FEASIBILITY STUDY
30 WATTS PER POUND
ROLLUP SOLAR ARRAY

Final Report

Contract No. 951971

REPORT NO. 40067-4 21 JUNE 19

RYAN

FEASIBILITY STUDY
30 WATTS PER POUND
ROLLUP SOLAR ARRAY

Final Report

Contract No. 951971

REPORT NO. 40067-4 21 JUNE 1968

Prepared by: R. D. Allen
R. E. Williams
B. Lake
A. J. Wellman

Approved by:
N. L. Olthoff
Program Director
Space Systems

This work was performed for the Jet Propulsion Laboratory, California Institute of Technology, as sponsored by the National Aeronautics and Space Administration under Contract NAS 7-100.

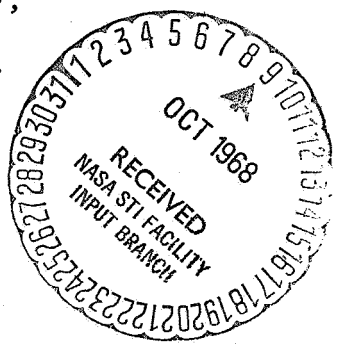

RYAN AERONAUTICAL COMPANY ◇ 5650 KEARNY MESA ROAD ◇ SAN DIEGO, CALIFORNIA

This report contains information prepared by the Ryan Aeronautical Company under JPL subcontract. Its content is not necessarily endorsed by the Jet Propulsion Laboratory, California Institute of Technology, or the National Aeronautics and Space Administration.

ABSTRACT

A preliminary design of the selected 30-watts/pound rollup solar array has been accomplished. Supporting technical analyses including electrical, loads, dynamics, stress, weights and thermal have been performed. The selection of materials and processes and the manufacturing feasibility have been investigated and fulfill the "state-of-the-art" constraints of the Design Specification. Special support equipment has been identified for handling the flexible solar panels and the complete array. Significant engineering tests were performed to substantiate the analytical approach and to verify the solar array design. A full scale model was fabricated and demonstrated to illustrate the deployment/retraction characteristics of the design. The selected solar array design produces 31.16 watts of power per pound of weight as established from a detail weights analysis and a solar cell electrical output of 10-watts/square foot at air mass zero, at 55°C and 1 A.U. equivalent solar intensity.

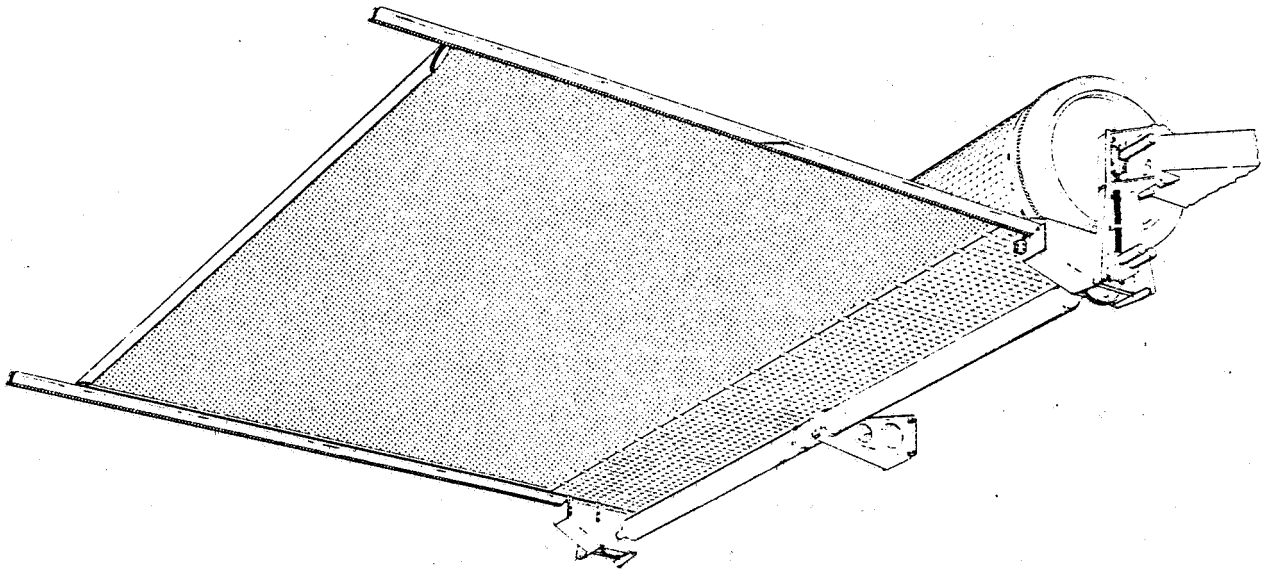

30-WATTS PER POUND ROLLUP SOLAR ARRAY

TABLE OF CONTENTS

TABLE OF CONTENTS (Continued)

TABLE OF CONTENTS (Continued)

TABLE OF CONTENTS (Continued)

TABLE OF CONTENTS (Continued)

LIST OF ILLUSTRATIONS

LIST OF ILLUSTRATIONS (Continued)

LIST OF ILLUSTRATIONS (Continued)

1.0 INTRODUCTION AND SUMMARY

This final report is submitted by the Ryan Aeronautical Company to the Jet Propulsion Laboratory in accordance with Article I, (a), (2) (iv) and Article II, Item (a) (8) of Contract No. 951971. The report presents the results of work performed from date of contract (23 June 1967) through 21 June 1968.

The data presented in subsequent sections are reported as summary information, developed in evolving a preliminary design of the solar array configuration. The detail investigations of subsystem and component evaluations and the parametric type analysis performed were reported in the Quarterly Reports (References 1, 2 and 3) which preceeded this report.

The selected rollup solar array configuration provides 1,000 square feet of solar cell area. This solar array configuration is composed of four Roll-up Solar Arrays each of which provide 250-square feet of gross solar cell area. The rollup solar array consists of four major elements:

- Vehicle Mounting Structure
- Wrap Drum/Panel Support Structure
- Wrap Drum
- Solar Panel

Design trade studies, analysis and development verification tests were conducted to select the most promising configuration. A detail preliminary design of the selected configuration has been performed. This design has been conducted in depth to identify all elements of the solar array. The major drawings which define the selected design are contained in Section 7.5. Detail stress, dynamic thermal and weights analysis has been performed to insure, with maximum confidence, conformance with the detail specification requirements.

Tests were performed during the study and preliminary design activities to identify suitable materials and to establish their characteristics. A full size drum with six substrate panels, mass loaded to simulate the 250-square foot solar panel, was tested to the 40g (0 to peak) sinusoidal launch environment. This test which is the most critical design environment was conducted to confirm the system dynamic characteristics and to substantiate the analytical predictions and to verify the critical elements of the solar array.

A full scale model was fabricated to demonstrate the deployment/retraction characteristics of the array design. This model is described with photographs of various extension positions in Section 2.7.

The calculated weight of the major elements of the 250-square foot rollup array is summarized as follows:

ITEM	CALCULATED WEIGHT - POUNDS
Array/Vehicle Mount	5.83
Drum/Panel Support	3.67
Drum Assembly	11.35
Panel Assembly	10.95
Deployment/Retraction System	7.26
TOTAL STRUCTURE	39.06
Solar Cell and Electrical @ 0.165 lb/ft^2	41.37
TOTAL	80.43 Pounds

A comparison of the selected rollup solar array performance characteristics with the contract and specification requirements confirm that the selected design will fulfill the objectives of the program.

CONTRACT REQUIREMENTS	SELECTED DESIGN CONFORMANCE
Power Output - 10.0 watts/square foot	10.0 watts/square foot
2 cm x 2 cm N/P 8 mil cells and mil cover glass	Same
Maximum number of cells per square foot - 225	224.
Gross cell area 250-square foot nominal	250.72
Power Output per solar panel - 2.5 KW	2.507
Nominal Panel Weight - 83.33 pounds	80.43
Power/Weight - 30-Watts/Pound	31.16

2.0 TECHNICAL DISCUSSION

2.1 APPLICABLE DOCUMENTS

a. System Specification No. SS501407, Rev. A, dated 4 January 1967, titled: ROLLUP SOLAR CELL ARRAY, 30-WATTS PER POUND, DETAIL REQUIREMENTS FOR.

b. Contract No. 951971, dated 26 June 1967, California Institute of Technology, Jet Propulsion Laboratory, for a FEASIBILITY STUDY, 30-WATTS PER POUND, ROLL-UP SOLAR ARRAY.

2.2 PROGRAM OBJECTIVES

The objective of this program has been to perform a design study and analysis, concluding with a preliminary engineering design, of a 250-square foot, rollup, solar array capable of producing 30-watts per pound, or greater. A part of this study has been devoted to evaluating the feasibility of manufacturing the rollup solar cell array from existing materials and technologies, or, from materials and techniques that could be developed to production use, one year from the conclusion of the Phase I study.

The design criteria defined in the detail specification (Reference 4) establish the electrical and mechanical features of the rollup solar cell array and the environmental constraints for selecting acceptable materials and processes. For clarification purposes the complete rollup solar array is defined as 1,000 square feet of displayed solar cell area, arranged on a spacecraft as four autonomous subarrays, each of 250-square feet. All further discussion in this report will therefore be concerned with an array area of 250-square feet.

The design study was also concerned with the equipment directly associated with support tasks for an array program, such as handling and transportation fixtures, product testing, etc. Likewise, fabrication feasibility studies were concerned with such supporting functions as repair and replacement procedures for damaged components and with development of reasonable increments of activity time for the design, development (fabrication), test and evaluation of a full scale prototype, solar array.

A further objective of Phase I was to assemble a model of the selected configuration which would adequately demonstrate the deployment/retraction characteristics of the design.

2.3 PROGRAM APPROACH

The approach employed to achieve the objectives of the program consisted of:

- The selection of the most promising rollout array concept that provides the following characteristics:
  - Design simplicity,
  - Maximum power/weight,
  - Positive deployment/retraction system,
  - Growth potential,
  - Minimized damage effects,
  - Analytically predictable, and
  - Manufacturing suitability.
- Trade-off studies and analysis to establish the most efficient design for the major subelements of the solar array.
- Preliminary design of the selected configuration and engineering development tests to verify the analytical predictions and/or design characteristics.
- Full scale solar array model fabrication and demonstration.

2.3.1 Concept Selection

In preparing Ryan's precontract proposal to conduct the Phase I Feasibility Study, work performed on previous deployable solar cell array concepts was reviewed for applicability to contract objectives, particularly a design

for a 50-square foot array, Figure 1, Reference 5. This experience encouraged Ryan to use the 50-square foot design as the baseline concept for an array capable of producing 30-watts per pound. Investigations had shown that the general arrangement was well-suited to the envelope described in the JPL Specification, Figure 2.

The design utilizes two extendible beams that continuously support a flexible, film-type substrate along each longitudinal edge. The beams, made of metal, are approximately circular in cross section when extended. They readily compress to the equivalent of flat metal strips, capable of wrapping about a cylindrical storage drum. Direction and support of the extended beams is provided by an arrangement of "guides" that are integral with the drum and drive system support structure. The solar cell layout, circuitry and connecting devices are designed to match the flexibiility of the substrate. A mechanical drive system, arranged to synchronously actuate both beams, is used to accomplish array deployment and retraction.

Experience gained in fabricating the full scale 50-square foot design lent confidence to the fabrication feasibility of a much larger array. Model fabrication and demonstration and component testing had established correlation with the original design philosophy and analytical methods that were used. There was sufficient evidence in each aspect that was considered to warrant selection of the design concept for initial study and evaluation. This decision then permitted an early detailed investigation of array subsystems that would otherwise have been deferred until conceptual studies were completed.

2.3.2 Trade-Off Studies

2.3.2.1 Design Studies

Studies were conducted during the initial phase of the contract considering suitable candidate concepts, materials and processes for each of the major items of the solar array. A matrix table was established and each of the items evaluated in order to establish the preferred design. Table 1 illustrates the matrix chart, identifies the items considered, their numerical evaluation and denotes the selected design concept.

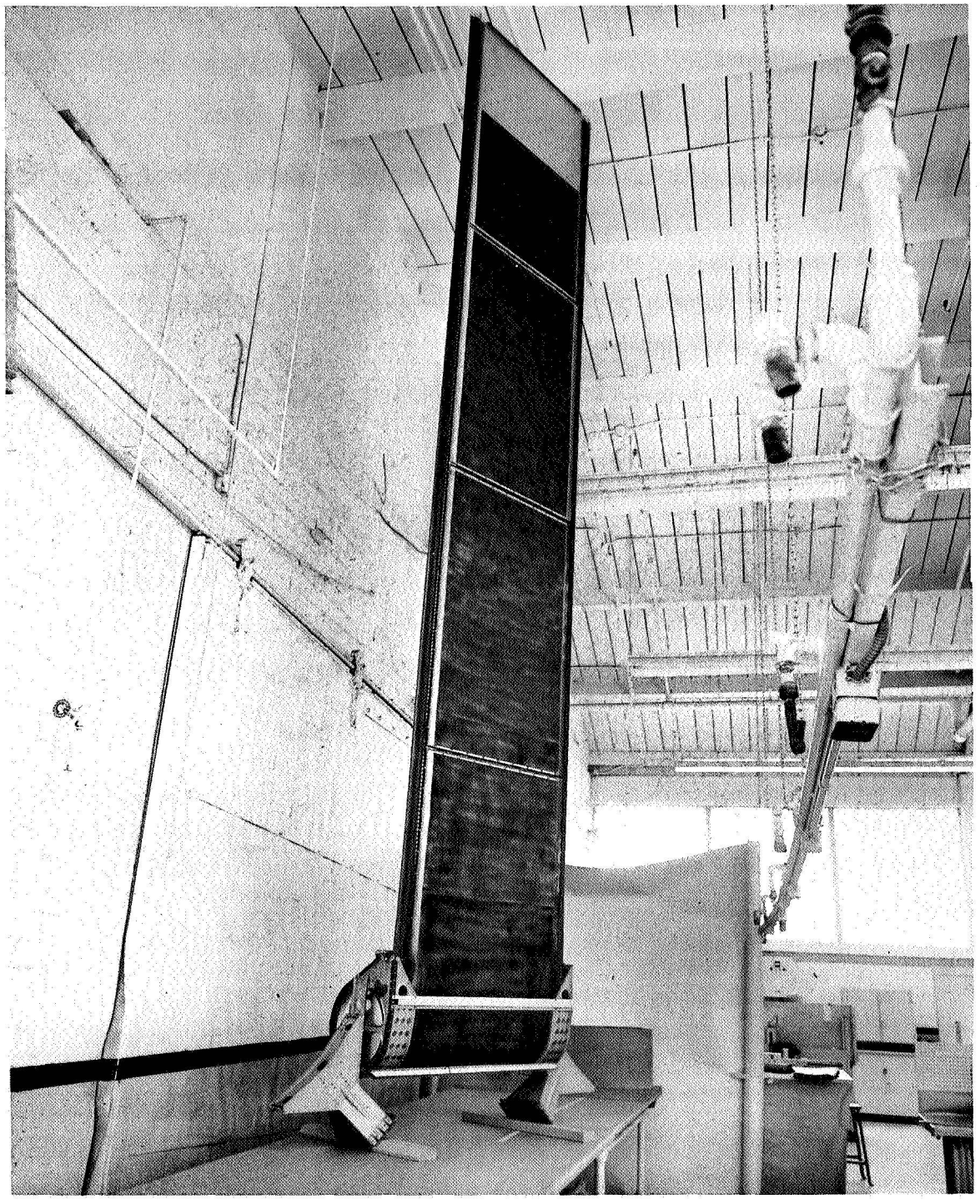

Figure 1 50 Square Foot Roll-Up Solar Array Vertically Deployed

NOTE: Dimensions in inches

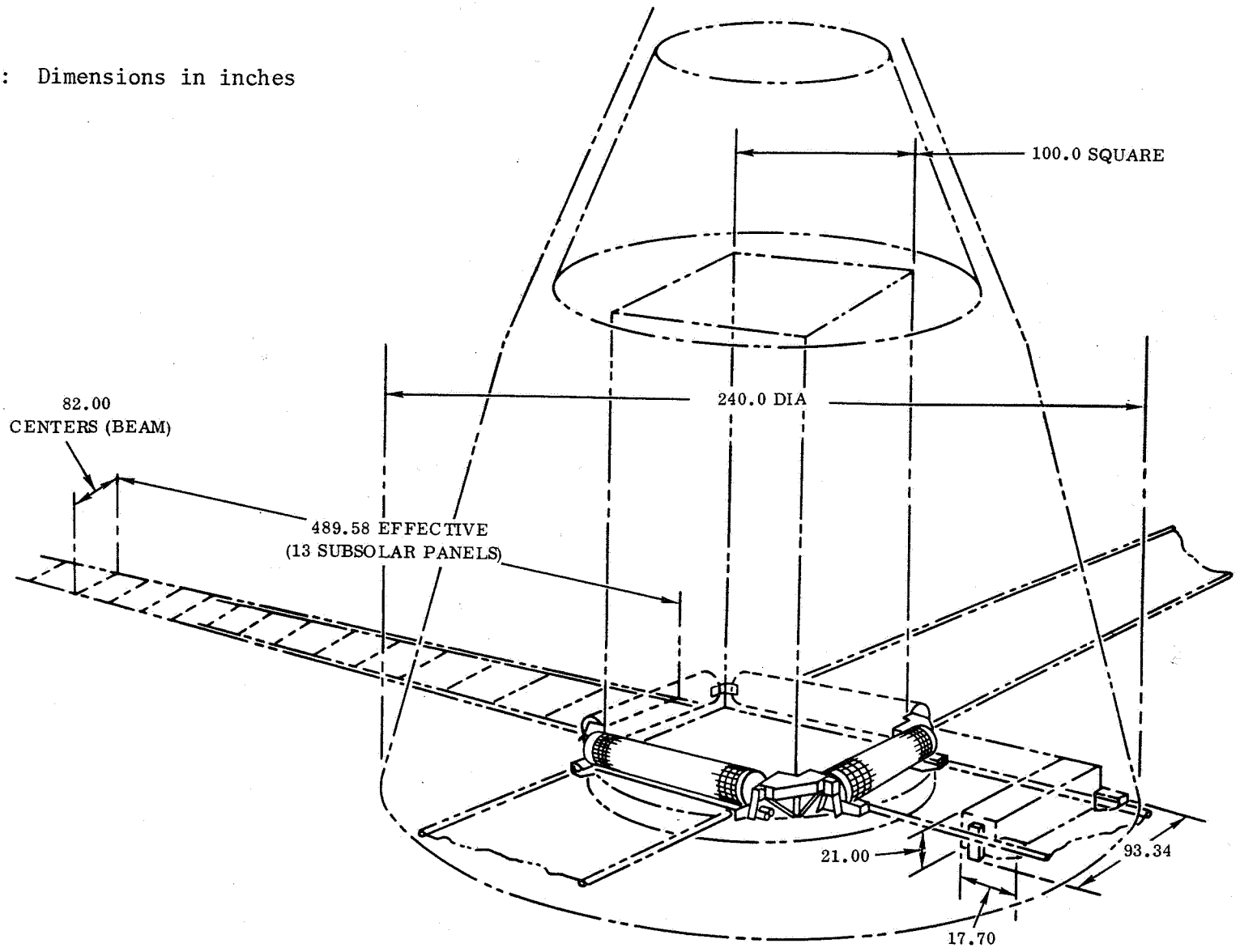

Figure 2 1,000 Ft^2 Roll Up Solar Array Installation

TABLE 1

TRADE STUDY SUMMARY

Item	Description	Concept No	Weight (overall weight effect)	Fabrication Feasibility	Reliability	Relative Cost	Comments	Final Evaluation
1. Drum/Beam Mounting	Fixed Drum and Pivoting Guide	1a	2		2	Equal	Design Based on JPL Model 208, Large Retracted Size Caused Excessive Guide Movement.	2
	Floating Drum and Fixed Guides	1b	1		1		System Eliminates Less Desirable Features of 208 Model.	1
2. Mounting to Vehicle	Tubular Mounting	2a	3		1	1	Dynamically Unfavorable	3
	"X" Form Mounting	2b	2		3	3	Dynamically Unfavorable	2
	Box Mounting	2c	1		2	2	Dynamically Acceptable	1
	Mounting with Shock Mounts	2d	4		4	4	Large Excursion of Shock Mounts (1:3) Makes Design Unfavorable	4
3. Substrate	Fiberglass	3a	2	3	2	3	Brittle and Prone to Handling Damage. Good Bonding Properties. Good Repairability and Tear Resistance.	2
	Mylar	3b	1	2	3	1	Relatively Good Handling Characteristics. Bonding Susceptible to Gamma Radiation Damage. Poor Resistance to Soldering Heat.	3
	Kapton	3c	1	1	1	2	Relatively Good Handling Characteristics. Bonding and Repairability Qualities Need Improving.	1
4. Beam	Titanium	4a	1	1	1	3	Needs Coatings to Reduce Larger Thermal Gradients.	1
	Beryllium Copper	4b	3	2	3	2	Best Thermal Properties	3
	Stainless Steel	4c	2	3	2	1		2
5. Drum Assembly	Chem Milled Magnesium Skin	5a	3	2	2	2		2
	Honeycomb Drum Skin (No Stiffeners)	5b	4	3	3	3		4
	Beryllium Skin With Stiffeners	5c	1	4	2	4	Considerable Fabrication Difficulty Due to Excessive Handling of Toxic Material. May Have Flaws in Sheet.	3
	Magnesium Skin with Lightness Holes and Stiffeners.	5d	2	1	1	1		1
6. Mechanical Drive System	Silicone to Silicone Friction Drive	6a	4	1	4	1		4
	Toothed Rack on Beam (Silicone or Polyurethane)	6b	2	2	1	2		2
	Toothed Rack on Beam (Formed Titanium Strip)	6c	1	4		4	This Shows Considerable Weight Saving on Other Schemes.	1
	Toothed Sprocket Wheel, Matching Holes in Beam	6d	3	3	3	3		3
7. Electrical Lead-Out	Coiled Continuous Harness	7a	3	1	1	1	Excessive Weight Approx. 400% Heavier than Internal Slip Ring.	2
	External Disc Slip Rings	7b	2	3	3	3	Difficulties due to Floating Drum	3
	Internal Sleeve Slip Rings	7c	1	2	2	2	Considerable Weight Saving Over Other Schemes	1
8. Motor Drive	Single Gearmotor Drive	8a	1	Equal	2	1	Failure of Single Motor Makes Roll Up Unit Inoperable.	2
	Double Gearmotor (Redundant Drive)	8b	2		1	2	Roll Up Unit Capable of Operating With One Motor Dead.	1
9. Cell Layout	180 Series	-	1	1	2	1	More Optimum Match to Converter and Conditioning Equipment.	1
	90 Series	-	2	2	1	2	Higher Power Loss Due to Higher Current.	2
10. Solar Cell Type	2 x 2 cm Bar Contact	-	-	1	1	3	Conventional Approach; Highest Reliability; Lowest Power	3
	2 x 2 cm Corner Dart Contact	-	-		2	2	Highest Power per Given Area	2
	2 x 6 cm Bar Contact	-	-	2	3	1	Good Area Utilization; Lowest cost Per Unit Area.	1
11. Bussing Material	Copper	Spectrolab DWG. SK-0007	3	3	2	2	Lowest Power Loss; Enhances Structure.	3
	Aluminum		1	1	3	1	Moderate Power Loss; Enhances Structure	2
	Copper - Clad Aluminum		2	2	1	3	Low Power Loss; Good Fabrication; Enhances Structure.	1
	Teflon Coated Individual Wire	-	6	-	5	5	High Weight; Difficult to Fabricate	6
	Teflon Coated Ribbon	-	5	-	4	4	Excess Weight	5
	Kapton Covered Ribbon	-	4	-	4	4	Excess Weight	4
12. Solar Cell Inter-Connections	Molybdenum, Silver Plate	-	4	2	1	3	High Cost, Difficult to Control Processing	2
	Copper, Silver Plate	-	3	1	1	1	Currently Used on Numerous Satellites.	1
	Aluminum, Nickel and Silver Plate	-	1	4	2	2	Difficult to Work.	3
	Aluminum, Copper and Silver Plate	-	2	3	3	2	Difficult to Work	4

2.3.2.2 Analytical Studies

Concurrent with the design studies analytical and parametric investigations were conducted to evaluate and substantiate each of the various candidate designs. The following basic tasks were accomplished:

a. Conducted a complete detailed weight analysis of the proposed design concept for use as a target design weight during the trade-off study and detailed work in Phase I. Weight contingencies were added whenever performance confidence was questionable. The watts/pound calculated from this target weight was based upon, (1) the baseline requirements of 10-watts/square foot, (2) a possible 4% factor above nominal structure weight to allow for materials and manufacturing tolerance variations.

b. Maintained a calculated power/weight monitor based upon various trade-off study concepts and detail design changes.

c. Analytically compared the effects, on panel structure and solar cell structural integrity, of the launch environments of sinusoidal vibration, acoustics, random vibration, and steady-state acceleration.

d. Used to advantage for analysis and refinement of this design the results as they became available, of the environmental qualification test of the 50-square foot rollup panel.

e. Conducted detailed sinusoidal dynamic analysis of the stowed configuration to find natural frequencies for use in determining load distributions for stress analysis. Refinements of the structural design were then made to minimize deflection of the stowed panel by decoupling the following basic structural components:

   (1) wrap drum

   (2) stowed panel

   (3) wrap drum end plates

   (4) spacecraft mounts.

f. Conducted thermal analysis of deployed panel to determine solar cell operating temperatures near Earth and Venus encounter. The baseline solar cell power output of 10-watts/square foot at 1 A.U. was verified. Effects on temperatures using Kapton and fiberglass substrates were analyzed.

g. Conducted circuit analysis to establish optimum cell arrangement and output voltage levels.

h. Investigated and optimized power transmission system.

i. Conducted component and materials suitability tests.

2.3.3 Preliminary Design and Analysis

A preliminary detail design of the selected solar array concept was conducted This design activity was extended in depth to include and identify all elements of the array and the preparation of drawings from which prototype hardware could be fabricated.

The analytical support was extended and refined to adequately substantiate and predict the characteristics of the array.

To support and verify the selected configuration, the following significant tasks were accomplished:

a. A 1/4-scale model of the array was fabricated to demonstrate the design features and was used to evaluate and improve the operational characteristics.

b. Conducted thermal analysis for use in approximating expansion and contraction of the panel relative to the space frame. This was used in calculating resulting induced solar panel loads and verified the necessity for a slip joint in the drum axial direction at one spacecraft mount.

c. Conducted thermal analysis of stowed panel for end-on solar flux conditions to determine magnitude of relative structure growth or contraction and resulting induced loads between substrate and beam guides.

d. Conducted full size drum and stowed panel mass sinusoidal vibration tests to verify the major design elements and the characteristic mode shapes and transmissibilities as used in the detailed stress and dynamic analysis.

e. Conducted sinusoidal vibration development testing of various solar cell matrices using various interconnect configurations and cell bonding techniques with the Kapton substrate.

f. Conducted breadboard testing of the extension/retraction motors to establish their operational characteristics and to verify the operational suitability of the deployment system.

g. Weight measurements were made of samples of representative solar cell installations to verify the pounds/square foot value used in the power/weight monitor and for detailed stress analysis.

2.3.4 Deployment Model

A full size rollup solar array deployment model was designed and fabricated to:

a. Demonstrate the deployment characteristics of the array design.

b. Confirm the manufacturing suitability of the selected design.

c. Confirm the minimal type of special support equipment for adequate support and handling of a large area rollup solar array.

2.4 CONFIGURATION DEFINITION AND STUDIES

This section presents a detailed description of the selected solar array design with a review of design trade studies where applicable, descriptions of ground support equipment and a discussion of the manufacturing feasibility of the array. Engineering drawings for each of the items discussed are presented in Section 7.5.

2.4.1 Functional Description

The solar array installation is shown in Figure 2. Four subsolar arrays each providing 250 square feet of solar cell area are mounted along the sides of the spacecraft. When extended the solar array provides 1,000 square feet of solar cell area capable of producing at least 10 kilowatts of raw power at air mass zero, at 55°C and 1 A.U. equivalent solar intensity. The power to weight ratio of the array is 31.16 watts/pound.

Each subsolar array consists of the following major elements:

- Solar Panel
- Drum Assembly
- Deployable Beams
- Extension-Retraction System
- Supports for Drum and Beams
- Spacecraft Mounting Structure

During launch the flexible solar panel is stowed on the wrap drum. When deployment is desired, two compressed tubular beams to which the panel is attached are extended from the rotating drum. The beams control the position of the panel during deployment and retraction.

Electrical power from the solar cells is collected by integral busses laminated to the panel substrate and transferred by means of slip rings through the wrap drum to the spacecraft.

2.4.2 Mechanical-Structural Design

2.4.2.1 Solar Panel

The solar panel consists of an assembly of thirteen subpanels with solar cells and one subpanel at the outer end providing a thermal blanket to protect the stowed array. The substrate is 0.001 inch thick Kapton type H with the power transmission bus integrally bonded between Kapton doublers along the substrate edges. The subpanels are connected to themselves and the deployable beams by means of flexible fiberglass tapes bonded with RTV-3145 adhesive.

The power transmission bus is 0.001 inch aluminum foil bonded to the substrate with FM-1044R adhesive. The aluminum foil bus is locally silver plated at areas where slots are provided in the Kapton insulation to permit solder connections. Solar cell submodules of 2 cm x 2 cm N/P silicon cells are bonded to the Kapton substrate with RTV-3145 adhesive. The cell layout and interconnections are described in detail in Section 2.4.3.

Polyurethane foam damper pads are bonded to the rear surface of the substrate to protect the solar cells during launch. The damper pads are arranged in a decreasingly dense pattern from the drum outboard to the tip of the panel.

The outer thermal blanket consists of two layers of Kapton Type H separated by foam pads. The exterior surfaces of the Kapton H have a vacuum deposited aluminum coating with an additional coating of silicon monoxide on the side facing the sun.

Trade studies (References 1, 2, 3) considered variations in the number and arrangement of the subpanels. Also, several edge attachment methods were evaluated including aluminum foil connectors and silicone rubber coated glass cloth tabs. Substrate materials investigated included fiberglass reinforced epoxy sheet, mylar, and Kapton films. Various arrangements and densities of damping pads using both silicone and polyurethane foam were considered in determining the optimum design.

Power bus provisions using flat ribbon, stranded wire and laminated foil conductors of copper or aluminum were compared.

Various silicone, epoxy and polyimide adhesives were evaluated for bonding the solar cells, substrate, power bus, and attachment tabs.

A thermal analysis was performed to determine temperature gradients and to compare methods of thermal control.

2.4.2.2 Drum Assembly

The drum assembly supports the solar panels in the stowed position. The drum is a magnesium sheet metal cylinder with flanged lightening holes incorporated on the cylindrical surface. The drum is stiffened internally with three equally spaced magnesium rings. Each end contains an adhesive bonded aluminum honeycomb sandwich bulkhead to which axis hubs of machined magnesium alloy are fastened.

A slip-ring assembly for power transfer is installed at one of the bulkhead hubs. Electrical lead-through inserts are provided at each end with adjacent access holes and covers.

Radial fence brackets are attached to the periphery of the drum near each end to insure correct beam alignment and to transfer stowed solar panel axial loads to the drum structure.

Trade studies considered the influence of drum diameter, length, and stiffness on the overall system efficiency. Magnesium and beryllium sheet metal drums along with aluminum or fiberglass faced honeycomb sandwich connections were evaluated (Reference 1).

Other factors considered were relative feasibility of fabrication and cost.

Alternate power transfer systems compared included slip rings, coiled cable and magnetic circuit.

2.4.2.3 Deployable Beams

The deployable beams provide support and control of the solar panels. The beams are connected at the outer end by an aluminum intercostal to which the solar panel is also attached.

The beams are constructed of titanium alloy (6Al-4V) 0.003 inch thick. The beam shape is a tubular cross section which can be compressed within its elastic limit to a flat configuration. Each beam is composed of an upper and lower surface which have been seam welded along the edges to provide the desired cross section. A corrugated strip of the same alloy is spot welded to one crown of the beam. This corrugated strip provides the rack portion of a rack and pinion gear drive system.

Trade studies considered various beam cross sections, gauges and materials including titanium, fiberglass, beryllium-copper and stainless steel. The beam section and properties were optimized in the titanium beam selected (Reference 1).

2.4.2.4 Extension-Retraction System

The extension-retraction system includes the drive motors, power transfer devices and associated control. During deployment and retraction, magnesium pinion gears at each end of a magnesium drive shaft engage the corrugated beam drive strip thus synchronizing the relative position of the two beams.

Deployment drive power is provided by a motor gear box system attached to the drive shaft. Double motors working through a differential gear box are used to provide redundancy. In the event one motor fails the remaining motor will extend the array at approximately half normal speed. Retraction drive is provided by a motor attached to the drum end hub.

In order to insure proper wrapping and unwrapping of the beam it is necessary to maintain tension on that portion of the beam between the drive pinion and the drum. This tension is produced by drag action of the retraction motor

during extension and the extension motor during retraction. The drag is produced by differential control of the motors through an electronic control system (Section 2.4.3). Limit switches shut off power to the motors when the array reaches either the fully deployed or retracted position

A redundant release clutch and a one way drive clutch are incorporated into the retraction motor drive. Their function is to permit the array to operate with a failed retraction motor. Though the retraction motor might fail to act as a brake, the array could be extended by the main deployment motors overriding the release clutch, causing it to slip. On retraction the deployment motors reverse and retract the unit; the one way drive clutch would overrun and allow the drum to turn. In this event, a tight wrap condition would not necessarily be assured. However, this is not critical for a retraction after launch. The release clutch also serves as a safety measure to prevent damage to the beam drive strip corrugations should the drive and wrap motors be out of phase.

Various deployment/retraction concepts were investigated during the study phase. One concept utilized the double gear motor and differential gear box attached to the drive shaft. The drum was driven simultaneously by a flexible belt powered by a pulley take-off from the drive shaft. Model tests showed that this system did not provide the desired tension in the beams required to achieve proper wrapping characteristics.

Other designs for the extension-retract system which were investigated were a friction drive utilizing a silicone rubber faced drive wheel, a rack and pinion drive utilizing silicone rubber drive strip, and a sprocket drive which engaged holes in the beam.

2.4.2.5 Drum and Beam Support Structure

The drum assembly is supported at each end of the drum axle by machined magnesium mounts. These mounts are attached to magnesium sheet metal box sections which support and position the deployable beams with glass reinforced teflon guides.

The drum axle bearings are caged in a magnesium guide which features stainless steel rollers and which are contained in the machined mounting track. The guide-track arrangement controls the position of the drum and allows for movement in a single plane as required as the diameter varies with the number of beam wraps. The drum is retained against the pinion extension gears by tension springs thus maintaining alignment of the drum-beam tangency with the beam support guides.

The drum support mounts provide the interface for attaching the solar array to the vehicle mounting structure. At one end a fixed attachment is made and at the opposite end a sliding fitting (axial direction of drum) is provided to allow for thermal expansion/contraction.

The box section which supports the beam guides also provides the extension motor, pinion gear and drive shaft mounting provisions. The beam guides are attached to the box structure in a manner which allows lateral freedom for possible substrate thermal contraction.

The preceeding trade studies included basic concepts for the mechanical compensation arrangement essential to adjustment of diameter change in the wrapped substrate during deployment or retraction:

a. A fixed drum with a pivoting guide. The beam guide is pivoted at its forward end and driven by a cam mechanism at the rear in such a manner that it follows the increasing or decreasing diameter of the wrapped drum.

b. Floating drum and fixed guides. With this scheme the drum rests on fixed drive and idler rollers. The drum center bearings work in slides on the fixed support structure. Heavy tension springs keep the drum in contact with the rollers. As the drum substrate increase or decreases in diameter the drum center rises or falls in the slide. (This was the basis of the selected concept.)

2.4.2.6 Array-to-Vehicle Attachment

The structural assembly that is used to mount four 250-square foot arrays to the spacecraft is a right angle box structure used at each of the four corners of the spacecraft. They are constructed of an aluminum sheet metal structure and are augmented with tubular bracing to the spacecraft corners. Each unit supports the end of an adjacent array by means of magnesium fittings. One fitting is designed for fixed attachment of the array; the other fitting is configured as a captive slide track which permits the array to wrap and its support structure to expand or contract in the direction of the wrap drum axis.

In the trade study phase, four schemes were investigated for the type of structure that would mount upon the spacecraft and support the array assembly:

a. A tubular mounting arrangement representing a truss made up of tubes, pin-jointed at intersections.

b. An X-frame design. It consists of an aluminum box structure in the form of an "X" which provides a common mounting for the end of one rollup unit and the opposite end of the adjacent unit. The structure is braced by tube struts for loads in the vertical plane.

c. A box-mount arrangement. The structure mounts to the corner of the spacecraft and provides a common support for two rollup units similar to the X-frame design. (Concept selected for detail design.)

d. A support structure with resilient-type shock mounts. A structural box attaches to the corner of the spacecraft utilizing shock mounts between the box member and the rollup unit. This scheme was the only concept investigated involving application of a mechanical damping device.

2.4.3 Electrical Designs

2.4.3.1 Solar Cell Installation

Cell Layout

Various solar cell layouts (i.e., module sizes, arrangements, and circuitry) were studied to determine the most satisfactory design. Prime attention was given to (1) cell layout per available area, (2) circuit-module designs, (3) interconnect configurations, and (4) general suitability of the solar cell installation for thin film, flexible substrate.

Layouts were investigated using the conventional 2 x 2 cm cells and also the large area, 2 x 6 cm cells. Use of the larger cells was studied because of potential gains in electrical output and the possibility of more efficient use of available substrate area. Interconnect concepts and solar cell contact designs were objects of intensive study.

Solar Cells

The silicon solar cell of 8-mil thickness, N on P configuration, was used in all studies.

Coverglass

Specific information regarding radiation spectrum anticipated to be encountered was not included; therefore, no detail studies were performed to optimize coverglass use. On these terms, the most suitable coverglass, considering cell output, cost, and handling was judged to be microsheets with an antireflective (AR) coating.

Conductor Leads

Study was devoted to various meterials and manufacturing techniques for conductor leads which would be used to collect series-connected cells into parallel circuitry (transversely across the array) and connect the flexible

longitudinal leads bringing collected power into the inboard end of the array. Conductor designs were considered which would be made from plastic shielded wire and/or ribbon, conductive metal foil, a bimetallic composite or plated base metal. Redundancy was assured in the array by planning for primary power transmission bus bars along both longitudinal edges of the array and connecting transverse module leads to both sides.

The two longitudinal transmission bus bars would terminate on terminal boards incorporated on the inboard end of the deployable substrate assembly.

Solar Cell-Substrate Interface

To evaluate this interface design, Mylar, Kapton H, and Kapton HF (Kapton H with Teflon) were considered. Studies stressed comparative evaluation of handling, adhesive application, and projected service life characteristics of the selected materials.

Diodes

Requirements for blocking diodes were studied but there appears to be no foundation for their use. Chief reasons for not using diodes are:

- The substrate is a nonconductive material and not subject to the short circuit hazards associated with use of metallic, rigid substrate.

- The fact that shadow effects are assumed to approach a complete eclipse of the array rather than local, concentrated area shadows.

Description of Selected Configuration

The solar cell area of each solar panel is 250.7 square feet utilizing 224 2 x 2 cm cells per square foot. The solar panel is composed of thirteen sub-panels each containing 4,320 individual cells connected in series-parallel in eight circuits. Each circuit consists of three cells in parallel by 180 in series (four subcircuits of 45 cells in series).

This configuration utilizing a 2 ohm base resistivity solar cell at a temperature of 55°C will generate approximately 76 volts at the maximum power point.

The subpanel layout is shown in Figure 3.

The area covered by cells on each subpanel is 76.83 x 36.81 inches. This configuration allows 45 cells to be placed in series on the panel and 96 cells in parallel.

The 2 x 2 cm cell is manufactured to 0.788 ±0.005 inch in both dimensions. The cell spacing is 0.010 inch between parallel solar cells and 0.017 inch between series connected cells. Spacing between solar cell submodules is 0.012 inch.

The layout has been made using upper side limits of cell dimensions to avoid possible interference between cells and to permit greater flexibility in assembly tooling.

Solaflex(R) series interconnects were selected to optimize circuit reliability. The design is illustrated in Figure 4.

All solder connections are redundant and accessible from the cell side surface of the panel.

The power transmission bus consists of 0.001 inch aluminum foil laminated on the substrate. Access for solder connections is provided by means of slots in the substrate insulation. Magnetic fields are minimized by utilizing multilayer foil conductors and by reversing juxtaposed circuits. The width of the longitudinal bus increases from the outboard to inboard end of the array to maintain a constant conductor resistance power loss of 0.10 watts per square foot. Flexible foil or expanded mesh jumpers are used to conduct the current across the subpanel joints. A main power bus is routed along each side of the subpanels for redundancy.

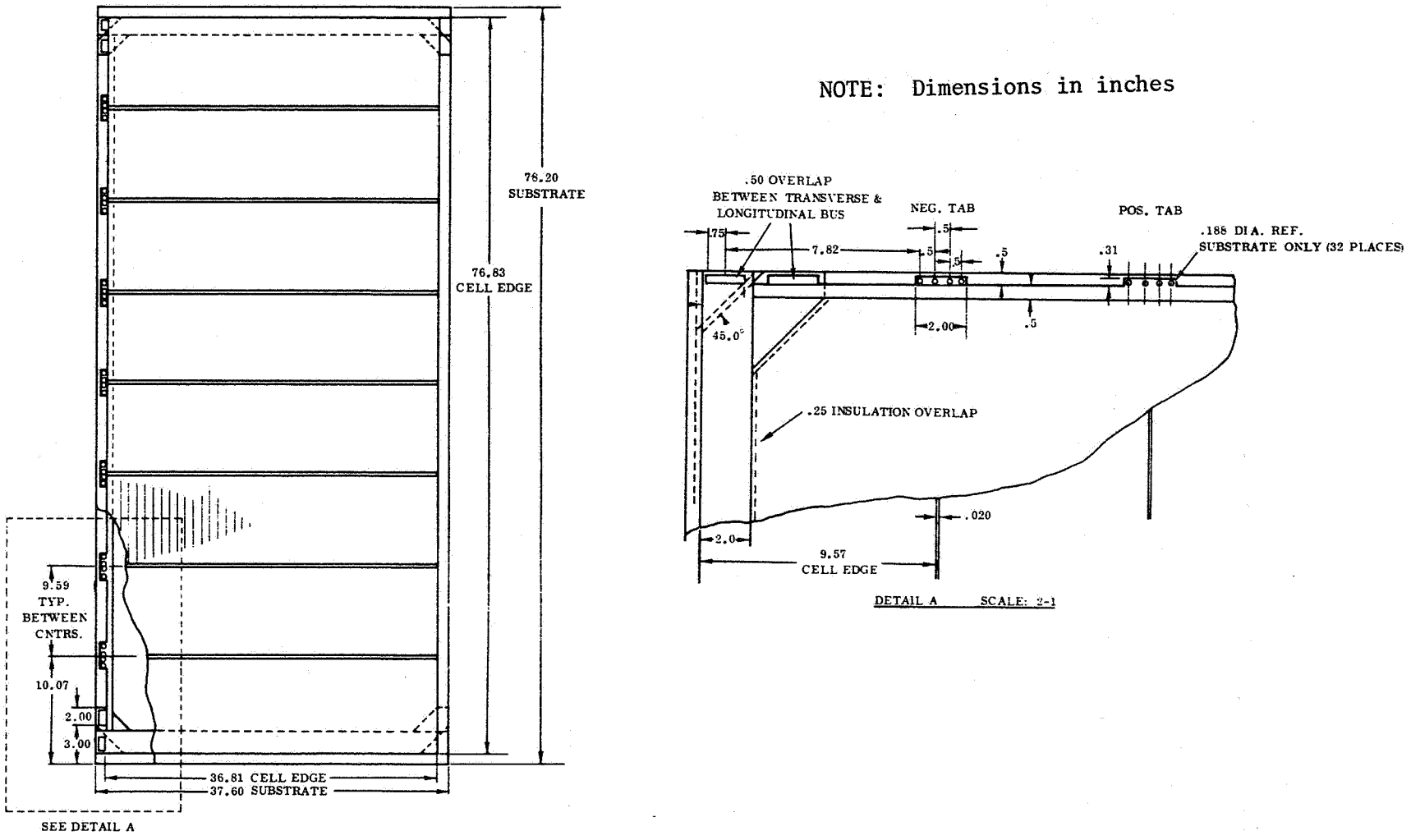

Figure 3 Solar Cell Module Layout For 2 x 2 cm Cells

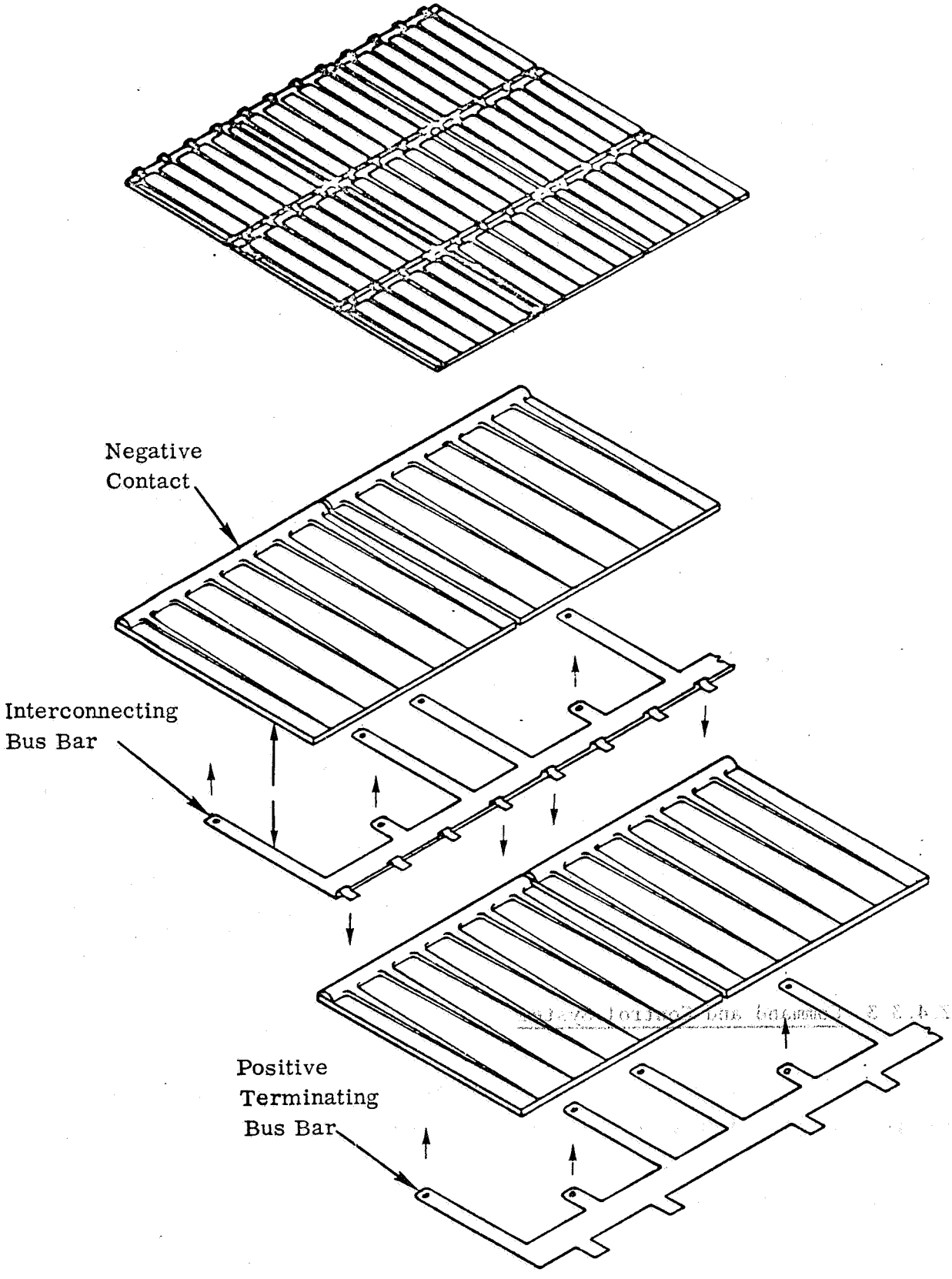

Figure 4 Typical Solaflex(R) Interconnections
For 2 x 2 cm Bar Contact, Solar Cells

2.4.3.2 Electrical Transmission - Array-to-Vehicle

This system transmits current generated by the solar cells from the deployed array to the spacecraft electrical system. The design must accommodate rotation of the wrap drum and consequently the harness and/or rotating conductor must be compatible with wrap drum operation.

Three designs were investigated in trade studies:

a. A continuous coiled harness. The continuous coil is formed so that during retraction the coil winds up and unwinds during deployment.

b. External disc slip rings. Several conductor discs separated by insulating strips are fixed to the end of the drum so that they rotate with the drum. Spring loaded, stationary pickup brushes mount to the array support structure and conduct current from the drum.

c. Internal slip rings. This method uses a series of slip rings and pickup brushes within the rotating shaft of the drum. The contacts are a series of rings inside the shaft that rotate with the drum. The pickup brushes are stationary, being fixed to the outside structure and inserted inside the rotating shaft.

Item (c), internal slip rings, were selected for incorporation in the detail design.

2.4.3.3 Command and Control System

The command switch would be actuated by the spacecraft data link and electrical power supplied through it to deploy or retract the panel.

Two limit switches are mounted on the guide support structure. One turns off power when the panel is fully extended; the other turns off power when the panel is fully retracted.

Control is accomplished by means of a closed-loop electronic servo-system which compares the load on the "driving" motor with the load on the "drag" motor. It adjusts the drag to insure that proper tension between the beams and the drum is applied during deployment or retraction.

Strain sensors (sensing motor torque) measure the load each motor is applying to the system and converts it to an electrical signal which is transmitted to the electronic control circuit. The electronic control circuit controls the amount of drag between the two drive motor units.

2.4.4 Materials and Processes

2.4.4.1 Selected Materials

Materials used in the design have been chosen with regard to the functional and environmental requirements of JPL specification SS501407A. The selection of materials has been based on their ability to meet the requirements of the design and to withstand deep space environment. Factors considered in evaluating materials included resistance to radiation, thermal cycling, and release of condensing gases. Also considered were methods of fabrication, assembly and ground handling. Several materials for each application were considered to determine the best choice.

Table 2 summarizes the materials used, properties and the basis for their selection.

There are some general areas of concern in selecting materials. First, all the material should have the properties required for the launch and flight environment.

Another consideration is the extent to which exotic or state-of-the-art materials are employed. Obviously, use of well known, proven materials avoids the risk involved with extensive employment of advanced materials undergoing development.

TABLE 2

SUMMARY OF MATERIALS USED

Application	Material	Radiation Limiting Dose (Rads) (ref 4)	Useful Temperature Range (°C) (ref 5)	VCM at 125 C (Weight %) (ref 6)	Reason for Selection
Solar Array					
Substrate	Kapton Type H (Dupont)	5 x 10	-260 to 300	0.09	Least weight - stability in space
Power Bus Conductor	Aluminum Foil 1100-EC	-	-	-	Least weight
Adhesive, Power Bus	FM-1044R (Am. Cyanamid)	10^8	-90 to 170	2.99	Flexible, thin, thermosetting
Interconnect	Copper	-	-	-	Reliability - proven use
Adhesive, Solar Cell	RTV 3145 (Dow-Corning)	10^7	-100 to 350	0.6*	Least weight - fabrication feasibility
Primer	90-198 (Dow-Corning)	10^7	-100 to 350	0.20*	Good adhesion to Kapton
Adhesive, Cover Slide	RTV 602 (General Electric)	10^7	-100 to 350	1.04	Reliability, proven use
Substrate attach Tabs	Woven Glass Fiber (Owens-Corning)	-	-	-	Flexible, high strength
Adhesive attach Tab	RTV 3145 (Dow-Corning)	10^7	-100 to 350	0.6*	Flexible, reliable bond
Damper Pads	Eccofoam FS (Emerson & Cumming)	10^7	-55 to 150	0.63	Least weight - flexible
Deployment System					
Beams	Titanium (6AL-4V)	-	-	-	High ratio tensile yield strength to modulus of elasticity
Beam Guide	Teflon (TFE) Glass Filled	5×10^7	-260 to 320	0.05*	Low friction - stable in space
Wrap Drum	Magnesium (AZ-31B)	-	-	-	Lightweight fabrication feasibility
Drum Bulkhead	Aluminum Honeycomb Sandwich	-	-	-	High stiffness to weight ratio - feasibility
Bulkhead Adhesive	FM-96U (Am. Cyanamid)	10^8	-200 to 170	0.01	Stable - reliable

(*estimated, additional data required)

TABLE 2 - CONTINUED

SUMMARY OF MATERIALS USED

Application	Material	Radiation Limiting Dose (Rads) (ref 4)	Useful Temperature Range (°C) (ref 5)	VCM at 125 C (Weight %) (ref 6)	Reason for Selection
Deployment System (Cont'd)					
Drum Slide	Magnesium (AZ-31B)	-	-	-	Lightweight - fabrication feasibility
Bearings, Drum Slide and Drum	Stainless Steel 440C	-	-	-	Nonmagnetic
Lubricant, Bearing	Electrofilm 4306 (Electrofilm, Inc.)	10^8	-150 to 220	0.09	Stable - Prevents surface adhesion
Torque Shaft	Magnesium (AZ-31B)	-	-	-	Lightweight - Fabrication feasibility
Bearing, Torque Shaft	Teflon (TFE) (Glass filled)	5×10^7	-260 to 320	0.05*	Low friction - stable
Drive Gear	Magnesium (AZ-31B)	-	-	-	Lightweight - fabrication feasibility
Lubricant Drive Gear	Electrofilm 4306	10^8	-150 to 220	0.09	Stable - prevents surface adhesion
Retaining Spring	Stainless Steel (316)	-	-	-	Nonmagnetic
Support Structure					
Drum Support	Magnesium AZ-31B	-	-	-	Lightweight - fabrication feasibility
Spacecraft Mount	Aluminum 7079	-	-	-	Strength - fabrication feasibility
Thermal Control Materials					
Array Cover	Kapton - VDA plus silicon monoxide (Sghjeldahl)	10^8	-260 to 320	0.09	Low a/e - lightweight
Structure Coating	Vacuum deposited aluminum	-	-	-	Low e - lightweight
Structure Undercoating	Cat-a-Lac 473-1-500 clear (Finch Paint Co.)	10^7	-90 to 170	0.82	Reliable - proved use

(* estimated, additional data required)

In the solar panel design, analytical consideration has been given to use of beryllium and advanced composites, but their use is not considered justified by the modest weight differences predicted when offset by the general risks related to fabrication problems, cost, and reliability of performance.

Another consideration of significance is the extent to which non-metallic materials are used and the types of non-metallic materials. These choices are particularly important because of the wide variation in properties with respect to environmental conditions and particularly because of the tendency of most to release volatile condensible materials (VCM) in the vacuum environment. Resistance to penetrating radiation of 10^7 rads must also be considered.

The selection of a material must be based on its ability to perform its design function with reliability. In most cases, the selected solar array employs materials which meet the objective of less than 1.0 percent weight loss and less than 0.1 percent VCM at 125°C and 10^{-6} torr.

In a few cases, in order to meet design function requirements, materials have been selected which, as prepared, exceed the desired limits of VCM. However, these materials will be either sealed in their design application or can be thermal vacuum cleaned to remove excess volatile material.

Table 3 summarizes the properties of various non-metallic materials chosen in the preliminary design. Some additional tests on composite elements are required to verify the acceptability of the materials as they are employed in the design.

Materials choices and their design relationship are discussed in the following paragraphs.

2.4.4.2 Solar Panel

The solar panel consists of the substrate, attach tabs, damping pads, power bus, solar cells, cover slides, cell interconnects and adhesives.

TABLE 3

NONMETALLIC MATERIAL-SUMMARY OF VOLATILE CONDENSIBLE MATERIAL
(Tested at 125°C and 10^{-6} Torr) (Ref. 1)

Application	Material	Weight Loss %	VCM Weight %	Lbs used per array	Lbs VCM per array at 125 C	Comment
Substrate	Kapton Type H	0.14	0.09	2.0	0.002	
Adhesive, Solar Cell	RTV 41	1.09	0.60	1.8	0.011	Confined under cell
Adhesive, solar Cell	RTV 3145		0.6*	-	--	Confined under cell
Adhesive, cover Slide	RTV 602	2.07	1.04	1.8	0.019	Confined on cell
VDA Base	Cat-a-Lac 473-1-500	1.09	0.82	0.10	0.001	
Adhesive, Bulkhead	FM 96U	0.15	0.01	0.15	0.000	
Lubricant, Bearing	Electrofilm 4306	0.67	0.09	0.1	0.000	
Adhesive, Bus Bar	FM-1044R	5.84	2.99	1.4	0.042	Sealed in Kapton
Damper Pad	Eccofoam FS	1.25	0.63	2.0	0.012	Requires thermal vacuum clean-up
Adhesive, Damper Pad	RTV 3145		0.6*	0.7	0.004	Requires thermal vacuum clean-up
Beam Guide	Teflon TFE glass filled		0.05*	0.25	0.000	

*Estimated, additional data required

Ref. 1. Muraca, R. F. and Whittick, W. S., Polymers for Spacecraft Applications Final Report, JPL Contract 950745, September 15, 1967.

The substrate material is Kapton Type H selected for its excellent resistance to the space environment. Kapton has a broad range of service temperatures from -250 to +400°C (Reference 7) and good radiation resistance up to 5×10^8 rads (Reference 8). Kapton has good handling properties except for low propagation tear strength (8 grams per mil). This is so low that provisions must be made in the design to prevent start of tears. Doublers are provided on all edges of the Kapton substrate. The aluminum foil power bus conductors which are integrally laminated to the Kapton provide additional edge strength.

The bus foil is bonded using FM 1044R adhesive and Kapton film insulation. FM1044R has been selected in this application because of its flexibility and reliable adhesion. It is a thin film, thermosetting adhesive which maintains its properties over the temperature range of the flight environment.

This adhesive is a nylon-epoxy type with relatively high (2.99 percent) VCM content. However, it is reasonable to use in this application because it is entirely contained between layers of Kapton which will prevent the release of volatile components.

Element tests can be conducted to verify the suitability of this configuration with respect to VCM content.

The power bus conductor is aluminum (1100 EC-grade) which has been shown in the trade study to have the lowest weight. The aluminum is silver plated locally where solderability is required. This technique, enabling repeated soldering operations during fabrication has been demonstrated in development testing (Reference 3).

Cell interconnections are made using silver plated copper conductors. This material selection is based primarily on the reliability of plating on copper compared to plating on molybdenum. (See Section 2.6.10.)

Damper pads are flexible polyurethane foam Eccofoam FS, 2.0 pounds/cubic foot.

The selection of this material is based primarily on the weight advantage over silicone foam which has densities of about ten pounds/cubic foot for the same damping characteristic. The service temperature ranges of silicone foam is -90°C to 315°C compared with -55°C to -150°C for the polyurethane foam. At the lower temperature limits, the flexible foams become rigid; however, the critical damping requirement exists at launch when temperature is not a factor.

A factor involved in the selection of damping material is the requirement for insignificant release of volatile condensing material. Both materials have VCM content in excess of 0.6 percent by weight at 125°C and 10^{-6} torr. Therefore, it will be desirable to thermal vacuum clean the pad material to reduce the VCM to a more acceptable level.

Adhesives selected for bonding solar cells, cover slides, and substrate edge attachment are all of the silicone RTV type. These selections are determined by design function requirements and the need for uniform properties in the space environment.

The adhesives proposed have been tested to verify their ability to withstand thermal cycling from -195°C to 140°C at 10^{-6} torr without degradation. (Reference 1 and 3.)

The cover slide adhesive is RTV 602 which is selected primarily for its reliability and proven use on successful space missions.

The solar cell adhesive selected is RTV 3145 (Dow Corning) which in testing exhibited superior adhesion to Kapton as well as consistent handling and curing characteristics.

RTV 3145 is a one component amine-curing silicone system which has met the needs for a flexible adhesive bond of titanium doublers to the flexible titanium beams used and tested in the Ryan 50-square foot solar array program. This is the basis for selecting the RTV 3145 to bond the flexible substrate attach tabs to the Kapton substrate and titanium beams.

As a class the RTV silicone adhesive have VCM content which exceeds the desired amount. Expected VCM content at 125°C and 10^{-6} torr is greater than 0.6 percent. This can be reduced to more acceptable levels by thermal vacuum cleaning the array after assembly.

A woven fiberglass tape is used for the flexible attach tabs connecting the substrate modules and the titanium deployable beam. The material selected is a 0.003 inch thick, 1.0 inch wide tape. The use of a dry glass tape with a woven edge provides the tensile strength (135 pounds/inch) and flexibility required.

Candidate materials for the substrate included Kapton, Mylar and fiberglass reinforced plastic. These materials were considered because of availability in thin sheet, and suitability for space environment. Silicone rubber or Teflon films are substantilaly heavier than the selected candidates.

A fiberglass-epoxy resin substrate had been previously selected for the 50-square foot solar array design in order to meet deployment and mid-course maneuver requirements. However, in this design, the reduced load requirements and weight objectives suggested consideration of very thin films.

Several adhesive systems were evaluated for use in the array. Structural adhesives considered include FM-1000, FM-1044R, and FM-96U (American Cyanamid); Narmco 225 and Narmco 329 (Whittaker Corporation); EPON 934 and EPON 956 (Shell Chemical Company); TR150-25 (Thermo Resist, Inc.); RTV-3145, Silastic 140 (Dow Corning), and GT-100 (Schjeldahl).

For solar cell adhesives, the following were considered: RTV 108, RTV 41, RTV 511, RTV 577, RTV 602 (General Electric); Sylgard 182 and 92-024 (Dow Corning).

These materials are generally acceptable to the specified environment with the epoxy and polyimide types being considered more resistant than the silicones.

In order to protect the solar cells in the stowed position during launch, a cushion or pad arrangement must be provided. Silicone foam materials having a density of 10 to 20 pounds/cubic foot were previously investigated and found suitable for sterilization, launch and space environment. In this design, lower foam densities were needed to meet weight objectives. Therefore, flexible polyurethane foam was evaluated and selected because of its more uniform properties at densities as low as 2.0 pounds/cubic foot.

2.4.4.3 Deployment System

The deployment system consists of the storage drum, the drum slide, bearings, retaining spring, the beam guides, deployable beams, the drive pinion and drive shaft.

The drum material is magnesium AZ-31B. This selection has been based on the analytical trade study which shows that magnesium adequately meets the launch loads. The structure is readily fabricated of sheet metal using spot welds or rivets. A protective coating of Dow 17 is applied for corrosion resistance.

The drum and bulkheads are an aluminum faced-aluminum honeycomb structure adhesive bonded with FM-96U. This selection was based on the high strength to weight ratio of the aluminum facings and the stiffness requirements of the launch environment. The sandwich structure is readily fabricated using FM-96U, an unsupported film adhesive which has reliable mechanical properties and meets the space environment requirements.

The drum slide is machined from magnesium AZ-31B which is selected for lightweight and fabrication feasibility.

The drum spindle bearings and drum slide bearings are stainless steel selected because of its hardness and nonmagnetic property.

The retaining springs are type 316 stainless steel selected to provide a nonmagnetic material of high mechanical properties.

The drive shaft and drive gear are of magnesium construction selected for lightweight and fabrication feasibility. The magnesium drive shaft is treated with Dow 17. The drive pinion is treated with Dow 19 and coated with Electrofilm 4306.

2.4.4.4 Support Structure

The support structure consists of the spacecraft mount and the drum support.

The spacecraft attachment is 7079 aluminum alloy, chosen during analysis for its stiffness in this application. The aluminum surface is polished to provide a low emittance for thermal control.

The drum support is made of AZ-31B magnesium. This selection is based on the low density of magnesium and its fabrication feasibility. The exposed surfaces of the support are coated with vacuum deposited aluminum for thermal control purposes. Dow 19 coating is applied for corrosion resistance and as a base for adhesion of Cat-a-Lac 473-1-500 clear epoxy coating used under the vacuum deposited aluminum.

During the design study various materials were considered for the structural and mechanical components of the array. The metals considered were aluminum, beryllium, beryllium-copper, magnesium, corrosion resistant steel and titanium. All of these metals are space qualified and present no significant environmental problems.

2.4.4.5 Beams

Titanium (6AL-4V) was selected because of its high ratio of tensile yield strength to modulus. In addition, it can be satisfactorily formed by annealing at temperatures from 1,000°F to 1,300°F. During the forming process an oxide surface is formed on the titanium which can be controlled to give satisfactory emittance values for thermal control.

The beam guide is machined from Teflon-reinforced with glass fiber. This material is selected for its reasonable strength and low coefficient of friction (0.04). Teflon will maintain useful properties from -200°C to +320°C.

Materials considered for the support beams include titanium, beryllium-copper, stainless steel and glass fiber reinforced plastic. Each of these candidate materials can be fabricated successfully into the beam configuration to meet functional and environmental requirements.

The feasibility of forming long metal beams (at least 40 feet) was considered. Titanium beams 20 feet long have been formed in a full length heat treat fixture (Reference 5). Longer beams can be fabricated by (1) extending the size of tooling fixtures and furnaces, (2) by using a continuous forming process, or (3) by incorporating splice joints in the beam. The use of splice joints is applicable. Several titanium beam test sections have been spliced by welding to produce a satisfactory joint. This method is also applicable to beryllium-copper and steel.

Equipment limitations oppose the use of larger tooling fixtures to produce beams 40 feet long. Continuous forming appears to be feasible with considerable promise but requires tooling development. Continuous forming would not be applicable to the reinforced plastic beams.

2.4.4.6 Lubricants

The lubricants have been selected to fulfill the design and manufacturing requirements and to provide satisfactory functional characteristics in and after a long time exposure to deep space environments. In previous space application greases and oils have been used but because of the low volatility constraint in this program, preference to use dry film lubricants because of their negligible release of volatile material and to preclude surface adhesion of the contact metals.

The dry film lubricants considered most acceptable are Electrofilm 4306, containing molybdenum disulfide, and MPB Corporation DL-5, tungsten disulfide. The four main areas to be considered for lubrication are:

a. Drum spindle bearings.

b. Drum slide rollers.

c. Drive shaft bushings.

d. Extension and retraction motor gear trains.

The drum spindle bearings and the drum slide rollers are made from stainless steel. The bearing races and the drum slide, rollers and roller track are coated with Electrofilm 4306.

The drive shaft is made from magnesium and is supported at each end by glass reinforced teflon sleeve bushings. No lubricant is considered necessary.

The lubricants for both the extension and retraction motor gear train will be selected to meet the design environments and to provide satisfactory functional characteristics. Suitable systems are available and have been proven in space applications.

2.4.5 Ground Support Equipment

The following are considered to be the major items of ground support equipment that will be needed.

a. Handling platform.

b. Rollout demonstration fixture.

c. Shipping container.

2.4.5.1 Handling Platform

The handling platform (Figure 5) consists of a pallet on which the subarray is assembled and remains attached except when the unit is assembled to a simulated spacecraft mounting or a vibration fixture. It has four brackets for mounting the drum end support structures. Single bolt lugs are provided near the corners of the pallet for attachment to the rollout demonstration fixture and also for securing to shock mounts in the shipping container. Convenient lifting handles are provided.

2.4.5.2 Rollout Demonstration Fixture

The rollout demonstration fixture (Figure 6) consists of:

- Four identical table sections (approximately 3' high x 8' wide x 12' long) equipped with rollers that support a lightweight, endless belt. The endless belt is driven at one end by an electric motor geared to drive at the approximate rate of the rollout deployment. The tables are bolted together to form a 48-foot long deployment platform capable of being broken down for transportation.

- A support gantry that suspends the stowed array is mounted on its handling pallet as a free-swinging pendulum. A linkage arm operates a variable resistance control which varies the endless belt motor speed. During deployment or retraction of the panel on the endless belt, any tendency of the belt to induce fore or aft drag on the system is registered as a swing from vertical and the belt drive motor power is varied to compensate.

2.4.5.3 Shipping Container

The shipping container (Figure 7) consists of a reinforced box structure that will accept the stowed subarray on its handling pallet. Attachment is accomplished by four vibration shock isolators.

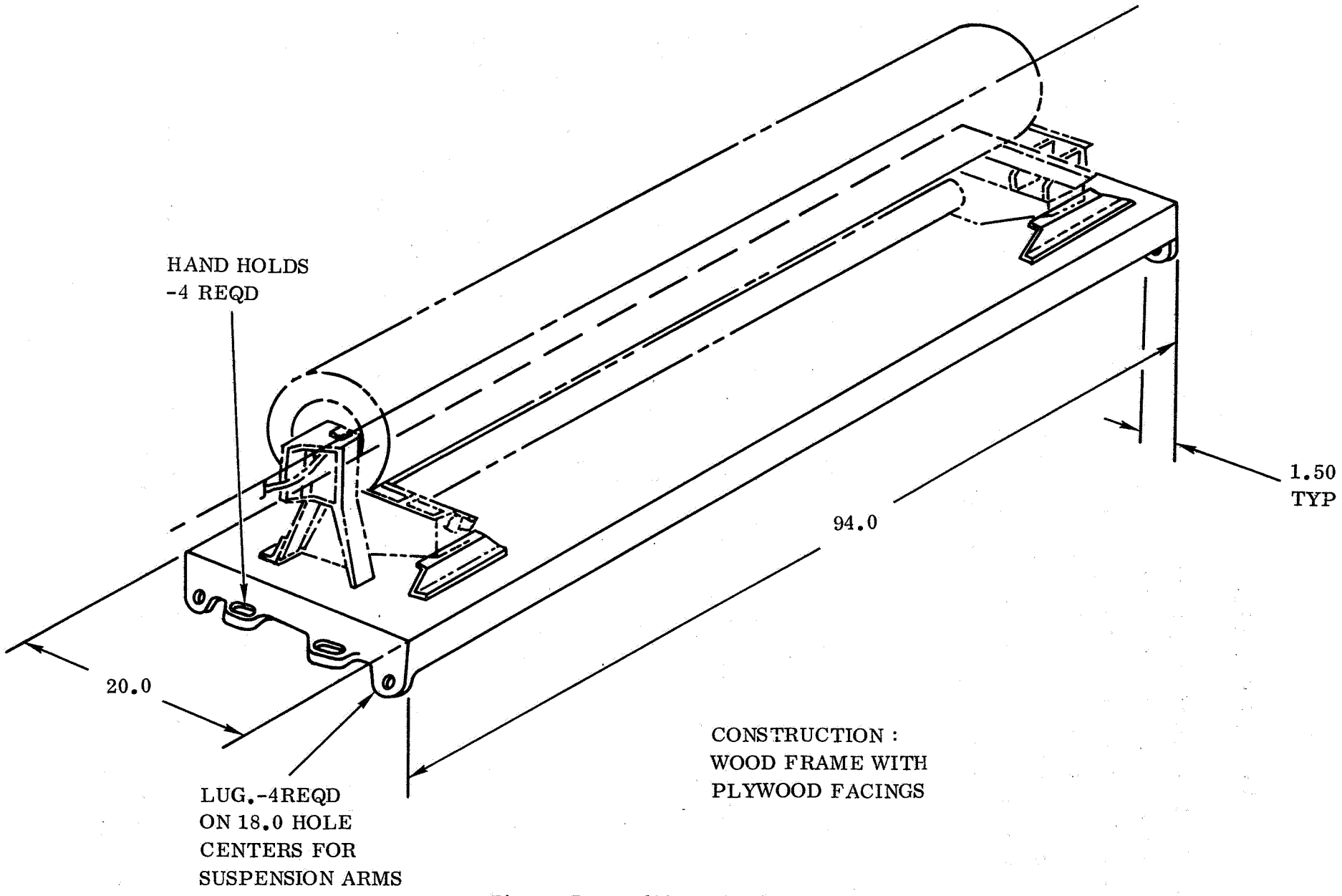

Figure 5 Handling Platform

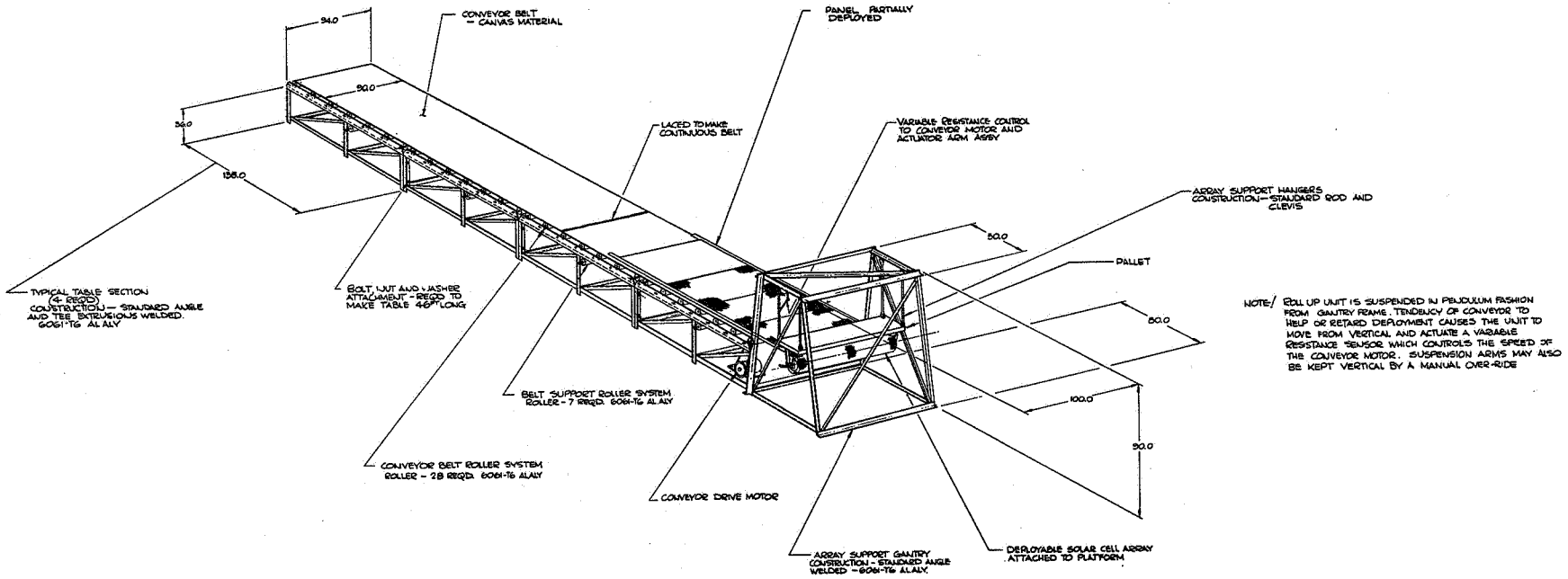

Figure 6 Rollout Demostration Fixture

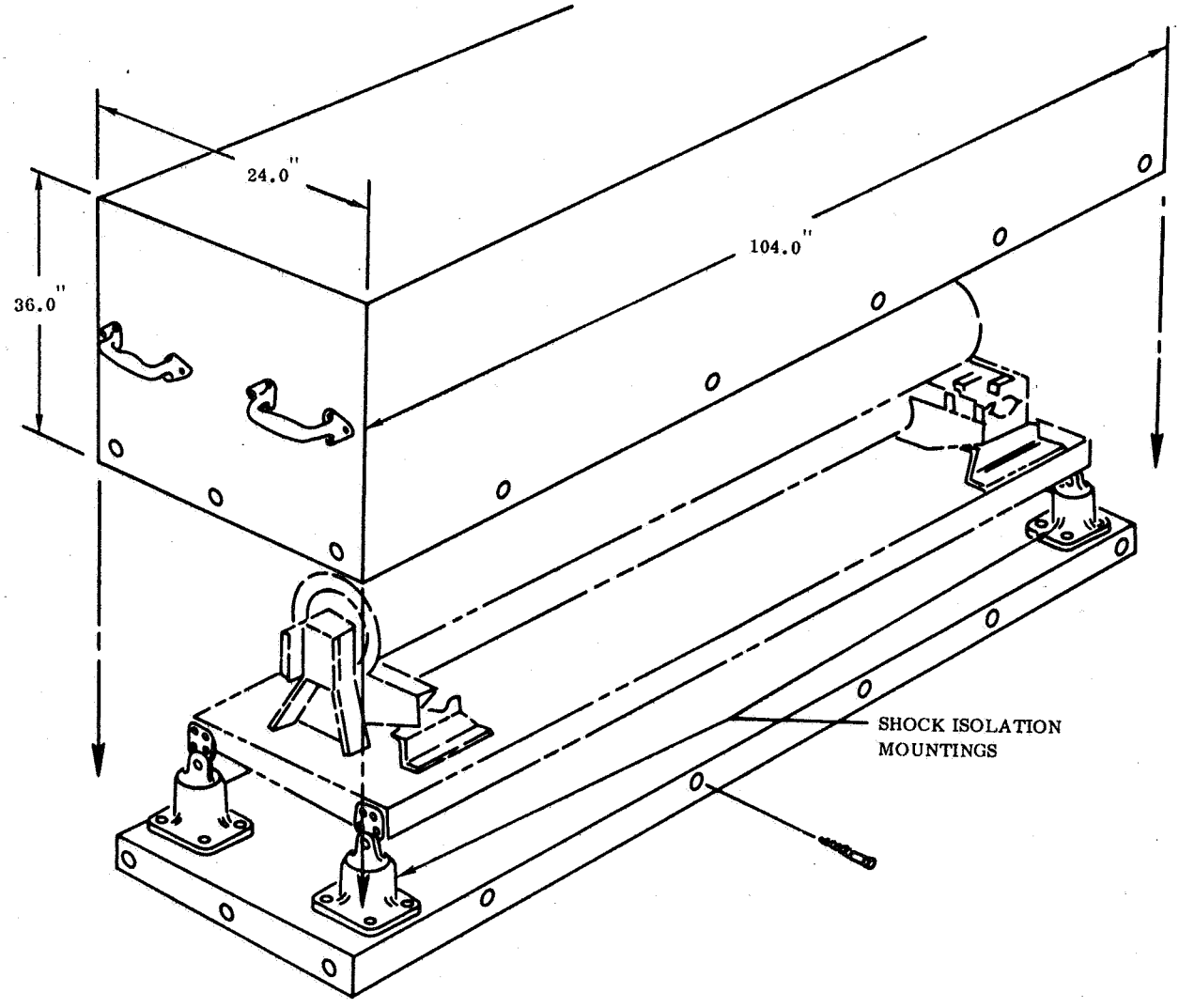

Figure 7 Shipping Container

2.4.6 Manufacturing Feasibility

A key element affecting the successful performance of a flight system is the feasibility of manufacturing the device to meet the design and functional requirements. From concept development through preliminary design, manufacturing feasibility has been a principal consideration.

Throughout Phase I, attention was given to the producibility of the array and its equipments. Trade studies particularly weighed the feasibility of component manufacture or the comparative ease of accomplishing processing which was unique to a design.

Major features of the design which are affected by the feasibility of fabrication include the deployable beams, the substrate assembly, the solar cell installation, the deployment system, the mounting structure and thermal control coating.

The design selected makes maximum use of established materials and processes. Structural components, electrical devices and process systems are used which can be realistically employed to meet design requirements.

A constraint of the contract was to limit material and processing selections to those considered practical realities within one year from the completion date of this contract. The Ryan concept is well within this constraint as evidenced by a review of the materials and processing that have been chosen (see Section 2.4.4). The exotic and new composite materials were not incorporated in designs. Viewed from a manufacturing standpoint, the engineering design is quite simple. Complex configurations have been avoided.

Substrate Assembly

There are many novel features incorporated in the solar panel assembly. All factors affecting manufacturing feasibility were investigated and methods developed to conform to design goals.

Adhesive systems and techniques for laminating foil bus conductors to Kapton H film were studied. Sample panels were prepared incorporating laminated aluminum bus bars, access slots for soldering, local silver plating, solar cell installation and interconnections.

Solar Cell Installation

Several adhesive systems for application of solar cells were studied. A method of roller coating was developed and demonstrated in fabrication of full size panels used for vibration test.

Methods of interconnection of solar cells and spacing were determined and demonstrated to optimize feasibility of assembly.

Solar cell installation methods were explored in the manufacture of solar panel segments to support test requirements and those specimens assembled for exhibit purposes. Working with full size subpanels of Kapton material and a correspondingly large area of cells and coverglass will require careful planning and diligent care in cell application operations to preserve the integrity of the basic one-mil thick plastic substrate. Repair techniques for replacement of damaged cells have been worked out and demonstrated. A special handling fixture was developed to assist installation of the cells and electrical connections.

The fixture is a multipurpose tool, providing means of transportation and handling support and also serving as a protective storage aid. Acceptance test procedures that validate the solar cell installation were resolved.

Deployable Beams

Manufacturing procedures for fabrication of 47-foot long deployable beams were established and demonstrated. Two full size beams with corrugated drive strip attached were manufactured for the deployment demonstration model. Materials requirements, tooling devices, handling methods, welding and splicing methods were determined to assure straightforward production of beam assemblies.

Demonstration Model

A critical consideration to contend with is the relatively large size of the array and the handling and assembly of foil gage materials used in manufacture of detail parts.

Fabrication of the full scale demonstration model (see Section 2.7), has substantiated nearly all major structural assembly manufacturing techniques. Assembly procedures and primary fixture requirements were established by this task.

Deployment System

The deployment system was incorporated in the full size model. The feasibility of fabrication and satisfactory performance of the system was demonstrated.

Thermal Control Coatings

The feasibility of the thermal control coating selected has been demonstrated on other space flight systems.

These coatings are feasible. Special handling is required which is similar to standard handling on space programs.

In summary, it is felt that manufacture and acceptance of the large area rollup solar array as presented in this report can be performed with good confidence. Development of new and untried methods and fabrication techniques is unnecessary.

2.5 ANALYSES AND STUDIES

This section describes the major analytical studies performed which are covered by the following general catagories:

- Structural/Mechanical and Thermal

- Electrical
- Reliability
- Weight

The method of approach is given together with the conclusion reached. Details of the analyses are incorporated in the Appendix.

2.5.1 Structural/Mechanical and Thermal Studies

2.5.1.1 Panel Aspect Ratio Study

This study was conducted to determine the optimum deployed panel aspect ratio, or length/width ratio defining the solar cell area, a criterion considered to be analogous to minimum weight design for the solar cell area required. By performance of this study, the wrap drum and deployable beam lengths were established.

The study was simplified by considering only those components whose weight will change, or effect an appreciable weight change in the total structure weight with a change in panel aspect ratio. These influencing components are the wrap drum, the deployable beams and the spacecraft mounts. Other components such as substrate, drive system, drum fittings and beam guides do not change as a function of aspect ratio, to significantly affect the results of the study.

The constraints set forth for the purposes of the study were:

a. That the wrap drum dynamic deflection remains constant.

b. That the deployable beam weight changes in direct proportion to a change in length, since the negligible in-space loads on the deployed beam do not require a change in beam cross section corresponding to a change in length.

For comparison a 12-inch diameter Mg drum and six-inch diameter Be and Mg drums were considered.

The curves in Figure 8 show the relative effect of aspect ratio change on the electrical power/weight ratio at 1 A.U. solar flux. Even though an optimum aspect ratio of 5.3 is shown, the design goal of 30-watts/pound can be met for ratios above 3.5. Little difference (approximately 1/2-watt/pound) results from the use of a six-inch diameter Be drum versus a 12-inch diameter magnesium drum. The 12-inch diameter magnesium drum was selected because increased dynamic translations of the stowed panel subject to sinusoidal vibration in the drum axial direction would become a problem on a six-inch diameter drum. This is due to the increased wrap stack-up of at least an additional 1.5 inches. Drums larger than 12-inch diameter were not considered because sufficient rigidity, for minimizing induced vibration loads to the stowed panel, of the resulting longer spacecraft mounts becomes increasingly difficult to obtain.

2.5.1.2 Deployment Beam Study

Preliminary analysis of beams used to carry the stowed panel, without longitudinal pretension, to its deployed configuration indicated that loads induced by spacecraft maneuver accelerations were insignificant for use in selecting a reasonable beam cross section compatible with handling and fabrication considerations. Also, a deployed panel natural frequency of 0.04 Hz could be met with a reasonable cross section. (For a detailed dynamic analysis, see Section 7.2.4 in this report.) Therefore, other criteria were used for design. The most critical of these are:

a. To provide a support which will maintain deployed panel flatness, to within ±10° of a theoretical plane when subject to normal-to-plane solar flux environment of 260 mw/cm^2.

b. To provide a panel support that possesses growth potential for increased panel size and/or load capability.

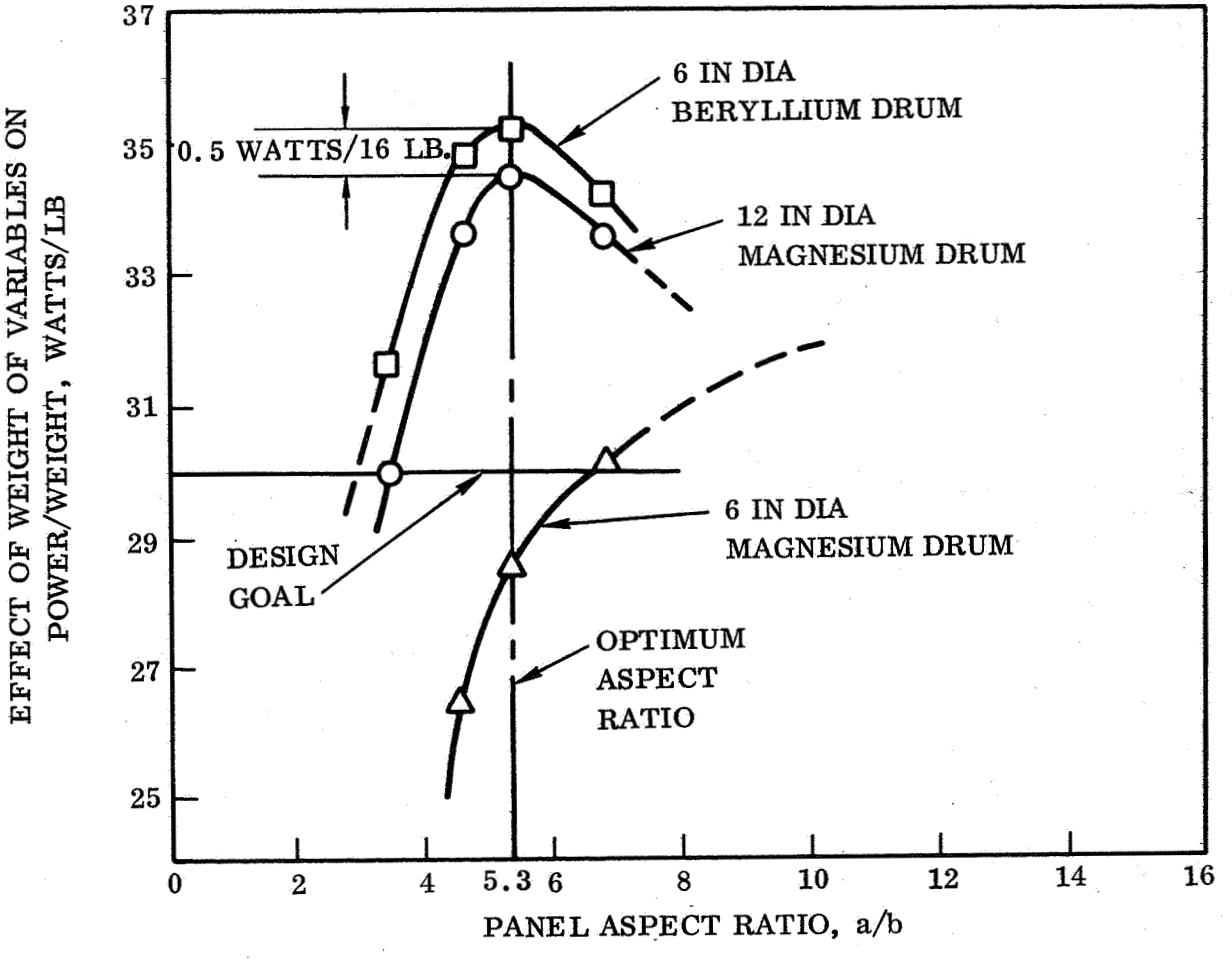

Figure 8 Aspect Ratio as Related to Power/Weight Objectives

c. To provide a panel support that, with possible degradation in strength capacity of beam elements, will not result in the loss or degradation of the solar panel.

To satisfy the basic requirements, a beam cross section is needed which can be stowed on a drum and after deployment be most efficient in providing the bending and torsional stability for the deployed panel subject to severe thermal environments. The latter of these requirements indicated a closed section, tubular type beam. Relative strength and weights of candidate materials considered to possess the desirable characteristics are shown in Figure 9.

This figure shows that even when considering small bending moments, a weight savings of approximately 30% is realized for 6AL-4V titanium with respect to the nearest alternate.

Once a beam design was established that could flatten for wrapping on a drum and return to full open cross section when deployed, the prime consideration for selecting material, diameter and sheet thickness is the 260 mw/cm^2 thermal environment. The beam must limit distortion of the deployed solar panel to within $\pm 10^\circ$ with respect to a theoretical plane. Two considerations in this regard are: (a) the panel distortion induced by the deployed beams when a thermal gradient exists and (b) the effect of the beams on reducing substrate distortion.

The allowable out-of-plane distortion constraint angle, θ shown in Figure 10 was reduced to $\pm 5^\circ$ for analysis to compensate for the effects of substrate inducing distortion.

Final selection of the beam was made after thermal analysis and a parametric study of thermal beam deflection versus weight of various beams of titanium, fiberglass, and Be-Cu materials, of varying diameters and of varying sheet thicknesses. The results of the study showed that if a beam sheet thickness is limited to 0.003-inch as a minimum for handling and fabrication reasons, the lightest beam to satisfy a thermal distortion constraint of angle $\theta = 5^\circ$ would be of fiberglass and have a diameter of less than 0.85 inch. This beam was not selected because (a) it is structurally weak for demonstration of such

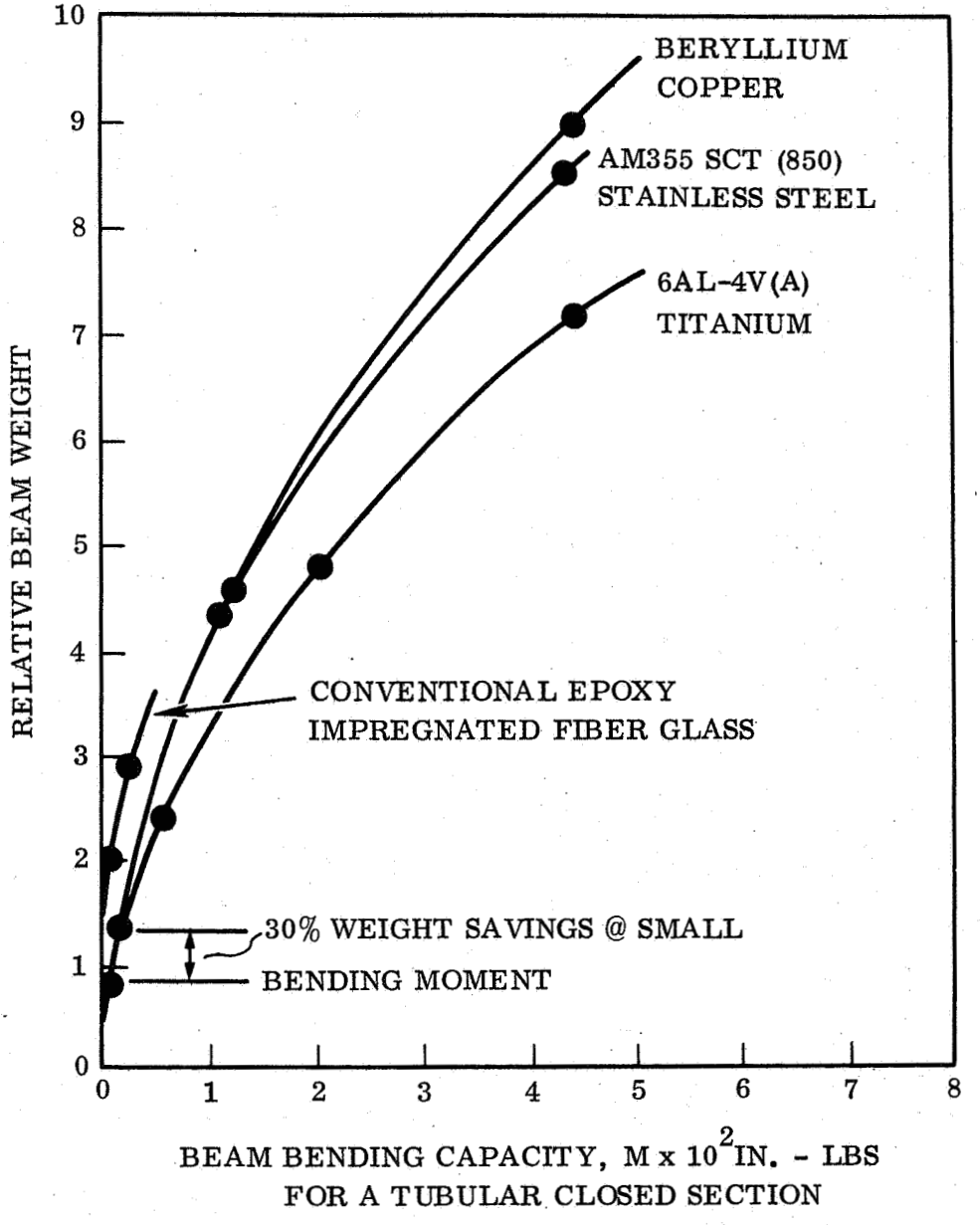

Figure 9 Relative Beam Weights of Various Materials Vs. Strength

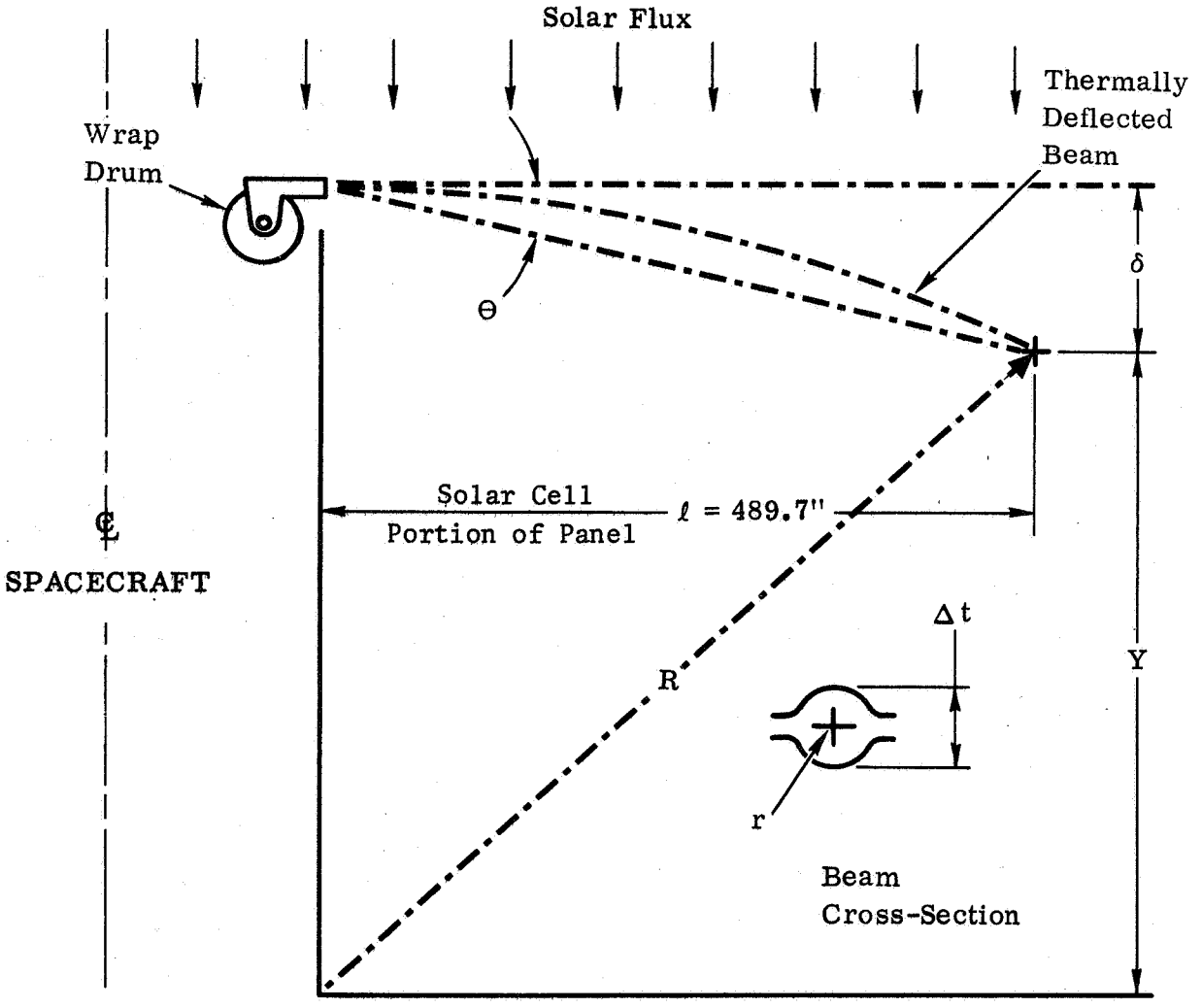

Figure 10 Edge View of Thermally Deflected Panel

a large panel in a 1-g field and (b) the operating temperature is high for fiberglass. The beam selected is 1.7-inch diameter and of 6AL-4V titanium alloy because (a) temperature effects on this material, approximately 385°F, are less critical, (b) it is more structurally compatible with a 1-g demonstration environment, (c) it meets the constraint requirements angle θ and (d) it is equal in weight to a fiberglass beam which would operate at temperatures of about 310°F. A Be-Cu beam was found to the heaviest.

2.5.1.3 Beam Tip Intercostal Study

Studies were made to justify the use of an intercostal between the deployable beams at the outboard end of the panel and to optimize the intercostal cross section compatible with minimum weight.

Results of analysis show that an unsupported outboard edge of the panel would vibrate excessively when in the stowed position and excited by launch vibration. Undesirable effects of excessive vibration of the unsupported edge are that fatigue failure could occur along the outboard attachments of panel to beams. Also, without a structural separation member at the beam tips with the panel in the deployed configuration in space, relative deflections of the panel and beams could cause disturbing perturbations.

A desirable advantage of the intercostal is the ability to hold the beam tips apart and control their position when deploying the panel over a roller support system in a 1-g field. Beam column loads induced under this condition were used for optimization of the intercostal. The more severe of the forementioned loading conditions, that is, induced vibration to the intercostal during launch, is reduced to insignificance by locating the intercostal such that it is snubbed against the panel wraps in the stowed position. Polyurethane low density foam applied to the intercostal will provide protective medium for the solar cells by attenuating vibration energy between the intercostal and stowed panel.

2.5.1.4 Wrap Drum Study

The basic considerations in selection of the wrap drum diameter and skin concept are (a) sufficient longitudinal bending stiffness to withstand launch vibration excitations, and (b) sufficient radial elastic stability to withstand radial pressures induced during launch if the wrapped panel is excited in a radial mode of vibration. Since this design features a drive through an auxiliary torque tube and the fact that torsion considerations are less severe than bending considerations, torsion is not important.

A wrap drum of 12-inches in diameter with magnesium skin was suggested in the panel aspect ratio study and was therefore pursued further in this study. Two design concepts were considered for comparison, (a) a magnesium skin drum and (b) a drum with the skin stabilized by honeycomb. In the case of the magnesium skin drum, internal rings are provided to stabilize the skin from buckling inward when subject to a radially induced vibration force from the wrapped panel. Holes in the skin are provided as an efficient means of minimizing weight where both radial stability and longitudinal stiffness are of concern.

The prime constraints considered for use in selecting the optimum drum are (a) minimum weight and (b) stowed panel dynamic deflection limited to 0.25 inch. The latter constraint minimizes the possibilities of vibration damage to the solar cell installation and minimizes the clearance required between stowed outer panel wrap and adjacent structure.

Analysis of a honeycomb skin stiffened drum on an equal bending deflection basis indicated that this concept would weigh more than the magnesium ring stiffened concept by an amount equal to the weight of honeycomb core and facing adhesives. A 1% weight savings would be realized using the honeycomb on an equal strength basis; however, dynamic deflections would be increased approximately 30% above that desirable for minimization of effects on the solar cells. Therefore, only the ring stiffened drum was pursued further in detail.

Ring-stiffened magnesium drums of various diameters and sheet thicknesses are plotted as a function of frequency in Figure 11 showing which diameter and sheet thickness combination results in a minimum weight drum in which the bending deflection at vibration resonance is no greater than 0.25 inch. Analysis assumed pin-ended support conditions at the end mount bearings, which has been verified by test on a full size drum. A drum of 12-inch diameter with a skin of 0.032 inch thick magnesium, 30% area lightening holes, two internal rings and a natural frequency of 50 Hz was selected. The ring spacing was selected to provide radial elastic stability of the drum skin subject to a dynamic radial load. This load was 0.61 pound/square inch based on a 50-g response acceleration of 2/3 of the stowed panel wraps vibrating in a radial breathing mode. The selected drum was analyzed for stresses in beam bending at vibration resonance using response accelerations of 50-g on the wrapped panel and found to be structurally satisfactory. The 50-g level was based on an effective dynamic transmissability of 10 to the stowed panel.

For comparison of the assumptions used in this study with test results, i.e., (a) that the drum supports the stowed panel in a beam bending mode of vibration and (b) that the stowed panel dynamic transmissability is 10, see Section 2.5.2.

2.5.1.5 Effects of Dynamics of Spacecraft Mount

Dynamic analysis of the proposed spacecraft mounts made of magnesium showed that they would not be sufficiently rigid to limit dynamic response to the stowed panel of 50-g. (The calculated natural frequency of the mount supporting the drum was 60 Hz where as a minimum a design frequency of 150 Hz should be maintained.) The result would be drum bending deflections greater than 0.25 inch, which was used as a constraint to minimize the possibility of solar cell damage.

The possible solutions were:

a. To use beryllium for the spacecraft mount or for the wrap drum in place of magnesium. No weight increase over the design proposed would result.

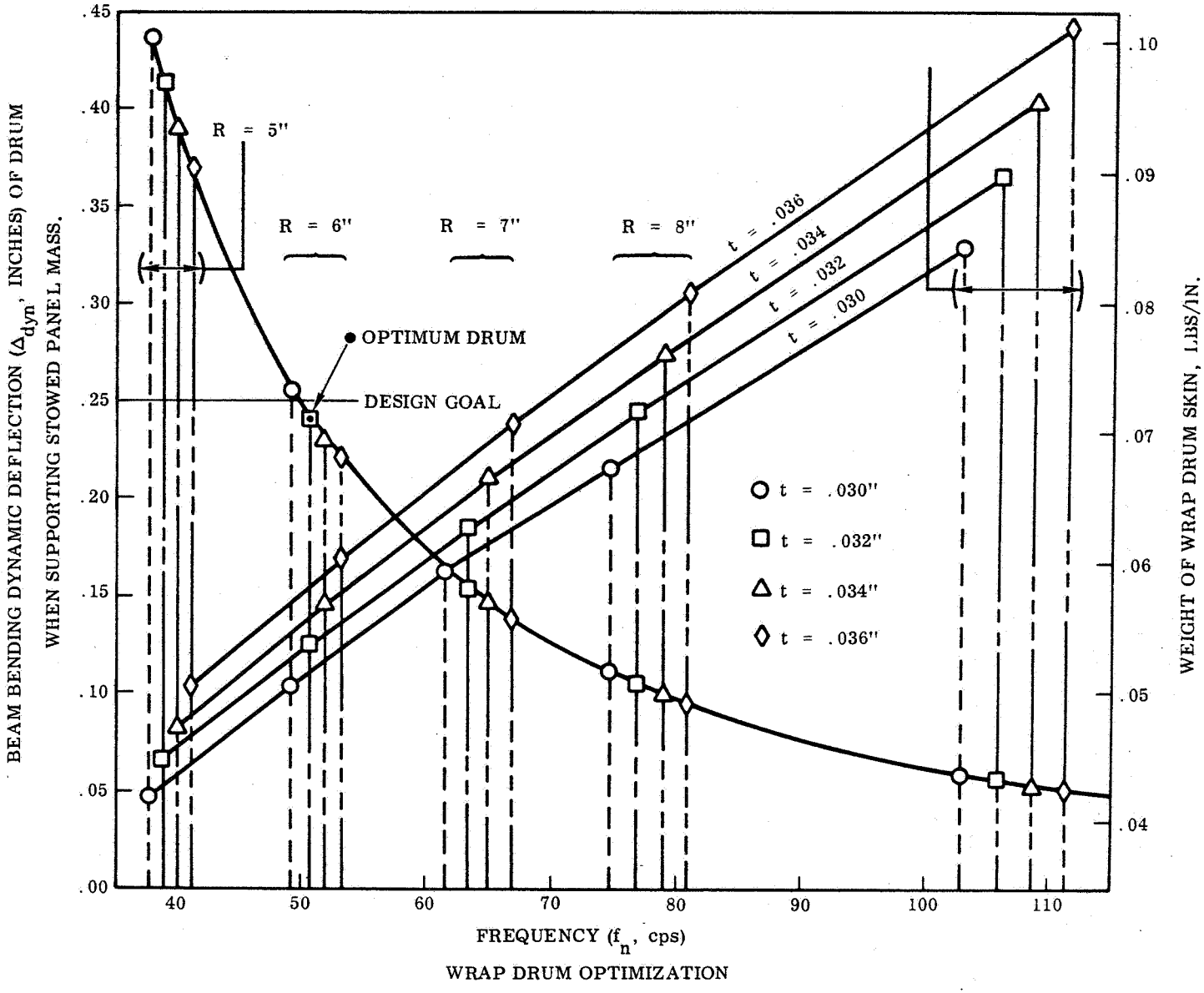

Figure 11 Wrap Drum Optimization

b. Increase spacecraft mount stiffness by increasing its cross section size and substitute for the proposed magnesium, material of slightly higher modulus of elasticity, but of little density increase, such as aluminum. The increase in weight was found to be small. A small change in panel aspect ratio was required due to a forced reduction in length of wrap drum to accommodate the larger mount.

c. Use shock pads of viscoelastic medium between the spacecraft mount and wrap drum to reduce dynamic excitations to the stowed panel. This possibility was discarded when analysis showed that a 1.4-inch deflection was required in the shock pads in all directions normal to drum axis to attenuate the excess energy. Dynamic motion of the stowed panel of this magnitude and an additional weight of about one pound were the factors which eliminated this concept.

d. Use a vibration snubber at the center of the wrap drum to reduce bending deflections. This possibility was discarded due to an additional weight of about two pounds for modification, neglecting additional spacecraft provisions.

The solution to this problem was to increase the spacecraft mount cross section size and use aluminum, effecting an increase in stiffness. Justifications were:

a. That the use of beryllium was not required.

b. Added weight is small.

c. Change in panel aspect ratio from 5.3 to 6.4 has small effect.

d. Design goal of 30-watts/pound can be met.

2.5.1.6 Drive Torque Tube Study

A study was made to determine which of two torque tubes (see Figure 12) design concepts would be of least weight, (a) a torque tube which must carry its own induced load at resonance in a sinusoidal vibration environment and sufficiently rigid to minimize bending deflection under these conditions and (b) one which

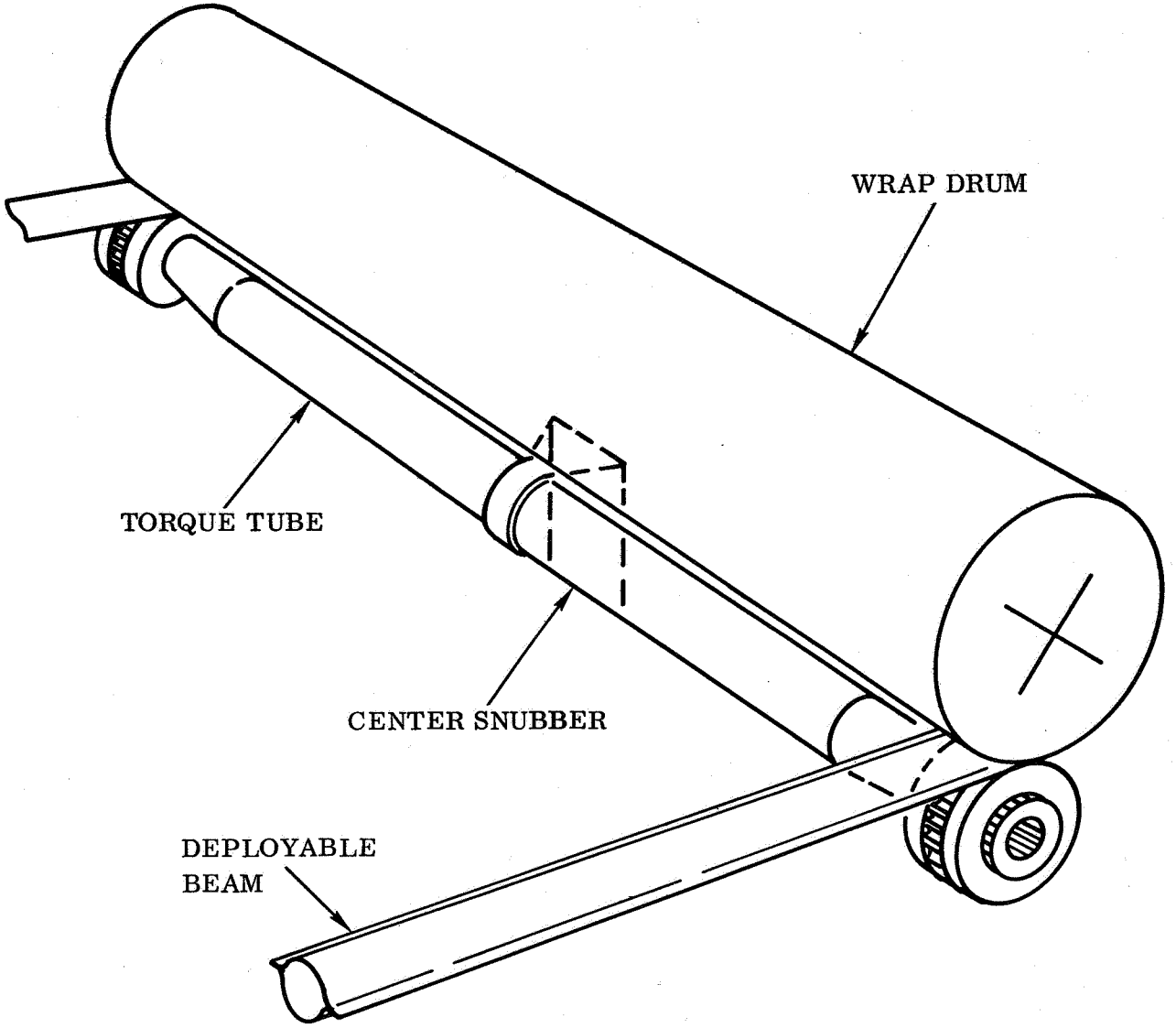

Figure 12 Torque Tube Installation

is snubbed against vibration at its center. In the weight comparison, it was assumed that a minimum sheet metal member could be provided on the spacecraft bus to mount the snubber; the weight of this member was not considered.

Holes in the tube wall were not considered since torsional deflection must be minimized; rather a tube of tapered wall thickness was considered for weight reduction where bending rigidity of an unsnubbed tube was of prime concern. The comparative weights of the basic tube if unsnubbed or snubbed were the same since torsional rigidity could not be sacrificed.

Dynamic analysis of an unsnubbed tube, using magnesium of 0.030 inch thick wall, showed that its natural bending frequency of 50 Hz would couple with that of the wrapped panel/drum bending mode, requiring additional spacing for the tube equal to 0.34 inch. The torque tube mounts would then increase in length, adding weight to both the mounts and drive sprockets which also increase in size. It was decided to eliminate the tube deflection by snubbing at its center; an additional weight of approximately 1/4-pound resulted. (The effect on the electrical power/weight ratio neglecting the spacecraft bus provisions would be small, about 1/10 watts/pounds.) The tube should be made of half-length tubes, supported at one end by the deployment guide sleeve mount and at the other by the center snubber. This should be done in such a way as to provide for thermal expansion/contraction at one supported end (center snubber) and provide for axial load reaction at the other end (guide sleeve mount).

2.5.1.7 Wrapped Panel Layer Separation Medium Study

The primary reason for use of a medium between the wrapped substrate layers is to prevent induced buffeting of solar cells during launch vibration excitations. The more critical environment of concern is the 4-g (0-Pk) sinusoidal excitation.

The separation medium should (a) be of low density to minimize weight and (b) have the proper spring rate to allow for some energy absorption and yet prevent excessive deflection, possibly causing solar cell contact and breakage at vibration resonances. Also of importance is the vibration damping provided by this medium when considering the wrap drum design.

Thermal studies performed in the trade-off study phase suggested that by limiting the medium to concentrated areas, not to exceed 40% of the solar cell area, will result in operating temperatures no greater than 131°F at 1 A.U., allowing an electrical output power of at least 10-watts/square foot. For maximum dynamic efficiency, these concentrated medium areas should be disc pads in shape.

The constraints set forth for analysis were that:

a. Dynamic deflection of the medium under sinusoidal excitation at resonance shall be no greater than 0.10 inch to prevent edge contact of solar cells.

b. That separation medium thickness shall be no greater than 0.15 inch to prevent excessive build-up of stowed panel thickness.

c. That the spacing between pads be limited to 2.5 inches maximum so that vibration deflection of the wrapped substrate is negligible between pads. An analysis based on pad deflection only is thereby made possible.

d. That the medium thickness be no less than 0.05 inch to prevent damage to solar cells subject to possible loads during wrapping on the drum.

e. That the medium thickness be constant on all wraps to facilitate ease of coordinating beam and panel wrap rates.

Selection of the optimum medium design on a minimum weight basis satisfying these constraints was made after plotting weight versus natural frequency of various configurations.

Figure 13 shows the plot of natural frequency of various medium configurations versus weight for each respective panel wrap.

These configurations vary in medium thickness and where the medium thickness and where the medium is less than a full blanket, the variable is pad center distance. Pad diameters were held constant at 0.75 inch, a diameter which appears to be optimum, by examination. A similar plot was made for silicone sponge medium.

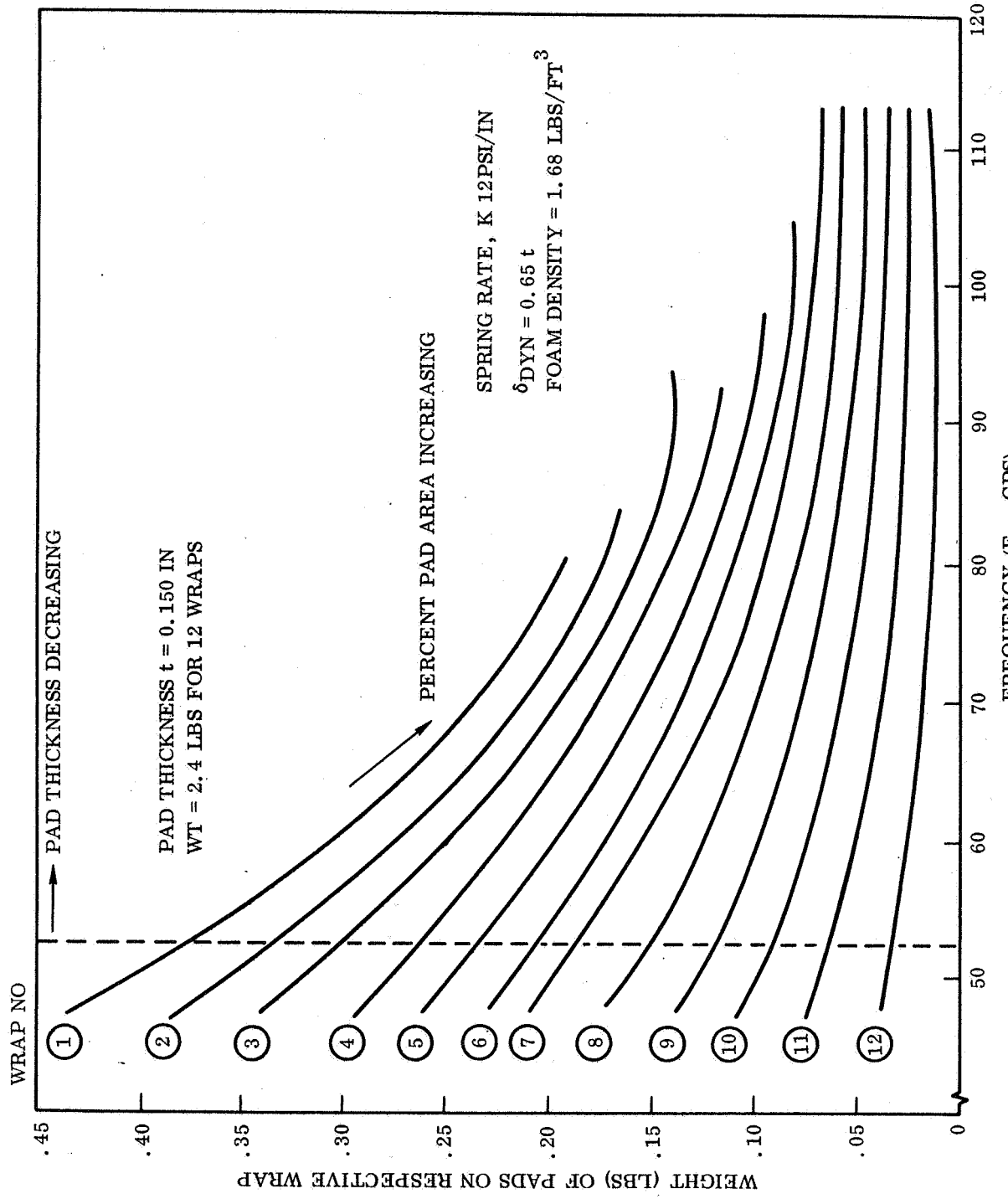

Figure 13 Weight Versus Frequency For Polyurethane Foam Pads

The lightest weight medium shown in Figure 13 for polyurethane foam will resonate at 52.5 Hz. Lighter weight configurations, to the right of the optimum vertical line, would have pad area coverage greater than 40% and result in excessive solar cell operating temperatures.

The study showed that the lightest weight medium will result using polyurethane foam. A nominal foam density of 2.0 pounds/cubic foot, about the minimum obtainable, will result in a total medium weight of 2.4 pounds as compared to 17.2 pounds for silicone foam of minimum obtainable density. The pad area coverage will vary from 38% on the second wrap to 14% on the outer wrap. The inner wrap, where loads are maximum, will be supported by a full blanket bonded to the drum. Bonding the blanket to the drum rather than to the substrate will prevent excessive temperature of the solar cells on the inboard subpanel.

For comparison of natural vibration frequency shown here with that found by test, see Section 2.5.2.

2.5.1.8 Stowed Panel Axial Vibration Dynamics

Large induced launch vibration excitations to the wrapped panel in the axial direction would cause excessive motion of the wrapped panel layers, possibly allowing the wraps to slip and displace relative to each other on the drum, or displace the two side deployment beams, which could then prevent normal deployment.

A study was conducted to determine the cross section and facing thicknesses of the wrap drum honeycomb end plates required to provide a minimum weight design sufficiently rigid to minimize excitation accelerations to the wrapped panel. This end plate optimization study was made prior to inclusion of a thermal slip joint at one end of the wrap drum; therefore, dynamic analysis of the finalized design which supports all load at one end plate is substantiated in Section 7.2.2.

If the stowed panel is excited at launch, a dynamic transmissibility of 6 to the wrapped panel is expected. Sample tests were conducted to determine what axial force can be transmitted between wrapped layers before slippage will occur. The friction restraint force which can be provided was found to be small compared to expected induced vibration loads. Therefore, relative motion of the panel wraps will be limited by a beam restraint at each end of the drum (see Figure 14.) Loads will be transmitted to the beams in tension by the panel-to-beam attach tabs. Loads are calculated to be 10-pounds/attach tab.

2.5.1.9 Deployed Panel Thermal Study

A thermal analysis was conducted to determine the effects on solar cell operating temperatures utilizing 1 mil fiberglass substrate versus 1 mil Kapton substrate. The study was conducted for two areas of the deployed panel approximating the extremes in percent radiation blockage areas provided by the polyurethane foam solar cell protection pads (39.3% and 9.8% areas were analyzed).

The results of the study show that the use of Kapton substrate with no more than 40% backside radiation blockage by the foam pads will yield a solar cell operating temperature no greater than 134.0°F at 1 A.U.; this corresponds to a solar cell power output of 10-watts/square foot at 1 A.U., the baseline requirement. The solar cells would operate at a temperature 8% higher using fiberglass substrate, resulting in a reduction in electrical power and a corresponding reduction in watt/pound.

The material thermal radiative properties used in the solar cell wrap configuration analysis were:

a. The solar absorptance of the array front face is $\alpha_s = 0.84$. The energy is absorbed at the cell after transmission through the cover glass.

b. Re-emittance on the front face is from the cover glass and the emittance is assumed $\varepsilon = 1.0$

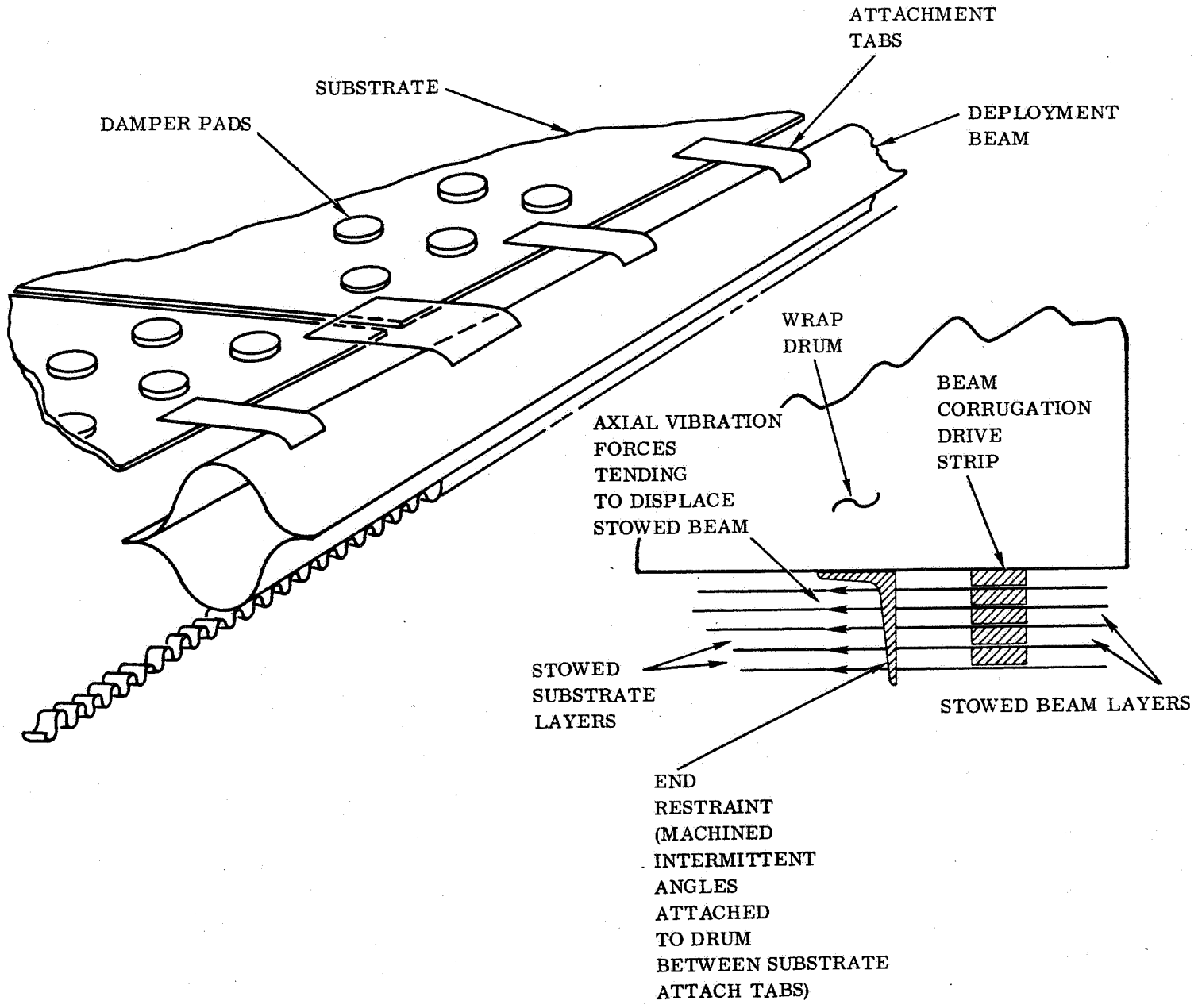

Figure 14 Axial Restraint Mechanism

c. Backside radiation losses occur by radiation from the Kapton surface, $\varepsilon = 0.35$ (measured), and by transmitted energy through the Kapton as radiated by the cell backface which is coated with adhesive (ε_{effect} from the cell surface after transmission is $\varepsilon = 0.34$).

d. Foam sponge $\varepsilon = 0.9$.

Radiative properties of the Kapton film were determined by laboratory measurements report in Section 7.4.

2.5.1.10 Effects of Stowed Panel End-On Solar Flux With No Thermal Control

An item given detailed consideration is an extreme case condition which occurs only if the array is not sun-oriented at the time of deployment. The stowed panel being oriented, end-on, to the solar flux at 1 A.U., the opposite end of the drum would radiate to deep space. Results of the study show that temperatures at the cold end of the drum would not drop below -20°F after reaching thermal stability in this attitude after six hours. A temperature difference in the stowed panel between extreme ends of the drum would reach 214°F after stabilization. Effects of this temperature differential are that tensile loads would be introduced in the substrate-to-beam attach tabs (due to contraction of the Kapton substrate relative to the wrap drum) which would be about equal in magnitude (10 pounds/tab) to the loads developed during launch sinusoidal vibration. However, should the panel be required to deploy under this thermal condition, where the stowed beams are pulled tight against the restraint fence, a larger increase in motor drive forces could develop. An analytical study, presented in Section 2.4.1.11, was therefore made to show that thermal control means can be employed to reduce the temperature difference of 214°F to 30°F; the effect on deployment will thereby be reduced to an acceptable level.

2.5.1.11 Thermal Study of Stowed Panel With Consideration For Effects of Thermal Control

A preliminary thermal analysis of array (in the undeployed state) was completed. Mission phases and vehicle orientations resulting in worst case gradients were considered.

The reduction of temperature gradients within the undeployed array required investigation. This gradient can be minimized by application of vacuum-deposited aluminum (VDA) to external surfaces and an additional wrap of low thermal emittance and solar absorptance (such as VDA on Kapton film) to cover the high emittance solar cells normally exposed on the wrap drum.

The approach to reducing temperature gradients within the retracted array is to insulate the structure from unwanted heat fluxes by selection of proper surface finishes to reduce the absorption of solar energy and radiation of thermal energy. In order to minimize the energy re-radiated by the external surfaces, and steady-state temperatures, it would be desirable to minimize both the α_s and ε of the external surfaces, at the same time maintaining a low α/ε ratio. This combination of surface properties will minimize the cooldown rate and inherent internal gradients during shadowing and solar exposure following shadowing. Flexible thermal control materials with the above characteristics are currently available "off-the-shelf" in sheet form. The coatings are manufactured by vacuum-depositing a thin layer of silicon monoxide over a reflective metal layer (usually vacuum-deposited aluminum) on either plastic film or foil, such as 0.0005 inch Kapton. Since the SiO layer is transparent to solar radiation in the UV and visible region, the solar absorptance is largely controlled by the metal coating while the emittance is a function of SiO thickness.

The solar panel, wrap drum and beam supports are particularly subject to large temperature variations because of the wide range of surface emittances of the various materials. Low thermal conductance, light weight and large size contribute also to difficulty in maintaining low temperature differentials between various parts of the unit.

The thermal model used for the preliminary analysis shown in Figure 39 accounts for 11 wraps of solar cells with Kapton substrate, 10 lateral divisions of the magnesium wrap drum, the torque bar, electrical motor and structural support ends. There are 37 nodes in all.

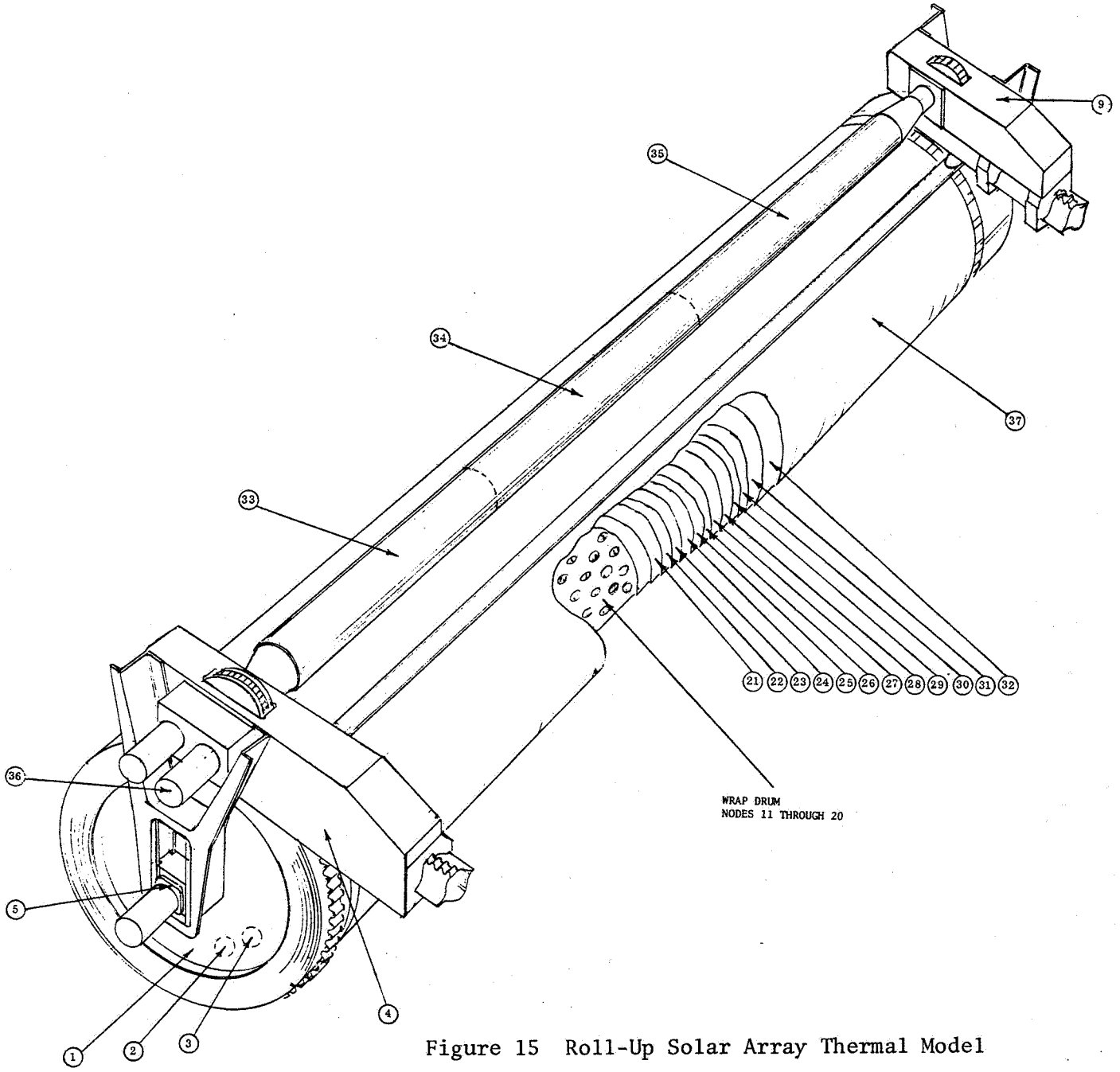

NODE	NOMENCLATURE
1	DRUM END OUTSIDE
2	DRUM END CORE
3	DRUM END INSIDE
4	DRUM SUPPORT
5	DRUM AXIS
6	DRUM END OUTSIDE
7	DRUM END CORE
8	DRUM END INSIDE
9	DRUM SUPPORT
10	DRUM AXIS
11	WRAP DRUM, AXIAL SEGMENT 1
12	WRAP DRUM, AXIAL SEGMENT 2
13	WRAP DRUM, AXIAL SEGMENT 3
14	WRAP DRUM, AXIAL SEGMENT 4
15	WRAP DRUM, AXIAL SEGMENT 5
16	WRAP DRUM, AXIAL SEGMENT 6
17	WRAP DRUM, AXIAL SEGMENT 7
18	WRAP DRUM, AXIAL SEGMENT 8
19	WRAP DRUM, AXIAL SEGMENT 9
20	WRAP DRUM, AXIAL SEGMENT 10
21	SOLAR PANEL, WRAP 1
22	SOLAR PANEL, WRAP 2
23	SOLAR PANEL, WRAP 3
24	SOLAR PANEL, WRAP 4
25	SOLAR PANEL, WRAP 5
26	SOLAR PANEL, WRAP 6
27	SOLAR PANEL, WRAP 7
28	SOLAR PANEL, WRAP 8
29	SOLAR PANEL, WRAP 9
30	SOLAR PANEL, WRAP 10
31	SOLAR PANEL, WRAP 11
32	PARTIAL WRAP
33	TORSION BAR, AXIAL SEGMENT 1
34	TORSION BAR, AXIAL SEGMENT 2
35	TORSION BAR, AXIAL SEGMENT 3
36	MOTOR
37	THERMAL CONTROL WRAP

Figure 15 Roll-Up Solar Array Thermal Model

Cold Soak in Shadow, Uncoated Configuration

When the uncovered solar array is deployed after an extended period in shadow, severe temperature gradients may be in existence. Computer analysis of the uncoated array temperature transients during a 10-hour shadow period (initial temperature = 70°F) showed that the maximum temperature difference between inner and outer wrap is achieved at 0.8 hour. The outer wrap was at -141°F while the inner wrap was at +55°F (see Figure 20). After 10 hours in shadow, the outer wrap was -240°F while the inner wrap was -160°F.

Cold Soak in Shadow, Configuration with Thermal Control Coatings

Coating the exterior portions of the structural support system with/low emittance VDA and including an additional panel wrap with a VDA coating greatly reduces temperature gradients during the cold soak. With VDA applied to an outer wrap, 10 hours of space exposure without external heating results in a maximum gradient between inner and outer layers of 22°F. The wrap temperatures and temperature difference are shown on Figure 16.

Cold Soak Followed by Two Hours of Solar Exposure - With Thermal Control Coatings

Application of vacuum-deposited aluminum to the undeployed solar array significantly reduces the rate of heat transferred to the array when exposed to the sun following a cold soak. However, since vacuum-deposited aluminum has a relatively high ratio of solar absorptance to thermal emittance (α_s/ε = 0.12 / 0.03) its steady-state temperature in sunlight is high. $T_{final} \cong 528°F$ near earth for this coating when backed by insulation. The transient response, however, is slow for objects with considerable thermal mass because of the low α_s. For this reason, the transient temperatures of wrap drum supports show a relatively slow rise in temperature in response to solar heating after a period of cold soak. Because of its low thermal mass the outer layer of vacuum deposited aluminum on Kapton shows a rapid response to heating from the sun.

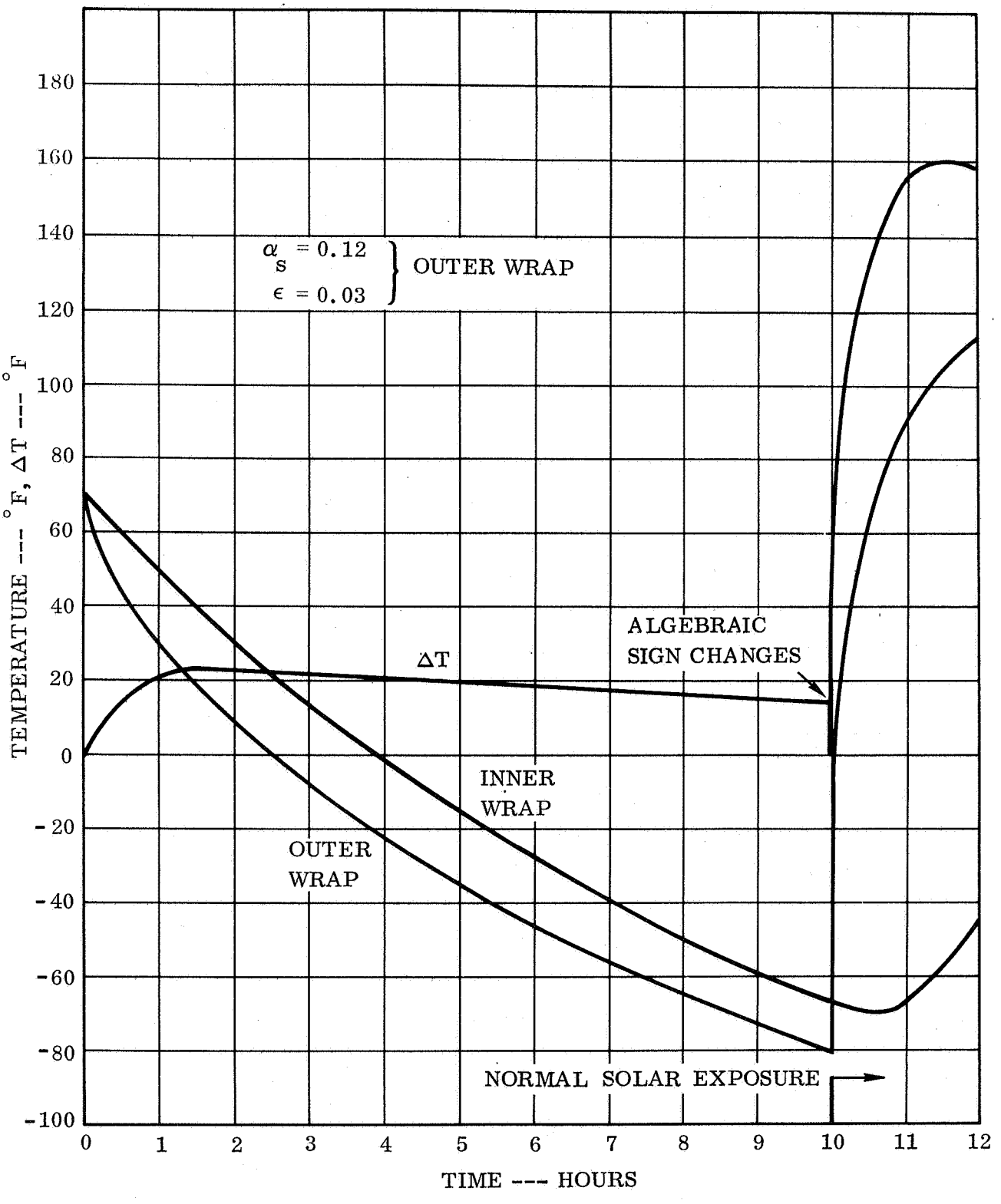

Figure 16 Temperature Response With Vacuum Deposited Aluminum Outer Wrap - Cold Soak Followed by Near Earth Solar Flux

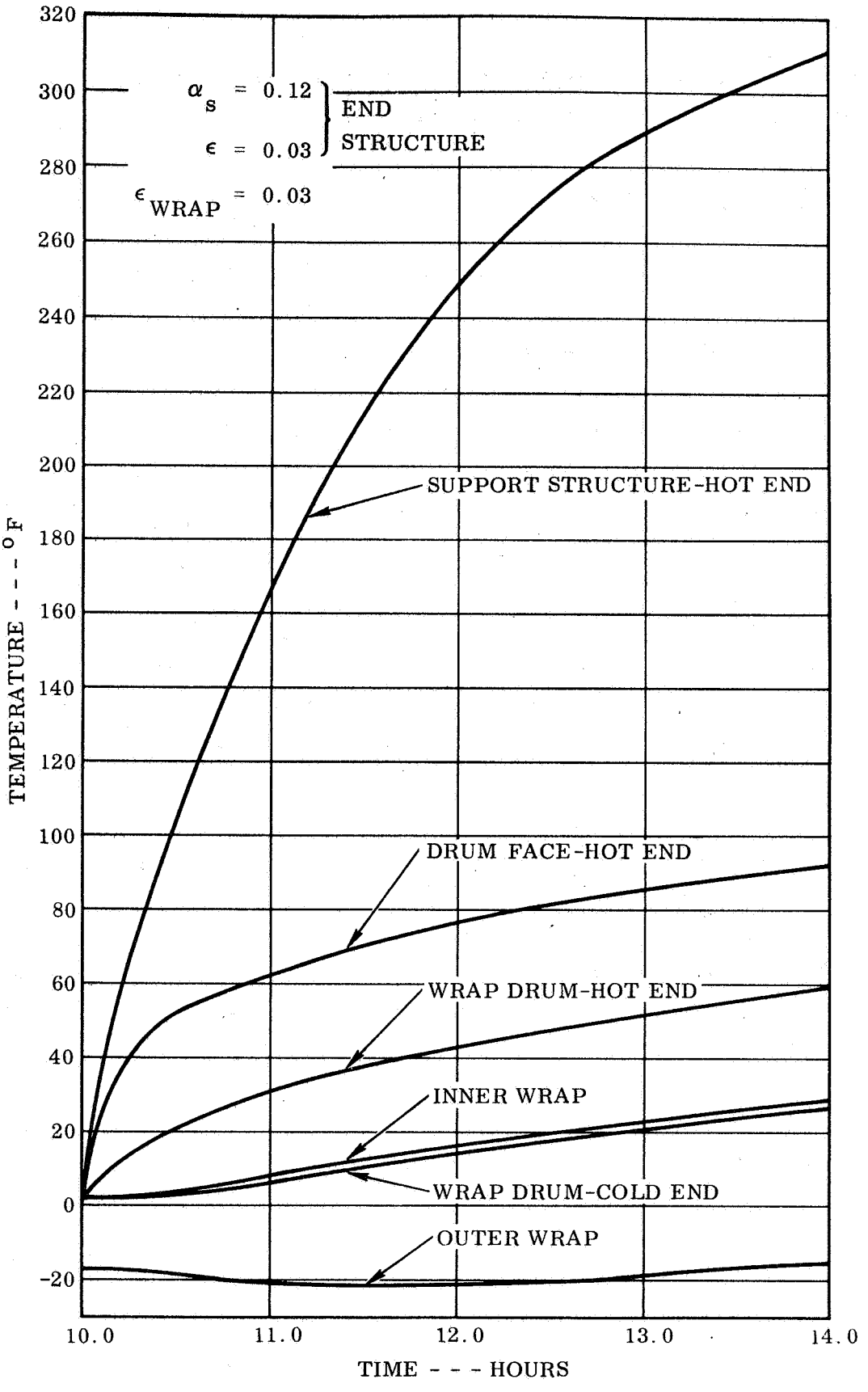

Figure 17 End-On Solar Exposure After 10-Hour Cold Soak, VDA on Outer Wrap and Structure (Near Earth)

Figure 17 shows the time-temperature response curve of array components for end-on solar heating after a 10-hour cold soak.

Proposed Thermal Design

Long term solar exposure of the retracted array, followed by a cold soak due to spacecraft or planet shadowing could result in temperature gradients more severe than those considered above for launch conditions.

The addition of aluminized Kapton with a thin coat of SiO offers a solution to this problem. An analysis was made using values of SiO coated VDA on the outer wrap with $\varepsilon = \alpha_s = 0.12$. Figure 18 shows the results of a 10-hour cold soak followed by 2 hours of solar exposure.

As expected, the inner to outer wrap temperature difference has decreased during the cold soak over that of the uncoated VDA. The temperature difference during solar exposure was decreased and the steady-state temperature will be reduced significantly (from approximately 580^{o}F for a near Venus Solar Flux).

To reduce temperature gradients within the undeployed array under conditions of solar exposure and shadow, it is proposed to include an additional panel wrap. The wrap will consist of the necessary additional beam length supporting two layers of aluminized Kapton separated by foam pads. The outer layer will have a sufficient thickness of SiO overcoat to result in an α/ε of approximately 1.0.

This design will result in a system which will minimize thermal gradients and shock in virtually any sequence of retraction and deployment in shadows or solar flux.

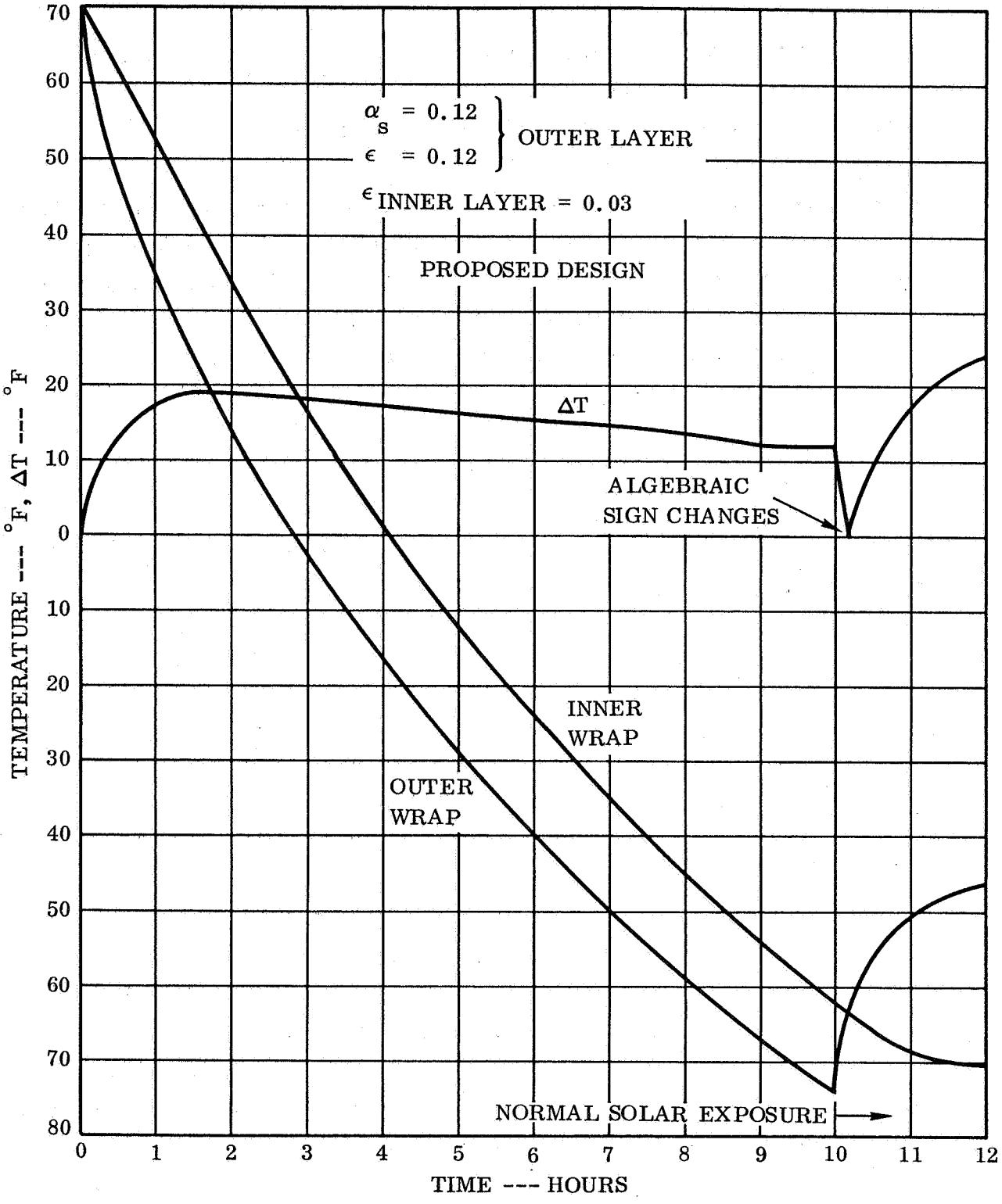

Figure 18 Temperature Response With SiO Over Two Layer Vacuum-Deposited Aluminum Outer Wrap - Cold Soak Followed by Near-Earth Solar Flux

Mission Analyses

Four phases of flight are significant from the point of view of thermal control of the solar panel arrays: (a) near earth in shadow; (b) near earth in solar flux; (c) cruise, and (d) near planet destination.

For near earth, cruise, and for near Mars or Venus, the thermal control design will employ the same general concepts. The system will rely heavily upon thermal isolation from the external environment with an inherent large time constant to eliminate sharp temperature excursions during various midcourse maneuvers, transition from shadow to sunlight and during retraction and deployment.

The solar absorptivity will be chosen with due regard to:

a. The effective solar absorptance due to radiosity effects (multiple inter-reflections of solar energy).

b. The possibility of ultraviolet degradation resulting from prolonged sun exposure, and

c. Micrometeorite penetration, Van Allen belt radiation and increases in solar flare activity.

The thermal emissivity will be chosen with due regard to:

a. The effective emittance due to radiosity effects.

b. Space and/or ground hold deterioration, and

c. Desired lower temperature limit and gradients during prolonged orientation with the array shadowed by the spacecraft umbra.

2.5.1.12 Thermal Stress Considerations

Thermal stress calculations are made to establish the characteristics of the array and to confirm the operational suitability when subjected to the extremes of thermal environments. The two critical thermal conditions considered are:

a. Cold Soak, (stowed configuration). Starting at 102°F ambient and cooling in planet shadow for 10 hours.

b. Venus Flyby, (deployed configuration). Starting at 70°F ambient, heated to a temperature of 231°F.

The thermal stress calculations are made considering that all structural elements are free of thermal stress at the ambient (70°F) temperature, and all thermal growths are related to condition a or b. Considerations are given to the panel in both the stowed and deployed conditions at the start of deployment or retraction. Further consideration was given to configurations both with and without an outer thermal control wrap around the drum and substrate in the stowed condition.

No problems were encountered with the deployment or retraction of the 50-square foot rollup panel after thermal heat soak in either the retracted or deployed soaking condition, which simulated near earth or near Venus conditions. During cold soak, thermal loads were developed, between the deployment beams and guides which resulted in an increase in friction and deployment retraction forces which in turn required higher output torque in the drive motor. These higher drive forces indicated the need for more effective thermal control means for the stowed panel.

The calculations and data in this section substantiate the thermal controls which are proposed to reduce the thermal loadings and to assure proper deployment and retraction.

Consideration is given to the use of aluminum for the tip intercostal instead of titanium. Originally in Phase I titanium was selected, but calculations for thermal considerations show that it is better to have the thermal expansion of the intercostal compatible with the drum. Calculations for the tip intercostal are shown in Table 4. Temperatures used in this table were taken from Figure 19 and Figure 20 for t = 9.5 hours which was the most critical condition.

Table 4 indicates that a very high end force in the intercostal could develop, if it were not for the fact that the beams give in the guides thereby relieving most of the intercostal load. Based on thermal expansion of the intercostal, Figure 21 shows that side loads (P) are induced in the beams as a function of beam deflection. The beam deflection is one half of the intercostal growth since there are two side beams. Table 4 indicates the desirability of an aluminum intercostal, and a thermal wrap on the drum, as indicated by the beam side forces (P).

The thermal wrap selected for study was a wrap of two layers of VDA and SiO coated Kapton around the stowed panel. The effect of beam side load (P) on measured motor torques is shown in Figure 22.

Further thermal stress studies were made on the stowed panel configuration. The outer layer of Kapton (substrate) is the most critical with respect to the wrap drum growth.

Results of stowed panel thermal stress calculations are shown tabulated in Table 5. Temperatures were taken from Figures 19 and 20.

By comparing the beam loads at the radial fence, the advantages of the thermal wrap can be seen. Side load on the beam is almost totally eliminated by using the thermal wrap.

The use of the thermal wrap provides an efficient method of controlling the thermal gradients and any induced loads. This control minimizes the substrate-beam attachment loads, reduces beam guide friction and deployment motor power requirements.

TABLE 4

INTERCOSTAL-DRUM THERMAL EXPANSION

Condition	Time Hours	Material	T_{AM}	T_{DR} (F°)	T_{INT}	Δ_{DR}	Δ_{INT}	Δ_{REL}	$f_{t,\ c}$ psi	P'	Ref. Fig. 34
* RU 1	9.5	AL	70	-158	-238	-0.2617	-0.3283	-0.0666	- 8,528	-240	4.40
RU 1	9.5	Ti	70	-158	-238	-0.2617	-0.1263	+0.1354	+26,247	+487	7.1
* RU 2	9.5	AL	70	- 58	- 71	-0.1469	-0.1503	+0.0034	435	- 12	0.0
RU 2	9.5	Ti	70	- 58	- 71	-0.1469	-0.0578	+0.0891	+17,385	+321	5.2
*Venus 2	--	AL	70	+231	+231	+0.1848	+0.0660	+0.0132	+ 1,690	+ 48	0.1
Venus 2	--	Ti	70	+231	+231	+0.1848	+0.0660	+0.118	+23,180	+248	6.5

	AL	Ti
α	- 12.9 (10^6)	5.0 (10^6)
E	- 10.5 (10^6)	16.0 (10^6)
Δ	$-\alpha L\ (\Delta t)$	

*RU - Rolled Up (stowed), (-1) No Thermal Wrap, (-2) With Thermal Wrap

DR ~ Drum

INT ~ Intercostal

Δ_{REL} ~ Differential Growth

Δ ~ Change in Length

P' ~ Theoretical Load, lbs

P ~ Actual Load Found by Test, lbs

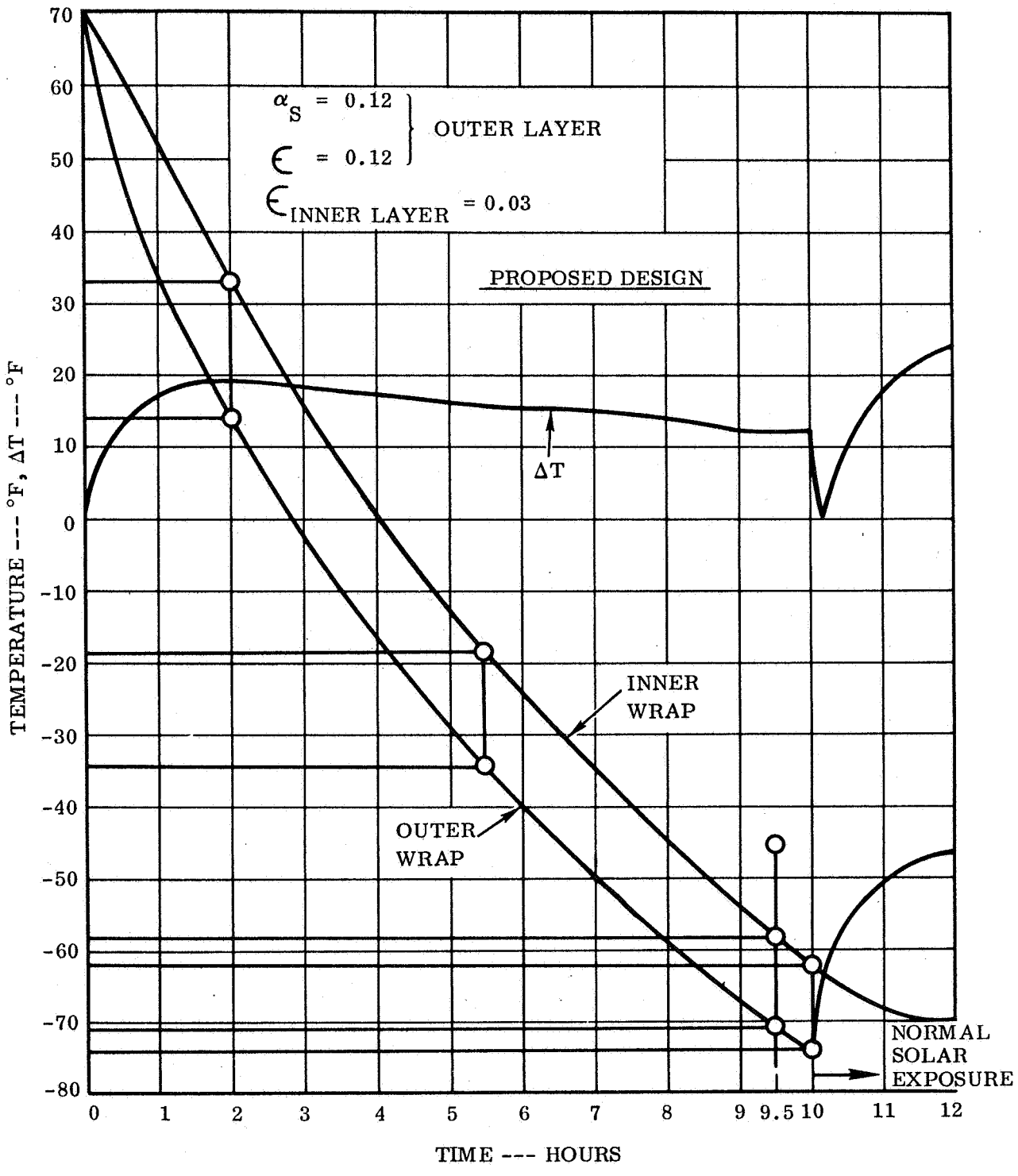

Figure 19 Temperature Response With SiO Over Two Layer Vacuum-Deposited Aluminum Outer Wrap (Cold Soak Followed by Near-Earth Solar Flux)

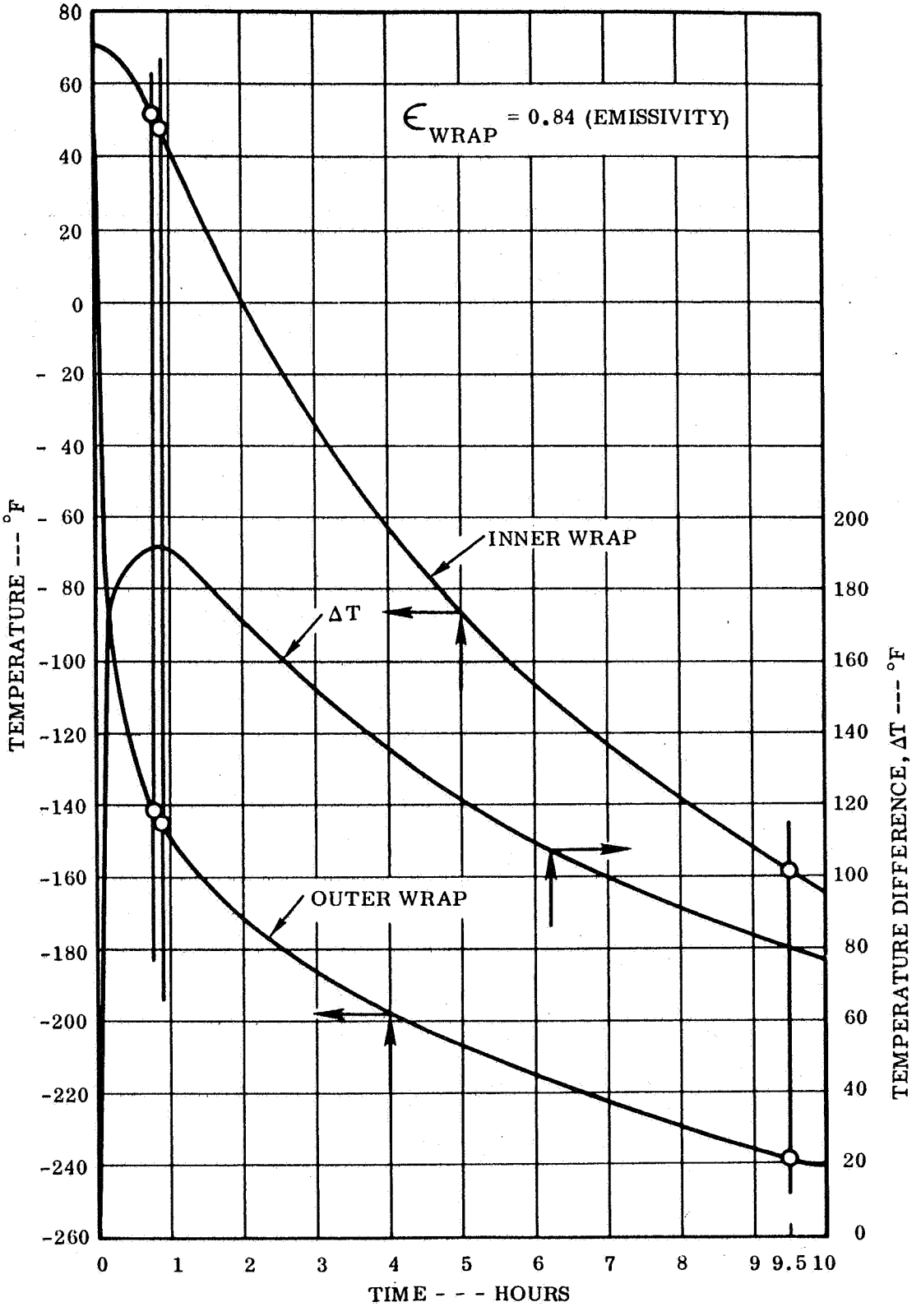

Figure 20 Temperature Response With "Exposed" Outer Wrap-Cold Soak

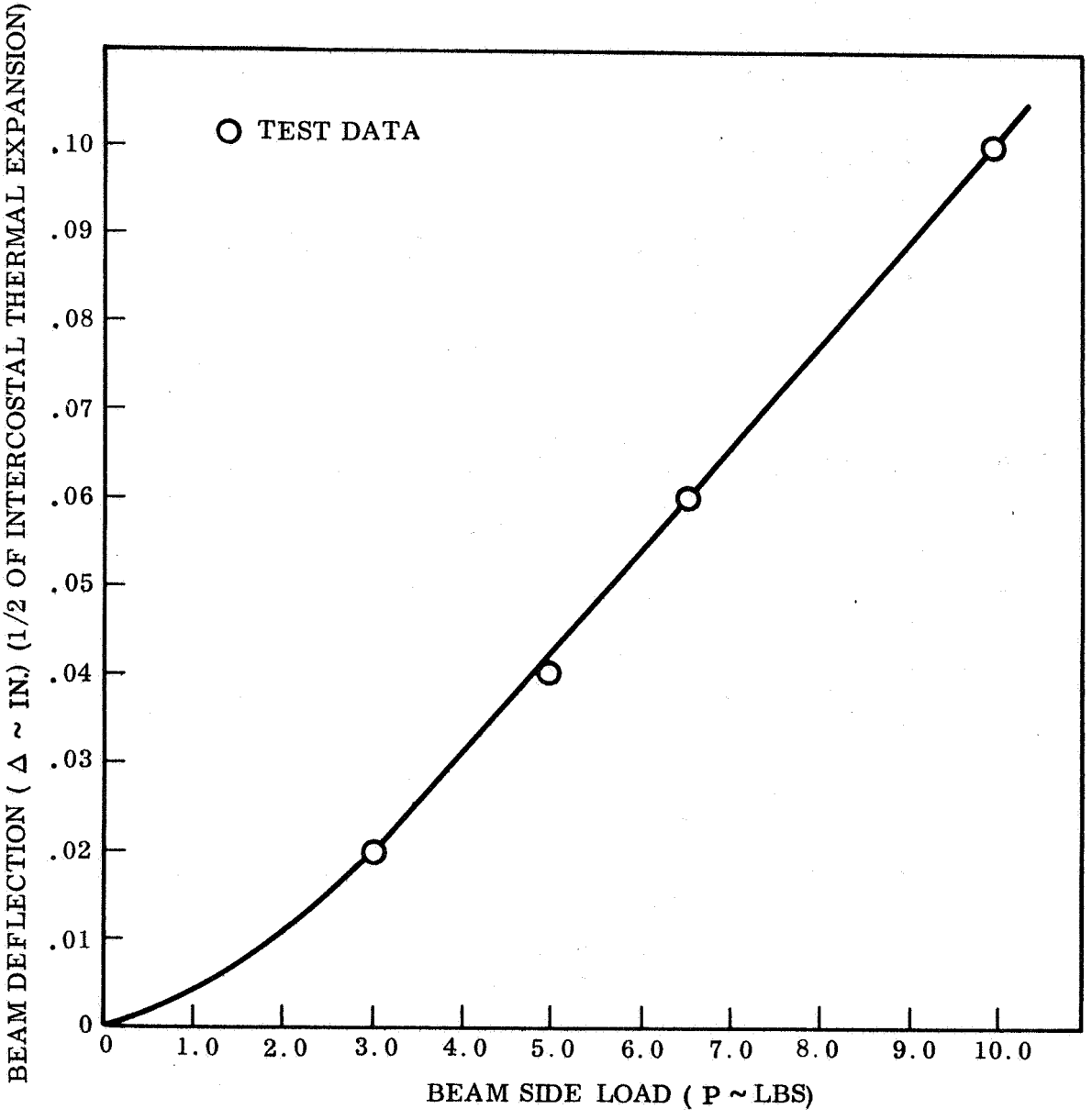

Figure 21 Beam Side Load Versus Beam Deflection

TABLE 5

STOWED KAPTON-DRUM THERMAL STRESSES

Condition	Time (Hours)	T_{AMB} F°	T_{DR}	T_{KAP}	Δ DR	Δ KAP	Δ^*	f_t psi	P (#)
*1	10.8	70	52	-142	-0.0208	-0.1843	+0.1735	+1,052	+6.46
*2	2.0	70	32.5	12.5	-0.0433	-0.0527	+0.0094	+ 57	+0.35

P ~ Actual Load Induced at Fence

A ~ Thermal Growth

DR ~ Drum

KAP ~ Kapton

*1 $\Delta = \Delta_{DR} - \Delta_{KAP}$

*2 P= End Load on Beam Fence

*1 No thermal wrap

*2 With thermal wrap

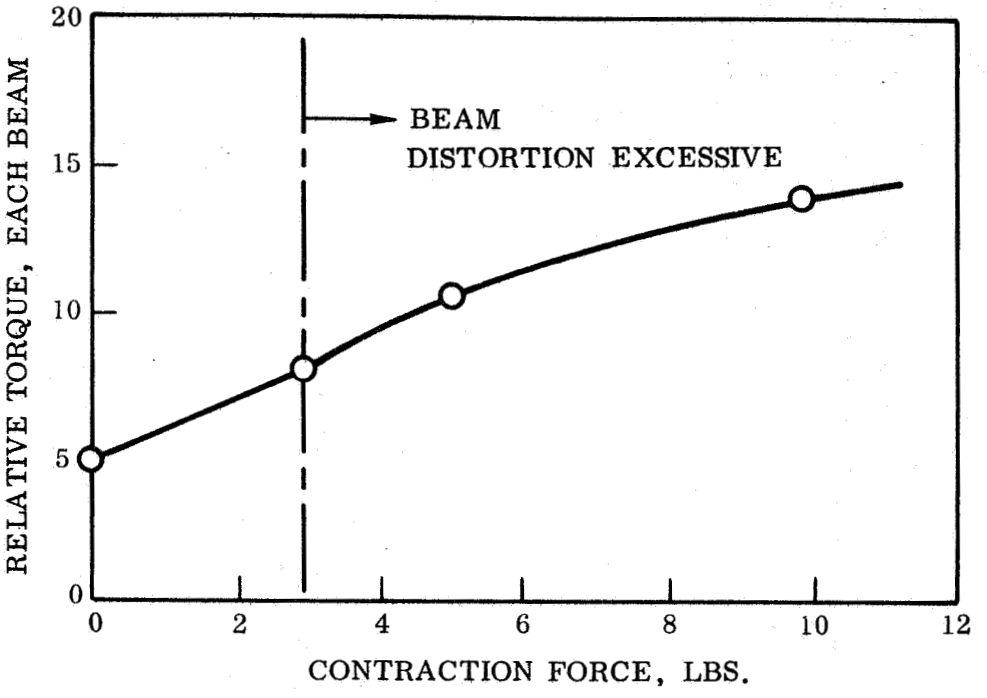

Figure 22 Relative Beam Drive Torque Versus Substrate Thermal Contraction Force

2.5.1.13 Deployment/Retraction System Drive Motor Requirements

The derivation of the equation and the determination of the retraction motor torque is shown in Reference 2. The equation for the motor torque is:

$$T = \frac{60\ F_b(V)}{\pi K\ (RPM)}$$

and the calculated torque

T = 33.3 inch-pounds at 6.0 RPM

Preliminary measurements obtained from the full size deployment model indicates that the torque required to retract the substrate in the horizontal mode is about 50 inch-pounds applied by the drum mounted motor. This torque is somewhat higher than predicted but is attributed to the friction between the substrate and support table. Further measurements will be made to verify the analytical predictions.

2.5.1.14 Study of Attachment of Panel Substrate to Deployable Side Beams

Studies were made to determine the maximum allowable spacing between tabs attaching the panel substrate and deployable beams. The attachment was studied for loads which might occur under the following conditions:

a. Deployment in a 1-g field over roller supports.

b. An arbitrary and conservative 0.2-g in-space steady state maneuver load.

c. Restraint required to resist axial load vibration.

A tab spacing of 4 inches on center was selected. Tab loading of 1 pound or less were determined for conditions a and b above and 10 pounds for condition c.

Analysis verified the use of 1-inch wide tabs of 0.002 thick silicone coated fiberglass bonded to the Kapton substrate in double shear and to the beam in s-ngle shear. The load is transferred by the tabs directly into the substrate which is stabilized against distortion by the aluminum electrical bus strip.

2.5.2 Electrical System Studies and Analyses

Discussion in this section reviews work performed with respect to the electrical equipments involved in the solar array, principally, considerations pertaining to the solar cell installation. Other investigations of electrical components were concerned with a design for control of the deployment-retraction drive system and an arrangement for accomplishing power transfer through the wrap drum to the spacecraft.

2.5.2.1 Solar Cell Installation Studies

2.5.2.1.1 Circuit Layout Analysis

The physical, mechanical, and electrical restraints which govern the design of a deployable rollup solar cell array will be discussed in the following paragraphs.

Area Utilization

Area utilization is defined as the maximum number of solar cells that can be bonded to a given area of substrate. Percent utilization is a function of solar cell size, spacing between cells, circuit termination design, substrate size and optimized circuit output power considerations.

Solar Cell Size

Area utilization or packing factor is based on industry standard sizes for solar cells currently being manufactured. For a 2 x 2 cm cell these dimensions are .788 ±.005 x .788 ±.005. Where 2 x 6 cm cells have been considered, these dimensions would be .788 ±.005 x 2.394 ±.005. The 2.394 ±.005 dimension for the 2 x 6 cm cell utilizes the .005 wasted space between 2 x 2 cells and increases the packing factor by 0.63 percent.

Solar Cell Spacing

Nominal spacing between parallel solar cells is 0.010 inch. This spacing achieves a parallel cell pitch (distance from one cell edge to the corresponding edge of an adjacent cell) of 0.798 inch. Nominal spacing of series connected cells is 0.017 inch. This spacing achieves a cell pitch of 0.805 inch. Upper size limits on cell size dimensions were selected to avoid the possibility of interference between cells and coverglass and to allow greater flexibility in assembly tooling.

Spacing between adjacent portions of a circuit will be 0.012 inch. Spacing between complete circuits will be 0.012 inch.

Circuit Layout

The major parameters to be considered at this time are substrate size, operating voltage, and magnetic field considerations.

The substrate laydown dimensions are 76.70 x 36.21 inches. The 36.21-inch dimension allows 45 2 x 2 cm cells to be placed in series. The 76.70 inches allows 96 2 x 2 cm cells in parallel plus appropriate intercircuit spacing.

Using 2 x 2 cm cells, each substrate will consist of 4,320 individual 2 x 2 cm cells connected in series parallel in eight circuits. Each circuit consists of 3 cells in parallel by 180 in series (4 subcircuits of 45 cells in series). The even number of circuits minimizes the magnetic field associated with the completed solar cell array.

Operating Voltage

A study of current space power conditioning equipment revealed that the optimum operating voltage should be in a range of 50 to 100 volts for maximum power conversion efficiency. The aforementioned configuration utilizing a 2-ohm base resistivity solar cell at a temperature of 55°C will generate approximately 76 volts at the maximum power point. This voltage is within the 50 to 100 volts considered optimum.

A second configuration consisting of 90 solar cells connected in series was considered. The voltage produced by this configuration was 38 volts, but the output current was doubled. The higher output current necessitated the installation of substantially heavier wiring. This configuration was consequently rejected.

2.5.2.1.2 Power Analysis and Trade-Offs

The following parameters established the baseline for an analysis of the large area rollup solar cell array.

a. Power output 10 watts per square foot of the solar cell area. This is the area covered by solar cells including intercell spacing.

b. Illumination intensity at air mass zero and 1 A.U. equivalent solar intensity.

c. Operating solar cell array temperatures assumed to be 55°C.

The general approach to the power analysis will be discussed in the sequence in which pertinent steps were performed.

Solar Cell Analysis

Typical I-V curves for 2 ohm and 10 ohm centimeter base resistivity solar cells in various thicknesses were selected from the report entitled "Performance of Very Thin Silicon Solar Cells", Reference 6. Appropriate extrapolation was performed to extract maximum power voltage and current at the specified operating temperature (55°C).

The I-V curves presented in the aforementioned report were for a 2 x 2 centimeter solar cell with a corner dart contact configuration.

The maximum power current and voltage were adjusted to reflect losses due to coverglass installation, assembly, and mismatch. Based on dimensions discussed in an earlier paragraph of this report, 224 solar cells measuring 2 x 2 cm will occupy an area of one square foot.

Three types of solar cell configurations were considered: the bar contact, large bar contact, and the corner dart contact. The latter offers the advantage of supplying a significantly higher power output for a given gross area of silicone, approximately 2.3 percent greater than the bar contact configuration solar cell.

Curves have been developed for power output per unit area versus solar cell thickness for both bar contact and corner dart contact cells with silicon base resistivities of 2 ohm and 10 ohm centimeters. These curves are presented in Figures 23 and 24.

2.5.2.1.3 Magnetic Moment Determination

The rollup solar panel has been designed in a manner to render the magnetic moment (M) and generated external magnetic field (B) minimum in values. This has been accomplished by alternating the direction of current flow in adjacent circuits for which the geometry is equivalent. Following is an analysis performed to determine the order of magnitude of the residual magnetic moment and external magnetic field.

Cross Configuration

For analysis purposes each individual solar cell circuit consisted of 180 2 x 6 cm N/P solar cells laid out in a configuration as shown below.

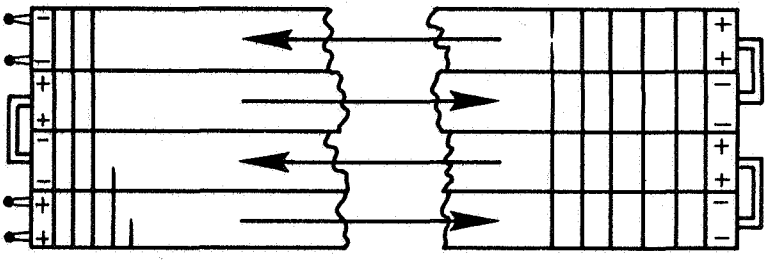

---56 series solar cells in each circuit leg---

The direction of the electron flow is indicated by the arrows. Eight such circuits are connected electrically in parallel with polarity of adjacent circuits being geometrically reversed. Parallel connection is accomplished by two strip bus bars of .001 inch thickness which are separated by .005-inch thick insulation. These bus bars run transverse to the direction of the panel and are connected to a redundant set of panel bus bars of the same cross-section and

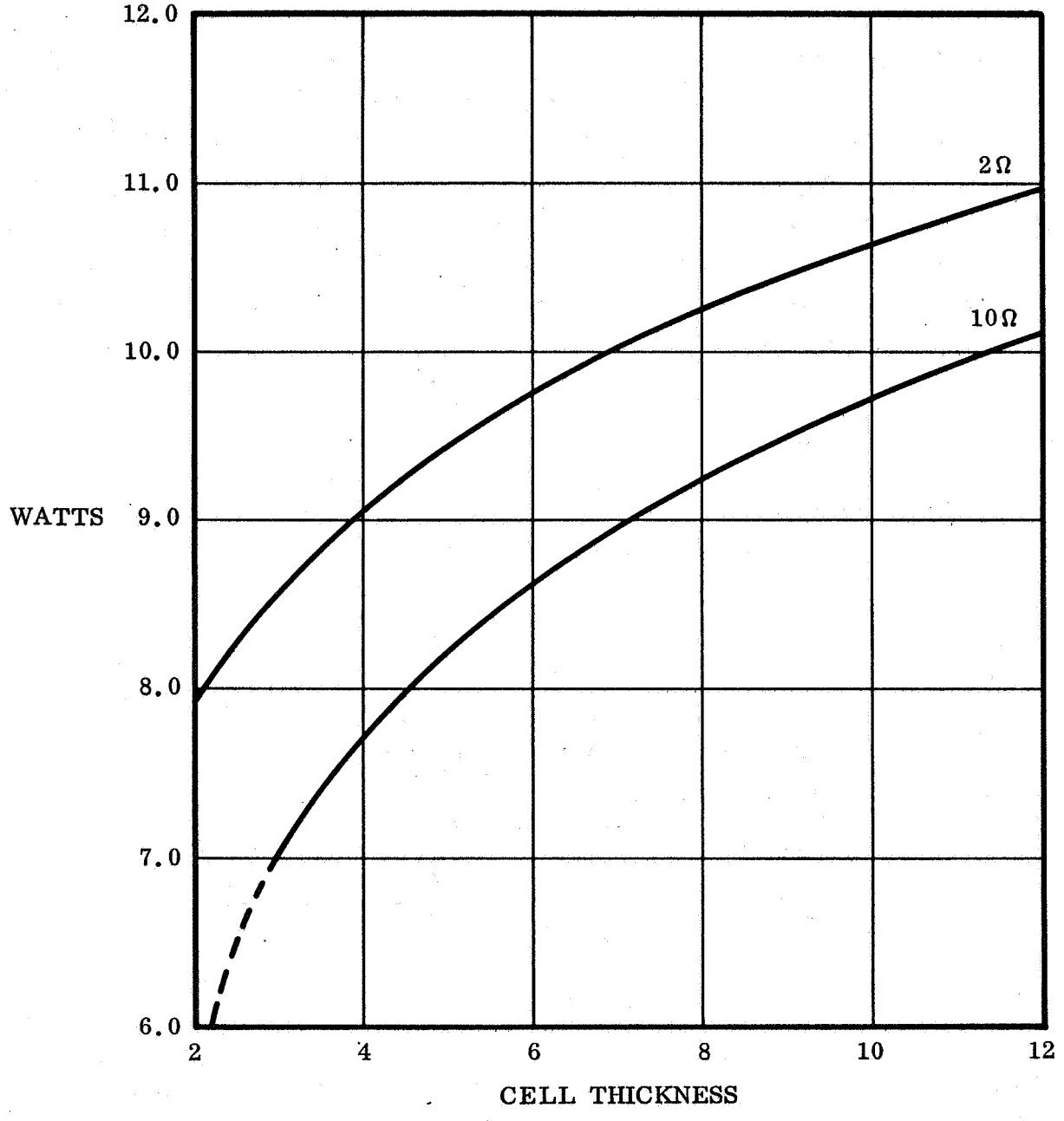

Figure 23 Power Output per Cell Thickness
(Watts/Ft.^{2}) 2 × 2 cm Bar Contact

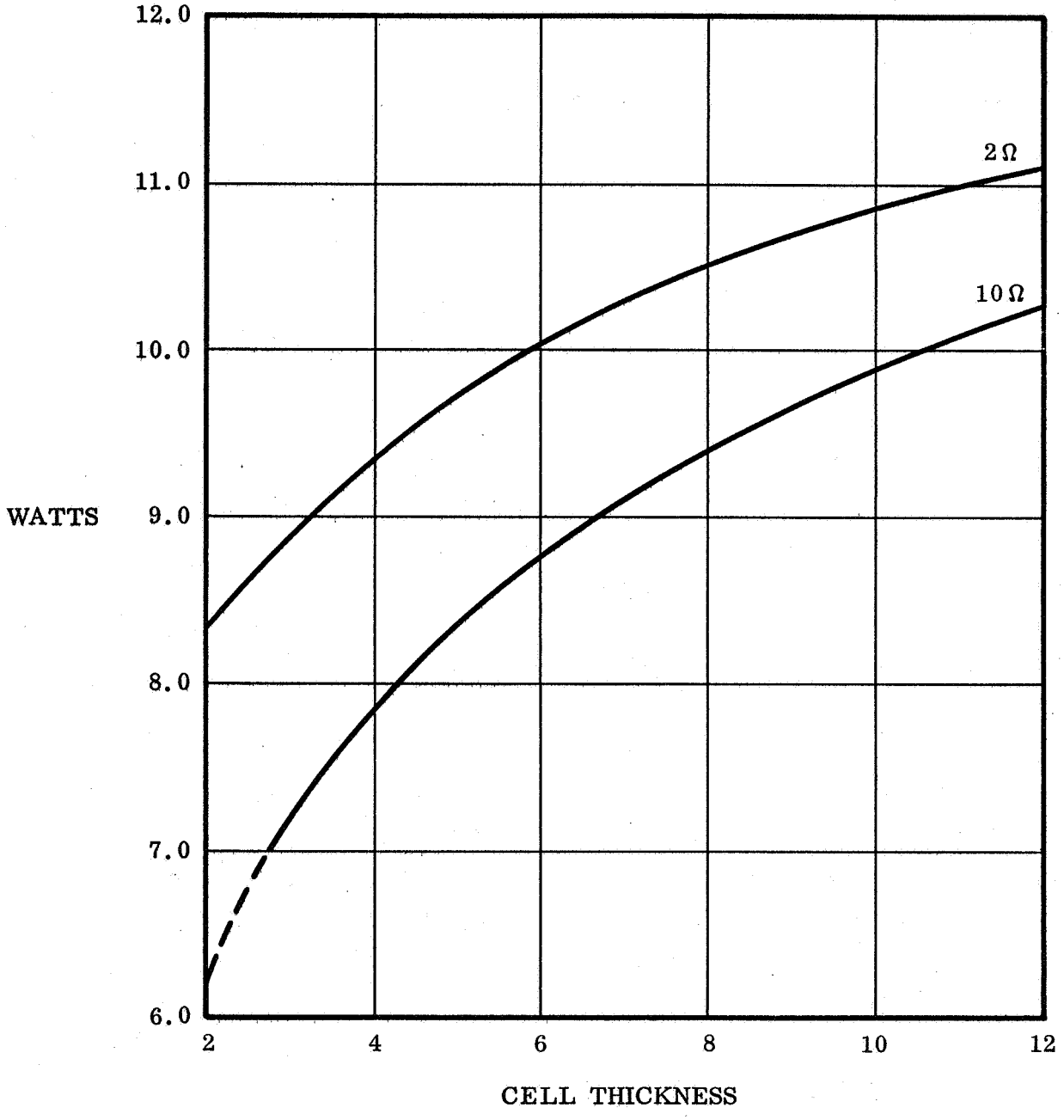

Figure 24 Power Output per Cell Thickness (Watts/Ft.^{2})
2 × 2 cm Corner Dart Contact

separation which run in a longitudinal direction. A total of 13 sets of 8 circuits are connected in this manner to the panel bus bars for a total of 104 circuits for the entire panel.

Magnetic Moment

The magnetic moment (M) is defined by the expression

$$M = \sum_{n=1}^{3} i\, a_n\, X_{o_n}$$

where i is the current, measured in amperes, and a_n is the projection of the circuit area in a plane for which X_{o_n} is the normal unit vector, and for which the three unit vectors are orthogonal.

In the case of the roll-out panel, it is convenient to define the orthogonal set of unit vectors as being normal, transverse, and longitudinal to the panel substrate in the extended position. Each component of the magnetic moment shall be considered in turn.

Normal Component of Magnetic Moment

The normal component of the magnetic moment for each individual circuit will be equal to the circuit current of 0.341 ampere times an effective area of $18 \times 90\ cm^2 = 0.162\ m^2$, which equals 5.52×10^{-2} ampmeter^2. Since adjacent solar cell circuits have reversed direction of the electric current, the contributions to the normal component of the magnetic moment from all the circuits on the panel will cancel in pairs. Thus, the normal component of magnetic moment will vanish.

Longitudinal Component of Magnetic Field

As a result of the collection of the current from each section of eight circuits by the transverse circuit bus bars for distribution to the longitudinal bus bars, a component of the magnetic moment in the longitudinal direction will exist.

A net effective current equal to $\frac{8 \times 0.341}{2} = 1.36$ amperes will traverse a loop bounded by the width of the panel, 1.95 meters and the mean separation of the bus bars which is 0.0015 inch - 3.75×10^{-5} meters. The area of this loop is then 7.31×10^{-5} m^2 and the magnetic moment contribution is 9.96×10^{-5} $ampmeter^2$. Since there are a total of 13 such bus bar loops, the total value of the longitudinal component of magnetic moment for the entire panel will be 1.3×10^{-3} amp $-m^2$.

Transverse Component of Magnetic Moment

The panel bus bars extend a distance of 12.15 meters along the length of the extended panel. The mean separation of these bus bars will be the same as in the previous case so that the total area of the current loops will be 4.56×10^{-4} m^2. The effective current passing through this loop will be one-half of that at the termination which is

$$\frac{8 \times 13 \times .341}{2} = 17.70 \text{ amperes}$$

The effective transverse component of magnetic moment for the panel is then computed to be 8.1×10^{-3} amp-m^2.

Reduction of Magnetic Moment

The components of magnetic moment in the transverse and longitudinal can only be reduced as a result of reducing the effective thickness between the bus bars. This may be accomplished only as a result of reducing the thickness of the bus bars and insulation. For mechanical stress considerations, this does not appear to be prudent.

Consideration of Magnetic Field Strength

It has not been stipulated at what position relative to the panel the magnetic field strength was to be evaluated, and if it were so stipulated it would be virtually impossible starting from basic definitions to perform such an evaluation (i.e., uses of law of Birot and Sevart). Certain generalizations, though, can be made, which would be of qualitative nature:

- As a result of the reversal of current direction in each of the individual circuits relative to its neighboring circuits, the component of the magnetic field normal to the plane of the panel will tend to average to zero at a given point in space. This approximation will be more accurate at greater distances from the panel.

- The magnetic fields resulting from the transverse and longitudinal bus bars will cancel for each pair of positive and negative bus bars except in regions very close to the bus bars and that region between the two bus bars. As a result of the additive effect, the magnetic intensity will be of the extreme values in the region between the bus bars. Since no ferromagnetic materials will be placed in this region, this field should not affect the operation of the solar panel or adjacent equipment.

2.5.2.1.4 Conductor Selections

Conductor selection was governed by three basic considerations. These were minimum weight, optimum power loss per square foot of panel area, and a minimum thickness buildup during retraction.

The following conductors were evaluated:

a. Teflon insulated stranded wire

b. Teflon insulated ribbon conductors

c. Kapton insulated ribbon conductors

d. Copper foil conductor

e. Aluminum foil conductor

f. Copper clad aluminum foil conductor

The first three items were eliminated due to excess weight.

Copper and aluminum foils were compared. The weight saving realized by using a 0.001-inch aluminum foil was 0.163 pounds. Problems associated with joining aluminum will be alleviated by silver plating the aluminum in the areas to be soldered.

A calculated conductor width table for aluminum (.001) is shown in Table 6.

Copper clad aluminum foil would be an excellent material for this application, but it is not available at this time. This foil would consist of a layer of aluminum between two layers of copper; layer thickness would be a 20:60:20 proportion. Handling and fabrication would be greatly simplified by the use of this material.

The aforementioned discussion was concerned with longitudinal bus bars which transmit power from the thirteen modules to the inboard end of the solar cell array.

The transverse collector strips which carry current from the positive and negative circuit terminations to the longitudinal bus will be 0.002-inch thick x 0.50-inch wide aluminum.

Feedthrough from the solar cell circuit terminations will be accomplished through the use of 0.002 by 0.100-inch silver-plated copper strips. Two strips will be used for each circuit termination to increase redundancy.

2.5.2.1.5 Blocking Diodes

Paragraph 3.7.1.2 of JPL Document No. 501407 states that the possibility of shadowing is to be considered. This shadowing was not due to any appendages on the spacecraft but would be more total in nature such as complete shadowing of the entire spacecraft. Because of this possibility, the use of circuit-blocking diodes is not being considered. The only question which applies here is whether or not the vehicle will enter into such a situation that diodes would be needed, since any increase in panel components will only lower overall reliability.

TABLE 6

CONDUCTOR WIDTH SUMMARY

(1 Mil Aluminum)

Panel Number	Conductor Width (inches)
1	0.706
2	1.367
3	1.980
4	2.546
5	3.065
6	3.535
7	3.960
8	4.290
9	4.573
10	4.810
11	4.998
12	5.138
13	5.235

Power/Weight Loss

The including of a blocking diode (or redundant diodes) to the circuits would produce approximately a 1.4% decrease in array power output. This is of the order of 35 watts. A typical weight for a diode employed for the circuits that was considered would be about 300 mg., or 31 gms total (62 gms for redundant diodes). This incurs a reduction in the power to weight ratio of the order of 1/2 watt per pound. This is an obvious drawback to the use of diodes.

Shorting Between Cells

Shorting has also been examined. Shorting can occur either between two cells or from a cell to the substrate. Neither occurrence is very likely. An analysis of open cell failures for the panel has shown that no more than one failure per module (circuit) would be expected under the desired total panel reliability of 0.99975. Experience has shown that the occurrence of cell shorts is much less likely than opens. Therefore, in the most conservative worst case only one cell short would occur in a module. Assuming that all modules had one such short (virtually impossible), the power degradation for the array would be less than 0.5 percent.

The specific power loss will depend upon the circuit's operating voltage point. One short will, however, drop the open circuit voltage of the affected circuit by 1/180 for 2 x 2 cm cell circuits. The circuit would consist of one 2 x 2 string, which is in parallel with two other 2 x 2 strings. To determine the effect new I-V curves are drawn showing this open circuit voltage drop, maintaining the same short circuit current. The effect on the operating power point, which is usually located on or near the flat part of the I-V curve near the maximum power point will then be negligible for the first one or two shorts. Further, if only one module has a short, the total panel open voltage drop would be less than that of one cell. Hence, even if a short between cells were to occur, the power degradation would be less than that lost to diodes. The number of random shorts needed to produce a power loss greater than that caused by diodes is much greater than would be indicated by the reliability analysis of all possible cell failures as described in the section on Reliability.

Shorting to Substrate

The last short possibility considered is that between cell and substrate. In view of the nature of the substrate material employed, a short could only occur at the panel edges. In such a case, a contact could possibly occur between the base of a cell and the positive bus -- assuming a tear in the insulating Kapton. This should be essentially self-healing with the heat generated producing a hole in the positive bus. The possibility of such a

failure in the Kapton appears to be extremely remote in view of the nature of the panel deployment.

Conclusions

Since the inclusion of diodes will add another failure possibility, i.e., that of diode open or short, since it will produce a loss in panel power, and since shadowing and shorting do not appear to be potentially serious power loss modes, the use of diodes is not recommended.

2.4.2.1.6 Radiation Degradation

The extent of radiation degradation to solar cells is dependent upon the environment of the cell. Hence for purposes of comparison of various coverslides, a general environment has been specified which will attempt to represent a realistic situation and at the same time facilitate calculations.

For this report a 10 ohm-centimeter N/P solar cell in a 1-year solar orbit at 1 A.U. (Astronomincal Unit) will be considered. This will neglect the effect of trapped protons and electrons near the earth. Thus, radiation damage will occur through protons emitted by solar flares and ultraviolet radiation. The former radiation primarily affects the cell by causing defects in the silicon crystal lattice, whereas the U.V. (Ultraviolet) radiation will primarily degrade the coverslide, and coverslide adhesives.

In vew of the fact that solar flares can differ widely in both intensity and energy distribution and that measurements of low energy protons (<5 MEV) are not available in any usable quantity, a certain amount of averaging and extrapolating must be made. It should be kept in mind that the numbers thus employed, although not necessarily conforming to any actual realized radiation environment, do represent theoretically plausible conditions based upon the experimental evidence now available.

Figure 25 shows the solar cell coverglass shield thickness as a function of the coverglass thickness with curves for microsheet (Microsheet Silica Corning No. 0211), lead potash (8871), and sapphire. The shield thicknesses for the 3 mil microsheet, 6 mil microsheet, and the 1.3 lead potash are obtained from these curves.

Since present data on cell particle degradation is based on experiments with 1 MEV electrons the proton flux must be converted into an equivalent 1.0 MEV electron flux. Figure 26 contains the information needed to make this conversion. The lead potash curve is labeled 0.015, the 3 mil microsheet is 0.019, and the 6 mil microsheet is 0.035 (their shield thicknesses). For the 6 mil microsheet all protons with energies less than 4.4 MEV are essentially absorbed by the coverglass and do not affect the cell. For the 3 mil microsheet the cutoff is at 3.1 MEV, and for the lead potash glass the cutoff energy is 2.7 MEV. The dosage received by the cell is obtained in the following manner. A flux and energy spectrum is assumed for the radiation environment. With a given exposure period the flux can then be converted to a dosage (number of incident particles per area). The proton dosage is then converted by integration (using Figure 26) into an equivalent flux of 1 MEV electronics. Then Figure 27 is used to determine cell degradation.

In the case of the 1 A.U. solar orbit, two different flux levels are considered. One will pertain to a probably expected environment and the second will pertain to a highly unlikely high radiation environment (a worst case). Since flux levels can vary widely over short periods of time (with solar flares), the dosage for 1 year will be more meaningful since it will essentially average out the random flux variations. For case 1, a dosage of 8×10^8 protons/cm^2 will be used, and for case 2 a dosage of 4×10^{10} protons/cm^2 will be used. The dosage curves versus time of exposure are shown in Figure 28, where P(<N) means the probability of no more than N particles/cm^2 being "seen" during the specified time interval. Curves 1 and 3 have been used.

Information on the energy spectrum to be expected is somewhat ambiguous. One reason is that the random solar flares, in addition to exhibiting different flux levels, also have different spectrums. Second, since primary flare measurements have been made on the earth, protons with energies below 4 MEV

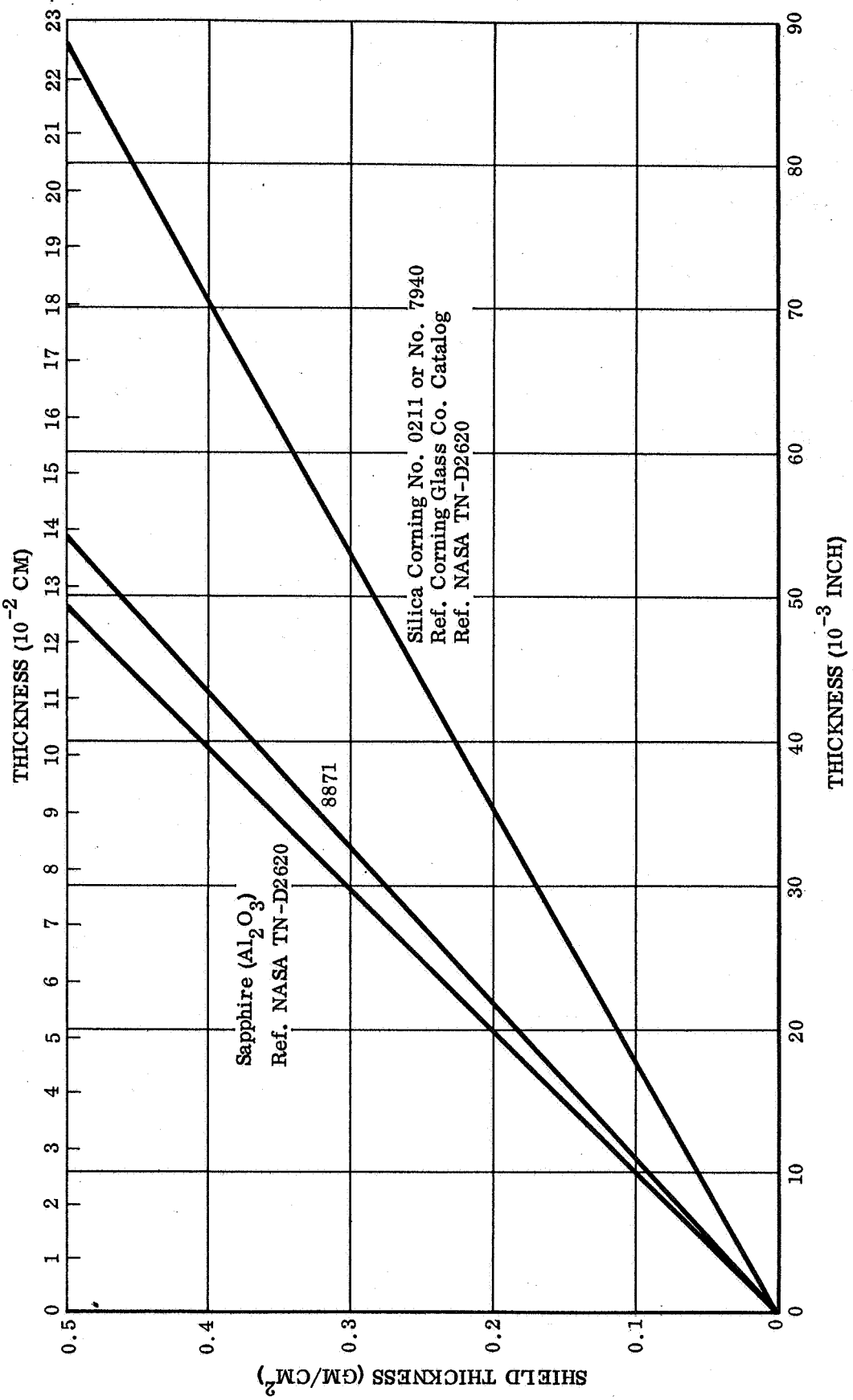

Figure 25 Solar Cell Coverglass Shield Thickness As Function of Thickness of Coverglass

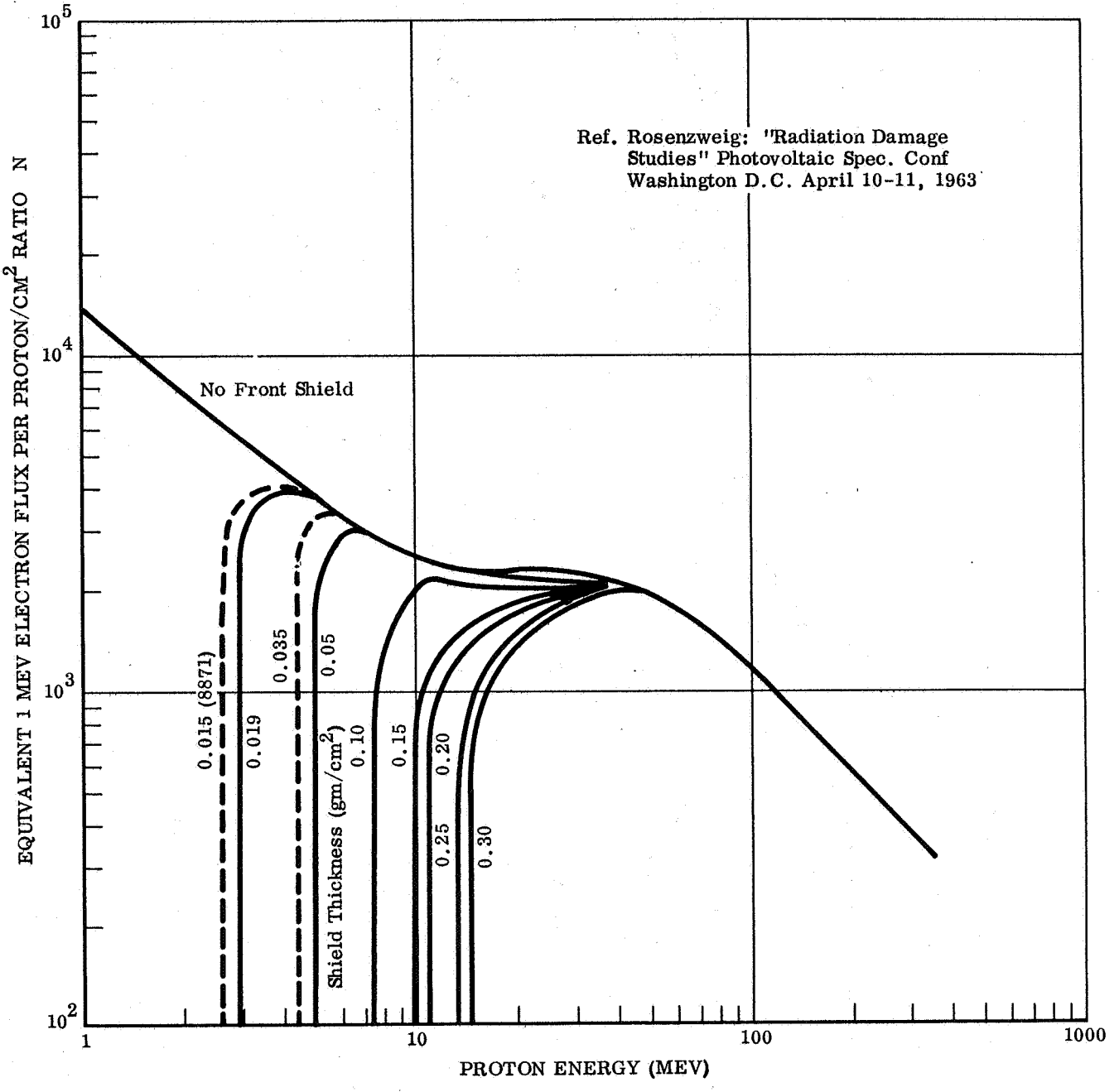

Figure 26 Solar Cell Damage Equivalent to 1 MEV Electronics As Function of Proton Energy Infinite Back Shielding

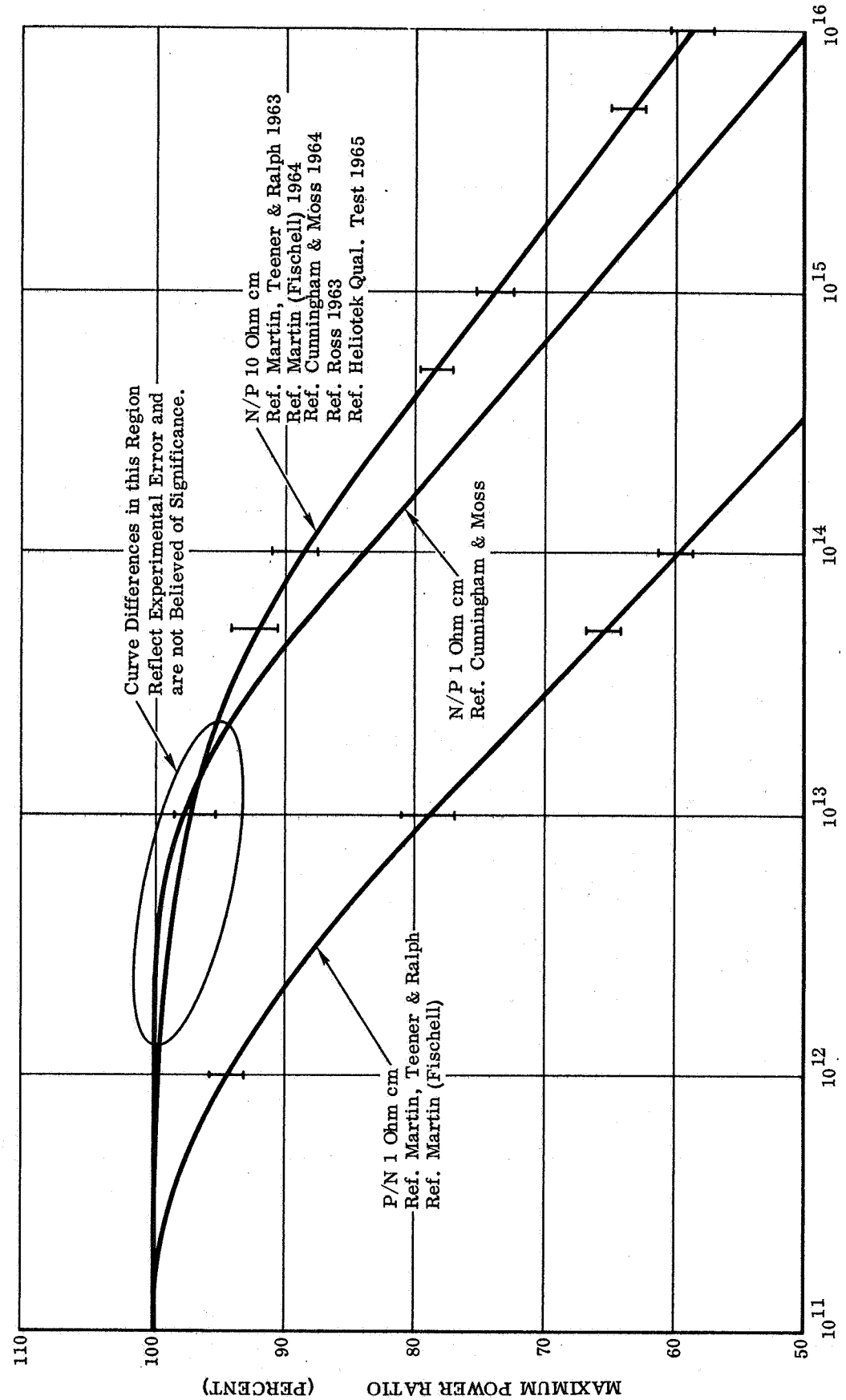

Figure 27 Effect of 1 MEV Electron Irradiation on Silicon Solar Cell Maximum Power Curves Derived From Experimental Studies Performed in Various Laboratories With Air Mass Zero Equivalent Sunlight, 28°

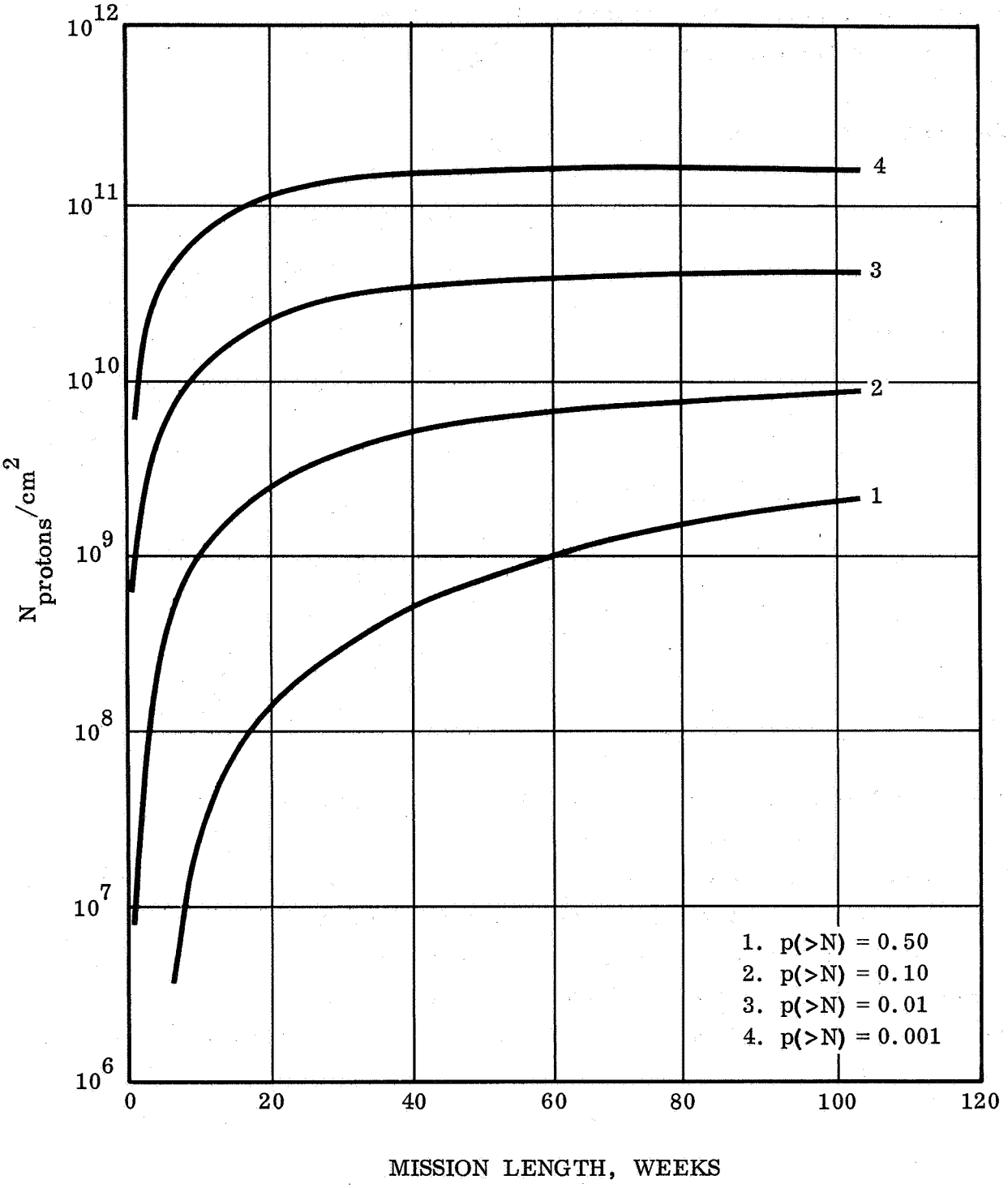

Figure 28 Mission Durations From 1 to 104 Weeks

cannot be measured due to absorption in the atmosphere. By averaging many flares and extrapolating spectral curves, we can expect to find approximately equal numbers of particles in the region 2.7 to 4.4 MEV, 4.4 - 30 MEV, and 30 MEV and greater. These approximations appear to be reasonable on the basis of the limited data in the low energy regions.

The results are summarized in the following charts.

PROTON DOSAGE	EQUIVALENT 1 MEV ELECTRON DOSAGE		
	1.3 Mil Lead Potash	3 Mil Microsheet	6 Mil Microsheet
8×10^7 P/cm^2	6×10^{12}	5×10^{12}	2.8×10^{12}
3.5×10^{10} P/cm^2	3×10^{14}	2.5×10^{14}	1.4×10^{14}

% DEGRADATION FOR 1 YEAR DOSAGE (Using Figure 27)

	8×10^8 P/cm^2	3.5×10^{10} P/cm^2
1.3 Mil	1.2%	18%
3 Mil	1.0%	17%
6 Mil	0.6%	13.5%

This degradation will represent the effect then of protons on the solar cell itself. The ultraviolet radiation will also produce some degradation. For 3 and 6 Mil microsheet coverslides this will be of the order of 3% for one year, depending on adhesives, filters, and coatings used. For the lead potash no quantitative data is presently available, although browning of the coverslide has been noticed. Measurements are now being made to determine the magnitude of the discoloring for various exposure times and will be considered when available.

2.5.2.2 Controls

Investigations were conducted to determine the problems associated with the use of DC permanent magnetic motors in the space environment. Essentially the same problems that are inherent in the slip rings are inherent in the DC motor with the added gear lubrication difficulty. Both areas are discussed in other sections of this report, and control of the motors is the subject of this section.

Deployment/Retraction Control System

The deployment and retraction of the array is accomplished through an electronic sensing system that controls the deployment and retraction motor. This system is designed such that, when deployment is commanded, both deployment and retraction motor are energized. By adjustment of current input the deployment motor is the superior force and beam and substrate deployment takes place but a lagging action occurs with the retraction motor imposing a drag on the system. This has the effect of a braking action on the drum and retards unwinding caused by the stored energy in the beams.

In the retraction mode both motors are energized but the deployment motor in this case is controlled to lag the wrap motor, thus producing a snug wrap. The electronic sensing system constantly monitors load and regulates current input to the motors. This system eliminates the need for a drag brake mechanism. The motors act as locks when current is off (see Figure 29).

Drive Motors

The investigation of electronic motors for the drive system consisted of selection and test of candidate motors in a simulated array deployment cycle. (Test description and results are discussed in Section 2.6.1 of this report.

Tests using the control system as conceived on the simulated test setup and the full-scale model indicated that noise generated by the motors and unpredictable differences in the motor and array mechanical system made current sensing and control impractical. An alternate consideration was a relatively

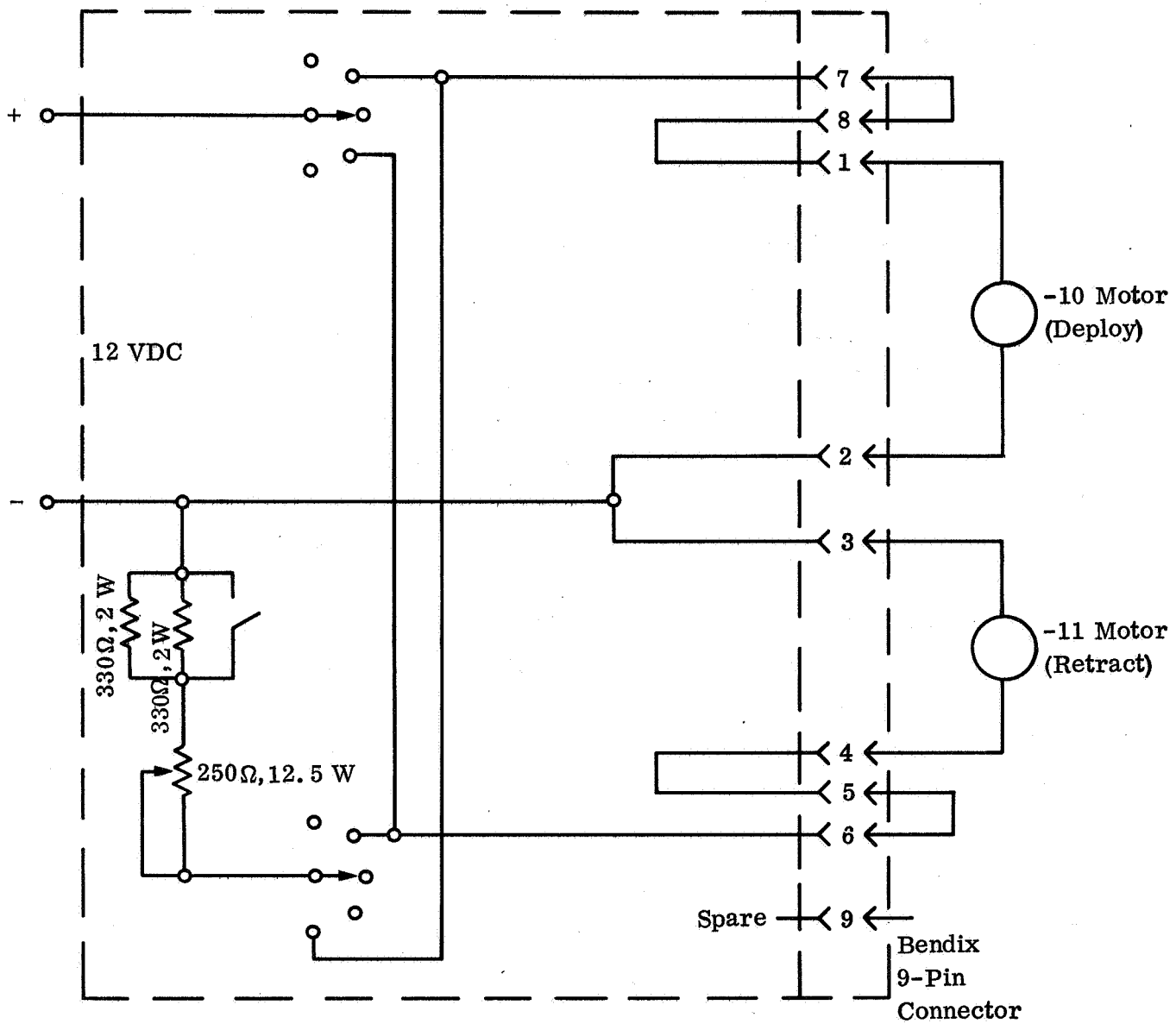

Figure 29 Schematic/Wiring Diagram Deployment Control Unit Full Scale Model

simple and accurate control parameter such as motor torque. The motor mount can be instrumented with strain gauges to produce an electrical signal proportional to torque. With both motor mounts instrumented the difference between the two electrical signals is proportional to the desired tension. A simple closed loop servo system can then maintain this electrical signal (the tension) constant regardless of other disturbances to the system.

Instead of controlling voltage to the retarding motor, however, it has been determined that the drag is produced much more simply and with greater accuracy by resistively loading the dragging motor. The dragging motor is a generator and produces a voltage. Increasing the load, i.e., decreasing the resistance across the terminals, increases the torque required to turn the shaft of the motor and thus the tension on the wrapping beams.

Test data taken on the full-scale model confirms the practicality of controlling tension by this method. The time required to deploy or retract the array with proper tension is plotted against drive motor voltage (see schematic below).

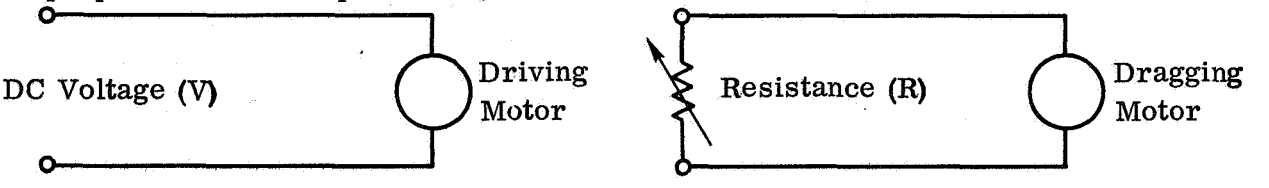

Schematic - Tensioning System

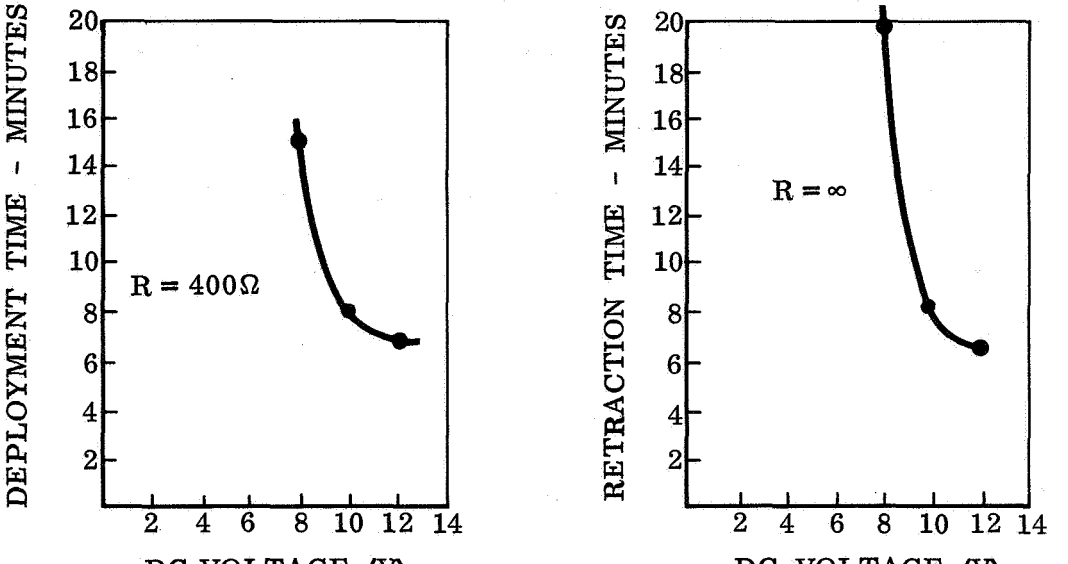

Deployment and Retraction Times Versus DC Voltage With Dragging Motor Resistively Loaded

2.5.2.3 Power Transfer

Calculations based on slip rings used in similar applications and on data supplied by Airflyte Electronics indicate that optimum slip ring performance at extreme vacuum and at the low speeds at which the solar array slip ring assembly will operate when the rings are of coin silver and the brushes are silver impregnated with molybdenum disulfide or niobium disulfide. Parameters for such a slip ring assembly are shown below.

Brush Material	Ag Nb S_2 Ag Mo S_2
Ring Material	Ag
Number of Rings	8
Brushes per Ring	2
Brush Area	0.017 square inch (200 amp/sq. in.)
Current per Circuit	5 amps maximum
Speed RPM	3 maximum
Potential Drop (Per Circuit	20 millivolts

This assembly would be 1.75 inches in diameter and 3.6 inches long. It would be mounted by means of 3.00 inch diameter flange, and would weigh less than 1 pound.

The contact resistance quoted is 4 milliohms per circuit. The power loss per circuit allowing 5 amps per circuit is:

I^2R = 100 milliwatts I = 5 amperes

R = 0.004 ohms

For the eight circuits the total power loss is:

8 x 100 = 800 milliwatts

2.5.3 Reliability Analysis

A reliability evaluation of the Solar Panel Array has been performed. A general mathematical model was developed to logically depict the relationships between the various system constituents and the detail specification requirements.

2.5.3.1 Reliability Mathematic Model

The reliability model (Figure 30) shows the probability of success predicted for each element and the aggregate. The prediction utilizes failure rates on parts and materials where data is available and performance estimates on other devices. Reliabilities are calculated for (1) and (10) deployment and retraction cycles. K-factors utilized during various phases such as launch, transition, deployment and post deployment are shown on the mission profile, Figure 31. Figure 32 shows the failure rates utilized in this analysis.

Discussion of Math Model

The principal mechanical loads on the Solar Array occur during the launch phase of the mission. The near zero gravity condition during other mission phases essentially eliminates all loading except those thermally induced. Stress due to thermal effects will be negated during design efforts by thorough thermal analysis and adequate control means. The other loads experienced by the substrate, drum and support structures occurs during retraction and deployment. The deployment and retraction loads are minor when compared to the launch conditions. Exposure time to the environment, in either case, is for very short periods. The failure rates of all devices are directly related to the use environment and the probability of success is inversely related to the environment exposure time. Therefore, the portion of the mission phase for all system elements (except the solar cells) that is most detrimental to probability of success is interplanet flight. This is due almost entirely to the extended time in transit and is true even though the in-transit failure rate is smaller than operational failure rates by 3 orders of magnitude.

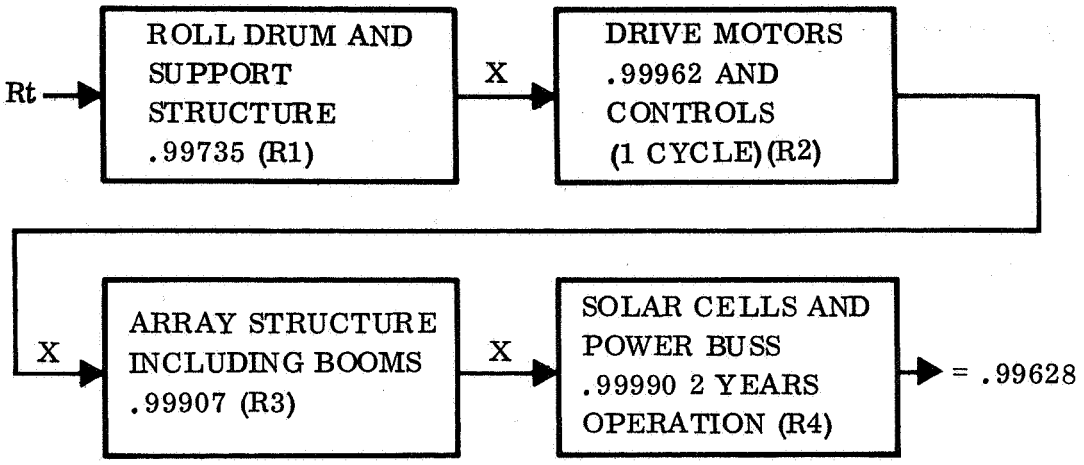

Figure 30 Mathematical Model

ESTIMATED MISSION EQUIVALENT TIME - SUB SOLAR ARRAY			
Mission Phase	K Factor	Mission Time (Hours)	Equivalent Time (Hours)
Launch	5.0	0.1	0.500
Array Deployment	1.0	0.115	0.115
Inter-Planet	0.001	12,500 (18 mo.)	12.500
Array Retraction	1.0	0.115	0.115
Total Mission Equivalent Time (MET)			13.230

Figure 31 Mission Profile

Subsystem	FR/10^6 hrs	Mission Equivalent Time (MET)	Reliability
Drum & Support Structures	200.00	13.23 hr	0.99735
Motor & Controls	78.96*	13.23 hr	0.99962
Array Structure	70.00	13.23 hr	0.99907
Solar Cell and Power Buss	7.00**	13.23 hr	0.99990
Complete System	355.96*	13.23 hr	0.99628

* Motor redundancy has the effect of reducing the Motor and Control effective failure rate to 3.96/10^6 hrs for deployment and 28.96/10^6 hours for retraction.

**See Solar cell section for discussion of multiple redundancy that provides high reliability which was converted to the failure rate shown.

Figure 32 Subsystem Failure Rates and Reliabilities

2.5.3.2 Mission Profile

Figure 31 depicts a probable mission profile for the Solar Panel Array System. Each of the mission profile elements is time phased and corrected by a K-factor which is indicative of the stress anticipated during that mission phase. The K-factors are patterned from similar factors used on other space programs such as the Apollo. Such time factoring, to represent various stresses encountered in a mission, has effects identical to failure rate factoring but reduces the overall computational requirements. The no load (gravity/acceleration free) condition during most of the mission plus the freedom from degrading atmospheric effects such as corrosion, drag, etc., provide an idealized environment during a large portion of the total mission.

2.5.3.3 Solar Array Structure

The selected structural design which features an unloaded panel substrate for the Rollup Solar Array has been analyzed to establish conformance with the reliability goal of 0.999 probability that the array structure will successfully function when subjected to the specification requirements. It is concluded that the design will meet or exceed the reliability objectives. This conclusion while not based on the conventional statistical prediction method is considered reasonable and valid based on the following considerations.

All materials and methods used in the design and manufacture of the array structure are current state-of-the-art. The materials selected are compatible with the intended space environment and have been successfully used on previous deep space missions.

Testing accomplished by Ryan on a similar structure (a 50-square foot rollup solar array) has developed confidence that the reliability objectives for the 250-square foot solar array can be achieved. The 50-square foot array has been deployed and retracted at room ambient temperatures approximately one hundred times without a critical structural failure occuring. A collapsible titanium beam, very similar to the beam design to be used on the 250-square foot array, was deployed from a drum and retracted 2,000 times without a failure of catastrophic nature. Some local buckling and cracks were evident but did not detract from functional capability. This simile is considered to

be subject design, even though conducted at room ambient temperatures and sea level pressures, as titanium is unaffected by space environment except for temperature (in this case, -150° to +300°F), a range that would have negligible effect on the properties of titanium. Extensive tests have also been conducted on the tab materials to be used to attach the substrate panels to the extendable beams. The tests demonstrated the feasibility of the attachment design and provided some statistical evidence of the suitability of the material.

Low temperature thermal vacuum tests of the 50-square foot array revealed a problem with thermal gradients between the substrate wrap and the support structure. The loads induced in this environment resulted in a failure of the substrate-to-beam attachment and buckling of the beams at the drum interface during low temperature deployment. This problem has been eliminated on the current design by providing flexible tab attachments between the substrate and beams, by thermal control surfaces for both the substrate outer wrap and for all exposed surface of the support structure thus minimizing the thermal gradients and by providing an extension drive system that precludes the possibility of buckling the beams. The experience gained provides insight for the current design and lends confidence in achieving the structural objective.

Full size drum-substrate sinusoidal vibration tests conducted during the Phase I activities correlated the analytical predictions and were accomplished without failure of the drum and related structural items.

Rollup Drum and Support Structures

The mechanical reliability aspects of the drum structure were carefully analysed during drum design efforts and safety margins exceeding specification requirements were employed. This effort plus the suitability of the materials employed for the intended environment will provide the level of reliability required to successfully complete the mission requirements. Evaluation test data will be utilized to provide assurance that the design will achieve reliability objectives.

The reliabilities shown for structures were derived empirically but are justified by adequate safety margins employed throughout the design. The relability potential of such structures is almost completely dependent on the thoroughness of stress analyses during design efforts, supported by verification testing. Millions of failure free hours on air frames and space structures evidenced the high reliability attainable by proper attention to design.

Reliability analyses of the data generated during evaluation tests of the 250-square foot array will be performed and the results reported.

These analyses will provide qualitative support of the array structure reliability and by diligent use of K-factors to identify fatigue phenomena, quantification of reliability parameters is possible.

Drive Motors and Controls

During deployment two motors are employed to extend the panel and a failure of either of the deployment drive motors or a failure of the retraction motor will not prevent successful deployment. During retraction one of the deployment drive motors is required to provide braking action. Operation of the retraction drive motor is also required. Thus, during retraction complete redundancy is not available. It is noted that while complete redundancy is not available, provisions are made through use of a slip clutch and free wheeling feature in the retract drive system so that under emergency conditions the extension motors can retract the panel by rotation of the drum through friction at the drive sprocket interface. The operational periods of the motors during a deployment or retraction are approximately 0.115 hours. This relatively short operational requirement in conjunction with the partial motor redundancy assures a high probability of success for one or several deployment and retraction cycles. One drive motor supplies deployment or retraction power, while the opposing motor serves as a brake. This feature provides continuous smooth retraction or deployment. Electronics sensing and compensation circuity is required for this feature. The parts utilized to provide this feature, like all other electronic or electromechanical parts used in this system, were selected for long term space use and are in conformance with current high reliability specifications. A list of the electronic and

electromechanical parts and their failure rates used in the 250-square foot array system are provided in Table 7.

2.5.3.4 Deployment Reliability

A successful deployment requires proper performance of all system elements except the solar cells and power bus subsystem. Utilization of redundant deployment motors provides such high levels of reliability that their effect on successful deployment is for practical consideration eliminated. The retraction provides braking torque to the roll drum during deployment but can be overcome by the deployment motor if the retracting motor should fail. The probability of one successful deployment, considers only the equivalent mission time required to complete a deployment.

$$R_d = 1 - (R1\ fr + R2\ fr + R3\ fr) \times (\text{MET of } 0.115 \text{ hour}) = 0.999965$$

The probability of success is the total probability of the motor and control circuitry completing one entire mission.

2.5.3.5 Retraction Reliability

Successful retraction requires proper performance of the retraction motor and one of the redundant deployment motors plus the other elements described above for deployment. The probability of success for one retraction, R_r, is:

$$R_r = 1 - (R1\ Fr + R2\ (Mod) + R3\ fr) \times \text{MET of } 0.115 = 0.999961$$

2.5.3.6 Deployed Array Reliability

The after-deployment reliability is dependent on successful performance of the solar cells and power distribution system, and the array support structure. These elements are shown as blocks R3 and R4 on the reliability model. The after-deployment reliability does not consider the launch, deployment or transit hazards. The reliability for a two year period is therefore:

TABLE 7

FAILURE RATE SUMMARY OF MOTOR AND CONTROL SUBSYSTEM

Ref	Qty	Part No.	Name	Remarks	
				FR/10^6 hrs	FR
S1, S2	2	MS27216-1	HM-Miniature Switch	1.0	2.0
CR1-CR4	4	IN4245	Diode/Motor Control	0.015	0.060
A1	2	A709	Operational Amp.	0.400	0.800
R1-R5	10	RNR60C	Hi Rel Resistors	0.006	0.060
CR1, CR2	4		Zener Diode	0.078	0.312
CR3, CR4	4	IN914	Diode	0.014	0.056
C1, C2	4		Capacitor Ceramic	0.010	0.040
Q1	2	2N3997	Power Transistor	0.160	0.320
R6, R7	2	RNR65C	Resistor (current sensor)	0.006	0.012
F1-F3	3		Fuse (1 ampere)	0.100	0.300
B1, B2, B3	3		Motors, Deployment and Retraction	25.000	75.000
	40			Total FR	78.960

R_{DA} = 1 - (R3 fr + R4 fr) x (8-hour mission equivalent time (MET)

= 0.99938

(For reliabilities greater than 0.99 R $e^{-\lambda t}$ is R = 1 - λt).

(fr = failure rate in failure per 10^6 hours).

2.5.3.7 Launch Reliability

The launch phase of the mission exposes all system elements to relatively high vibratory stresses. The roll drum and support structures absorb the majority of the launch stresses and are the most likely element to receive damage during this mission phase. Solar cell damage is unlikely due to the damping provided by resilent foam discs between roll layers. The flexible beams in the stowed condition absorb little if any stress. The launch phase K-factor was selected to provide a degradation factor which is representative of the launch environment.

The launch probability of success was determined by considering each system element's probability of failure only during the time launch stress is imposed.

The probability of successfully completing the launch phase of the mission is:

R_L = 1 - (R1 fr + R2 fr + R3 + R4 fr) x (MET) of 0.5 hour = 0.99984

2.5.3.8 Total Mission Probability of Success

The success of a complete mission requires successful performance of all subsystems for the entire mission. Mission probability of success was calculated for a complete mission consisting of launch, transit time, one deployment, and two years operation. Mission probability of success is also shown for a complete mission with 10 deployment and retraction cycles.

R_t for one deployment = 1 - (R1 fr + R2 fr + R3 fr + R4)

x (MET of 13.23 hours) = 0.99628

R_t for ten deployments = 1 - (R1 fr + R3 fr + R4 fr)

x (MET) of 13.23 hours)

x (10x deployment and retraction probability of success) = 0.995.

2.5.3.9 Solar Cell Reliability Analysis

Reported herein are the results of the reliability analysis performed on the proposed design of a solar cell power supply for a rollup array.

Included is a failure effect analysis and reliability model with appropriate calculations of system reliability and maximum anticipated power degradation.

The panel configuration consists of 13 subpanels. Each subpanel contains eight circuits (modules). The circuits consist of 540 2 x 2 cm solar cells, three in parallel by 180 in series. All wiring and connections will be redundant. An array lifetime of two years will be used for reliability calculations.

2.5.3.10 Solar Cell Failure Analysis

Failures Resulting in Complete Loss of Solar Cell Power

Short Circuit Failures

A short circuit of a solar cell results when a conducting path exists between the upper and lower surface of a cell. The most probable cause for this type of failure is a contact between the lower surface of the cell and the lead from the submodule bus bar which is connected to the top surface of the same cell. This will result in a short circuit of the affected cell. There will be a slight variation in the operating voltage in that string resulting in a correspondingly small power degradation. For a single short this power degradation will be of the order of one-half percent for the affected string when operating at no failure maximum power voltage. The total panel power degradation will depend on the panel's operating voltage; however, typically

a total power degradation of the order of 1/10 percent per failure will result for the entire panel. Quality control inspection of the intercell connections substantially eliminates the possibility of occurrence of such a failure. The probability of occurrence of this failure is therefore assumed to be zero.

A second source of shorting is caused when the negative bus contacts the positive bus causing complete loss of power for the whole panel. The design as proposed will use Kapton H film insulator between both busses thick enough to prohibit any possible arcing. Quality control inspection of the assembly with bus bars and insulation will eliminate any human induced failures introduced during fabrication. The probability of such a failure occurring will also be zero.

For a 2 x 2 cm cell with the Solaflex(R) connections there are three solder points on the lower surface and four on the upper surface which gives a probability of open failures of the order of 10^{-16} and 10^{-12} for the lower and upper surface, respectively.

An open circuit cell failure may result from the fracture of a cell. The probability is extremely small for such a failure not being detected during preliminary inspections or occurring during normal operating conditions. An open circuit failure caused by the separation of the electrode grid from the upper surface of a cell may result from thermal cycling of the cell and/or vibration of the cell. If all possibilities of open circuit failure for normal operation are considered, the probability of an open circuit failure of an individual solar cell is no greater than 3.2×10^{-5} per 1,000 hours.

Investigations of cell fracturing have shown that due to the use of extended Solaflex(R) solder tabs, open failures will result in only a very small part of all cell failures.

Cell Failure Probabilities

For the 2 x 2 cm cell configuration the probability of "n" failures, out of a total of N cells, can be written as

$$n_{P_N} = \frac{N-n}{(n-N)!n!} \; P^n \; (1 - P)^{N-n}$$

where P is the probability of failure for one cell during a two year period. For the 2 x 2 cm cell P equals 7.7×10^{-5}. Thus, the probability of losing "n" 2 x 2 cm cells in the proposed panel (56,160) will be

$$n_{P_{56160}} = \frac{56160!}{(56160 - n)!n!} \; P^n \; (1-P)^{56160 - n}$$

The values of $n_{P_{56160}}$ for n = 0, 1, 2, 3, 4, 5, 6, are

n = 0	0.007259
n = 1	0.035754
n = 2	0.088056
n = 3	0.144575
n = 4	0.178022
n = 5	0.175365

The sum of the n_{P_N} from n = 0 to n = K will be the probability that no more than K of the N cells will fracture. This can be called the reliability of no more than K failures, or R_K.

$$R_K = \sum_{(n = 0)}^{K} n_{P_N}$$

Sixteen (16) cell failures will be given an R_K of 0.999918, i.e., there is a probability of 0.99918 that during a two year mission no more than 16 cells will fracture. Employing this figure in the total panel reliability (including wiring, insulations, etc.) a total reliability of 0.99975 can be achieved. This calculation will be shown later.

The 16 cell failures will distribute themselves among the 13 subpanels. The probability of n failures within a single module will be $n_{P_{4320}}$.

Values for n = 1, 2, 3, and 4 are:

n = 1 0.259

n = 2 0.049

n = 3 0.006

n = 4 0.00004

This indicates that the probability of three cells failing in the same subpanel will be approximately 1/40 the probability that one will fail. Since only 16 failures are considered this would imply that in the worst case the failures will distribute themselves such that ten subpanels have one cell failure each and three subpanels have two cell failures each. By examining np_{540} the distribution of failures among the eight circuits (modules) (each with 540 cells) can be found.

We get for n = 1, 2, 3

n = 1 0.045

n = 2 0.001

n = 3 0.00002

Thus, the probability of two failures occurring in one circuit is 1/45 the probability that one failure will occur. Since in the worst case, a subpanel will have at most two failures, the most probably distribution along the circuits would be for two circuits to have one failure each, and six circuits to have no failures.

For the 2 x 2 cm cells then, a total panel probability of 0.99975 can be achieved with 16 failures distributing themselves in the worst case among the 13 subpanels, each with eight circuits, as described above. This would represent a power loss for the panel of approximately 0.05 percent, based on cell fracture power losses.

2.5.3.11 Wiring Reliability and Failure Analysis

Total Panel Reliability

The total panel reliability, R, will depend upon the total reliability of the solar cells, R_x, and the panel wiring reliability, R_1.

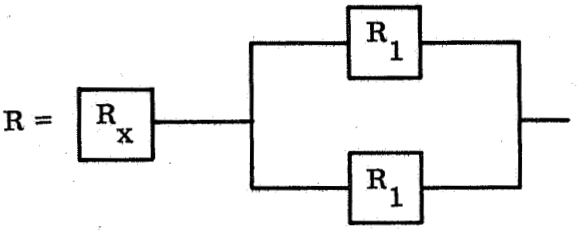

$$R = R_x \left[1 - (1 - R_1)^2\right]$$

Panel Wiring Reliability

The panel wiring reliability will depend on the positive longitudinal bus reliability, R_2, the inter bus insulation, R_3, the negative longitudinal bus reliability, R_4, the positive longitudinal bus to transverse bus solder connection reliability, R_5, the negative longitudinal bus to transverse bus solder connection, R_6, and the subpanel wiring reliability, R_7,

$$R_1 = R_2 \cdot R_3 \cdot R_4 \left[R_5 \cdot R_6 \cdot R_7\right]^{13}$$

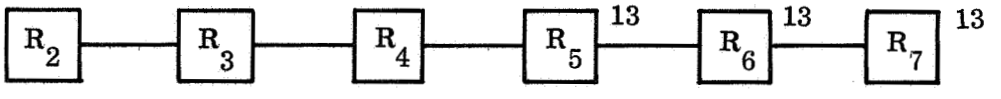

Subpanel Wiring Reliability

The subpanel wiring reliability, R_7, depends on the positive transverse bus reliability, R_8, the negative transverse bus reliability, R_9, the positive circuit to transverse bus connection reliability, R_{10}, the negative circuit

to transverse bus connection reliability, R_{11}, and the reliability of the interbus insulator, R_3,

$$R_7 = R_8 R_3 R_9 \left[R_{10} R_{11}\right]^8$$

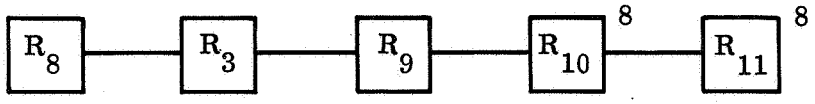

R_{10} (and R_{11}) will depend on the circuit bus bar to transverse subpanel solder connection reliability, R_{14}, (R_{15}).

$$R_{10} = R_{14}\left[1 - (1-R_{13})^2\right]$$

$$R_{11} = R_{15}\left[1 - (1-R_{13})^2\right]$$

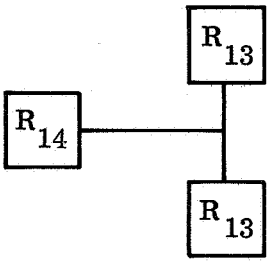

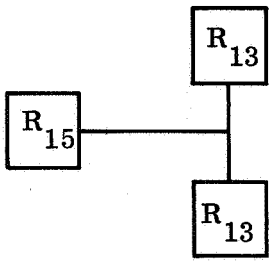

	Component Failures/Hour	Reliability for Two Years
R		0.999
R_1		0.999 999
R_2	1.0×10^{-11}	0.999 999 8
R_3	1.0×10^{-11}	0.999 999 8
R_4	1.0×10^{-11}	0.999 999 8
R_5	1.0×10^{-11}	0.999 999 8

	Component Failure/Hour	Reliability for Two Years
R_6	1.0×10^{-11}	0.999 999 8
R_7		0.999 999 8
R_8	No failures have occurred to present time	1.0
R_9	No failures have occurred to present time	1.0
R_{10}		0.999 999 999 999
R_{11}		0.999 999 999 999
R_{13}	1.0×10^{-11}	0.999 999 8
R_{14}	No failures have occurred to present time	1.0
R_{15}	No failures have occurred to present time	1.0

2.5.4 Weight Study

The weight of the array includes all items required up to the array/spacecraft interface.

The weight studies made continuing use of data derived from the 50-square foot rollout panel program.

A continuing weight monitor was maintained throughout the program (see Figure 33). The monitor reflects the effects of various trade studies and the progressively more exact definition of components during the detail design phase. A major factor influencing the dip in the monitor curve at approximately the 85% point in the trade study phase, was the requirement for increased rigidity in the spacecraft mounts. This requirement became evident from data derived during vibration testing of the 50-square foot rollout panel. The general downward slope between the second quarter and third quarter was the result of full development of details and the appraisal of weight attributed to the details. The downward trend between the third quarter and completion of the

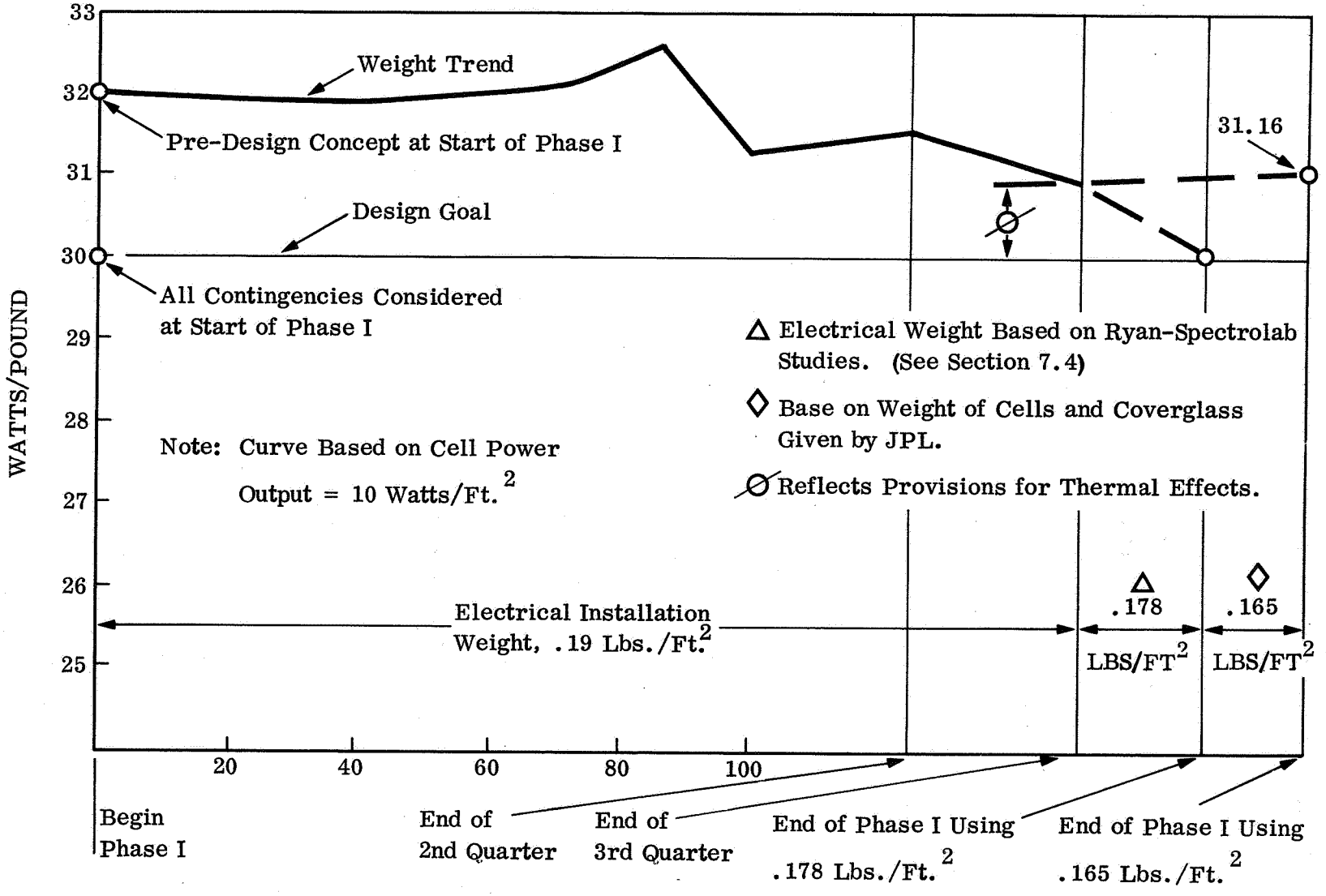

Figure 33 Power/Weight Monitor

task was due to provisions for thermal effects. The major provisions affecting weight during this period were the incorporation of a thermal coated blanket on the outer substrate wrap and a slip fitting in the mounting bracket to accommodate thermal growth.

The weight monitor chart also shows the weight allocated to the electrical installation during various periods of the program. It is noted that the original assumption of 0.09 pound/square foot was carried from the inception of this program to the end of the third quarter. During the last quarter a value of 0.178 pound/square foot, based on studies and actual weight developed by Ryan and Spectrolab, was used in the weight analysis. Recent information from JPL establishes the weight of 2 x 2 cm cells at 0.17 grams and 3 mil cover slips at 0.065 grams. Based on these values the electrical installation weight is reduced from 0.178 pound/square foot to 0.165 pound/square foot.

The watts/pound capability of the array is calculated based on nominal drawing tolerances and sheet thicknesses, using the baseline 10 watts/square foot cell power output.

$$\text{Watts/pound} = \frac{(10)\ (\text{Solar Cell Area})}{\text{Weight}}$$

where;

Solar Cell Area = 250.72 square feet

Nominal Array Weight = 80.451 pounds

$$\text{Watts/Pound} = \frac{(10)\ (250.72)}{80.451} = 31.16$$

Detail weight data is incorporated in Section 7.3 of the Appendix.

2.6 DESIGN DEVELOPMENT TESTS

The following tests were conducted to determine the effects of the more critical design environments on those components which contribute significantly to the efficiency of the total array. The results were used for deriving

loads for detail stress analysis, optimization of the proposed design and comparison with assumptions made in the early phases of the program.

2.6.1 Drive Motor System Test

Tests were conducted to determine the feasibility of providing tension in the deployable beams, between the beam drive pinion and the drum, by differentially varying the output of the deploy and retract motors. Two different motors, one 27 vdc rated at 100-inch-pounds torque and the other 24 vdc rated at 262 inch-ounces were used. The measured torque-speed characteristics of these motors are shown in Figure 34 and 35. This test data was used to determine motor control parameters.

Tests were then performed to demonstrate that the above mentioned tension could be obtained by varying the load between the driving motor and the drag motor (see Figure 36). The two motors were connected so that they rotated in the same direction and the voltage to each was controlled. The motors were interconnected mechanically by a cable attached to a sheave at each motor output shaft. Cable tension was measured by a load cell. Analysis has shown that a maximum of ten pounds can be applied to the teeth of the corrugated drive strip on the beams, therefore, the tests were run at tensions between two and ten pounds. Test data shows that by controlling the voltage to the dragging motor a constant tension can be maintained in the cable between the motors.

2.6.2 Dynamic Characteristics Test of Wrapped Panel Layer Separation Medium

A structural damping characteristic test (reported in Reference 2) of a small section of panel with polyurethane foam pads on the back and wired solar cells on the opposite side was conducted. The purpose of this test was to determine the amount of sinusoidal dynamic energy which can be transmitted through a representative pad configuration at resonance.

The specimen was draped over and attached to a rigid fixture, simulating the wrapped panel on the stowage drum in a 1g field without pretension (see Figure 37). Dynamic transmissibilities were obtained at various resonant

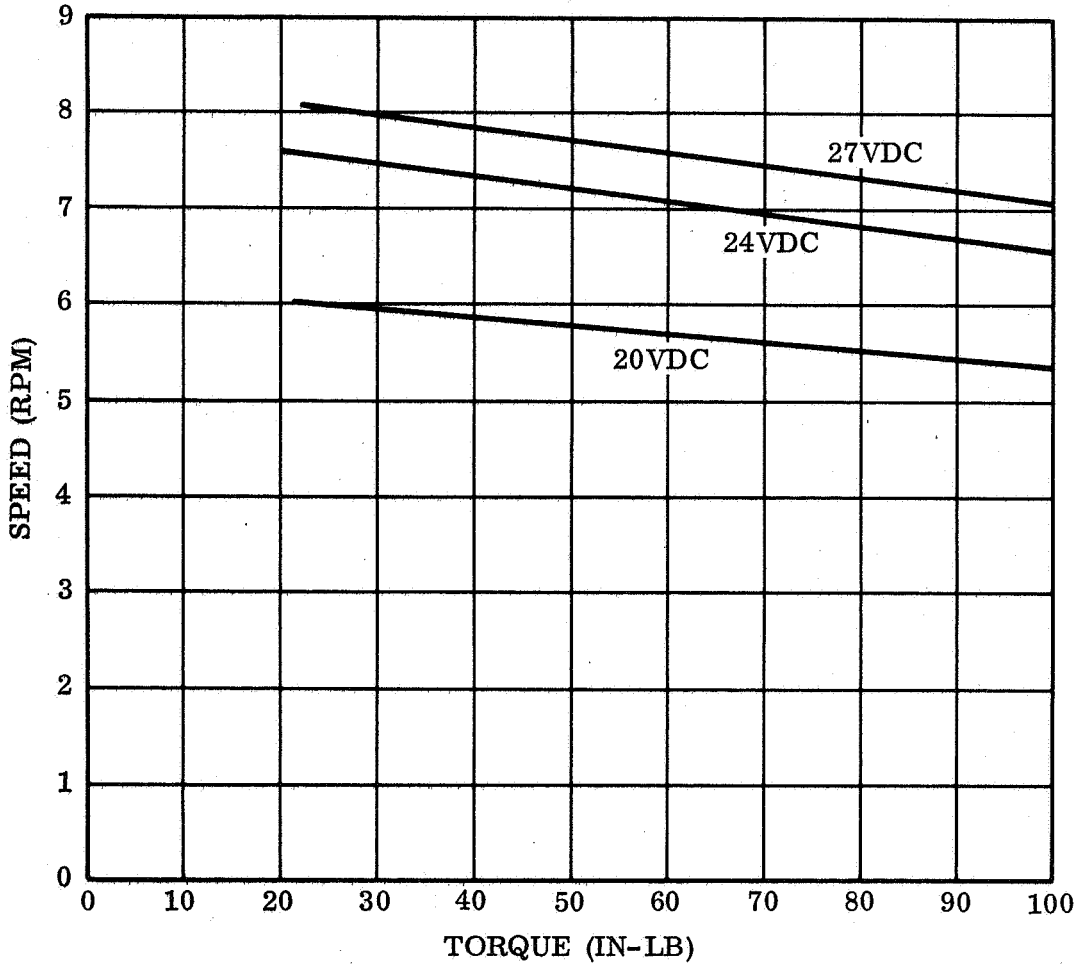

Figure 34 Speed Versus Torque, At Various Input Voltages, 100 Inch-Pound Motor

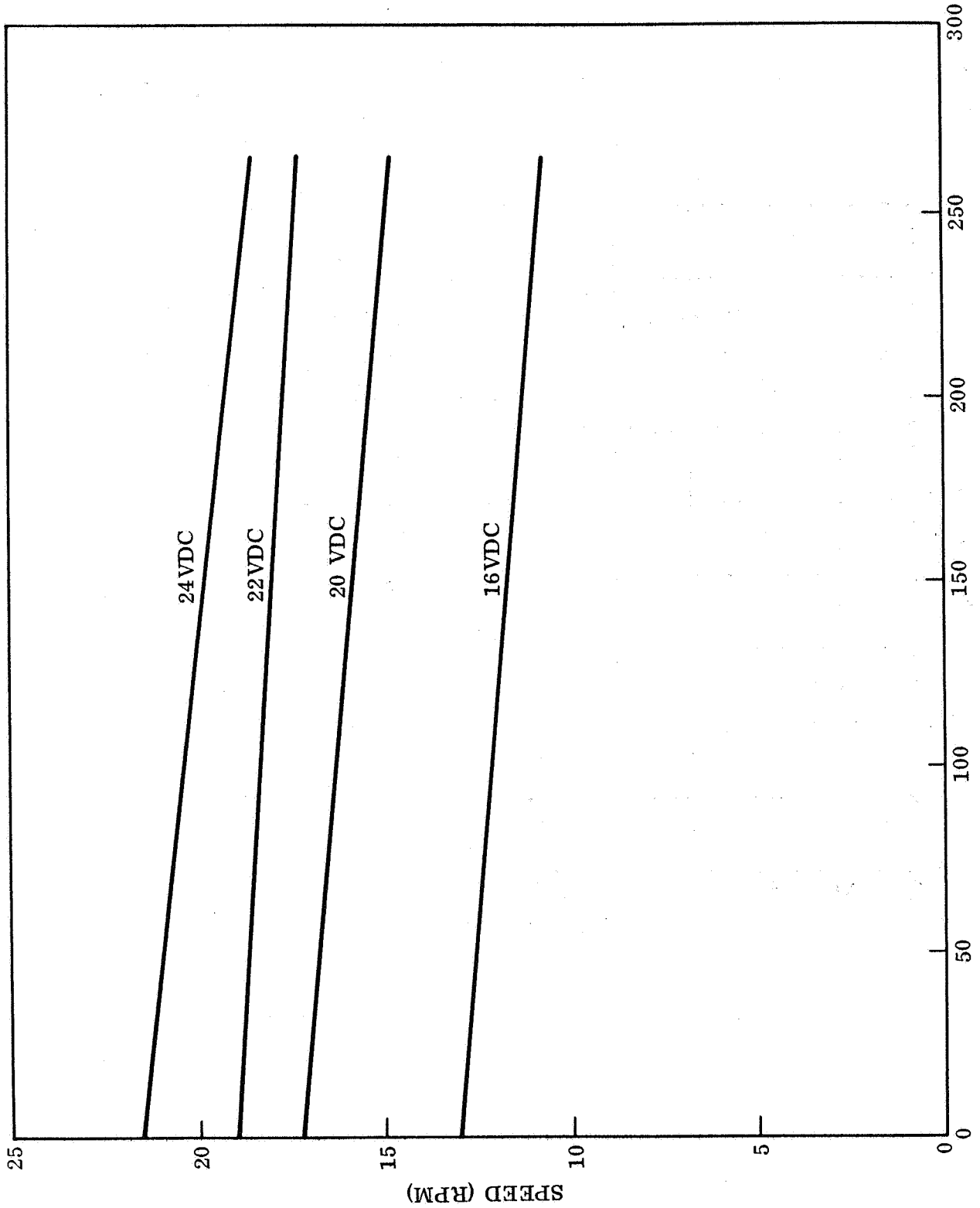

Figure 35 Speed Versus Torque, At Various Input Voltages, 262 Inch-Ounce Motor

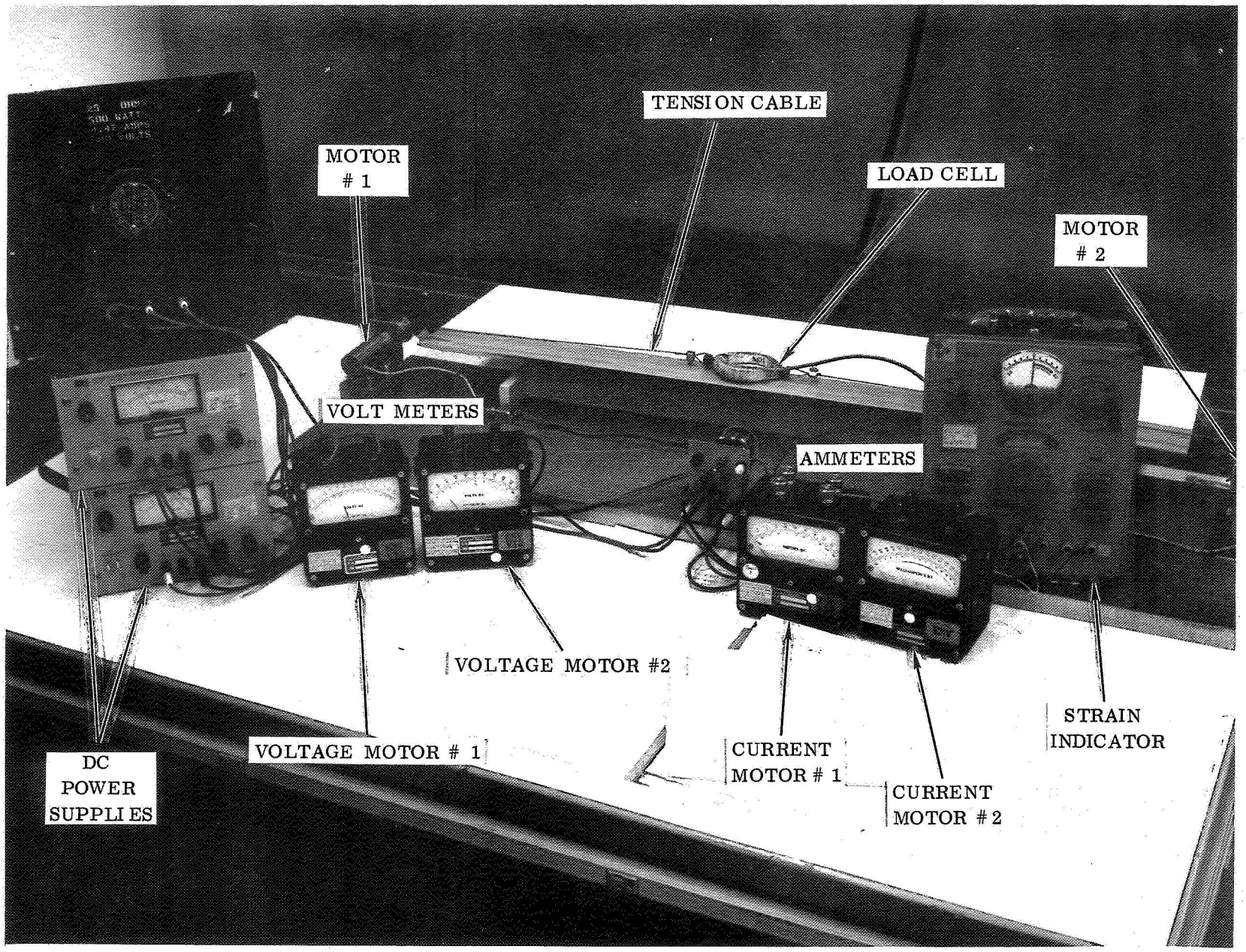

Figure 36 Motor Control Test Setup

frequencies for different levels of sinusoidal excitation up to 3g (0-Pk). Results show a transmissibility of approximately 4 to 1 at the stowed panel design frequency, rather than 10 to 1 used in early analysis for foam pad configuration design.

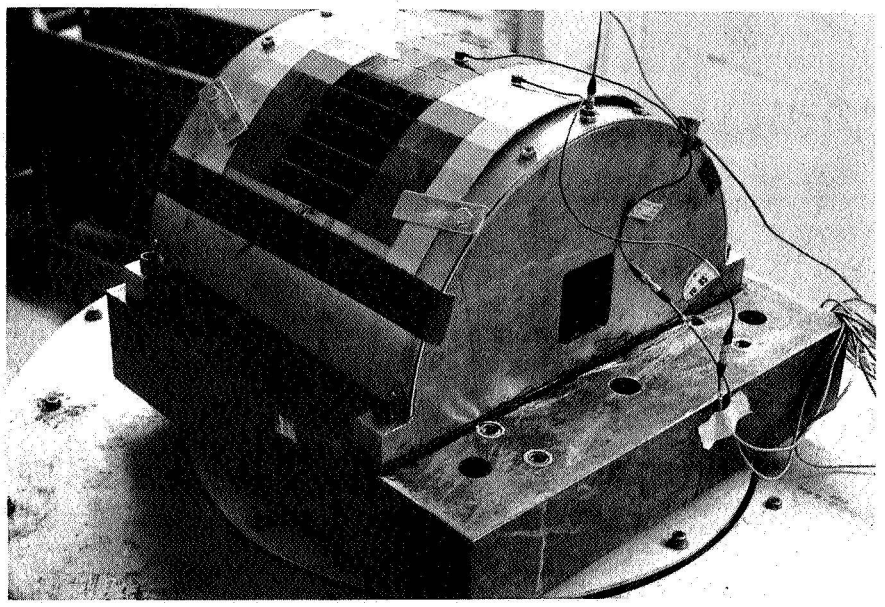

Figure 37 Damping Pad Test Setup

2.6.3 Sinusoidal Vibration Test of Stowed Panel Excited Normal to Wrap Drum Axis

To optimize and verify the design it was considered necessary to substantiate assumptions and obtain data in the following important areas:

- Suitability of 1 mil Kapton.
- The response acceleration of the large stowed panel mass.
- Substantiation of the design assumption that the load distribution on the wrap drum would be characteristic of a pin ended beam vibrating at critical resonance (see illustration on following page).

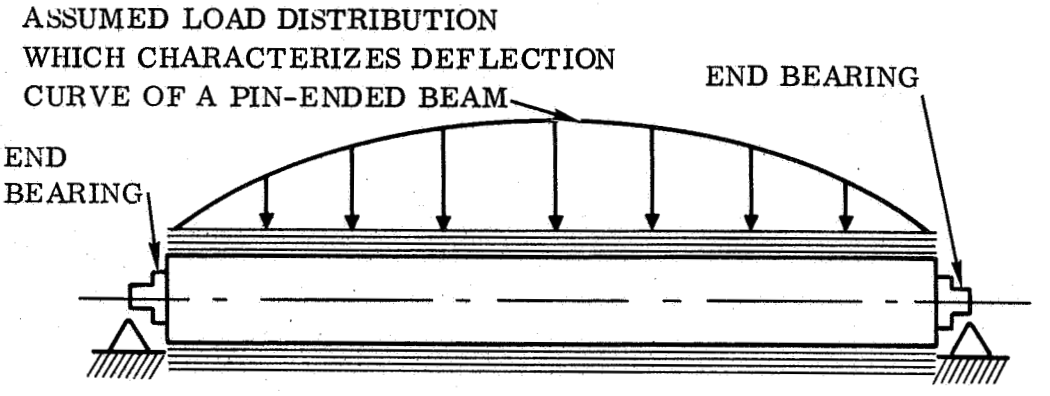

WRAP DRUM SUPPORTED AT END BEARINGS

- Verification that the deflection of the drum, under vibration would not exceed the 1/4 inch deflection established as a Ryan requirement.

- Determination of the dynamic transmissibility through the drum and end bearings at the stowed panel resonance.

A full size wrap drum, 12-inches in diameter of 0.032 magnesium per Ryan Drawing No. 400U023 was installed in a rigid aluminum fixture at each end support bearing, (see Figure 38). Dynamic analysis showed that the stowed panel mode and wrap drum resonance modes would be lower than the spacecraft mount resonance mode and that dynamic transmissibility through the spacecraft mount at those resonances would be 1 to 1, justifying a test without the use of spacecraft mounts.

Six full width substrate panels of 1 mil Kapton were used. Each substrate panel was covered with 2 x 2 dummy chips except for an area in center to which was applied a 9-1/2" x 9-1/2" solar cell matrix consisting of 2 x 6 cells

not interconnected. The weight of the dummy chips used on the six substrates was equivalent to the total weight of solar cells for the full solar panel consisting of 13 substrates.

The back of the substrate panels had 0.15 inch thick, 2 pounds/cubic foot polyurethane foam damping pads representing the area coverage established by analysis. The panels were carefully wrapped, without pretension, around the drum. Tests were conducted by first applying one wrap and then successively adding wraps. After each addition of a panel wrap; a test was made and the mode shapes, resonance frequency, and response accelerations were recorded. Since two of the six wraps had dummy chips of copper which represented 50 percent of the total solar cell installation mass, care was taken in testing to evaluate the influence on test results.

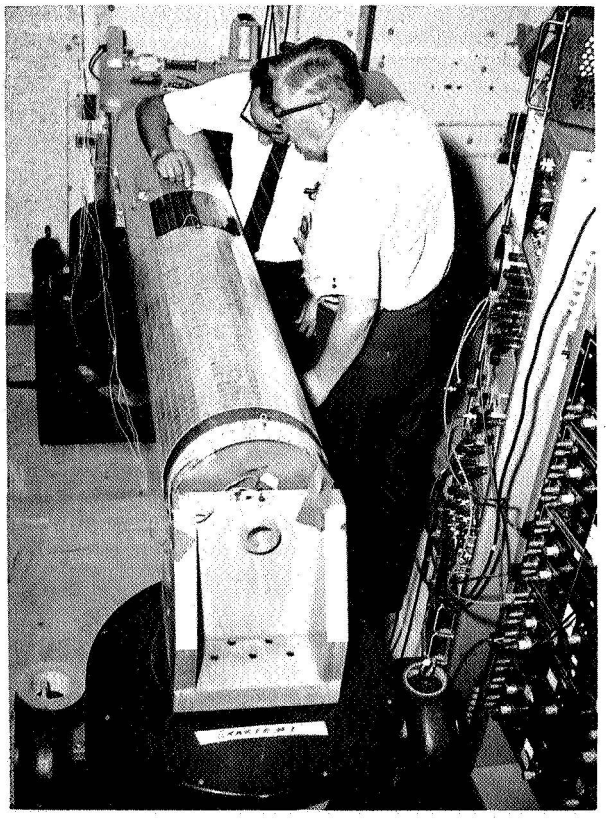

Figure 38 Test Setup - Stowed Panel Vibration Test

Test Results

Each successive wrap after the third had little effect on the dynamic characteristics, with the exception of panel and drum transmissibilities. Damping provided by the stowed panel appeared to increase as the wraps were added, but the increase appears to be negligible after the sixth wrap is added (see following test curve).

At the critical resonance (stowed panel, 30 Hz), transmissiblities through the drum end plate were the same with the fifth and sixth wraps (1 to 1) and transmissibilities through the drum mount bearings were 1.17 with all six wraps.

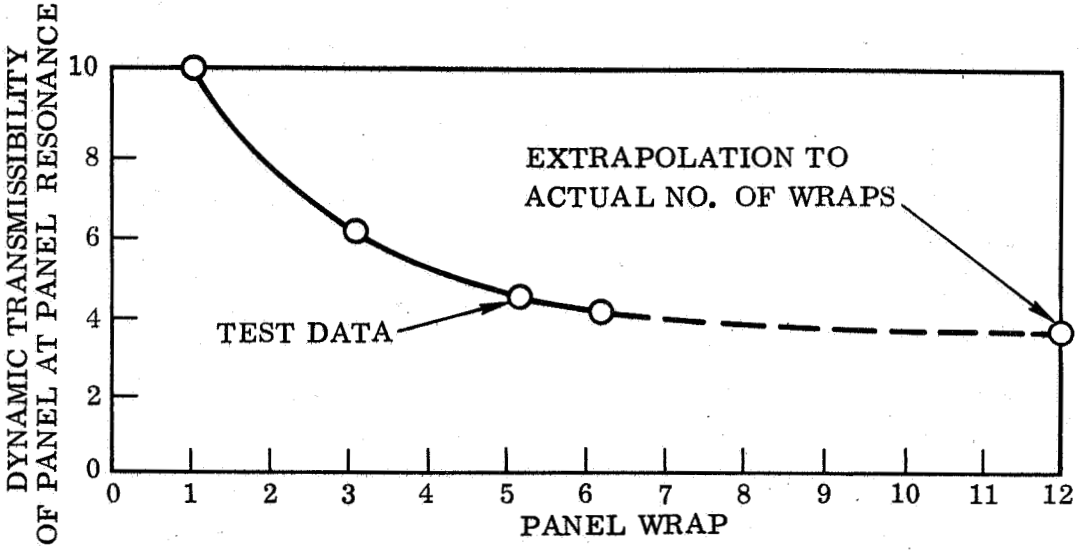

The drum and stowed panel resonances were found to be completely decoupled. The drum, in actuality is not loaded by the stowed panel motion as a beam in bending as was assumed. As a result the magnesium proposed for the drum material has sufficient stiffness and may be reduced in thickness to save weight (0.025 from 0.032 inch).

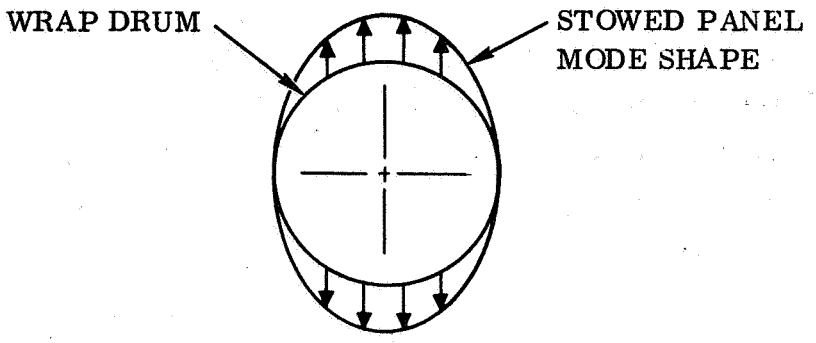

CRITICAL RESONANCE
(STOWED PANEL ELLIPTIC
MODE SHAPE)

A monitor of the stowed panel wraps at the maximum deflection mode shape (30 Hz) showed that all wraps were vibrating in phase, and that at lower excitation levels the mode was radial in shape, changing to the elliptic shape (more critical shape) at forcing excitations above 1g (Pk); there was no other change, with the exception of a reduction in panel transmissibility (from 8.6 to 4) at the 4g (Pk) excitation. The maximum stowed panel deflection was 0.20 inch at the 30 Hz mode, which is within the 0.25 inch limit set by Ryan in the design.

The tests showed that it is necessary to provide 100 percent bond area at the cells when using thin membrane type substrate material of low modulus of elasticity. No failures of the solar cell cover glass combination occurred; however, some solar cell interconnects on the matrices of each panel wrap were found broken as a result of testing. There was 108 minutes of accumulated cycle time on the inner wrap and 10 minutes on the outer wrap.

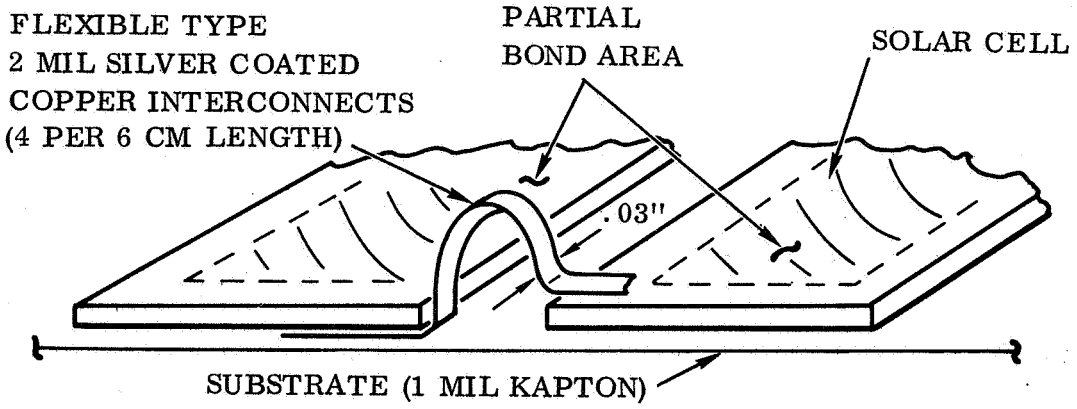

CROSS-SECTION OF SOLAR CELLS SHOWING AREA OF DAMAGE OF INTERCONNECTS

2.6.4 Solar Cell Interconnect Vibration Evaluation Tests

This section discusses the sinusoidal vibration evaluation test program which was conducted to determine a suitable solar cell interconnect compatible for use with a thin membrane substrate.

Purpose of Test

To find the best interconnect and bond method (partial or 100 percent bond area) which is compatible with sinusoidal loading under conditions simulating that which occurred during the full size drum vibration test, where the deflection was 0.2 inch single amplitude measured at the outer wrap in the plane of vibration at the elliptic mode.

Specimen Configurations for Evaluation

Configuration	Description
1	2 x 6 cm (14 mil) cell with copper flexible interconnects (4 per 6 cm length) with cell bond area in the center of cell only.
2	2 x 2 cm (12 mil cell and 3 mil cover) with copper flexible interconnects (12 per 6 cm length) with cell bond area in center of cell only.
3	2 x 6 cm cell with Molybdenum flexible interconnects (4 per 6 cm length) with 100 percent cell bond area.
4	2 x 6 cm cell with copper flexible interconnects (4 per 6 cm length) with 100 percent cell bond area.

Configuration	Description
5	2 x 6 cm cell with copper flexible interconnects (12 per 6 cm length) with 100 percent cell bond area.

Each specimen had a wired solar cell matrix (6 x 10) bonded at the center of an 8-1/2" x 10-1/2" 1-mil Kapton substrate with dummy chips covering the balance of the substrate area.

Test Setup

The specimen was draped to simulate the wrapped conditions over a six-inch radius rigid aluminum cylindrical half-section fixture. The fixture had 0.75 inch diameter x 0.15 inch thick damping pads on 1.9 inch centers attached to its surface. The specimen was clamped at its two ends to the fixture as shown in Figure 39. The fixture was mounted to a sine wave vibration exciter and the specimen response accelerations monitored using a miniature accelerometer attached to the solar cell coverglass at the center of the specimen in the plane of excitation. Input excitation levels were controlled from an accelerometer mounted to the fixture in the plane of excitation. Each specimen was mass loaded, to give the desired amount of force in the specimen when driven at 18g response at a frequency of 20 Hz. This characterized a loading distribution similar to that obtained during vibration test of the full size drum.

Test Results

The interconnect failure rate is plotted in Figure 40.

Specimen Configuration	Weight lbs/ft^2	Remarks
1 - Poorest	0.2390	Not enough interconnects with small bond area.

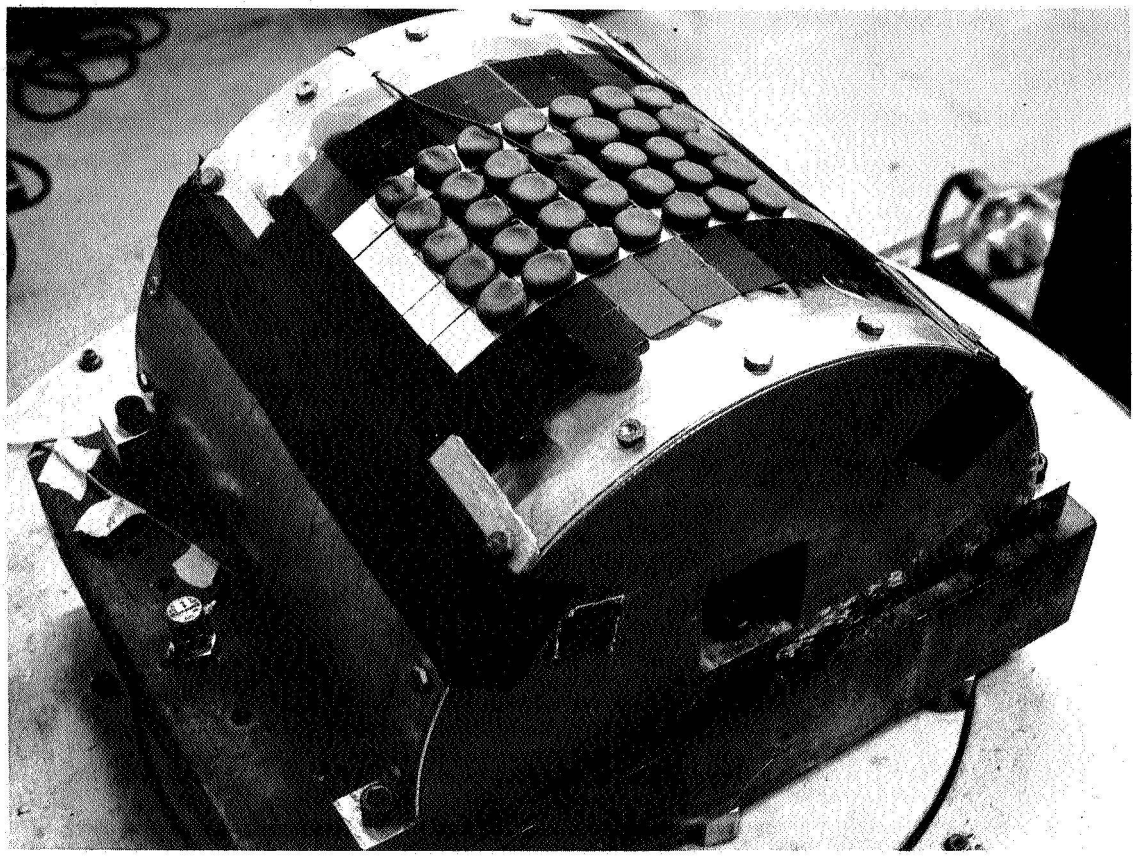

Figure 39 Test Specimen Mounted To Vibration Fixture

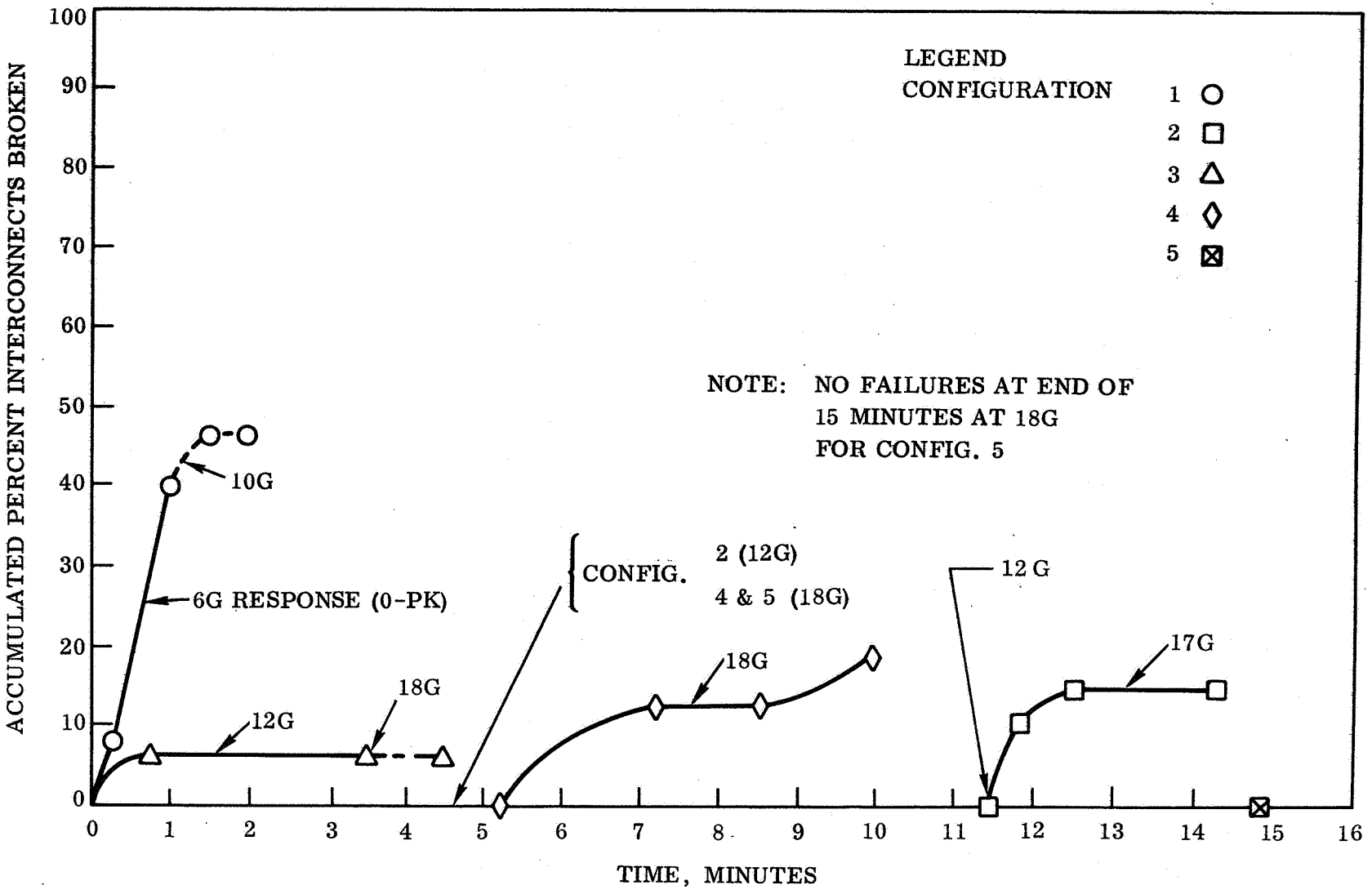

Figure 40 Failure Rate History of Solar Cell Interconnect Configurations

Specimen Configuration	Weight lbs/ft^2	Remarks
2 - Better than No. 1	0.2322	Greater number of interconnects affected results with respect to No. 1.
3 - Better than No. 2	0.2221	Either larger bond or different interconnect material affected results with respect to No. 2.
4 - Better than No. 3	0.2322	Larger bond area is better. Copper interconnect seems to be better.
5 - Best	0.2659	Larger bond area with greater number of copper flexible interconnects is best. No failure at 15 minutes and 18g.

The above listed weights should be considered as relative, only, because the solar cells used were thicker than 8 mil, in which case the weight should have been about 0.174 pound/square foot using 3 mil covers. The breakdown however, does show consistency in weight, regardless of interconnect configuration.

The radial force at 18g response for the specimens is calculated as:

$$(\text{lbs/ft}^2)\ (\text{g response}) = (1.61)\ (18) = 29\ \text{lbs/ft}^2$$

which approximates the 31 pounds/square foot loading at the solar cells on the outer wrap of the full size test drum.

Conclusions

The configurations which satisfactorily passed the evaluation test were No. 4 and 5. The desirable configuration characteristics are:

- 100 percent solar cell bond area

- flexible interconnects
- 2 mil copper interconnect material
- 12 interconnects per each 6 cm cell length.

2.6.5 Panel Axial Loads - Launch Environment

The severity of axial vibration and its effect on proper deployment was shown by the test performed on the 50-square foot rollup panel. In the 30-watts/pound array intermittently spaced fence brackets are installed at either end of the wrap drum to restain the axial motion of the panel and beams when the drum is excited along its major axis. The calculated force at each bracket induced by the substrate is approximately 10 pounds limit, Reference 2.

A static load test of a wrapped beam section was conducted to verify the capability of the substrate attachment tabs, the retaining brackets, and the flattened beam to withstand the calculated design loads. The design load was applied without failure (see Figure 41).

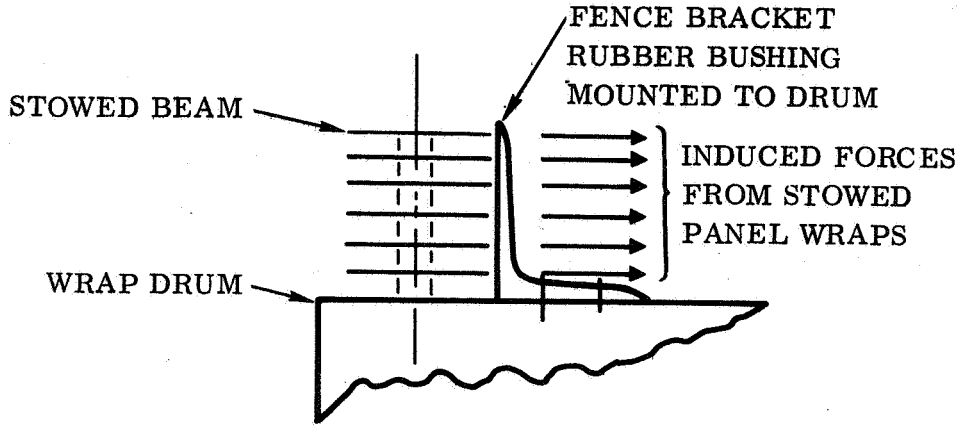

Figure 41 Fence Bracket

2.6.6 Adhesive Evaluations - Environmental

An evaluation of various adhesive systems for solar cells was performed to measure compliance of these systems with paragraph 3.3.1c of JPL Specification SS501407A. The purpose of the test was to establish whether (a) adhesive properties suffered any appreciable degradation when thermal cycled in a high vacuum and (b) the adhesives showed an appreciable weight loss after being subjected to high and low temperature extremes in a high vacuum.

Tests were conducted on the following adhesives:

RTV 602	RTV 41
Sylgard 182	RTV 511
Siliastic 140	RTV 577
Schjeldahl GT-100	RTV 3145

Samples were prepared by casting a controlled thickness of adhesive between two cylindrical bars suitable for tension test. Specimen preparation is described in detail in Reference 1.

Each sample was weighed and numbered before test and the weight recorded from an analytical balance. One control sample was then selected from each group of three adhesive samples and withheld from thermal vacuum. The remaining samples were subjected to ten cycles from -195°C to 140°C at 1×10^{-6} torr, with a 90 minute cycle and temperature stabilization dwell at the extreme temperatures.

When thermal vacuum testing was complete, samples were re-weighed and a tensile test was then conducted on the samples to check any degradation in adhesvie strength.

Stress strain curves were plotted for each of the test samples after the thermal vacuum tests. The curves of similar samples were compared for any gross deviations (±10 percent) from the control samples. Any deviation in excess of 10 percent would indicate a severe degradation in the adhesive.

None of the samples, with the exception of the Schjeldahl GT-100, showed any appreciable degradation due to thermal cycling in a vacuum.

Table 8 sumarizes the test results. Test details are reported in References 1 and 3. Test results for RTV 602, Sylgard 182 and Silastic 140 were inconclusive due to sample damage and have therefore been omitted from this summary.

TABLE 8

EFFECT OF THERMAL VACUUM ON ADHESIVES

(10 Cycles From -195°C to 140°C at 10^{-6} Torr)

Material	Weight Loss Percent	Tensile Strength Change Percent
RTV 577	1.2	-5.3
RTV 511	0.4	+15.0
RTV 41	0.3	+4.8
RTV 3145	0.3	-3.0
Silastic 140	0.2	-8.5

2.6.7 Adhesive Bonding Tests

Screening tests were conducted on Kapton bonding using various epoxy, silicone and polymide adhesives (Reference 1).

Solar cell bonding was evaluated by performing peel tests. Kapton splicing was evaluated by performing lap shear and peel tests. Adhesives tested included RTV 41, RTV 511, and RTV 3145 for solar cell bonding. Kapton splicing adhesives tested were FM 1044R, Narmco 225, FM 964, TR-150-25 and Narmco 329.

The results of these tests indicated that the best flexible adhesive systems were RTV 3145 for cell bonding and FM 1044R for Kapton splicing.

The test results of several adhesives are summarized in the following table. Detailed test procedures and results are presented in Reference 1.

	Adhesive	Primer	Peel Strength psi	Shear Strength psi
Kapton to Solar Cell	RTV 411	SS4044	2.7	---
Kapton to Solar Cell	RTV 511	SS4004	1.4	---
Kapton to Solar Cell	RTV 3145 (cells only)	1200	3.5	---
Kapton to Kapton	FM 1044R	---	2.3	>109*
Kapton to Kapton	TR-150-25	---	---	141
Kapton to Kapton	Narmco 329	---	0.2	> 92*

*Kapton film failed in tension

2.6.8 Substrate Edge Attachment

Tests were conducted to measure joint strength and failure modes of the beam to substrate edge attachment. Tests on rigid metal connectors and flexible silicone rubber coated glass cloth were conducted (References 1 and 3). Results of the flexible tab tests indicated that a shear strength of 138 psi was obtained in glass fiber to titanium bonds using RTV 3145 and 1200 primer on the mating surfaces.

Additional tensile shear strength tests were performed using woven glass fiber tapes bonded to Kapton with RTV 3145. Test results are presented on the following page:

TENSILE SHEAR STRENGTH OF GLASS FABRIC TO KAPTON BONDS WITH RTV 3145

Material	Primer	Shear Strength (psi)	Failure Mode
Tape 4538-S910 (Carolina)*	None	50	To Kapton
Tape 4538-S910 (Carolina)	90-198 (Kapton)	55	To Kapton
Tape 4538-S910 (Carolina)	1200 (Kapton)	49	To Kapton
Tape 138 (Fiber Mfg. Co.)*	None	25	To Kapton
Tape 138 (Fiber Mfg. Co.)	90-198 (Kapton)	47	To Kapton
Tape 138 (Fiber Mfg. Co.)	1200 (Kapton)	53	To Kapton

*Tape dimensions 1.0 inch wide x 0.003 inch

The tests indicate that a suitable edge attachment can be made using glass fiber tape. The design selected uses a flexible glass fiber woven tape 1.0 inch wide by 0.003 inch thick bonded to the titanium beam and Kapton substrate with RTV 3145.

2.6.9 Plating Method for Aluminum Bus Bar

The design of the array requires electrical connections to be made to the aluminum bus by soldering. A silver clad aluminum foil had been previously considered. However, it would be desirable to provide a silver plated surface, only in the areas to be soldered. The surface should be capable of soldering and desoldering so that rework can be performed if required.

Test samples consisting of a sheet of aluminum bonded between two sheets of Kapton were prepared with slots two inches long by 1/4-inch wide, provided in the Kapton. The aluminum connection areas, were brush-plated using Selectron No. 2 Activator, Selectron acid high speed copper and Selectron silver plating solution. Copper foil strips, 1/8-inch wide by 0.0015-inch thick were soldered to the plated surface using Kester 1544 flux and SN-53 solder. The strips were desoldered and soldered again, as noted, and pull tests performed as shown in Table 9.

TABLE 9

PEEL STRENGTH OF PLATED ALUMINUM FOIL SOLDER CONNECTIONS

Specimen	Plating Process	Solder/Desolder Cycles	Peel Strength (lbs/in. width)	Failure Mode
1	Activator/silver	1	4.5	Silver-aluminum separation
2	Activator/silver	1	4.9	Silver-aluminum separation
3	Activator/silver	5	2.1	Silver-aluminum separation
4	Activator/copper/ silver	1	5.3	Copper-aluminum separation
5	Activator/copper/ silver	1	6.8	Copper-aluminum separation
6	Activator/copper/ silver	5	3.1	Aluminum tore
7	Activator/copper/ silver	5	3.6	Copper-aluminum separation

The tests indicate either of the two plating systems provide acceptable adhesion. The Activator/copper/silver system is preferred.

2.6.10 Solar Cell Interconnection Test

This test was conducted to measure the effect of thermocyling one hundred times from -148°F to +168°F with a temperature gradient of 54°F/minute on the following bus bar materials:

a. Aluminum with copper flash and silver plate

b. Aluminum with nickel flash and silver plate

c. Copper with silver plate

d. Molybdenum (silver clad)

Physical investigation included discoloration, fatiguing, and separation of solder joints from the solar cell.

All cells used were bar contact 2 x 6 cm. Molybdenum and aluminum with copper and silver plating modules used six cells. The copper with silver plate modules used four cells. The aluminum with nickel and silver plating used eight cells.

The modules were placed on three shelves with Kapton tape in the test chamber.

Three modules were placed in the chamber; molybdenum was added at the 50th cycle. One-hundred cycles were run from +168°F to -148°F with a minumum temperature gradient of 54°F per minute between hot and cold stabilization. Once stability of the chamber occurred, thermocouples were given a five-minute stabilization time. When stabilization was completed temperature was held for an additional one minute for the timed soak period. All modules, upon the completion of each ten cycles, were removed from the chamber and inspected for any discrepancies, as described before. This procedure was carried out for one-hundred (100) cycles (fifty for molybdenum) at which time the test was complete.

The bus bar assemblies were inspected under a thirty (30) power stereomicroscope for discoloration, buckling and various other visible problems mentioned earlier.

Each solder connection between cell and bus bar was pried, under magnification, to observe any sign of brittling or separation. When inspection was complete the modules were replaced in the chamber.

Results

Of the four modules tested degradation was evident in three. The two aluminum bus bar samples; i.e., with nickel and silver plate, and copper and silver plate, showed a tendency to stretch and wrinkle slightly over one-hundred cycles. The molybdenum showed signs of severe discoloration on two of the

six bus bars, after forty cycles. Further investigation, however, revealed this to be an oxidation of the silver plating. The copper with silver plate bus bas showed virtually no sign of any degradation.

Several broken tabs and a few cracks were noted at the cell junction. This, however, can be attributed to fatigue from handling, as it was practically impossible to remove and replace without bending slightly. No solder failures were noted.

The tests indicate that copper with silver plate would provide an acceptable interconnect. However, further thermal vacuum testing with 2 cm x 2 cm solar cells bonded to Kapton substrate must be conducted to verify the selection of copper interconnects.

A previous test program indicated that the silver-clad molybdenum was capable of withstanding temperature gradients far in excess of the 54°F per minute. The principal problem associated with molybdenum is the difficulty of obtaining vendors capable of plating molybdenum. This problem could have a profound influence on any large program with an accelerated delivery schedule.

2.7 MODEL DESCRIPTION

The full size deployment model has been designed and constructed to incorporate all significant features of the subsolar array design. Figures 42, 43, 44, 45, and 46 are photographs of the model with the substrate retracted, partially deployed horizontal, fully deployed horizontal, partially deployed vertical and fully deployed vertical. The major elements of the model are as follows:

Wrap Drum

The wrap drum is full size, fabricated from 0.032 gage magnesium skin and supported internally with three "Z" section rings. The drum skin is perforated with flanged lightening holes to minimize the weight. The end bulkheads are made from a plywood sandwich with titanium skins designed to be dynamically similar to the actual array bulkheads.

Drum/Beam Support Structure

The drum support structure is machined from aluminum extrusions and provides the support track for the drum-axle mounted teflon slide. The machined sections are riveted to aluminum sheet metal box sections which serve as the mounting for the teflon beam guides and for the deployment motor, pinion gear and drive shaft.

Substrate Assembly

The substrate assembly consists of thirteen 37 x 38-inch subpanels made from one mil Kapton H film. The panels are attached to the titanium support beams with 1.0 inch wide fiberglass tabs spaced at approximately 4.0 inches. The tabs are bonded to the Kapton and to the beams with RTV-3145 adhesive. The panels are interconnected with the fiberglass tabs at approximately 4.0-inch spacing. Scored styrofoam sheets are bonded to each of the thirteen panels to simulate the solar cells.

Polyurethane pads and simulated transverse and longitudinal bussing are incorporated to represent the actual solar panel installation.

The deployment beams are full size 3 mil 1.7-inch diameter 6Al-4V titanium and were fabricated by welding two 18-foot sections and a 7-foot section together to achieve the 43-foot total length. The corrugated drive strip was made from commercial pure titanium and welded to the beams prior to forming and assembly.

Deployment System

The deployment system as presented by the model is functionally identical to the system proposed for the solar array. The system consists of a deployment motor mounted to one of two pinion gears. The gears engage the corrugated drive strips attached to the deployment beams. The gears are connected by a torque shaft which synchronizes the deployment rate of the beams and solar panel.

A second motor is mounted on the drum-axle slide and provides the power for retracting the solar panel.

During the deployment cycle the gear mounted motor supplies power to the rack and pinion system which extracts the beams and substrate from the wrap drum. The retraction motor provides a dragging torque to maintain uniform deployment and tight beam wraps on the drum. Retraction of the solar panel is accomplished by supplying power to the retraction motor. During this cycle of extension motor supplies a dragging torque to insure proper wrapping of the beams and substrate on the drum.

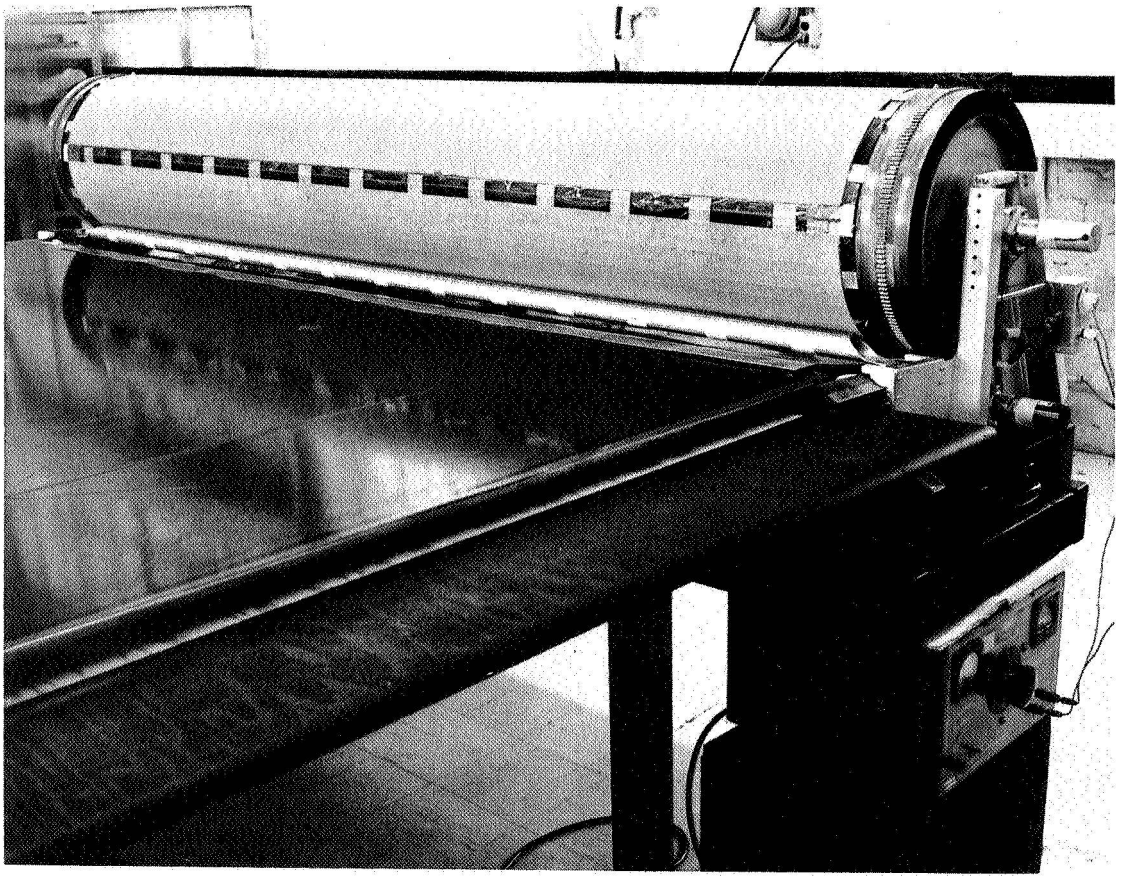

Figure 42 Full Scale Model - Substrate Retracted

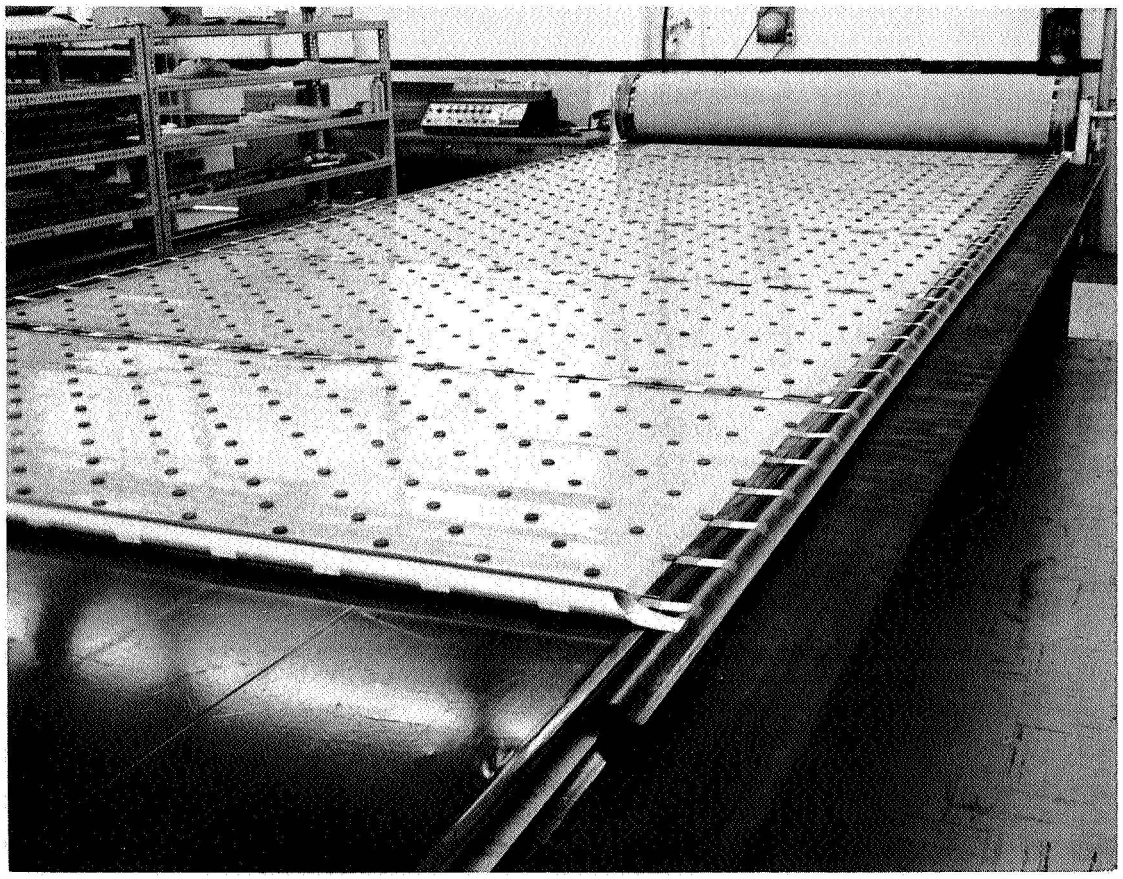

Figure 43 Full Scale Model - Partially Deployed, Horizontal

Figure 44 Full Scale Model - Fully Deployed, Horizontal

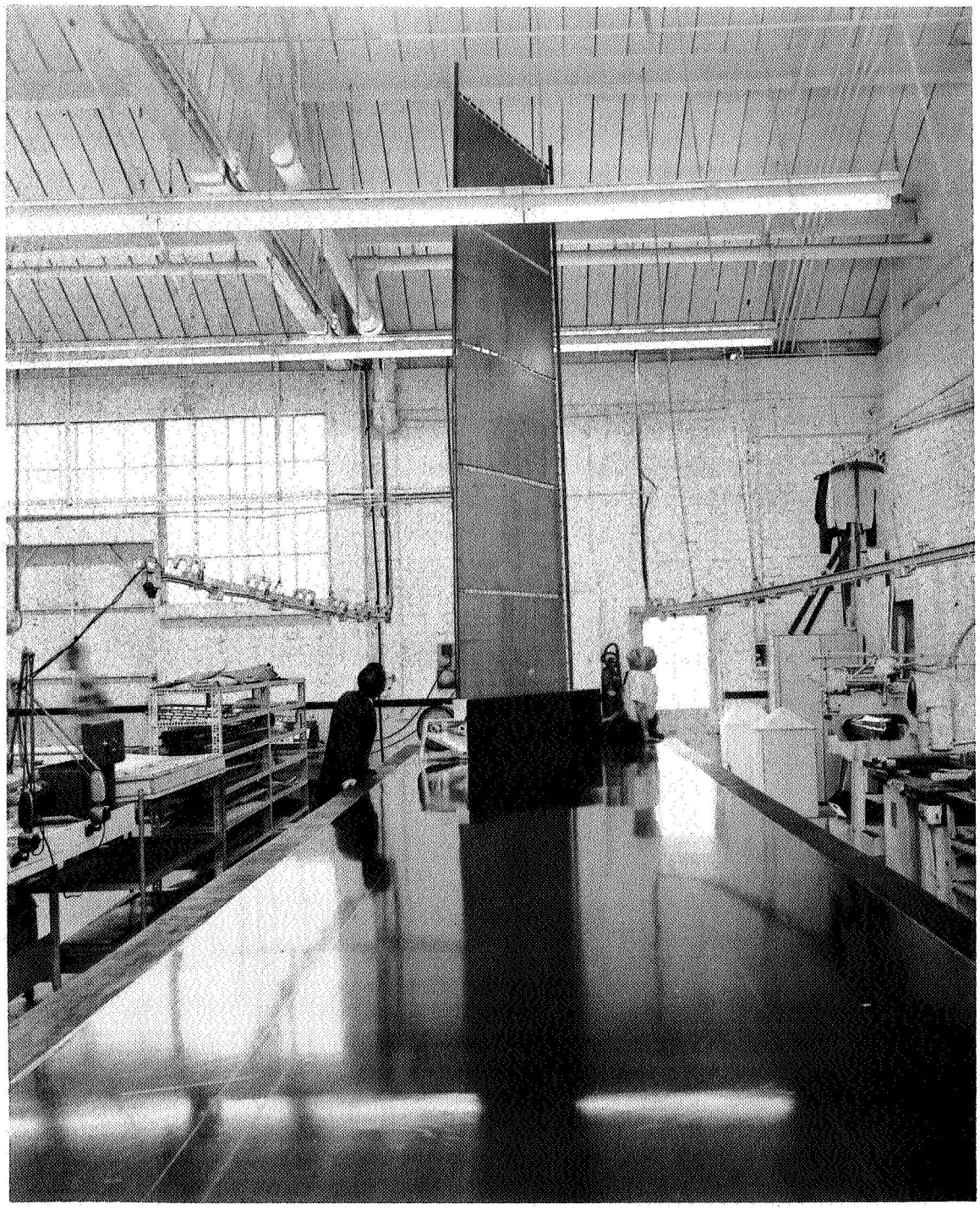

Figure 45 Full Scale Model - Partially Deployed, Vertical

Figure 46 Full Scale Model - Fully Deployed, Vertical

3.0 CONCLUSIONS

The results of the Phase I program show that technology is currently available which will permit the development of a 250-square foot flight-type array in the immediate future. It has been shown that the manufacturing processes are feasible, repair and replacement of damaged components may be readily achieved, handling, transportation and product test support equipment is straight forward and that the design goal of 30-watts per pound can be achieved. This conclusion is based not only on the results of the design and analytical studies performed but also upon parallel experience with the 50-square foot rollout panel, component development testing and the development of the 30-watts/pound full scale model.

The studies were conducted in depth and included analyses of dynamic properties, loads, stress, weights, thermal effects, electrical performance and reliability. Additionally, engineering drawings were evolved which define the final assembly, subassemblies and each component in detail.

Both the design and the analytical effort made direct use of experience obtained from the 50-square foot rollout panel, resulting in improvements to details of the concept and elimination of problem areas. Some of the important applications of this related experience are found in the:

- Development of a positive, synchronized system for extending and retracting the beams.

- Development of a substrate to beam attachment which provides improved flexibility.

- Development of a means to prevent excessive axial movement of the beams and substrate under launch vibration conditions.

- Incorporation of a thermal control system to eliminate excessive loads due to differential expansion/contraction.

- Determination of the required rigidity of the array to spacecraft mounts.

Verification testing accomplished on components for the 250-square foot array has established confidence in the analytical and design approach. A broad range of items were tested extending from simple material specimens to a full scale drum with a dynamically similar solar panel.

A realistic calculated weight has been established. The calculated weight is based upon a detailed weight breakdown derived from the engineering drawings which accurately define the geometry and materials of the components. All critical components shown on the drawings were substantiated by stress analysis.

Proof of principle has been shown through the operation of the full scale model. This model has incorporated the features depicted in the proposed design and cycling of the system has demonstrated repeatable, trouble free operation. The model has shown the feasibility of manufacture through the incorporation of Kapton substrates and deployable beams with integral corrugated drive strips. Both of these items are of gauge, size and configuration expected to be used in prototype solar array. Other components of the system are considered conventional from the standpoint of fabrication and assembly.

4.0 RECOMMENDATIONS

The Phase I program has substantiated the practicability of a 30-watt per pound solar array in the 10.0 kw size range.

Results of the study justify the implementation of Phase II of the 30-watts/ pound program. While refinement of design detail would be anticipated during Phase II, no basic change to the concept is expected.

5.0 NEW TECHNOLOGY

One item of a "New Technology" nature was identified in the performance of this contract. That is,

Descriptive Title --

The Application of Ultra Thin Solar Cell Coverslides

Names of Innovators --

Robert Oliver

Edward Zimmerman

Progress Report Disclosure --

General description given in the Second Quarterly Report, Ryan Report No. 40067-2, dated 15 January 1968, Feasibility Study, 30-Watts Per Pound Rollup Solar Array, Contract No. 951971.

Page Reference to Disclosure --

Initial disclosure found on page 22 of the report.

Disclosure Data --

A new technology report was submitted to NASA-JPL, 5 March 1968.

6.0 REFERENCES

1. First Quarterly Report on the Feasibility Study, 30-Watts Per Pound, Rollup Solar Array, Report 40067-1, Ryan Aeronautical Company, 10 November 1967.

2. Second Quarterly Report on the Feasibility Study, 30-Watts Per Pound, Rollup Solar Array, Report No. 40067-2, Ryan Aeronautical Company, 15 January 1968.

3. Third Quarterly Report on the Feasibility Study, 30-Watts Per Pound, Rollup Solar Array, Report 40067-3, Ryan Aeronautical Company, 15 April 1968.

4. System Specification No. SS501407A, Rollup Solar Cell Array, 30-Watts Per Pound, Detail Requirements for, Jet Propulsion Laboratory, California Institute of Technology, 4 January 1967.

5. California Institute of Technology, Jet Propulsion Laboratory, Contract No. 951107, dated 14 May 1965, titled, Development, Design and Fabrication of a Prototype Deployable Large Area Solar Array Supporting Structure; Ryan Concept Model No. 208.

6. E. L. Ralph, Performance of Very Thin Silicon Solar Cells, Heliotek, Division of Textron Electronics, Inc., Presented at 6th Photovoltaic Specialists Conference, Cocoa Beach, Florida, 28-31 March 1967.

7. Spacecraft Materials Guidebook, Jet Propulsion Laboratory, California Institute of Technology, Pasadena, California.

8. Goetzel, Rittenhouse and Singletary, Space Materials Handbook, Lockheed Missile and Space Company, Addision-Wesley Publishing Company, Palo Alto, California, 1965.

9. S. P. Timoshenko and S. Woinowsky-Krieger, Theory of Plates and Shells, Second Edition, McGraw-Hill Book Company, New York, 1959.

10. Roark, R. J., Formulas for Stress and Strain, McGraw-Hill Book Company, Inc., New York, N. Y., 1954.

11. D. J. Peery, Aircraft Structures, McGraw Hill Book Company, New York, 1949.

12. MIL-HDBK-5A, Metallic Materials and Elements for Flight Vehicle Structures, Department of Defense, Washington 25, D.C., 8 February 1966.

13. S. P. Timoshenko, Vibration Problems in Engineering, Third Edition, D. Van Nostrand Company, Inc., Princeton, New Jersey, September 1961.

14. E. F. Bruhn, Analysis and Design of Flight Vehicle Structures, Tri-State Offset Company, Cincinnati, Ohio.

15. Hi-Shear Corporation Standards Manual, High Strength and High Temperature Fasteners for the Aero-Space Industries, Torrance, California.

16. Lockheed Structures Manual, Stress Memo No. 110, May 1954.

7.0 APPENDIX

7.1 STRESS ANALYSIS

Stresses and resulting safety margins presented in this section are for the more critical of the design load environments given in the JPL Specification. The analysis that has been conducted includes all the primary weight contributing structural components of the rollup panel and its relatively large in scope to give a significant degree of confidence to the calculated weights in Section 7.3 and the resulting watts/pound capability given in Section 2.5.4. The work presented supersedes that given in Quarterly Reports since drum axis induced loads are now reacted at only one of the panel spacecraft mounts; this is a result of the incorporation of spacecraft interface thermal slip joint at the other spacecraft mount. The analysis is based on loads derived using a more realistic electrical installation weight of 0.165 pounds/square foot, whereas earlier analysis assumed a more conservative weight of 0.19 pounds/square foot.

Loads, buckling allowables, and section properties are based on nominal sheet thicknesses. Dynamic loads are treated as static loads. Some conservation is introduced into the design by using dynamic (0 to Pk) load values rather than rms values. Elastic buckling of any one element of a composite cross section is treated as an ultimate failure under dynamic conditions to assure that fatigue due to "oil canning" action will be eliminated. Design loads, used for analysis and derived from limit acceleration given in the JPL Specification, were compared to material yield and ultimate allowables as follows:

Yields allowable $\geq$ design limit load

Ultimate allowable $\geq$ 1.25 design limit load.

Considerations for reliability, fabrication, handling and cost have in some cases taken precedence over design loads and have resulted in high margins of safety.

A summary of the lower margins of safety for the basic components analyzed is presented in Table 10.

7.1.1 Wrap Drum Spindle

The final drum-spindle and end plate configuration incorporates the design of a drum axial direction slip joint. Thus at the slip joint end of the drum there is no axial load, all the axial load being taken out at the fixed end. This configuration means that the loads at the fixed end have increased, and the stress analysis given in Reference 3 has been modified to reflect that change in loading. The design change resulted in increasing the stiffness of the fixed end structure while decreasing the structural stiffness at the slide end. The actual stress levels were conservative, since the drum was designed for dynamic stiffness. Also, the stress analysis does not reflect any addition of loadings due to dynamic excitation occurring simultaneously in the three principal (orthogonal) axis directions. Allowable stress levels were based upon allowable cyclic stresses for 10^5 cycles for the material used, and as such was considered to be the limit stress allowable. The cyclic stress was considered to be completely reversible. At 200 cps this would be equivalent of 8.33 minutes $[10^5/200(6)]$ at resonant condition. However, since stress margins were low, the actual time would be increases considerably. On the basis of the above stress allowables for limit loads, ultimate margins were considered to be less critical in all cases.

The stress analysis of the drum spindle mounting follows. The schematic loads on the drum end support structure is shown in Figure 47.

$P'_x = P'_y = 359$ lb. Ref: p. 7.1-7

$P_{p/t} = 30$ lb. in P_y direction $W = 65.0$ lb.

$P_{ax} = aQ\, W_{dr} = (4.0)(5.0)(65.0) = 1300$ lbs.

All of the axial load is taken in one end. The auxiliary drive has been eliminated and the pre-tension spring has been placed along the Y axis.

Table 10 Summary of Stress Margins of Safety

COMPONENT	TYPE LOAD (DYN)	CRITICAL LOADING ELEMENT	MARGIN OF SAFETY	ALLOWABLE BASIS
Wrap Drum Hub				
a. Fixed End	P_{axial}	Flange Bending	0.75	Fatigue Limit
b. Slide End	Moment	Flange Bending	0.20	Fatigue Limit
End Plate - Wrap Drum				
a. Fixed End	P_{axial}	Inner Hub	High	Fatigue Limit
b. Slide End	Moment	Inner Hub	High	Fatigue Limit
Wrap Drum	P_{axial}	Drum crippling, fixed end	0.30	Crippling Ult.
Spacecraft Mount	Combined	Skin Crippling	High	Crippling Ult.
Guide Sleeve and Drum Mount Fitting	Combined	Flange Bending	0.37	Fatigue Limit
Tip Intercostal	1 g field Demo.	Beam Column Crippling	0.18	Crippling Ult.
Deployment Beams	In-Space Accel.	Beam Bending Crippling	High	Crippling Ult.

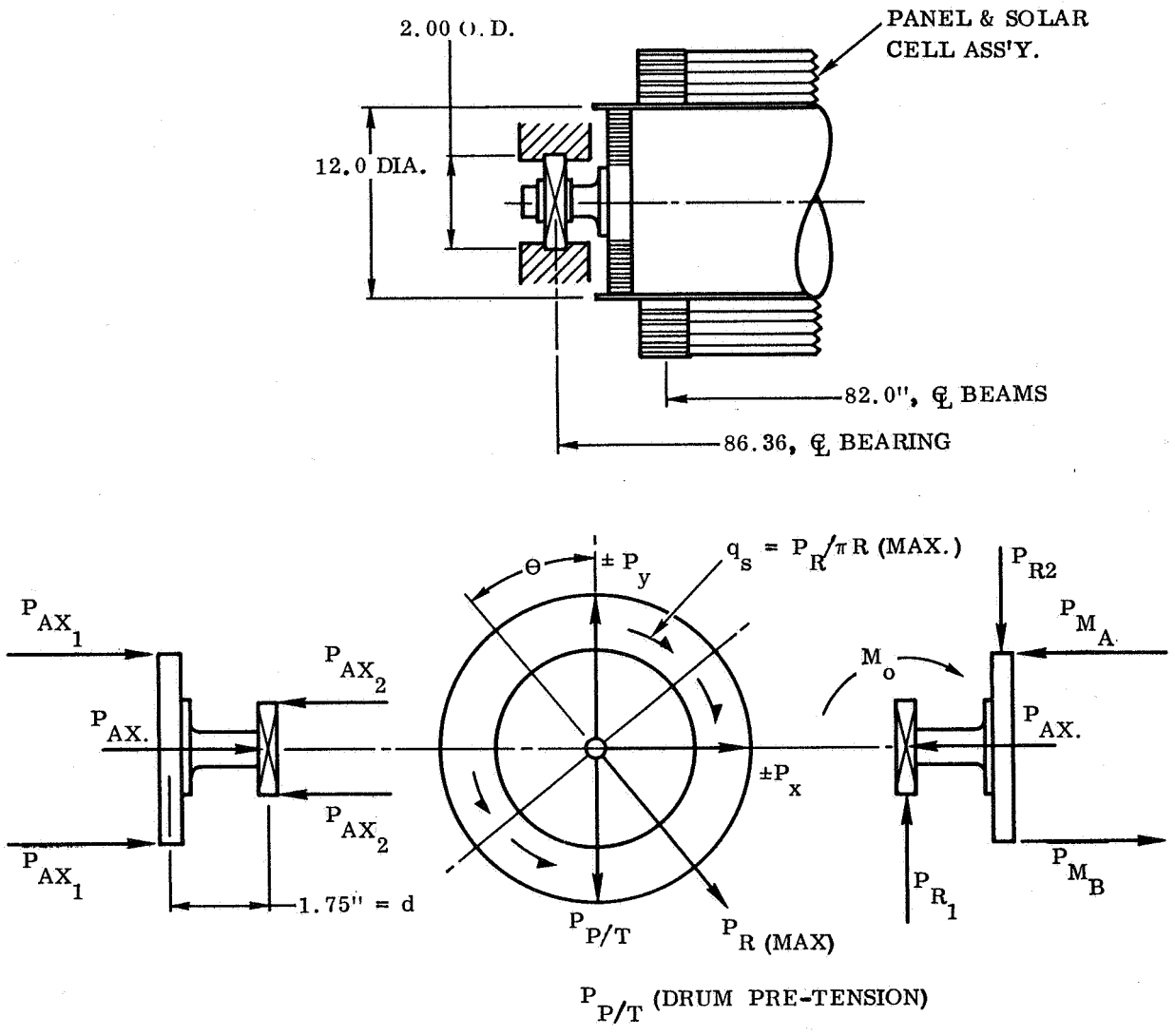

Figure 47 Loads - Drum End Support

$P_x = P' = 359$ lb.

$P_y = P'_y + P_{p/t} = 359 + 30 = 389$ lb.

$P_r = P_x \mapsto P_y = 359 \mapsto 389 = 529.34$ lb.

$\text{Tan } \theta = P_x/P_y = 359/389 = 0.92289$

$\theta = 42° \; 42.22'$

$q_s = P_r/\pi R = 529.34/6\pi = 28.08$ lb/in

Dynamics - End Reactions - Uniformly Distribted Load

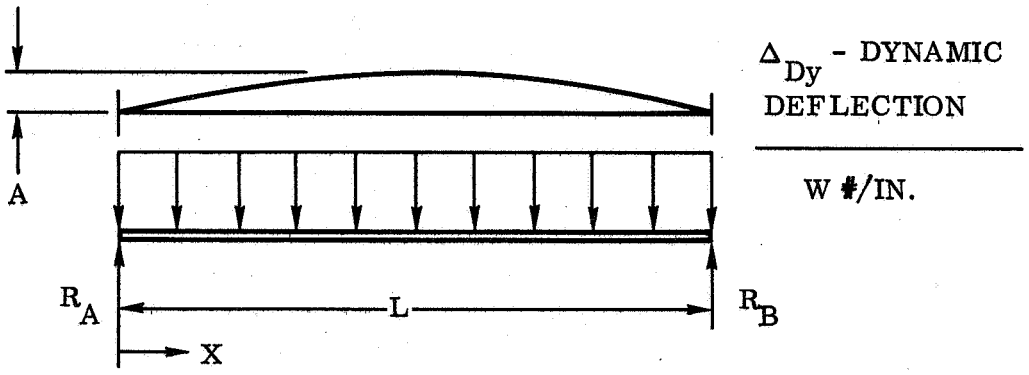

$\Delta_{Dyn} = A \; (\text{Sin } px) \; (\text{Sin } \omega t)$ (Ref: 13,p. 324)

$Q = (T.R.^2 - 1)^{\frac{1}{2}}$

T.R. = transmissibility (force)

Q = Dynamic amplification (deflection)

a = dynamic input G's

At centerline of beam (x = L/2)

$\Delta_{Dyn} = (aQ)\ \Delta_{st}$ (assumed for dampened beam)

$pL = \pi, 2\pi, 3\pi \ldots$

$\text{Sin } pL = \text{Sin } \pi = 1.0$

$\Delta_{Dyn} = A\ (\text{Sin } pL)\ (\text{Sin } \omega t) = A \qquad (\omega t = \pi/2)$

$A = (aQ)\ \Delta_{st} \sim \Delta_o$

$\Delta_{st} = 5WL^4/384\ EI$

$R_A = R_B = F/2$

$\dot{\Delta}_{Dyn} = (aQ'\Delta_{st})\ (\text{Sin } pn)\ (\text{Sin } \omega t) \ldots$

$\ddot{\Delta} = (aQ\Delta_{st})\ (\text{Sin } px)\ \omega^2\ (\text{sin } \omega t) = d^2\Delta/dx^2$

$dF = dM\ (A_{cc}) = -\ (W\ dx/g)\ (aQ\omega^2\Delta_{st})\ \text{Sin } px\ \text{Sin } \omega t$

(A_{cc} = acceleration, $\ddot{\Delta} = d^2\Delta/dx^2$)

$$F = -\ (W\ aQ\omega^2\Delta_{ST}/g)\int_o^L \text{Sin } pn\ \text{Sin } \omega t\ dx$$

For fundamental mode $pL = \pi \ldots$

$$F = -\ (W\ aQ\omega^2\Delta_{ST}/g)\int_o^{\pi} \text{Sin } px\ \text{Sin } \omega t\ dx$$

$$F = -\ (WaQ\omega^2\Delta_{ST}/g)\left[-\text{Cos } px\ \text{Sin } \omega t/P\right]_o^{\pi}$$

Disregarding periodic function, $\text{Sin } \omega t = 1$ (max)

$F = (WaQ\omega^2\Delta_{ST}/pg)\ (\text{Cos } \pi - \text{Cos } o)$

$$*F = -2waQ\omega^2\Delta_{ST}/pg \quad (1)$$

$$p = \pi/L \ , \ 2\pi/L \quad (2)$$

$$\omega^2 = (2\pi f_n)^2 = (2\pi)^2 \ (\pi/2)^2 \ (5g/384\Delta_{ST})$$

$$\omega^2 = \pi^4 \ 5g/384\Delta_{ST}$$

$$F = 2waQ \ (\pi^4 \ 5g/384\Delta_{ST}) \ \Delta_{ST}/pg$$

$$F = -10waQ\pi^4/p384 = -10wa \ (TR^2 - 1)^{\frac{1}{2}} \ \pi^4/384 \ (\pi/L)$$

$$F = \underline{-10wL(a) \ (T.R.^2 - 1)^{\frac{1}{2}} \ \pi^3/384}$$

$$R_A = R_B = \underline{F/2 = 5wL(a) \ (T.R^2 - 1)^{\frac{1}{2}} \ \pi^3/384}$$

for $W = 0.664$ lb/in and $T.R = 4.0$

$$\underline{R_A = R_B = 358.5 \text{ lbs}}$$

$$*R_A = R_B = \omega^2 \ (aQ\Delta_{ST}) \ w/(\pi/L)g$$

$$\underline{R_A = R_B = \omega^2\Delta_o wL/\pi g}$$

7.1.1.1 Hub

In the analysis of the hub, the stresses have not been combined for various directions of loadings. This is based on the assurance that the drum will not be dynamically excited in more than one direction at a time, at the maximum peak acceleration excitation.

a. Fixed End

P_{AX} = ±1300 lb. limit

P_R = ±530 lb.

n = 6 bolts

n' = 2 bolts

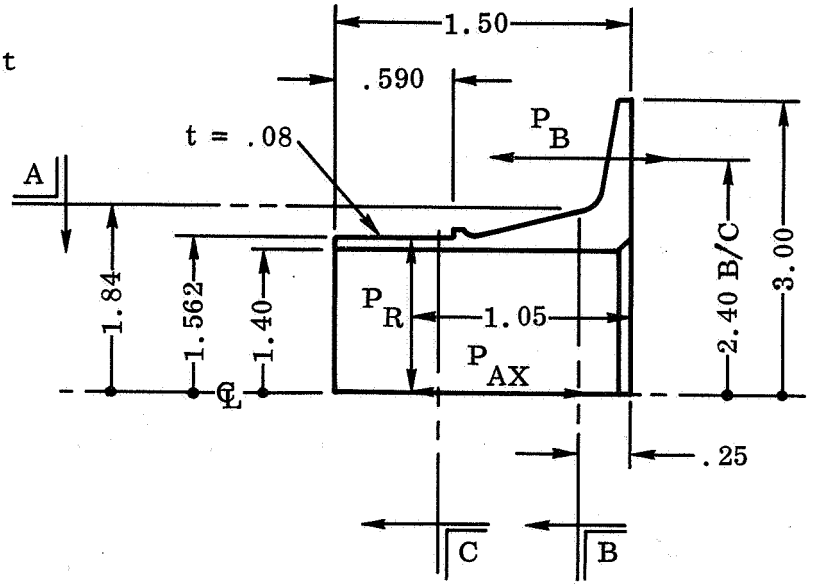

1) Axial Loading

$P_{B1} = P_{AX}/n = 1300/6$

P_{B1} = 217 lbs.

2) Lateral Loading

$P_{B2} = d_1 P_R / n' d'$

d' = 2.4 Cos 30° = 2.078 lb., d_1 = 105 in.

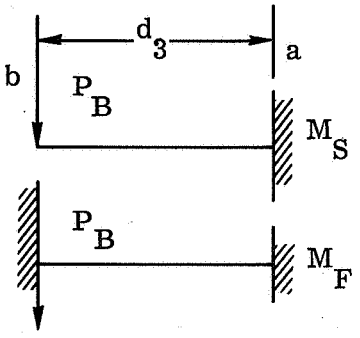

P_{B2} = 1.05 (530)/(2) (2.078)

P_{B2} = 134 lb. limit

(a) Section A-A - Flange Bending

Flange is assumed to be cantilever with 50% end fixity at load application point "b" due to bolt clamping

$d_3 = (d - d_A)/2 = (2.40 - 1.84)/2 = 0.28$ in.

$t = 0.17$ in.

$b = (1.84/2) = 0.92$ (Side 60° Δ)

$M = (M_S + M_F)/2 = (P_B d_3 + .5\ P_B d_3)/2 = 0.75\ P_B d_3$

$f_b = 6M/bt^2 = 6\ (0.75)\ P_B d_3/bt^2$

(1) $f_{b1} = 4.5\ P_{B1} d_3/bt^2 = 4.5\ (217)\ (0.28)/0.92\ (0.17^2)$

$f_{b1} = 10{,}284$ psi limit (Axial Load)

(2) $f_{b2} = 4.5\ P_{B2} d_3/bt^2 = 4.5\ (1.34)\ (0.28)/0.92\ (0.17)$

$f_{b2} = 6{,}350$ psi limit

$F'_{ty} = (0.9)\ 20{,}000 = 18{,}000$ psi, for 10^5 cycles

90% F_{ty} for 2.0 thick magnesium plate

Ref: (12) - Tables 4.2.1.0(b) and 4.3.1(c)

M.S. $= F'_{ty}/f_{b1} - 1 = 18{,}000/10{,}284 - 1 =$ <u>+0.75</u>

(b) Section B-B - Ref: p. 7.1-8

$f_t = P_B/A + C_D\ 6M/bt^2$

$t = 0.20$ in. $d_m = 1.40 + 2\ (2.0)/2 = 1.60$ in.

$A - bt = \pi d_m t/n = \pi(1.6)\ (t)/6 = .83776t = 0.16755$

$M = k\ P_B\ (d - d_m)/2 = (0.80)\ P_B\ (2.4 - 1.6)/2 = 0.32\ P_B$

k = moment end fixity factor - Ref: p. 7.1-8

C_D = moment decay factor for a tubular section. Ref: (10) - Case 11, p. 271

$C_D = e^{-\lambda x} (\text{Cos } \lambda x + \text{Sin } \lambda x)$

$X_B = 0.25$, $h = 0.20$, $r_m = d_m/2 = 0.80$, $\mu = 0.3$

$\lambda = \left[3(1 - \mu^2)/r_m h^2\right]^{1/4} = \left[3\ (0.9)/0.8\ (0.2^2)\right]^{1/4} = (84.375)^{1/4}$

$\lambda = 3.0308$

$\lambda_x = (3.0308)\ (0.25) = 0.7577$ Rad. $= 43° 24.8'$

$e^{-\lambda x} = 0.46874$

$\text{Sin } \lambda x = 0.68725$ $\qquad$ $\text{Cos } \lambda x = 0.72641$

$C_D = .46874\ (0.72641 + 0.68725) = 0.6626$

$f_t = P_B/A + C_D\ 6M/bt^2 = P_B/.16755$

$+ .6626\ (6)\ (.32\ P_B)/(.83776)\ (.2^2)$

$f_t = (5.968 + 37.964)\ P_B = 43.932\ P_B$

(1) $f_{t1} = 43.932\ P_{B1} = (43.932)\ (217)$

$f_{t1} = 9{,}533$ psi limit

(2) $f_{t2} = 43{,}932\ P_{B2} = (43.932)\ (134) = 5887$ psi limit

(c) Section C-C $t = 0.08$ Ref: p. 7.1-8

$d_m = 1.56 - 0.08 = 1.48$ in. $r_m = d_m/2 = .74$

(1) $f_t = P/A = P/\pi d_m t = P/\pi(1.48)\ (0.08) = 2.688\ P_{AX}$

$f_t = 2.688\ (1300) = 3{,}494$ psi ultimate tension for axial load

(2) $f_s = P_r/\pi r_m t = P_r/\pi\ (.74)\ (.08) = 5.377\ P_R$

$f_s = 5.377\ (530) = 2850$ psi limit

The above hub was designed for a high dynamic rigidity, although stress margins are conservative.

b. Hub - Slide End

$P_R = \pm 530$ $P_{AX} = 0$ Equations for fixed-end are applicable

1) Section A-A $t = 0.12$

$f_b = 4.5\ P_{B2}\ d_3/bt^2 = (4.5)\ (134)\ (.33)/.92\ (.12^2)$

$f_{b2} = 15{,}020$ psi limit

$d_3 = (2.40 - 1.74)/2 = 0.33$

2) Section B-B $t = 0.15$ $d_m = (1.40 + 0.15) = 1.55$

$A = \pi d_m t/n = \pi 1.55\ t/6 = 0.81158t = 0.121737$

$\lambda = \left[3\ (1-\mu^2)/r_m t^2\right]^{\frac{1}{4}} = \left[3\ (0.9)/0.775\ (0.15^2)\right]^{\frac{1}{4}}$

$\lambda = (154.8387)^{\frac{1}{4}} = 3.5275$

$\lambda x = 3.5275\ (0.25) = 0.881875$ Rad $= 50°\ 31.7'$

Sin $\lambda x = 0.77194$ Cos $\lambda x = 0.63570$

$e^{-\lambda x} = 0.46288$

$C_D = 0.46288\ (0.63570 + 0.46288) = 0.50851$

$M = kP_b(d - d_m)/2 = 0.8\ P_B\ (2.4 - 1.55)/2 = 0.34\ P_B$

$f_b = P_B/A + C_D 6M/bt^2 = P_B \left[1/0.12174 + (0.50851)\ (6)\ (0.34)/0.81158\ (0.15^2) \right]$

$f_b + (8.214 + 56.807)\ P_{B2} = 65.021\ P_{B2}$

$f_b = 65.021\ (134) = 8{,}713$ psi limit

3) Section C-C

$f_t = 2{,}850$ Ref: Fixed End (same)

M.S. Section A-A

M.S. $= F_{bu}/f_{b2} - 1 = 18{,}000/15{,}020 - 1 = \underline{+0.20}$ limit

Conclusions

The stresses in the fixed end portion of the hub are somewhat conservative. The hubs were designed to give good dynamic rigidity. The procedure used for finding flange bending stresses is considered to give conservative results.

7.1.1.2 End Plates

Due to the fact that the hub-end plate and drum attachment is not an exact condition, the stress analysis endeavor was to establish the maximum limits of the induced stresses. The final stress condition, therefore is intermediate to those limits shown in Table 11. This approach was taken due to the fact that all these areas are redundant, and do not conform to the exact condition given in the derivations of the plate equations. The stresses in all cases are low, due to the fact that the end plate was designed for dynamic rigidy. The stresses shown have not been considered as being dynamically additive, since it is considered that the vibration direction would not be excited simultaneously. Attention is called to the introduction of Section 7.1.1 for a discussion of the configuration to be analyzed.

The fixed end plate is shown in Figure 48. The fixed end plate has intermediate boundry conditions between the following limits:

Outer Edge	a)	Simply supported
	b)	Fixed
Plate Center	a)	Full plate
	b)	Hub configuration

The following general equations apply:

$$f_b = M_{EQ} \ (C/I)$$

where,

$$M_{EQ1} = K_1 \ P_{AX} \text{ and } M_{EQ2} = K_2 \ M_o = K_2 \ P_R d$$

The primary analysis consists of determining the limit of K_1 and K_2 for the various loading conditions above.

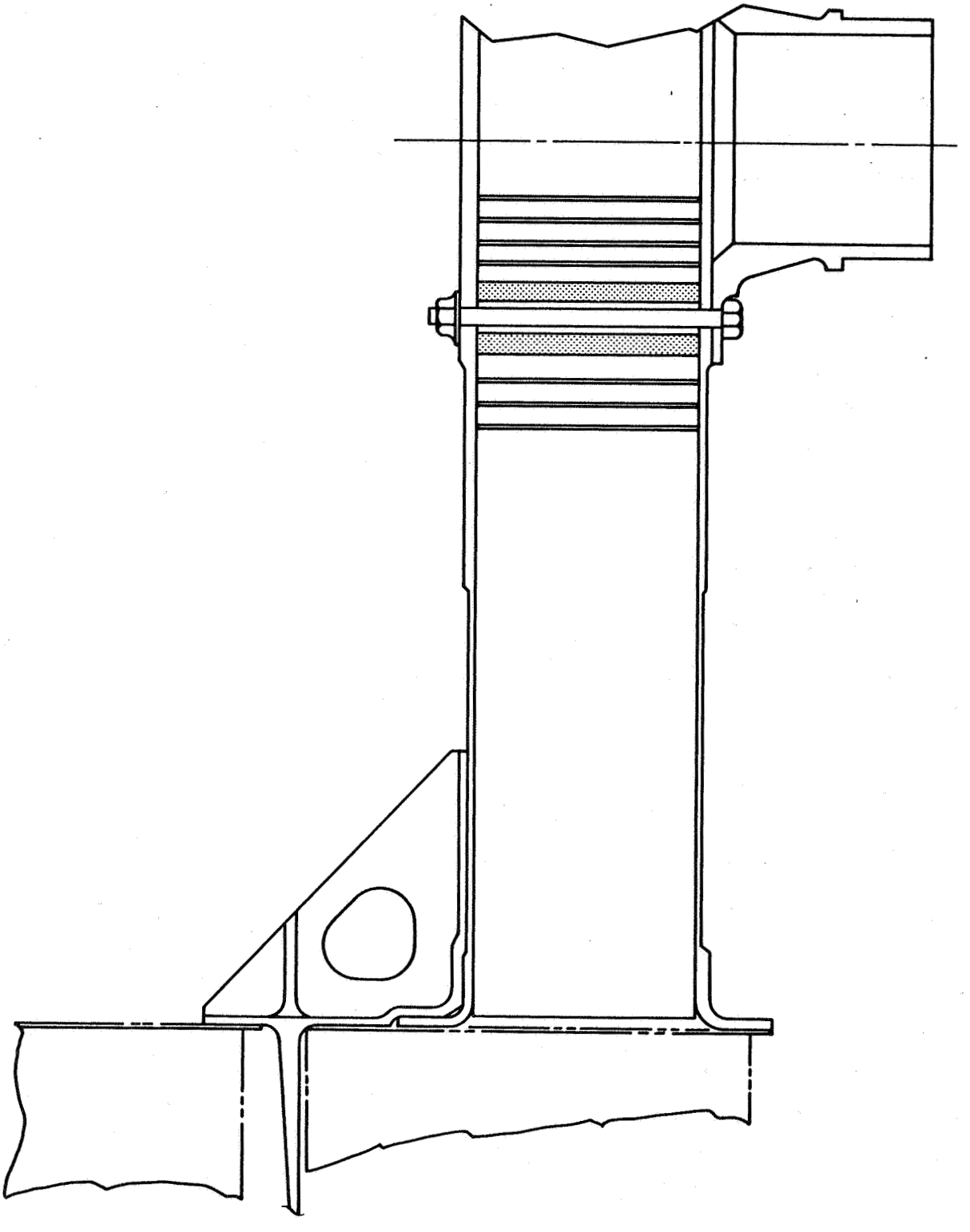

Figure 48 End Plate Configuration - Drum Fixed End

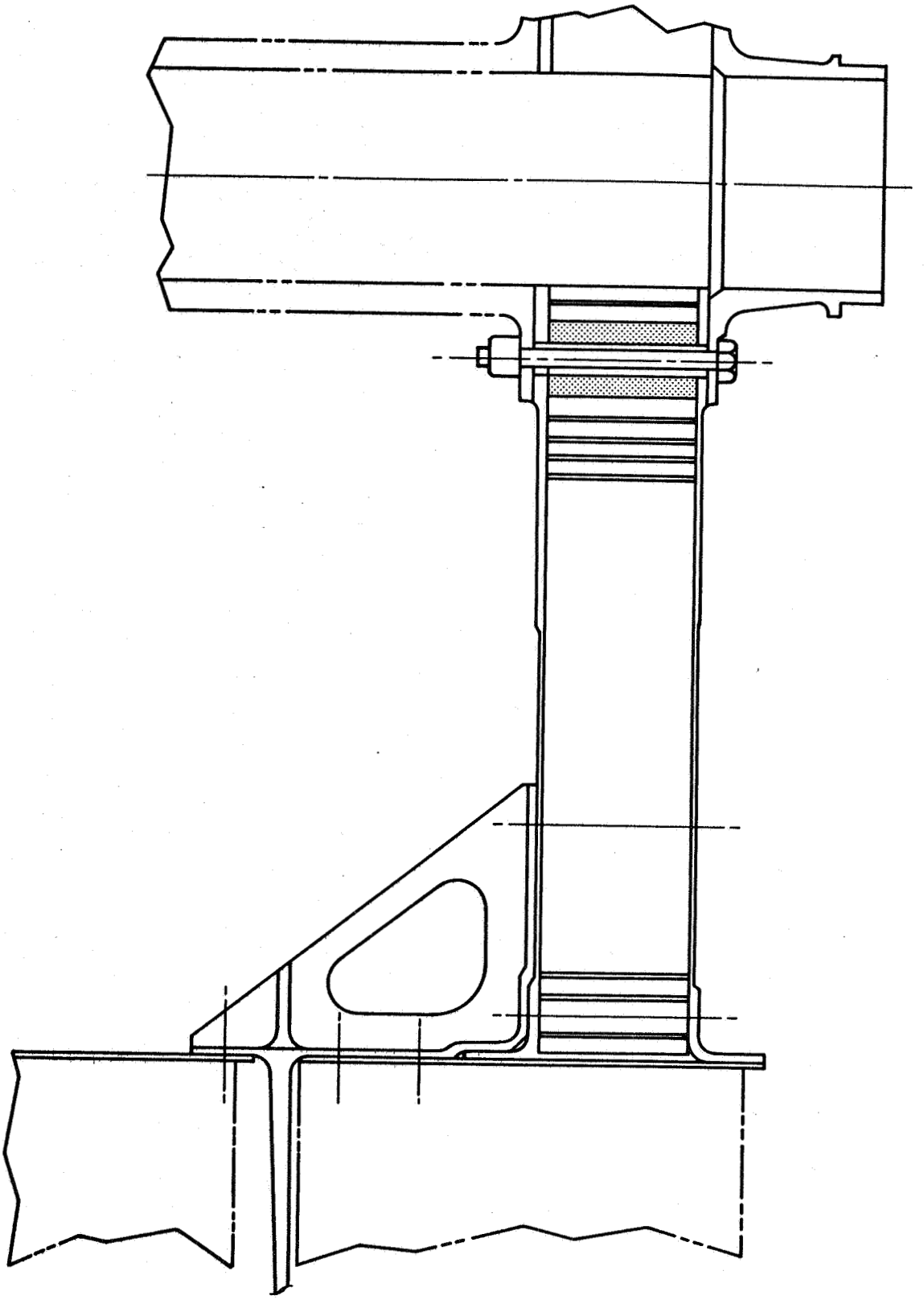

Figure 49 End Plate Configuration - Drum Slide End

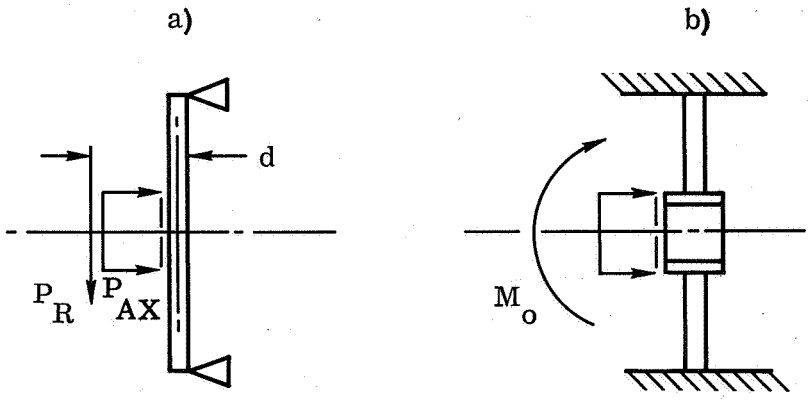

1a) Simply Supported 1b) Fixed

2a) Full Plate 2b) Hub Configuration

"a" Configuration is the least stiff of the configurations, and "b" has maximum stiffness.

$M_o = P_r d = 530\ (1.05\ (1.05 + 1.5/2) = 954$ in-lb

a) Hub Configuration

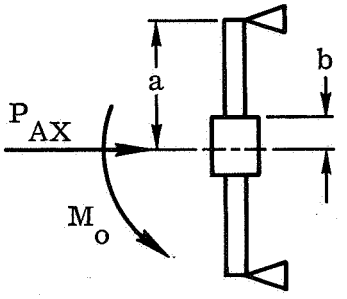

1) Simply supported (outer edge)

Ref: (9) - Case 8, p's. 42, 61

Dimension "b" is taken to be 1.2 in.

$a = r = 6.0$ in.

$a/b = 6.0/1.2 - 5.0$

For axially loaded plate

$f_b = K_s P_{AX}/h^2 = 6\ M'_{EQ}/h^2$ at the hub attach point

$M_{EQ1} = K_S\ P_{AX}/6 \qquad K_1 = K_S/6$

$K_s = 1.745$ $\quad K_1 = 1.745/6 = \underline{0.2908}$

For moment loading Ref: (10) P. 194 and 216 - Case 5

$f_b = \beta M_o/ah^2 = 6M_{EQ2}/h^2$ at hub attach point

$b/a = 1.2/6.0 = 0.20 \quad \beta = 3.27$

$M_{EQ2} = \beta_s M_o/6a = 3.27\ M_o/6(6) = 0.09083\ M_o$

$\underline{K_2 = 0.09083}$

2) Fixed Outer Edge

(a) At hub attach, axial Case 6 - Ref: (9)

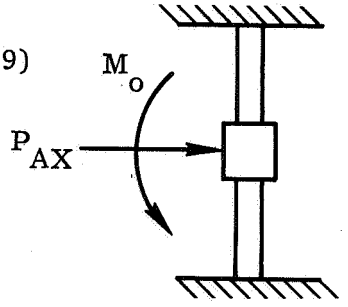

$M_{EQ1} = K_F\ P_{AX}/6$

$K_F = 1.13 \quad K_1 = 1.13/6 = 0.0188$

For M_o

$M_{EQ2} = \beta_F M_o/6a \quad \beta_F = 4.52$ (Case 10) Ref: (10)

$M_{EQ2} = 4.52\ M_o/6\ (6) = 0.1256\ M_o$

$\underline{K_2 = 0.1256}$

(b) At Outer Edge (a) due to P_{AX}

$$f_b = 3P/2\pi h^2\left[1 - 2b^2\ \text{Ln}\ (a/b)/(a^2 - b^2)\right] = 6M_{EQ}/h^2$$

$$M'_{EQ1} = (p/4\pi)\left[1 - 2b^2\ \text{Ln}\ (a/b)/(a^2 - b^2)\right] = K'_1\ P_{AX}$$

$$K'_1 = \left[1 - (1.2^2)\ \text{Ln}\ (6.0/1.2)/(6.0^2 - 1.2^2)\right]/4\pi$$

$$K_1' = [1 - (1.44)\ (1.609)/(34.56)]\ /4\pi = (1 - 0.06704)/\pi 4$$

$$K_1' = 0.07424$$

(c) For M_o use proportionality of K_1/K_2 (inner)

$$K_2'/K_1' = K_2/K_1 \qquad K_2' = K_1'\ K_2/K_1$$

$$K_2' = 0.07424\ (0.1256)/(0.188) = \underline{0.0496}$$

b. Full Plate Configuration

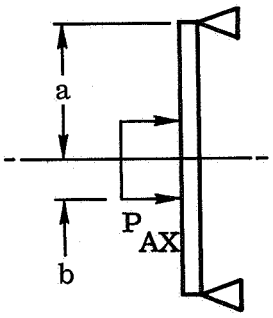

1) Simply supported - outer edge

Ref: (10) - Case 3, p. 194 (m - 1/μ)

$$f_b = P_{AX}\ K_S/h^2 = 6\ M_{EQ}/h^2$$

$$M_{EQ1}\ (P_{AX}/4\pi)\left[(1 - \mu)/2 + (1 + \mu)\ \text{Ln}\ (a/b) - (1 - \mu)\ b^2/2a^2\right]$$

$\mu = 0.3 \qquad a = 6.0 \qquad b = 1.2$

$$M_{EQ1} = (P_{AX}/4\pi)\ (1.0 - 0.3)/2 + (1 + 0.3)\ \ell n\ 5.0 - (1 - 0.3)\ 1.2^2/2\ (6.0^2)$$

$$= (P_{AX}/4\pi)\ [(0.70/2) + 1.3\ (1.609) - (0.70/2)\ (1.44)/36.0]$$

$$= P_{AX}\ (0.35 + 2.0917 - 0.0140)/4\pi = 2.4277\ P_{AX}/4\pi$$

$M_{EQ1} = 0.1932\ P_{AX}$ at centerline of plate $K_1 = .1932$

$M_{EQ2} = .09083\ M_o$ Ref: p. 7.1-17, $K_2 = .09083$

2) Fixed Outer Edge - Ref: (10) Case 8, p. 196

$$M'_{EQ1} = (P_{AX}/8\pi)\ (1 + \mu)\left[2\ \text{Ln}\ (a/b) + b^2/a^2 - 1\right]$$

$$M_{EQ1} = (P_{AX}/8\pi)\ (1.0 + 0.30)\left[2\ \text{Ln}\ 5.0 + 1.2^2/6.0^2 - 1\right]$$

$$M_{EQ1} = P_{AX}\ (1.3)\left[(2)(1.609) + 0.040 - 1\right]/8\pi$$

$$M_{EQ1} = 0.0898\ P_{AX} \qquad K_1 = 0.0898$$

$$M_{EQ2} = 0.0496\ M'_o \qquad K_2 = 0.0496$$

3) At Outer Edge

$$M'_{EQ1} = (P_{AX}/4\pi)\ (1 - b^2/a^2) = P_{AX}\ (1 - 1.2^2/6.0^2)/4\pi$$

$$M'_{EQ1} = 0.96\ P_{AX}/4\pi = 0.07639\ P_{AX} \qquad K'_1 = 0.07639$$

For M_o, use proportionality of K_1, K_2 (inner)

$$K'_2 = K'_1\ K_2/K_1 = (.07639)\ (.0496/.0898)$$

$$K'_2 = .0422$$

Moment of Inertia

$$I = 2Ad^2 = 2t_f d^2$$

$$C/I = \left[(t_c + 2t_f)/2\right] / \left[2t_f + (t_c + t_f)^2/4\right]$$

$$C/I = (t_c + 2t_f)/t_f\ (t_f + t_c)^2$$

$t_c = 1.50$ $\qquad t_f = 0.035$ (center section)

$$C/I = \left[1.5 + 2(0.035)\right] / \left[0.035\ (1.5 + 0.035)^2\right]$$

$$C/I = 1.57/.035\ (1.535)^2 = 19.038 \qquad \text{at inner section}$$

$f_b = M_{EQ}\ (c/I) = 19.038\ M_{EQ}$

$f_{b1} = 19.038\ M_{EQ1} = 19.038\ (K_1)\ P_{AX} = 19.038\ (1300)\ K_1 = 24{,}749.4\ K_1$

$f_{b2} = 19.038\ M_{EQ1} = 19.038\ (K_2)\ M_o = 19.038\ (954)\ K_2 = 18{,}162.3\ K_2$

For $t_c = 1.5$ $\quad t_f = 0.025$ at outer section

$c/I = 1.55/0.025\ (1.525)^2 = 26.666$

$f_b = M_{EQ}\ (c/I) = 26.666\ M_{EQ}$

Results of the above equations are tabulated in Table 11.

c. Honeycomb Plate - Slide End

($P_{AX} = 0$) The only loading is normal to the hub (P_R). The equations developed for hub bending for the slide end will be considered applicable with a 10% factor added to account for increased stresses due to cutout at center of plate.

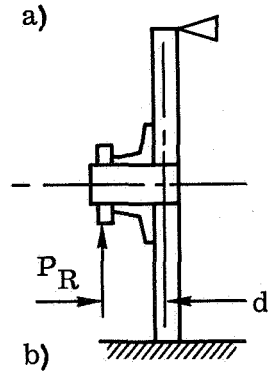

The following equations are applicable.

$f_b = M_{EQ}\ (c/I)$

$M_{EQ} = K\ K_2\ M_o = (1.10)\ K_2\ (821.5) = 903.65\ K_2$

K_2 (same as for previous case)

K = 1.10 (10% factor for cutout at centerline of plate)

$M_o = P_R d = 530\ (1.05 + 1.0/2) = 821.5$ in-lb

$C/I = (t_c + 2t_f)/t_f\ (t_f + t_c)^2$

Table 11 End Plate Stress Summary

FIXED END - PLATE							SLIDE END
OUTER EDGE	CENTER SECTION	K		M_{EQ} *1	f_b *2	POINT	f_b *3
S.S.	Full	K_1	0.19320	251.16	4,782	Inner	--
S.S.	Full	K_2	0.09083	86.65	1,650	Inner	3,043
S.S.	Hub	K_1	0.29080	378.04	7,197	Inner	--
S.S.	Hub	K_2	0.09083	86.65	1,650	Inner	3,043
Fixed	Full	K_1	0.08980	116.74	2,222	Inner	--
Fixed	Full	K_2	0.04960	47.32	901	Inner	1,661
Fixed	Full	K_1'	0.07639	99.31	2,648	Outer	--
Fixed	Full	K_2'	0.04220	40.26	1,074	Outer	1,414
Fixed	Hub	K_1	0.18800	244.40	4,653	Inner	--
Fixed	Hub	K_2	0.12560	119.82	2,281	Inner	4,208
Fixed	Hub	K_1'	0.07424	96.51	2,574	Outer	--
Fixed	Hub	K_2'	0.04960	47.32	1,262	Outer	1,662

*1 $M_{EQ1} = K_1 P_{AX} = 1300 K_1$

$M_{EQ2} = KM_o = 954 K_2$

*2 $f_{b1} = 19.038 M_{EQ1}$, $f_{b2} = 19.038 M_{EQ2}$

$f'_{b1} = 26.666 M'_{EQ1}$, $f_{b2} = 26.666 M'_{EQ2}$

*3 $f_b = 33,501 K_2$ and $33,501 K_2'$

$t_c = 0.90 \qquad t_f = 0.025$

$C/I = \left[0.90 + 0.025\ (2)\right] / 0.025\ (0.90 + 0.025)^2$

$C/I = 0.95/0.025625 = 37.073$

$f_b = (K\ K_2\ M_o)\ (C/I) = K_2\ (1.1)\ (821.5)\ (37.073) = 35{,}501\ K_2$

Results are tabulated in Table 11 for the two conditions: a) simply supported outer edge and b) full fixed outer edge.

d. Fixed End

$M.S. = F_{tu}/f_b - 1 = 25{,}000/7197 - 1$ High

$F_{ty} = 25{,}000$ psi for 10^5 cycles $K_T = 1.5$

Ref: (12) - Figure 3.3.1.6

Conclusions

Table 11 shows the maximum stresses at both the inner plate area and the outer attach boundary. None of the stresses are critical. The end plates were designed to give high dynamic stiffness. The end plate stresses are actually less than the maximum values given in the table since the boundary conditions are intermediate between the simply supported and fixed condition.

The stresses given in Table 11 are for the dynamically decoupled condition of the three axis dynamic loading. Not included, is the one (1) g loading in earth vertical plane.

7.1.2 Wrap Drum

The primary stresses in the wrap drum are wall crippling stresses due to axial loading directions. Since in a portion of the drum skin, 30% of the material was removed due to lightening holes, due allowance was made to critical values to compensate for the removal of material. Attention is called to the introduction of Section 7.1.1 for a discussion of the configuration to be analyzed.

Axial Load (P_{AX})

$P_1 = P_{AX}/\pi d = 1300/\pi(12) = 34.48$ lb/in

Bending Load (M_o)

$L = \pi d\ (60/360) = \pi d/6$ load is assumed distributed over 60° arc

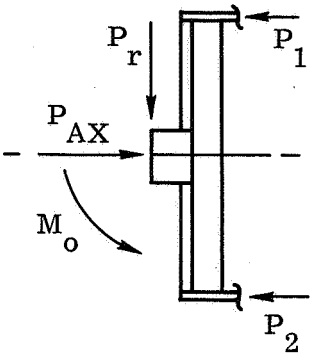

$P_2 = M_o/dL = 954/\left[(12)\pi\ (12)/6\right]$

$P_2 = 12.653$ lb/in $\qquad M_o = P_r d$

Drum skin has 70% lightening holes ∴

$t_{eff} = 0.7\ t = 0.7\ (0.025) = 0.0175$ in.

$r/t = 6.0/0.0175 = 343$

L = 27 in. between support rings

$Z = (L^2/rt)\ (1 - \mu^2)^{1/2} = 27^2\ (1 - 0.3^2)^{1/2}/(6)\ (0.0175)$

$Z = 729\ (0.9539)/0.105 = 6{,}623$

$K_C = 1.3\ (10^3)$ Ref: (14), p. C8.4 Figure C8.2

$F_{CCR} = K_c \pi^2\ Et^2/L^2\ (12)\ (1 - \mu^2)$

Material Mag. $E = 6.5\ (10^6)$ $\qquad t = t_{eff} = 0.0175$

$F_{CCR} = 1.3\ (10^3)\pi^2\ (6.5)\ 10^6\ (.0175)^2/27^2\ (12)\ (1 - 0.3^2)$

$F_{CCR} = 3{,}208$ psi

$f_{cy} = P_1/t_{eff} = 34.48/0.0175 = 1970$ psi Limit

$f_{cu} = 1.25\ f_{cy} = 1.25\ (1970) = 2463$ psi ultimate

M.S. $= F_{CCR}/f_{cu} - 1 = 3208/2463 - 1 = \underline{0.30}$ (ultimate)

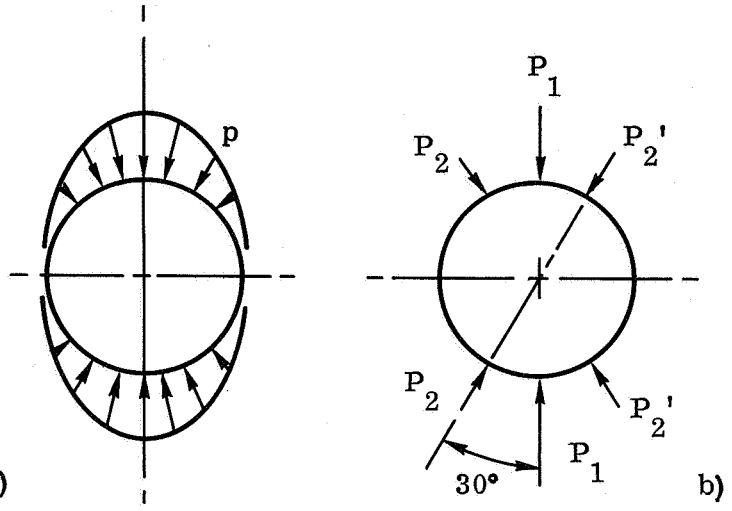

The drum radial loading is shown in Figure a) above. This loading is due to the substrate and wrap dynamic oscillations on the drum. The predominant radial mode is the elliptical mode shape as confirmed by Ryan tests. The eliptical loading in Figure (a) has been idealized simply as shown in Figure (b). The loading of configuration (b) is used for analysis of the drum intermediate stiffeners.

Loads - The total sprung weight in the radial mode is as follows:

		Pounds
1) Solar cell and electrical		41.366
2) Panel assembly (portion)		5.680
	Total	47.046

The above weight is distributed over 76.5 inches of drum length.

$w = W/L = 47.046/76.5 = 0.615$ lb/in

The transmissibility of the outer wrap was found by test to be (Q = 4.0). Since the inner wrap transmissiblity is approximately zero, the average transmissibilities for all wraps is taken to be (Q = 2.0). Only a fraction of the sprung weight is effective in a given coordinate direction. 33% of the total sprung weight is allocated to be effective in each of the directions in Figure (a).

$$p_T = kaQw = 0.33\ (4)\ (4)\ (0.615) \cong 3.26 \text{ lb/in.}$$

$$p_1 = p_T/2 = 3.26/2 = 1.63 \text{ lb/in.}$$

$$p_2 = p_2' + p_T/4 = 3.26/4 = 0.815 \text{ lb/in.}$$

The distance between drum frames is 27.0 inches.

$$P_1 = p_1 L = 1.63\ (27) = 44.01 \text{ lb. limit}$$

$$P_2 = p_2' = P_1' L = .815\ (27) = 22.01 \text{ lb. limit}$$

$$P_{N2} = P_1 + 2P_2 \text{ Cos } 30° = 44.01 + 2\ (22.01)\ (0.866) = 82.12$$

For a given load P in a ring where r/t is large

$$M = Pr\ (\text{Sin } \theta/2 - 0.3183)$$

a. $\theta_1 = 0 \qquad P = P_1 \qquad \text{Sin } \theta = 0$

$$M_1 = -0.3183\ P_1 r$$

$$\theta_2 = 30° \qquad P = P_2 \qquad \text{Sin } \theta = 1/2$$

$$M_2 = P_2 r\ (0.25 - 0.3183)$$

$$M_2 = -0.0683\ P_2 r$$

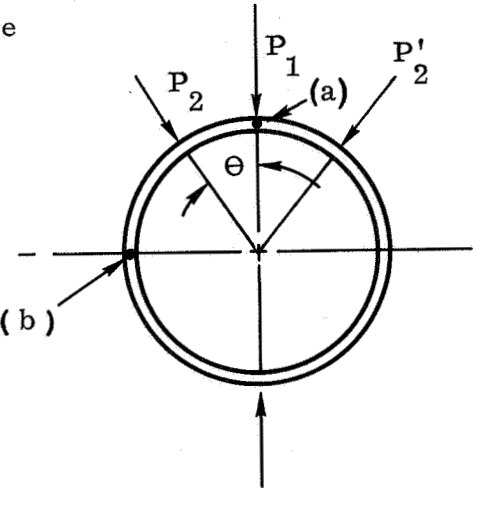

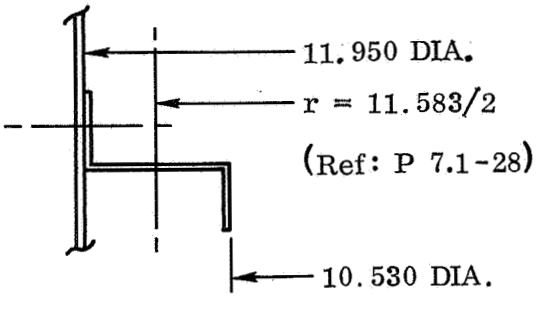

$\theta_2' = 330°$ $\quad P = P_2'$ $\quad \text{Sin } 60° = 0.866$

$M_2' = P_2' r\ (0.433 - 0.3183)$

$= 0.1147\ P_2' r = 0.1147\ P_2 r$

$\sum M_a = r\ (0.0464\ P_2 - 0.3183\ P_1)$

b. (Point "b")

$\theta_1 = 90$ $\quad \text{Sin } \theta = 1.0$

$M_1 = P_1 r\ (0.50 - 0.3183) = 0.1817\ P_1 r$

$\theta_2 = 60°$ $\quad \text{Sin } \theta = 0.866$

$M_2 = P_2 r\ (0.433 - 0.3183) = 0.1142\ P_2 r$

$\theta_2' = 120°$ $\quad \text{Sin } \theta = 0.866$

$M_2' = 0.1147\ P_2 r$

$\sum M_b = \sum M = r\ (0.1817\ P_1 + 0.2294\ P_2)$

For $r = 5.7915$ $\quad P_1 = 44.01$ $\quad P_2 = 22.01$ lb.

$M_A = 5.7915\ [0.0464\ (22.01) - 0.3183\ (44.01)] = -75.215$ in.-lb.

$M_B = 5.7912\ [(0.1817)\ 44.01 + (0.2294)\ (22.01)] = +75.554$ in.-lb.

$$f_b = P/A \pm MC/I \qquad P \sim P_N$$

At point b,

$$f_{b2} = -82.12/2.385t - 75.554\ (0.5265)/0.1778t$$

$$= (-34.432 - 223.730)/t = -258.162/t$$

For t = 0.025,

f_{b2} = 10,500 psi limit, compression (inner flange)

b/t = (0.30 - 0.025)/0.025 = 11.0

F_{cr} = 17,000 Ref: (16)-SM110

M.S. = $F_{cr}/f_{b2u} - 1 = 17{,}000/1.25(10.326) - 1 = 0.35$

Note: Since skin is 0.025, use 0.028 ring for higher rivet values.

For outer skin stresses (Pt. A),

$$f_c = MC/I = -75.215\ (0.2085)/(0.1778t)$$

f_c = 3528 psi limit

Effective width of skin:

$$\omega = 0.85t\sqrt{E/f_c}$$

$$= 0.85\ (0.025)\sqrt{6.5(10^6)/3228(1.25)}$$

= 0.853 inch, each side of rivet line

$$\omega_{eff} = 2\ (\omega) = 2\ (0.853)$$

= 1.706 inch (Adequate)

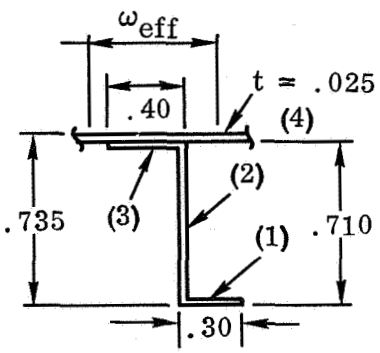

Moment of inertia

ω_{eff} = 1.00 in. assumed

	b	h	A	d	Ad	Ad^2	I_o
1	0.275	t	0.275t	--	--	--	--
2	t	0.735	0.735t	0.3675	0.2701t	0.09927t	0.03309t
3	0.375	t	0.375t	0.700	0.2625t	0.18375t	--
4	1.000	t'	1.000t	0.723	0.723t	0.52272t	--
			2.385t		1.2556t	0.80574t	0.03309t

$\overline{x} = \Sigma Ad/\Sigma A = 1.2556t/2.385t = 0.5265$ in. = C

$I_{NA} = 0.80574t + 0.03309t - (0.5265)\ (1.2556t)$

$I_{NA} = 0.1778t$

$C' = 0.735 - \overline{X} = 0.735 - 0.5265 = 0.2085$ in.

7.1.3 Spacecraft Mount

The aluminum mount is designed primarily for sufficient rigidity to prevent modal coupling with the stowed panel critical sinusoidal vibration resonance (30 Hz) if excited, normal to the drum axis, during launch vibration. Dynamic analysis presented in Reference 1 showed that the spacecraft mount natural frequency meets this requirement of ≥ 150 Hz set by Ryan in the trade-off study phase. This assures the transmissibilities through the spacecraft mount at the critical panel mode to be 1 to 1. That analysis was based on full load reaction capacity between the spacecraft mount and space frame. Since provisions have been made in the finalized design for a thermal slip joint at one mount-space vehicle interface, the mount design

was altered to react all load excited in the drum axis direction at one mount only; dynamic analysis of this final mount configuration is given in Section 7.2.1.

Stress analysis performed on the finalized design is presented in this section. Positive margins of safety are shown for the more critical mount stress condition when the mount resonance of 238 Hz is excited at 4g (Pk) sinusoidal excitation. A transmissibility of 5 to 1 in the drum axis direction and 4 to 1 in the two orthogonal axes was used to determine the loads for this condition. Analysis presented here is conservative by assuming that the sinusoidal excitations in the drum axis direction and the two orthogonal axis directions occur simultaneously at the spacecraft mount resonances in the respective directions. Under actual test qualification conditions, sinusoidal excitations will exist in only one direction at a time.

a. Fixed End

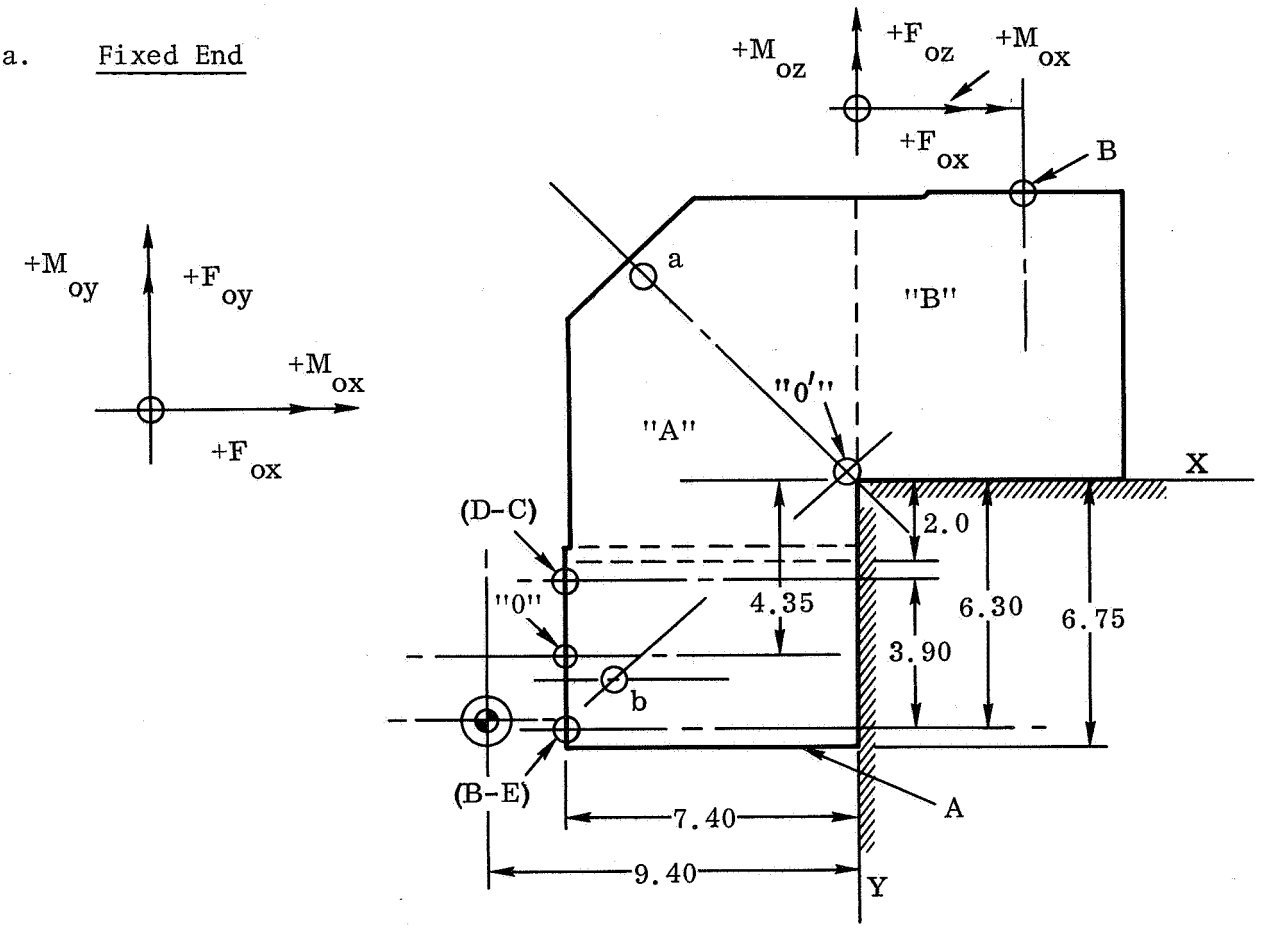

The loads for the above mount were developed in pages 7.1-41 to 7.1-44 for point "0". Two critical cases are given in the following table.

	A	B	C
M_{ox}	+2416	+4817	-142
M_{oy}	-321	+3301	-321
M_{oz}	+4168	-1903	-2004
P_{ox}	+548	+170	+548
P_{oy}	-1543	+1039	+1543
P_{oz}	+578	+578	+578

Signs are given for a given set of conditions. All signs may be reversed simultaneously.

1) Shear Stresses Web "A". Shear loading is reduced by the load taken out in the braces in proportion to the spring constants. Ref: p. 7.2-5

(a) Direct Shear

$$F_s = F_{oy}\ K_\omega / \Sigma K = F_{oy}\ (686{,}012/730{,}959) = 0.939\ F_{oy}$$

$$f_{s1} = F_s/2tL = 0.939,\ F_{oy}/2\ (.05)\ (12.52) = 0.750\ F_{oy}$$

(b) Torsion $q = T/2A$

$$T = M_{ox} + F_{oz}\ (4.35 - 6.75/2) = M_{ox} + 0.975\ F_{oz}$$

$$f_{s2} = q/t = T/2At = (M_{ox} + 0.975\ F_{oz})/$$
$$(6.75)\ (4.25)\ (0.05)\ (2)$$

$$f_{s2} = 0.3486\ (M_{ox} + 0.975\ F_{oz})$$

2) Bending Stresses. Assuming full effective width of skin, Ref: 7.1-31 and braces effective in proportion to spring rates, Ref: pages 7.2-8, 9.

(a) Y-Axis - Ref: 7.2-9,10

$$M_y = (M_{oy} + 7.2\ F_{oz})\ K_y/\Sigma K = (M_{oy} + 7.2\ F_{oz})(192{,}758)/293{,}299$$

$$M_y = 0.792\ M_{oy} + 5.704\ F_{oz} \qquad \text{Ref: p. 7.1-31}$$

$$f_{by} = M_y\ C/I = M_y \left[4.25/2\ (4.9221) \right] = (0.792\ M_{oy} + 5.704\ F_{oz})\ (0.4317)$$

(b) Z-Axis Bending Spring Rates - Ref: p. 7.2-5

$$M_z = (M_{oz} - 7.2\ F_{oy})\ K_z/\Sigma K = (M_{oz} - 7.2\ F_{oy})(686{,}012)/730{,}959$$

$$M_z = 0.939\ M_{oz} - 6.761\ F_{oy}$$

$$f_{bz} = M_z\ (C/I) = 0.481\ (0.939\ M_{oz} - 6.761\ F_{oy}) \qquad \text{Ref: p. 7.1-32}$$

I_y - full effective width of skin -8.0 in.

$$I_y = 3\ (4.25)^3\ (0.04)/12 + 2\ (8.0)\ (0.05)\ (4.25/2)^2 + (2)\ (3)\ (0.5)\ (0.04)\ (4.25/2)^2$$

$$I_y = 0.7677 + 3.6125 + 0.5419$$

$$I_y = 4.9221\ \text{in.}^4$$

$$c_y = 4.25/2 = 2.13\ \text{in.}$$

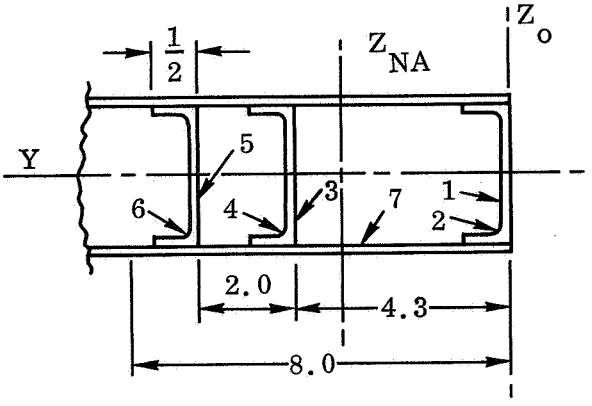

About Z_o Axis:

element	b	h	A	d	Ad	Ad^2	I_o
1	2.125	0.040	0.085	6.02	0.0017	0.00003	--
2	0.040	0.500	0.020	0.25	0.0050	0.00125	0.00042
3	2.125	0.040	0.085	4.32	0.3672	1.58630	--
4	0.040	0.500	0.020	4.55	0.0910	0.41405	0.00042
5	2.125	0.040	0.085	6.32	0.5372	3.39510	--
6	0.040	0.500	0.020	6.55	0.1310	0.85805	0.00042
7	0.050	8.0	0.400	4.00	1.60000	6.40000	2.13333
			0.715		2.7331	12.65478	2.13459

$$\bar{y} = \Sigma Ad / \Sigma A = 2.7331/0.715 = 3.8225 \text{ in.}$$

$$I_{NA} = 2 \left[12.65478 + 2.13459 - 3.8225\ (2.7331)\right]$$

$$= 2\ (4.3421) = 8.6842$$

$$c_u = 8.0 - \bar{y} = 8.0 - 3.8225 = 4.1775$$

$$c_u/I = 4.1775/8.6842 = 0.481$$

$$A_t = 2\ (0.715) = 1.430 \text{ in.}^2$$

Direct Stresses - Ref: p. 7.1-32

$$f_c = P/A = F_{ox}/A = F_{ox}/1.430 = 0.700\ F_{ox}$$

Results of the previous equations are tabulated in Table 12.

Critical Shear Stress (edges between clamped and simply supported)

$a/b = 4.5/(4.5/2) = 2.0$

$K_s = 9.0$ Ref: (14) p. C5.7

$$F_{scr} = \pi^2 K_s E (t/b)^2/12(1 - \mu^2) = K_s \pi^2 (10.3) (10^6) (0.05)^2/(2.25)^2(12)(.9)$$

$$F_{scr} = 0.25908 (10^6) K_s/54.675 = 4739 K_s = 42,651 \text{ psi}$$

Critical Compressive Stress:

$a/b = 2.0$ $K_c = 6.0$ Ref: (14) p. C5.2

For edges between clamped and simply supported,

$$F_{ccr} = \pi^2 K_c E (t/b)^2/12(1 - \mu^2) = 4739 K_c = 28,434$$

The above stresses are tabulated in Table 12.

From Load Case "A"

$$R_s = f_s/F_{scr} = 2,196/42,651 = 0.052 \text{ limit}$$

$$R_c = f_c/F_{ccr} = 8562/28,434 = 0.301 \text{ limit}$$

M.S. = $1/(R_s \mapsto R_c)(1.25) - 1$ (ultimate crippling) High

Loads applied independently, but increased by ratio of 83/(4.0)(5.0) in Y direction and 83/(4.0)(4.0) in X and Z direction, Ref: p. 7.1-29

"Y" direction, F_x and $F_z = 0$ Ref: p. 7.1-34

$$f_s = f_{s1} + f_{s2} = (83/20)\left[1175 + 0\right] = 4876 \text{ psi}$$

Table 12 Mount Stress Summary - Fixed End

STRESS LOAD	f_{s1} $.939\ F_{oy}$	f_{s2} $M_{ox} + .975\ F_{oz}$	f_{by} $.792\ M_{oy}$ $+5.704\ F_{oz}$	f_{b2} $.939\ M_{oz}$ $-6.761\ F_{oy}$	$f_c = f_x$ F_{ox}
A	-1449 lbs	+2980 lbs	+3043	+14,346	+548
f	1157 psi	1039 psi	-1314	-6900	-348
Σf	f_s = 2196		f_c = 8562 psi		
B	+976 lbs	+5381 lbs	+5911	-8812	+170
f	780 psi	1876 lbs/in^2	-2552	-4239	-119
Σf	f_s = 2656		f_c = 6910 psi		
C	+1449 lbs	+422 lbs	+3043	-12,314	+548
f	1157 psi	147 lbs/in^2	-1314	-5923	-348
Σf	f_s = 1304		f_c = 7585 psi		

F_{scr} = 42,651 t = 0.050

f_{bz} = 7004 (83/20) = 29,067

F_{ccr} = 28,434 t = 0.050

Increasing t to 0.065

F_{scr} = 42,651 $(65/50)^2$ = 72,080 Use F_{sy} = 36,000

F_{ccr} = 29,067 $(65/50)^2$ = 49,123

R_s = 4876/36,000 = 0.135

R_c = 29,067/49,123 = 0.592

$M.S._u = 1/(1.25)\ (R_s \mapsto R_c) - 1$

$= 1/(1.25)\ (0.607) - 1 = \underline{0.32}$

% increase of material 0.065/0.050 -1 = 30%

Use 25% since margin is high and not all mount elements need be increased.

Tubular Braces

Brace 0' - a P is proportional to spring rate

Y $P_1 = 1.220\ P_{oy}\ (0.50) = 0.61\ P_{oy}$ Ref: p. 7.2-3

Z $P_2 = 2.073\ P_{oz}\ (0.05) = 1.039\ P_{oz}$ Ref: p. 7.2-8

Note $K/\Sigma K$ = 0.50 has been conservatively assumed to account for softness that could exist in the missile substructure.

$P = P_1 + P_2 = 0.61\ P_{oy} + 1.039\ P_{oz}$

P_{oy} = 1543 lb. P_{oz} = 578 lb. Ref: p. 7.1-29, 30

$P = (0.61)\ 1543 + 1.039\ (578) = 1542$ lb. limit

Tube 1.0 diameter - 0.049 I = 0.016594 A = 0.1464

L = 11.35 Ref: p. 7.2-2 $E_c = 10.3\ (10^6)$, 7079 A1

$P_{cr} = \pi^2\ EI/L^2 = \pi^2\ (10.3)\ (10^6)\ (0.016594)/(11.35)^2$

P_{cr} = 13,095 lb.

$f_c = P/A = 1542/0.1464 = 10{,}533$ psi limit

$F_{ccr} = KET/R = .3\ (10.3)\ (10^6)\ (0.049)/0.5$ local crippling

F_{ccr} = 302,282 psi

M.S. = $F_{cy}/f_c - 1$ High

The above tubing sizes were selected for spring rate.

Lugs - Brace Ends

P = 1542 lb. Ref: Above (limit)

Alum 7075, F_{tu} = 75 ksi assume K_t = 0.92 lug

$A_t = P_u/K_t\ F_{tu} = 1542\ (1.25)/0.92(75{,}000)(2)$

$A_t = 0.027935/2$

at = $A_t/2 = 0.007$ a = 0.007/t

t	a	w
0.050	0.140	0.560
0.075	0.011	0.500
0.100	0.070	0.420

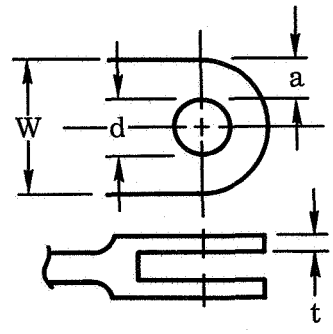

$w = 2a + d = 2a + 0.28$ (0.28) diameter includes bushing allowances per two lug clevis

Use $w = 0.600$ and $t = 0.08$

$w/D = 0.60/.28 = 2.14$

$K_t = 0.95$ Ref: (14) p. D1.7

$P_u = K_t F_{tu} A_t = 0.95\ (75{,}000)\ (0.08)\ (0.60 - 0.28)$

$P_u = 1824$ lb. ultimate/lug

Shear Tear Out

$e/D = 0.60/2(0.28) = 1.07$ $D/t = 0.28/0.09 = 3.11$

$K_{bru} = 0.80$

$P_{bru} = K_{bru} F_{tu} A_{br} = 0.80\ (75{,}000)\ (0.08)\ (0.28) = 1344$ lbs./lug

$t/d = 0.08/0.28 = 0.29$ $K_{bry} = 0.93$

$P_{bry} = K_{bry} F_{ty} A_{br} = 0.93\ (62{,}000)\ (0.08)\ (0.28) = 1291$ lbs. ult.

$M.S. = P_{bry}/P - 1 = (2)\ (1291)/1542 = \underline{0.67}$

Bolt Shear, Consider No. 10- 0.188 Hucks, either Alum or Ti.
[$F_s = 1270$ lbs. SSH (Al); $F_s = 2690$ SSH (Ti); Ref: 15(Hi Shear Manual)]

Lug - Mount End, Magnesium

F_{tu} = 33 ksi F_{ty} = 21 ksi

Lug size K_t = 0.5 assumed

$A_t = P_u/K_t F_{tu}$ = 1.25 (1542)/ 0.5(33,000)

A_t = .117

at = $A_t/2$ a = 0.059/t for,

t = 0.25 a = 0.236 w = 752

Use t = 0.26 w = 0.70

W/D = 0.70/0.28 = 2.50 K_t = 0.55

$P_u = K_t F_{tu} A_t$ = 0.55 (33,000) (0.26) (0.70 - 0.28)

P_u = 1981 lbs.

Shear Tear Out

e/D = 0.70/2(0.28) = 1.25 K_{bru} = 1.25

$P_{bru} = K_{bry} F_{ty} A_{br}$ = 1.25 (33,000) (0.26) (0.28)

P_{bru} = 2999 lbs.

t/D = 0.26/0.28 = 0.93 K_{bry} = 1.20

$P_{bry} = K_{bry} F_{ty} A_{br}$ = 1.2 (21,000) (0.26) (.028)

P_{bry} = 1835 lbs.

M.S. = P_u/P -1 = 1981/1.25(1542) -1 = 0.03 (ultimate)

Curves are known to be conservative in yield.

b. Slide End

F_{oy} = 0 Loads Ref: p. 7.2 - 1

M_{ox}	+1134*	+1134**
M_{oy}	-321	+3301
M_{oz}	+1082	+175
F_{ox}	+548	+170
F_{oz}	+578	+578

* Condition A and B ** Condition C

The stresses are calculated the same as for the fixed end with the exception that the thickness, t, has been reduced and F_{oy} = 0

$$f_{slide} = f_{fixed} (t_f/t_{SL})$$

t_{SL} = 0.032 t_f = 0.05 t_f/t_{SL} = 1.56

Results of stresses for the above loads are tabulated in Table 13, and were computed the same as the stresses on p. 7.1-34, equations p. 7.1-30 through 31 modified by the factor f_f/t_{SL} = 1.56 increase.

Critical Shear Stress

a = 5.3 b = 2.35 t = 0.028

a/b = 5.3/2.35 = 2.26

K_s = 9.0 Ref: (14) p. C5.6

$$F_{scr} = \pi^2 K_s E (t/b)^2/12(1 - \mu^2) = \pi^2 K_s (10.5) 10^6 (0.028)^2/ 2.35^2(10.8)$$

$$F_{scr} = 0.081247 \quad (10^6) K_s/59.643 = 12,259 \text{ psi}$$

Critical Compressive Stress

$$K_c = 7.0$$

$$F_{ccr} = (7.0) (0.081247) 10^6/59.643 = 9536 \text{ psi}$$

$$M.S. = F_{ccr}/f_{cu} -1 = 9536/1.25 (4290) -1$$

M.S. = <u>High</u>

Table 13 Mount Stress Summary - Slide End

STRESS LOAD	f_{s1} .939 F_{oy}	f_{s2} M_{ox} + .975 F_{oz}	f_{by} .792 M_{oy} + 5.704 F_{oz}	f_{bz} .939 M_{oz}	$f_c = f_x$ F_{ox}
A & B	0	1698	+3043	+1016	+548
f	0	923	-2049	-762	-598
Σ f	± 923		-3409		
c	0	1698	+5911	+164	+170
f	0	923	-3981	-123	-186
Σ f	± 923		-4290		

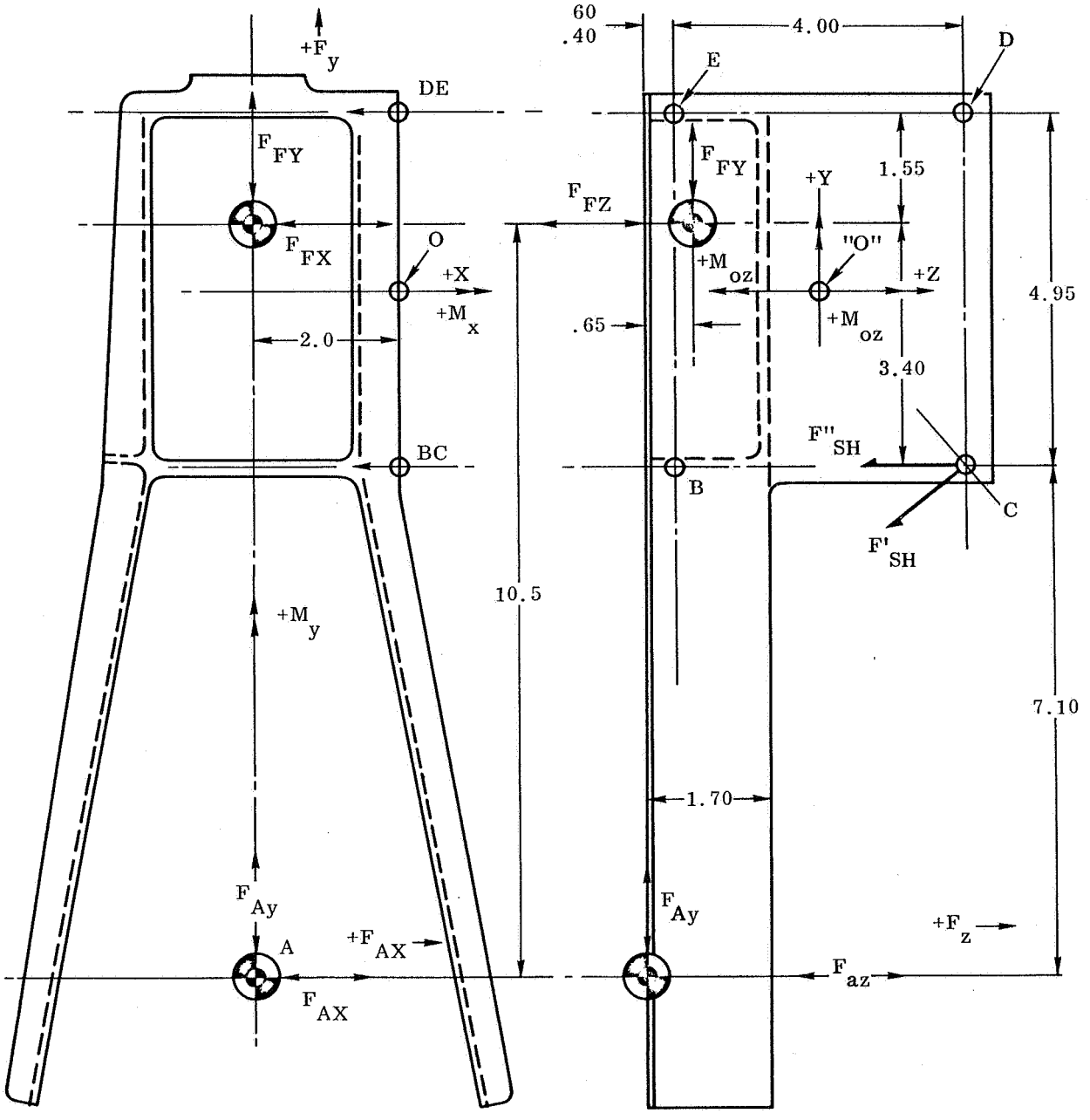

Figure 50 Support Fitting - Beam Guide Sleeve

W_a = 6.308 lbs. Total drive system weight assumed acting at one end.

a = 4.0 g's 0 - Pk Q_{TR} = 10.0

$F_a = (aQ)\ W_a = 40.0\ (6.308) = 252.32$ lbs. limit

Acting in the drum and driveshaft directions

$F_{ax} = F_{ay} = (0.75)\ F_{aax} = 0.75\ (252.32) = 189.24$ lbs.

W_f = 64.544 lbs. Ref: p. 7.1-2 Q = 5.0

The entire axial load is taken at fixed end

$F_f = aQW_f = (4.0)\ (5.0)\ (64.544) = 1291$ lbs. limit

F_{fx} = 359 lbs. F_{fy} = 389 lbs. Ref: p. 7.1-6

ΣM_{BC}, $(F_b' + F_e')\ 4.95 = -F_{ax}\ (7.10) + F_{ay}\ (2.0) + F_{fx}\ (3.4) + F_{fy}\ (1.05)$

$F_d' = F_e' = [(7.10 + 2.0)\ 189.24 + 3.4\ (359) + 389\ (1.05)]\ 2\ (4.95)$

$F_d' = F_e' = 3351/9.9 = 339$ lbs.

ΣM_{be}, $(F_c'' + F_d'')\ (4.0) = F_{ax}\ (.4) + F_{az}\ (2.0) + F_{fx}\ (0.30) + F_{fz}\ (2.0)$

$F_c'' = F_d'' = [(0.4)\ (189.24) + 2.0\ (252.32 + 1291) + 0.3\ (359)]\ /2\ (4)$

$F_c'' \pm F_d'' = 3270/8.0 = 409$ lbs. limit

ΣM_{de}, $(F_b' + F_c')\ (4.95) = F_{ax}\ (12.05) + F_{ay}\ (2.0) + F_{fx}\ (1.55) + F_{fy}\ (2.0)$

$F_b' = F_c' = [189.24\ (12.05 + 2.0) + 1.55\ (359) + 2.0\ (389)]/2\ (4.95)$

$F_b' = F_c' = 3993/9.9 = 403$ lbs. limit

ΣM_{cd}, $(F_b'' + F_e'')\ (4.0) = F_{ax}\ (4.4) + F_{aax}\ (2.0) + F_{fx}\ (3.75) + F_{fax}\ (2.0)$

$$F_b'' = F_e'' = \left[4.4\ (189.24) + 2.0\ (252.32 + 1291) + 3.75\ (359)\right] /8.0$$

$$F_b'' = F_e'' = 5102/8.0 = 638 \text{ lbs. limit}$$

The above effective moments were combined to give the maximum loading on bolt reactions.

Σ Normal Attach forces (Tension Compression)

$$F_b = K\ (F_b' + F_b'') = (1.10)\,(403 + 638) = 1145 \text{ lbs. limit (maximum)}$$

$$F_c = K\ (F_c' + F_c'') = (1.10)\ (403 + 409) = 893 \text{ lbs. limit (maximum)}$$

$$F_d = K\ (F_d' + F_d'') = (1.10)\ (339 + 409) = 823 \text{ lbs. limit (maximum)}$$

$$F_e = K\ (F_e' + F_e'') = (1.10)\ (339 + 638) = 1075 \text{ lbs. limit (maximum)}$$

K = 1.10 was used to account for reaction redundancy since reactions are statically indeterminant shear reactions.

ΣF_o, $F_{sh}' = \Sigma F_z/4 = (252 + 1291)/4 = 386$ lbs.

ΣM_o, $(4)\ (2.0 \leftrightarrow 2.48)\ F_{sh} = -F_{az}\ (9.58) + F_{ay}\ (2.4) + F_{fax}\ (.93) + F_{fy}\ (1.75)$

$$F_{sh}'' = \left[958\ (252.32) + (2.4)\ (189.24) + (0.93)\ (1291) + 1.75\ (389)\right] /12.744$$

$$F_{sh}'' = 373 \text{ lbs.} \qquad F_{sh} = F_{sh}' + F_{sh}'' = 759 \text{ lbs. (cons.)}$$

$$F_{bs} = F_{cs} = F_{ds} + F_{es} = 1.10\ (F_{sh}) = 1.10\ (759) = 410 \text{ lbs. limit}$$

About Point "O"

$$\Sigma M_{ox} = -F_{az}\ (9.85) + F_{ay}\ (2.4) + F_{fz}\ (.93) + (1.75)\ F_{fy}$$

$$\Sigma M_{oy} = -F_{az}\ (2.0) + F_{ax}\ (2.4) = F_{fz}\ (2.0) + F_{fx}\ (1.75)$$

$$\Sigma M_{oz} = +F_{ax}\ (9.58) + F_{ay}\ (2.0) - F_{fx}\ (.93) - 2.0\ F_{fy}$$

$$\Sigma F_{ox} = F_{ax} + F_{fx}$$

$$\Sigma F_{oy} = F_{ay} + F_{fy}$$

$$\Sigma F_{oz} = F_{az} + F_{fz}$$

The above moments and forces are tabulated below, for ± directions of dynamic load that give critical load (maximum) conditions.

Ref: Equations above

	F_{dy}		M_o, F_o	F_{dy}	M_o, F_o	F_{dy}	M_o F_o	S/C* Coordinates
F_{ax}	+ 189	M_{ox}	- 147	+ 189	+ 2416	- 189	+ 4817	M_{ox}
F_{fx}	+ 359	M_{oy}	- 2004	+ 359	+ 4168	+ 359	- 1903	M_{oz}
F_{ay}	+ 189	M_{oz}	- 321	+ 189	- 321	+ 189	+ 3301	M_{oy}
F_{fy}	+ 389	F_{ox}	+ 548	+ 389	+ 548	+ 389	+ 170	F_{ox}
F_{az}	+ 252	F_{oy}	+ 578	- 252	+ 578	- 252	+ 578	F_{oz}
F_{fz}	+ 1291	F_{oz}	+ 1543	- 1291	- 1543	+ 1291	+ 1039	F_{oy}

Maximum values above are: (limit)

M_{ox} = ± 4817 in.-lb. M_{oy} = ± 4186 in.-lb. M_{oz} = ± 3352 in.-lb.

F_{ox} = ± 548 lbs. F_{oy} = ± 578 lbs. F_{oz} = ± 1543 lbs.

*These are the actual spacecraft coordinate directions, which are converted for use in the mount stress analysis.

At the slide fitting end F_{az} and F_{fz} = 0 with only F_x and F_y acting. Critical conditions are tabulated below:

F_{dy}			M_o, F_o	F_{dy}	M_o, F_o
F_{ax}	+ 189	M_{ox}	+ 1134	- 189	+ 1134
F_{fx}	+ 359	M_{oy}	+ 1082	+ 359	+ 175
--	--	M_{oz}	+ 321	--	- 3301
F_{ay}	+ 189	F_{ox}	+ 548	+ 189	+ 170
F_{fy}	+ 389	F_{oy}	+ 578	+ 389	+ 578

7.2 DYNAMIC ANALYSIS

Dynamic analysis was performed on major weight contributing components of the panel to assure that supporting structure, such as the spacecraft mount and wrap drum end plates, would be sufficiently rigid to minimize sinusoidal launch excitations to the stowed panel; to effect this, a decoupled condition must exist between the stowed panel and wrap drum modes and the supporting structures. Also, detailed dynamic analysis of the deployed panel modes were made to show compliance with the JPL Specification requirement of $\geq$ 0.04 Hz.

Analysis has been based on nominal drawing sheet thicknesses and dimensions. Ambient room temperature conditions are considered to exist during launch and were therefore used for analysis of all but the deployed panel, which modes would be excited only in space. Temperatures used in the deployed panel analysis are 358°F for the deployment beams, determined by thermal analysis (see Section 2.5.1.2) for the maximum heat flux of 260 mw/cm^2 given in the JPL Specification.

7.2.1 Spacecraft Mount

7.2.1.1 Drum Axial Direction Stiffness

The dynamic analysis takes into account that all the axial load is reacted at one end. The mount was analyzed in two directions - the drum axial direction and the mount normal direction (spacecraft thrust direction).

$\alpha = 45°$

$\text{Tan } \alpha_1 = 5.1/6.2$

$\text{Tan } \alpha_1 = .82258$

$\alpha_1 = 39° \ 26.4'$

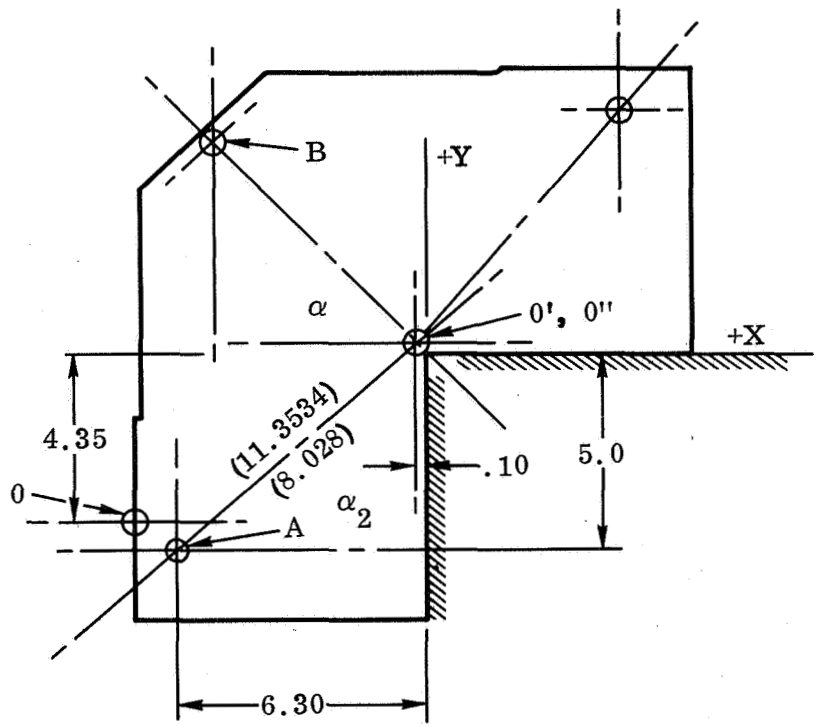

Brace "AQ" 45° in true plane

$$h' = \left\{ 2 \left[(5.0 + .1)^2 + (6.3 - .1)^2 \right] \right\}^{\frac{1}{2}} = 11.3534 \text{ in.}$$

$$h'' = (5.0 + .1) \leftrightarrow (6.3 - .1) = 8.028 \text{ in.}$$

Critical load conditions at Pt "O" are Ref: p. 7.1-44.

	A	B		A	B
M_{ox}	- 2416	+ 4817	F_{ox}	+ 548	+ 170
M_{oy}	- 321	+ 3301	F_{oy}	- 1543	+ 1039
M_{oz}	+ 4168	- 1903	F_{oz}	+ 578	+ 578

Ref: p. 7.2-3, 7.3-6

$\Sigma M_{o''}$, $P_y = P_{oy}\ (7.3/6.3) = 1.16\ P_{oy}$

Drum Axial Load (F_{oy}): Loading in Braces

a. Brace AO' - Y Direction Loading in Plane of Mount (Figure (a)

$P' = P'_y/\text{Sin}\ \alpha_2 = P'_y\ (1.57413)$

In plane of brace $\alpha_3 = 45°$

$P_a = P'/\text{Cos}\ \alpha = (P'_y)\ (1.57413)\ (1.4142)$

$P_a = 2.226\ P'_y \sim P_1$

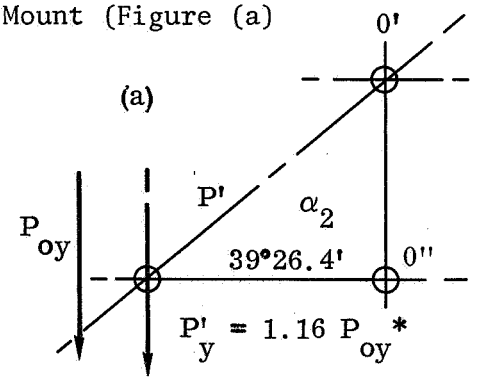

*$P_y = 1.16\ P_{oy}$ REF: p 7.2-2

b. Brace BO'

$P_b = P''_y/\text{Sin}^2\ 45° = 2.0\ P''_y$ *$P_y = 1.16\ P_{oy}$ Ref: p. 7.2-3

$P'_y + P''_y = P_y = 1.16\ P_{oy}$

Proportioning P_{oy} in Proportion to Stiffness above,

$P'_y = P_y\ (2.0)/(2.0 + 2.226) = 0.473\ P_{oy}$

$P''_y = P_y\ (2.226)/(4.226) = 0.527\ P_{oy}$

$$P_a = 2.226\ P_y' = 2.226\ (0.473)\ P_y = 1.053\ P_y^* = 1.22\ P_{oy}' = P_1$$

$$P_b = 2.00\ P_y'' = 2.0\ (.527)\ P_y = 1.054\ P_y = 1.22\ P_{oy} = P_2$$

In Brace AO

$$P_{ad} = P_y/\text{Tan}\ \alpha_2 = P_y\ \text{Cot}\ \alpha_2 = P_1\ 1.2157 \sim P_3$$

$$U_T = (P^2 L/2AE)_1 + (P^2\ L/2AE)_2 + (P^2\ L/2AE)_3$$

$L_1 = 11.5$ $\quad L_2 = 10.5$ $\quad A_1 = A_2 = 0.1464$ $\quad$ 1.0 diameter x 0.049

$E = 10.5\ (10^6)$ Alum. 7079 $\quad L_3 = 6.0$

$$A_3 = 2\ (.05)\ (5.0) + 2\ (0.04)\ (3.9 + 1.0) = 0.892\ \text{in.}^2$$

$$U_T = (1.22)^2\ P_{oy}^2\ (11.5)/2(0.1464)(10.5)(10^6)$$
$$+ (1.22)^2\ P_{oy}^2\ (10.5)/2(0.1464)(10.5)(10^6)$$
$$+ (1.2157)^2\ P_{oy}^2\ (6.0)/2(0.892)(10.5)(10^6)$$

$$\Delta_y = dU/dP_{oy}$$

$$\Delta_y = \left[P_{oy}/10.5\ (10^6)\right]\ (17.1166/0.1464 + 15.6282/0.1464 + 8.868/0.892)$$

$$\Delta_y = 233.609\ P_{oy}/10.5\ (10^6)$$

$$K_T = P/\Delta = 10.5\ (10^6)/233.609 = 44{,}947\ \text{lb./in.}$$

Note: Braces were assumed to be fully effective in axial direction because of mount shape, since any kick-up forces and deflections are restricted by 3rd brace as well as braces OA and OB counteracting kick-up deflections.

$\Delta_{lax} = h\gamma = P_s h/2tLG \qquad (\gamma = f_s/G)$

$G = 4.0\ (10^6) \qquad h = 7.3$ Ref: p. 7.2-6

$L = 12.52$ Ref: p. 7.1-30

$\Delta_l = P_{oy}\ (7.3)/2\ (.05)\ (12.52)\ (4.0)\ (10^6)$

$\Delta_l = 1.4577\ P_{oy}/10^6$

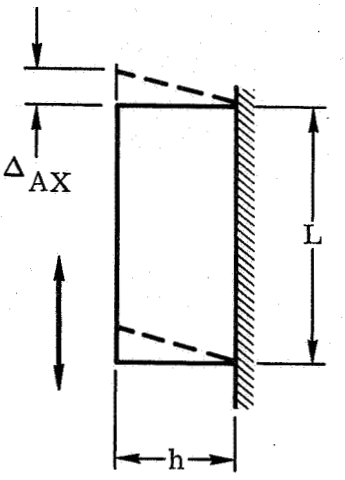

The entire length of shear panel is assumed to be effective since the shape of the mount allows shear panel end reactions to carry around the corner. The above shear panel deflection must be combined with the support fitting deflection.

$K_s = P/\Delta = 10^6/1.4577 = 686{,}012$ lb./in.

For Shear Panel and Truss Only

$K = K_t + K_s = 44{,}947 + 686{,}012 = 730{,}959$ lb./in.

Support Fitting:

$\Sigma M_B \qquad 3.9\ F_a = 2.0\ P_{ax}$

$F_a = 0.513\ P_{ax}$

$F_b = -0.513\ P_{ax}$

$\Delta_b = PL/AE$

$\Delta_b = 2\ \omega_{eff}\ t_1 + 4.9\ t_2$

$\Delta_b = 2\ (1.0)\ (0.05) + 4.9\ (0.04)$

$\Delta_b = 0.296$

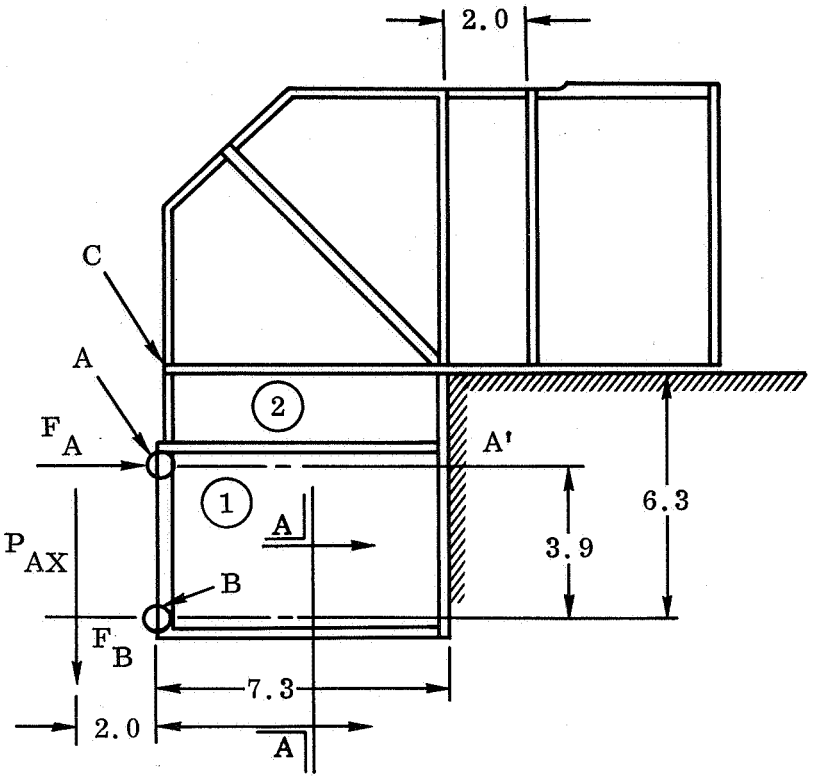

E = 10.5 (10^6) - 7075

L = 7.3

$\Delta_b = P_{ax}\ (7.3)/(0.296)\ 10.5\ (10^6)$

$\Delta_b = P_{ax}\ 2.349/10^6$

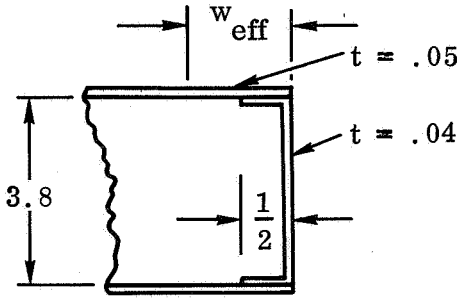

SECTION "AA"

At Point "A" the Deflection is a Result of

1) Axial load in member (A-A')

2) Bending in beam (BAC)

3) Shear deformation in panel (1) and (2) in direction of F_a

1) Axial Loading

$\Delta_{al} = 2.349\ P_{ax}/10^6$ (equal to Δ_b, above)

2) Beam Bending

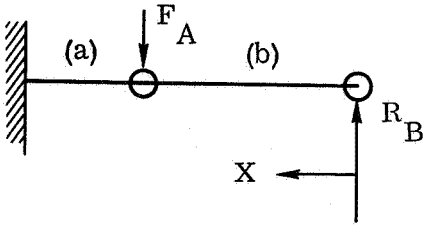

$$\Delta_a = \left[R_b\ (X^3 - 3L^2X) + 3\ F_a\ a^2\ X\right]/6EI$$

$$R_b = (3a^2\ L - a^2)\ F_a/2L^3$$

L = 6.3 in. a = 2.0 in. b = 6.0 - 2.0 = 4.3 in.

$$R_b = \left[3\ (2.0)^2\ (6.3) - (2.0)^3\right] F_a/2\ (6.3)^3 = 67.6\ F_a/500.094$$

$$R_b = 0.1352\ F_a = (0.1352)\ (.513)\ P_{ax} = \underline{0.06936\ P_{ax}}$$

For x = b = 4.3 in.

$$\Delta_a = \left[R_b\ (b^3 - 3L^2b) + 3\ F_a a^2 b\right]/6EI$$

$$= \left\{ 0.06936\ P_{ax} \left[(4.3)^3 - 3\ (6.3)^2\ (4.3)\right] + 3\ (0.513)\ P_{ax}\ (2.0)^2\ 4.3 \right\}/6EI$$

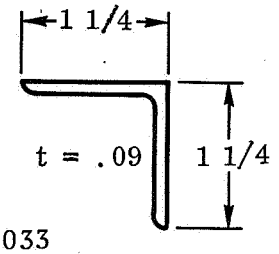

$$\Delta_a = (P_{ax}/EIO)\left[-29.9978 + 26.4708\right]/6$$

Equivalent "I" for 1-1/4 - 1-1/4 - 0.09∠ I = 0.033

$$I_t = 2I = (2)\ (0.033) = 0.066\ (2\ \text{angles})$$

$$E = 10.5\ (10^6)$$

$$\Delta_{a2} = P_{ax}\ (3.527)/6\ (10.5)\ (10^6)\ (0.066)$$

$$\Delta_{a2} = 0.8482\ P_{ax}/10^6$$

$$K_2 = P/\Delta = 10^6/0.8482 = 1.1789\ (10^6)\ \text{lb./in.}$$

$$K_1 = P/\Delta_a = 10^6/2.349 = 0.4258\ (10^6)\ \text{lb./in.}$$

3) Panel Shear Deformation - This is equivalent to a shear lag situation

$\Delta_{a3} = F_a kb/2tG$ - This equation is based on $b_1 = b_2$, it will not be in too much error to consider $b = (b_1 + b_2)/2 = b_{avg}$

$b_1 = 5.3 \quad b_2 = 2.0 \quad b = 3.65$

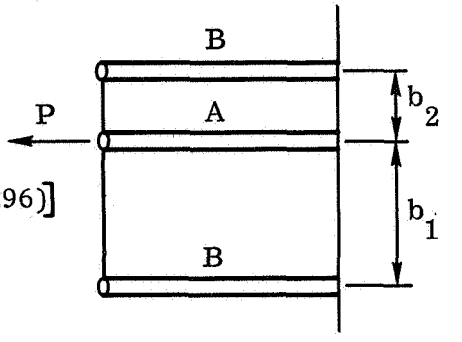

$k^2 = (2tG/bE)\ (1/A_a + 1/2\ A_b)$

$= [2\ (0.05)\ (4.0)/3.65\ (10.5)]\ [1/3\ (0.296)]$

$= 0.4/34.0326 = 0.01175 \qquad k = 0.1084$

$\Delta = (0.513\ P_{ax}/2)\ (0.1084)\ (3.65)/2\ (0.05)\ (4.0)\ 10^6$

$\Delta_{a3} = 0.203\ P_{ax}/0.8\ (10^6)$

$\Delta_{a3} = 0.2537$

$K_3 = P/\Delta = (0.8)\ 10^6/0.203 = 3.9414\ (10^6)$ lb./in.

$K_a = K_1 + K_2 + K_3 = (0.4258 + 1.1789 + 3.9414)\ 10^6$

$K_a = 5.5461\ (10^6)$

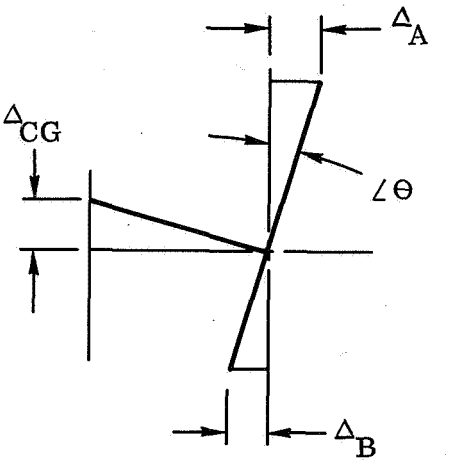

$\Delta_a = P/K = P_{ax}/5.5461\ (10^6)$

$\Delta_a = 0.1803\ P_{ax}/10^6$

$\theta = (\Delta_a + \Delta_b)/L$

$= (0.1803 + 2.3490)\ P_{Ax}/10^6(3.9)$

$\theta = 0.6485\ P_{ax}/10^6$

$\Delta_{2cg} = R\theta = (2.0)\ (0.6485)\ P_{ax}/10^6$

$$\Delta_{2cg} = 1.2971\ P_{ax}/10^6$$

$$\Delta_{cg} = \Delta_{1cg} + \Delta_{2cg} = (1.4577 + 1.2971)\ P_{ax}/10^6$$

$$\Delta_{cg} = 2.7548\ P_{ax}/10^6$$

$$K_b = P/\Delta = 10^6/2.7548 = 363{,}003 \text{ lb./in.}$$

$$K_{cg} = K_t + K_b = 44{,}947 + 363{,}003 = 407{,}950 \text{ lb./in.}$$ Ref: p. 7.2-4

$$f_n = \sqrt{K_g/w}\ /2\pi = \sqrt{(407{,}950)\ (386.1)/75}\ /2\pi$$

$$f_n = (10^3/2\pi)\ (2.10013)^{\frac{1}{2}}$$

$$f_n = \underline{230.6 \text{ Hz}}$$

7.2.1.2 Spacecraft Thrust Direction

Ref: p. 7.2-2 $P = 1.16\ P_{oz}$

a. Member AB is Assumed Pinned

$$d_1 = 8.0281 \mapsto 6.2 = 10.1435$$

$$d_3 = 5.1 \mapsto 6.2 = 64.45^{\frac{1}{2}} = 8.0281$$

$$d_1 \mapsto d_3 = 6.2 \mapsto 5.1 \mapsto 8.0281 = 11.3534$$

$$P_1 = P/\text{Sin}\ \alpha_1 = P\ 10.1435/8.0281$$

$$P_b = P_1/\text{Sin}\ \alpha_2 = P_1\ (11.3534/8.0281)$$

$$P_b = P\ (10.1435)\ (11.3534)/(8.0281)^2$$

$$P_b = 1.7869\ P = 2.0728\ P_{oz}$$

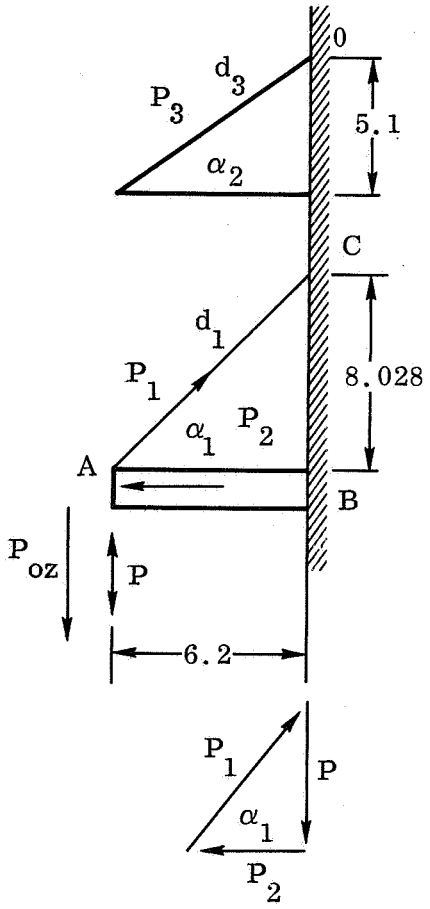

$P_2 = P\ (6.2/8.0281) = 0.7723\ P = .8959\ P_{oz}$

$A_1 = 0.1464\ in.^2$ 1.0ϕ - 0.049 Ref: p. 7.2-4

$A_2 = 1.430$ Ref: p. 7.1-36

$U = (P^2L/2AE)_b + (P^2L/2AE)_2$

$U = (2.0728P)^2\ (10.5)/2\ (0.1464)\ E + (0.8959P)^2\ 6.2/(1.43)2\ E$

$\Delta = dU/dP = (P/E)\left[2.0728^2\ (10.5)/0.1464 + (0.8959)^2\ (6.2)/1.43\right]$

$K = P/\Delta = E/(308.151 + 3.480)$

$K_1 = 33,694$ lb./in.

b. Bending Stiffness, Beam AB is Assumed Cantilevered

$\Delta = PL^3/3EI = P\ (9.3)^3/3E(4.9221)$ Ref: p. 7.1-31

$K = P/\Delta = (3)\ (10.5)\ 10^6\ (4.9221)/(9.3)^3$

$K_2 = 192,758$ lb./in.

Note: 9.3 inch length was used as this is distance to mounting bracket (load) Ref: p. 7.2-5

c. Member OB Ref: p. 7.2-2 Assume 50% Effective

$K_3 = K_1\ (1/2) = 33,694/2 = 16,847$ lb./in.

$K_z = \Sigma K = 33,694 + 192,758 + 16,847 = 243,299$ lb./in.

$f_n = (Kg/w)^{\frac{1}{2}}/2\pi = \left[243,299\ (386.1)/(75/2)\right]^{\frac{1}{2}}/2\pi$

$$f_n = (2.505)^{\frac{1}{2}}/2\pi = 1582.7/2\pi = \underline{251.9} \text{ Hz}$$

In the vertical direction the sprung mass is distributed equally (1/2) to each end.

7.2.2 Wrap Drum End Plate

This section takes into account the slide and fixed end concept of drum mounting (i.e., all drum axial loading is taken at the fixed end, with the slide end acting as an expansion joint in the drum axial direction). The slide end can take loading in the drum lateral directions (X and Y axes). The dynamic model of the fixed end portion of the drum is shown in Figure 51.

The following revised weights were used:

	Pounds
Panel assembly	11.198
Wrap drum assembly	12.357
Solar cell installation	41.366
Total	64.921

This is the total sprung weight acting through the end plate at the drum fixed end.

The deflections of plates are given on page 7.2-17, 18 for various fixity conditions of the inner and outer edges (boundary conditions). The latest configuration has a hub attachment in the center which will be assumed to be 40% effective in relation to the full plate (Ref: Figure 52).

1) Simply Supported Outer Edge

$$y = 90.703 - (0.40)\ (90.703 - 63.042)\ (P/16\pi d)$$

$$y = 80.039\ (P/16\pi D) \text{ for 40\% effective hub}$$

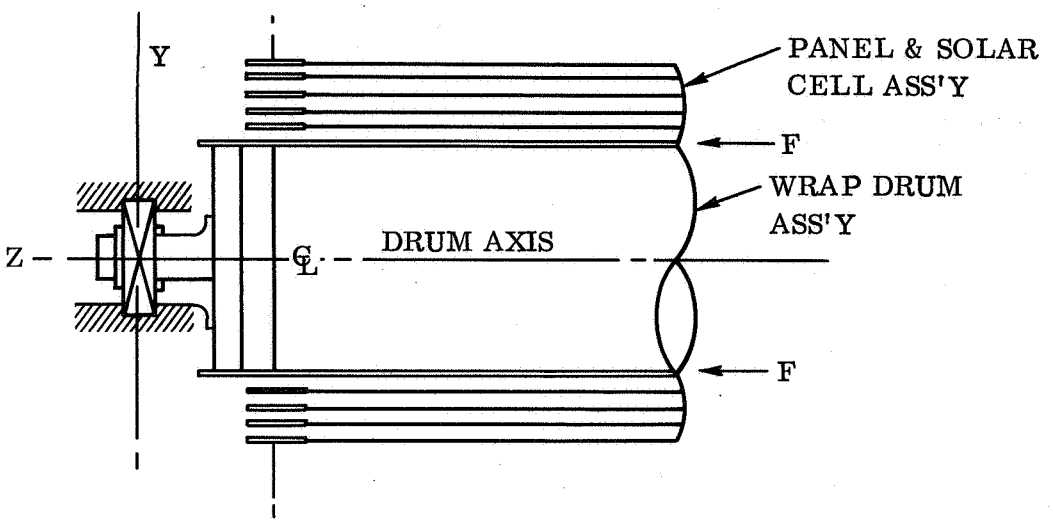

VIEWED AS A MODEL

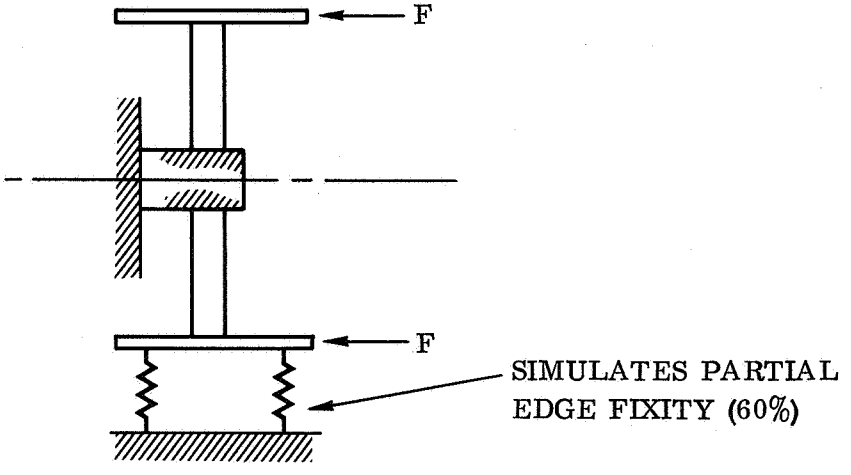

Figure 51 End Plate Dynamic Model

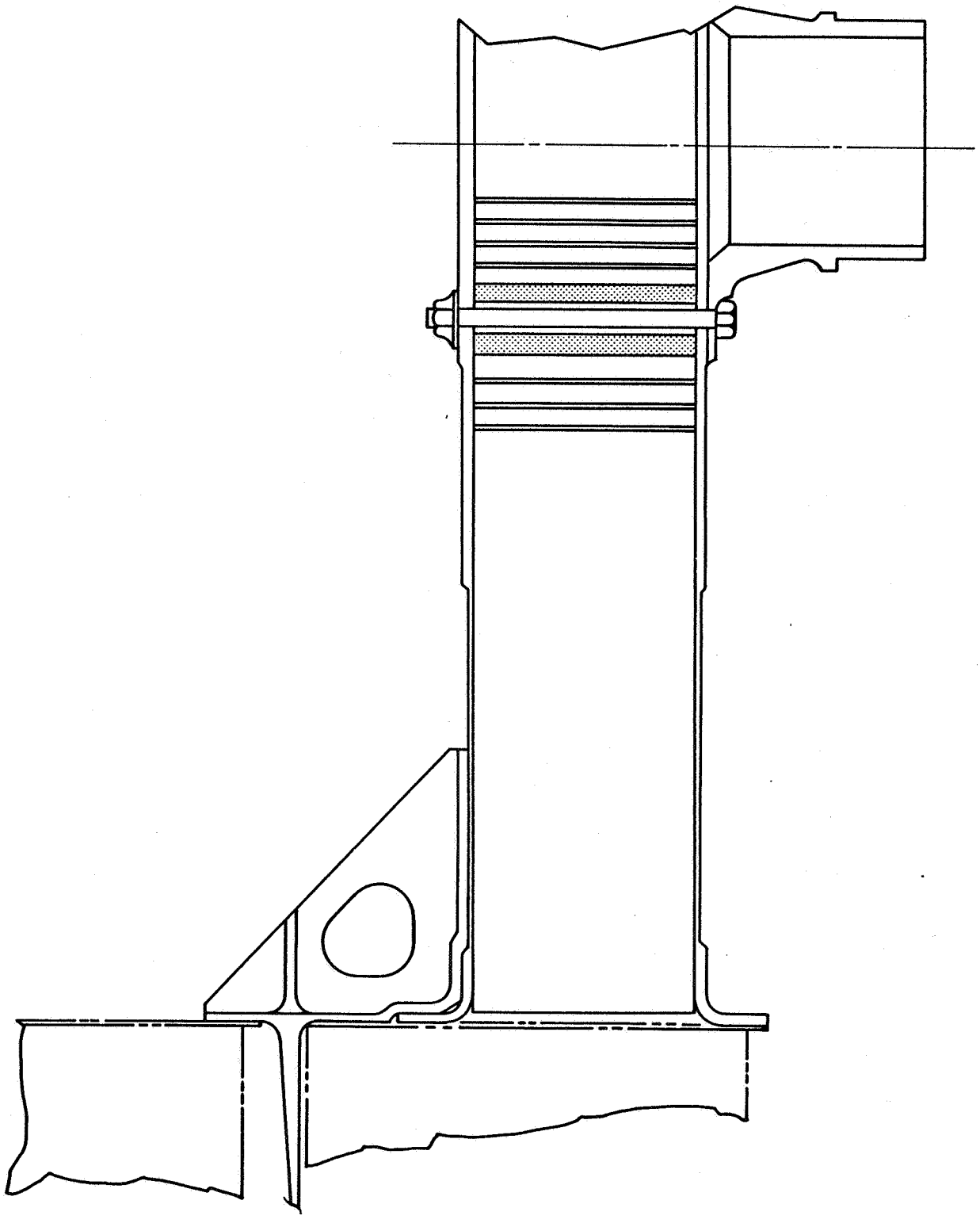

Figure 52 End Plate Layout - Fixed End

2) Fixed Outer Edge

$y = 36.0 - (0.40)\ (36.0 - 21.077)\ (P/16\pi D)$

$y = 30.031\ (P/16\pi D)$ for 40% effective hub

Gussets have been added to the drum-end plate attachment area (Ref: p. 7.2-13) which stiffens the attachment area.

It is further assumed that the outer edge is 60% fixed so that:

$y = 80.039 - (0.6)\ (80.039 - 30.031)\ (P/16\pi D)$

1) $\underline{y = 50.034\ (P/16\pi D)} = y_{st} \cong P/D$

2) $D = 5.833\ t_f\ t_c\ t\ 10^6$ Ref: (14)

$P = W = 64.921$ Ref: p. 7.2-11

3) $f_n = 3.1273/y^{\frac{1}{2}} = (3.1273^2\ D/P)^{\frac{1}{2}} = (0.150645D)^{\frac{1}{2}}$

4) $\Delta_{dyn} = (12.309/f_n)^2 = 151.5115/f_n^{2}$*

Results are tabulated in Table 14. Selection of actual skin thicknesses will be made on the basis of stress and system dynamics requirments (Ref: Sections 7.2.1 and 7.1.1). Also tabulated, is the end plate spring rate.

$K = P/\Delta = P/(50.034\ P/\pi 16D) = 16\pi D/50.034$

5) $K = 50.266\ D/50.034 = 1.0046D$

---

*For $a = 4$

$Q = (T.R^2 - 1)^{\frac{1}{2}} = 3.873$

The natural frequencies are shown in Table 14. It was desired to have a minimum f_n = 150 Hz. All end plate configurations with 1.5 inch cores exceed this requirement.

Table 14 Dynamic Summary of Natural Frequencies and Spring Rates

t	t_f	t_c	D	f_n	Δ_{dy}	K
1.500	0.030	1.440	378,000	238.63	0.00266	379,739
1.500	0.032	1.436	402,057	246.11	0.00250	403,906
1.500	0.036	1.428	452,314	261.03	0.00222	454,395
1.500	0.040	1.420	496,972	273.62	0.00202	499,258
1.500	0.044	1.412	543,589	286.16	0.00185	546,090
1.500	0.048	1.404	589,646	298.04	0.00171	592,358
1.500	0.050	1.400	612,465	303.75	0.00164	615,282

Dimensional Data:

$a = r_o = 6.0$ in. $\quad \mu = 0.3162 \quad \mu^2 = 0.10$

$b = r_i = 1.05$ in.

a. Simply supported Plate with Hub Refs: (9) and (10)

$$y_m = (P/16\pi D)\left\{ \left[a^4 (3 + \mu) - b^4 (1 - \mu) - 2a^2 b^2 (1 + \mu) - 8a^2 b^2 \text{Ln } (a/b) - 4a^2 b^2 (1 + \mu) (\text{Ln } a/b)^2\right] / \left[a^2 (1 + \mu) + b^2 (1 - \mu)\right] \right\}$$

$$y_m = (P/16\pi D)\left\{ \left[6.0^4 (3.3162) - 1.05^4 (0.6838) - 2 (6.0^2) (1.05^2) (1.3162) - 8 (6.0)^2 (1.05^2) \text{Ln } 6.0/1.05 - 4 (6.0^2) (1.05^2) (1.3162) \text{Ln}^2 (6.0/1.05) \right] / \left[6.0^2 (1.3162) + 1.05^2 (0.6838)\right] \right\}$$

$$y_m = (P/16\pi D)\left\{ \left[4297.80 - 0.83 - 104.48 - 317.52 \text{ Ln } 5.7143 - 208.96 \text{ Ln}^2 5.7143\right] / \left[46.6293\right] \right\}$$

$\text{Ln}_e\ 5.7143 = 1.743 \quad \text{Ln}^2\ a/b = 3.038$

$$y_m = (p/16\pi D)\ (2986.42/46.6293)$$

$$y_m = \underline{64.042\ (P/16\pi D)} \qquad (1)$$

b. Fixed Edge Plate With Hub Refs: (9) and (10)

$$y_m = (P/16\pi D)\left\{ a^2 - b^2 - \left[4\ a^2\ b^2\ \mathrm{Ln}^2\ (a/b)\right]/(a^2 - b^2)\right\}$$

$$y_m = (P/16\pi D)\left\{ 6.0^2 - 1.05^2 - 4\ (6.0)^2\ (1.05)^2\ (3.038)/(6.0^2 - 1.05^2)\right\}$$

$$y_m = (P/16\pi D)\left\{ 34.8975 - 482.31/34.8975 \right\}$$

$$= (P/16\pi D)\ (34.8975 - 13.8208)$$

$$y_m = \underline{21.077\ (P/16\pi D)} \qquad (2)$$

c. Simply Supported Plate with Hole Refs: (9) and (10)

$$y_m = (P/16\pi D)\left[(a^2 - b^2)\ (3 + \mu)/(1 + \mu) + 4a^2\ b^2\ (1 + \mu)\ (\mathrm{Ln}\ a/b)^2 /(1 - \mu)(a^2 - b^2)\right.$$

$$y_m = (P/16\pi D)\left[(6.0^2 - 1.05^2)\ (3.3162)/(1.3162) + (4)\ (6.0^2)\ (1.05^2)\ (1.3162)\ (3.038)/(0.6838)(6.0^2 - 1.0^2)\right]$$

$$y_m = (P/16\pi D)\left[87.9252 + 634.82/23.863\right]$$

$$y_m = P/16\pi D\ (87.9252 + 26.603) = \underline{114.528\ (P/16\pi D)}$$

d. Fixed Edge Plate with Hole Refs: (9) and (10)

$$y_m = (P/16\pi D)\left\{a^2 - b^2 + \left[2b^2\ (a^2 - b^2) - 8a^2\ b^2\ (\mathrm{Ln}\ a/b) + 4a^2\ b^2\ (1 + \mu)\ (\mathrm{Ln}\ a/b)^2\right] / \left[a^2\ (1 - \mu) + b^2\ (1 + \mu)\right]\right\}$$

$$y_m = (P/16\pi D) \left\{ 6.0^2 - 1.05^2 + \left[2\ (1.05^2)\ (6.0^2 - 1.05^2) - 8\ (6.0^2)\ (1.05^2)\ (1.743) + 4\ (6.0^2)\ (1.05^2)\ (1.3162)\ (3.038) \right] / \left[6.0^2\ (0.6838) + 1.05^2\ (1.3162) \right] \right\}$$

$$y_m = (P/16\pi D) \left\{ 34.8975 + \left[76.9500 - 553.428 + 634.820 \right] / 23.1657 \right\}$$

$$y_m = (P/16\pi D)\ (34.8975 - 6.835)$$

$$y_m = \underline{41.733\ (P/16\pi D)}$$

e. Simply Supported Plate Refs: (9) and (10)

$$y_m = (P/16\pi D) \left[a^2\ (3 + \mu)/(1 + \mu) \right]$$

$$y_m = (P/16\pi D) \left[6.0^2\ (3.3162)/1.3162 \right]$$

$$y_m = \underline{90.703\ (P/16\pi D)} \quad \text{at centerline} = y_o$$

$$y_x = y_o \text{ Sin } \pi x/2r = y_o \text{ Sin } \pi\ 4.95/2\ (6.0) = y_o \text{ Sin } 1.3 \text{ (Rad)}$$

$$y_x = 90.703\ (P/16\pi D)\ (0.964) = 87.438\ (P/16\pi D)$$

latter is more exact - former is conservative

Comparing relative deflection for three type plates and for both fixed and simply supported outer edges.

1) Simply Supported Outer Edge

Full Plate $y_m = 90.703\ (P/16\pi D)$

Center Cutout $y_m = 114.528\ (P/16\pi D)$

Center Hub $y_m = 65.042\ (P/16\pi D)$

2) Fixed Outer Edge

Full Plate $y_m = 36.000\ (P/16\pi D)$

Center Cutout $y_m = 41.733\ (P/16\pi D)$

Center Hub $y_m = 21.077\ (P/16\pi D)$

$\therefore y_m = K\ (P/16\pi D)$ the average K for the above conditions is 61.434.

7.2.3 Wrap Drum and Stowed Panel

The magnesium wrap drum is designed to be sufficiently rigid to limit maximum dynamic deflection to $\leq$ 0.25 inch when excited normal to the drum axis with 4g (Pk) launch sinusoidal vibration. The 0.25 inch was set by Ryan as a design goal to minimize induced bending stresses in the solar cells and to reduce the spacing necessary between the stowed panel outer wrap and the drive torque tube. Analysis performed in Phase I (Reference 1) shows the lightest weight wrap drum of magnesium which will limit panel deflection to 0.25 inch is about 12 inch diameter of 0.032 thick skin. Stress margins of safety were +0.22 based on beam bending analysis.

The drum stress analysis, based on the drum being loaded as a pin-ended beam in bending at resonance and assuming that the drum supports the stowed panel as small incremental masses, was found to be conservative. A full size drum with stowed panel was sine vibration tested normal to the drum axis, and it was found that:

a. The stowed panel does not act as small incremental masses supported by the drum. Rather, the stowed panel has a critical resonance mode, elliptic in shape, which does not load the drum in bending.

b. Maximum vibration deflection at the elliptic mode did not exceed the 0.25 inch design goal.

c. Assumption of pin-ended drum conditions at the bearings was verified.

d. The drum bending mode is insignificant since it is completely decoupled from the stowed panel elliptic mode and the stowed panel wraps provide a large amount of damping of this mode. This allows a reduction in skin thickness from 0.032 to 0.025.

The measured maximum dynamic deflections were within the 0.25 inch design goal. The stowed panel mode was 30 Hz, as compared to the 50 Hz calculated.

7.2.4 Deployed Panel

This analysis shows that the two deployment beams are sufficiently rigid to effect a deployed panel vibration natural mode of at least 0.04 Hz. Considerations for panel membrane, or coupled mode, are also given. The analysis contained in Reference 1 shows that margins of safety are high for any in-space accelerations and that the beam thermal properties are such that it will not exceed the deployed flatness requirement of $\leq 10°$ out of plane. Analysis presented in this section is based upon maximum beam temperature conditions (358°F), when receiving 260 mw/cm^2 solar flux.

7.2.4.1 Cantilevered Panel Mode

The deployed beam is shown (Figure 53) schematically below:

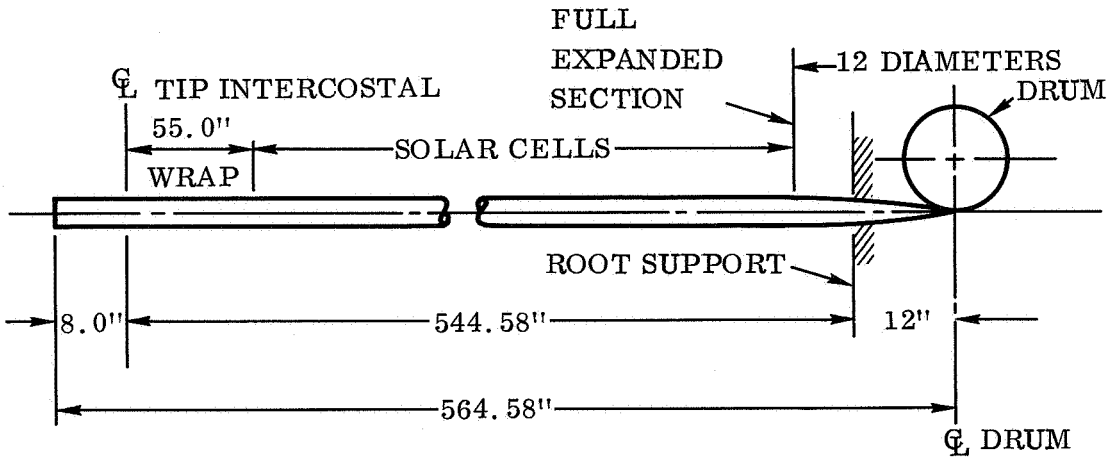

Figure 53 Deployed Beam Schematic

The last wrap of the stowed panel is a thermal reflecting wrap and does not have solar cells mounted to the substrate. For this reason the effective dynamic length was taken as the distance to the centerline of intercostal only, since the last wrap and beams are relatively light with respect to the solar cell weight. The total weight of the panel was then distributed over the effective dynamic length of 544.58 inches, from the root support.

The weight used in the dynamic analysis was taken as:

a.	Solar Cell Installation	41.336 pounds
b.	Substrate and Beams	10.923 pounds
c.	Tip Intercostal	0.263 pound
	TOTAL	52.522 pounds

The linear distributed weight per beam is therefore:

$$w = W/2L_B = 52.522/(2)\ (544.58) = 0.048 \text{ pound/inch/beam}$$

The beam cross section used to calculate the fundamental cantilever bending frequency is shown in Figure 54.

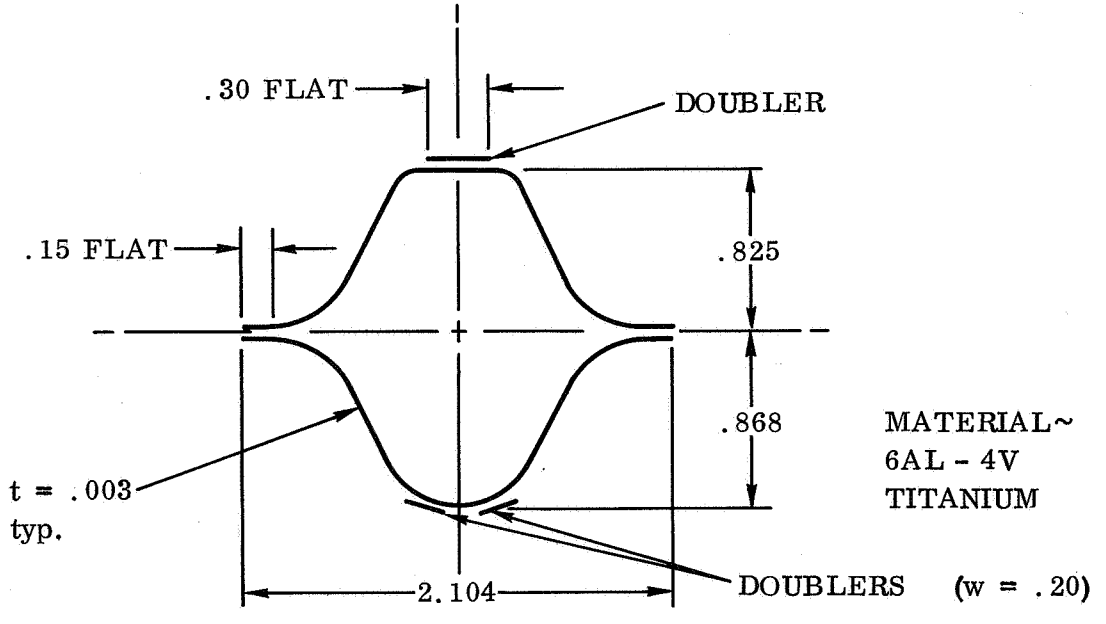

Figure 54 Side Beam Cross Section

In calculating the fundamental cantilever bending frequency, the following dimensions and properties were used:

$L = 544.58$ inches	$E = 14.9\ (10^6)$ - Ti at 350°F
$w = 0.048$ pound/inch	
$I = 1.1377t$	$t = 0.003$
$K = 1.20$	This is a factor to account for beam doubler and the effect of beam flattening at the root section. (0.97 x 1.24 = 1.20)

$$I_{eff} = KI$$

The basic frequency equation is,

$$f_n = C\sqrt{g\ E\ (KI)/WL^4}$$

$$= (0.56)\left[386.1\ (14.9)\ 10^6\ (1.2)(1.1377)\ (0.003)/\ (0.048)(544.48)^4\right]^{\frac{1}{2}}$$

$$f_n = 0.0414\ (Hz)$$

Beam doublers as shown in Figure 54 will be used for a distance of 125 inches outboard of the beam root support.

Summary

The frequency (f_n) of the cantilever mode meets the requirements of a minimum f_n of 0.040 Hz, with the use of beam doublers.

7.2.4.2 Panel Torsional Mode

The torsional model is shown schematically in Figure 55.

The basic dynamic equation for the torsional vibration mode is:

$$f_n = (n\pi/2)\sqrt{GJ\ g/\alpha\ I_p\ L^2}$$

G = Torsional modulus of elasticity

J = Section polar area moment of inertia

g = Gravity constant

α = Weight per unit length

I_p = Section mass moment of inertia

L = Length of panel (effective)

n = 1, 3, 5 torsional mode number

The above equation is derived as follows, for the torsional vibration of a shaft of constant cross section and uniformly distributed mass.

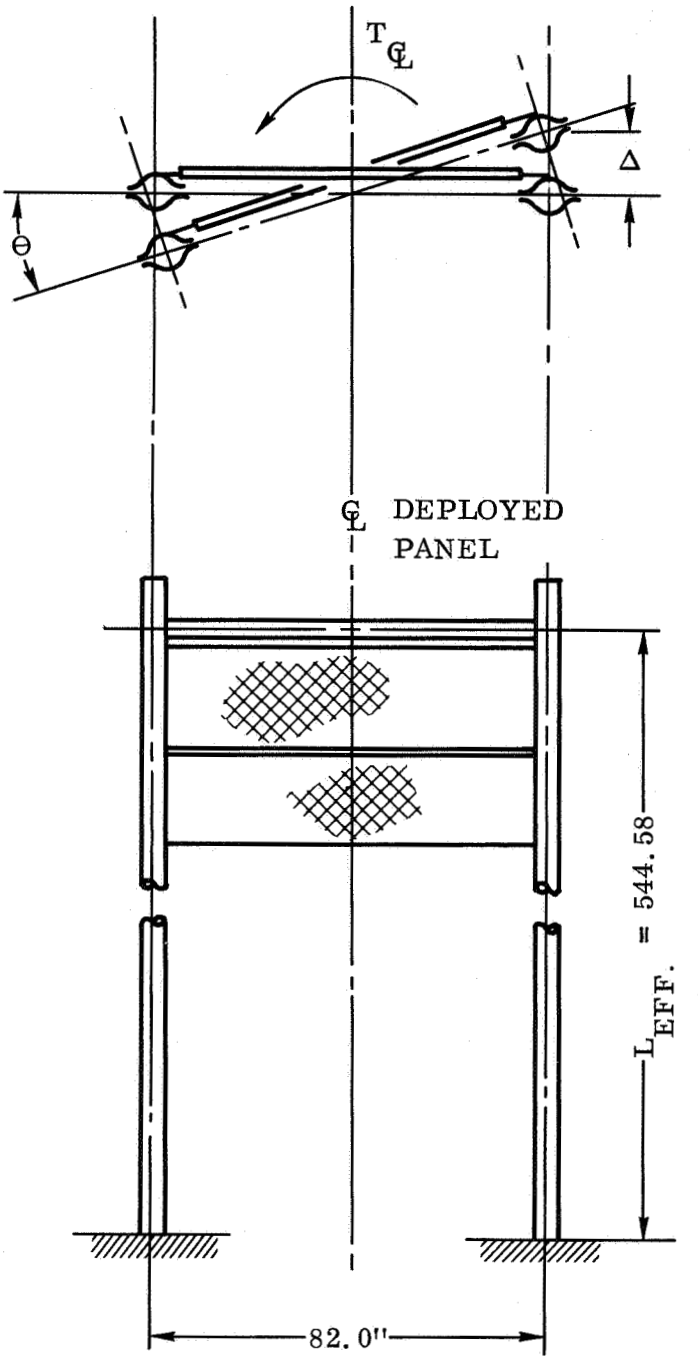

Figure 55 Torsion Mode Schematic Model

Ref: (13) p. 299-322, 336

$$\left[(\gamma I_p/g)\ \partial^2\theta/\partial t^2\right]dx = \left[GJ(\partial^2\theta/\partial x^2)\right]dx$$

$$\partial^2\theta/\partial t^2 = (GJg/\gamma I_p)\ (\partial^2\theta/\partial x^2)$$

$$\underline{\partial^2\theta/\partial t^2 = a^2(\partial^2\theta/\partial x^2)} \qquad \text{Wave Equation}$$

For Circular Shaft

$$\theta = TL/JG \qquad K_t = T/\theta = JG/L$$

$$J = I_p = I_x + I_y = (2)(\pi r^4/4) = \pi r^4/2$$

$$I_{mass} = mr^2dx/2 = (\pi r^2\gamma/g)(r^2dx/2) = (\gamma dx/g)(\pi r^4/2)$$

$$I_{mass} = (\gamma I_\rho/g)dx \qquad \gamma = \text{Weight/Unit Length}$$

$$a^2 = GJg/\gamma I_p \qquad \text{For Walled Section} \qquad (1)$$

$$a^2 = Gg/\gamma \qquad \text{For Circular Section} \qquad (2)$$

The general solution to equation (1) is

$$\theta = \psi(A\ \text{Cos}\ pt + B\ \text{Sin}\ pt)$$

$$\partial\theta/\partial x = \psi\left[f(t)\right] \qquad \partial^2\theta/\partial x^2 = \psi\left[f(t)\right]$$

$$\partial\theta/\partial t = \psi(-A_p\ \text{Sin}\ pt + B_p\ \text{Cos}\ pt)$$

$$\partial^2\theta/\partial t^2 = \psi(-A_p^{\ 2}\ \text{Cos}\ pt - B_p^{\ 2}\ \text{Sin}\ pt)$$

Substituting the above derivatives in Equation (1)

$$-p^2\ \psi\left[f(t)\right] = a^2\ \psi\left[f(t)\right]$$

$$\underline{\partial^2 x/\partial x^2 + (p^2/a^2)\ \psi = 0}$$

Solution to the above differential equation is

$$\psi = C \text{ Cos } px/a + D \text{ Sin } px/a$$

At $x = 0$ $\quad (\psi)_{x=o} = 0 \quad \therefore \quad C = 0$

$$\psi = D \text{ Sin } px/a$$

$$\theta = \psi\,[f(t)] = D/\text{Sin } px/a)\,[f(t)] \qquad D = \theta_o$$

$$\theta = \theta_o \text{ Sin } px/a\ f(t)$$

At $x = L$ $\quad \theta = \theta_o$ for $f(t) = 1$

$$\text{Sin } pL/a = 1 \qquad pL/a = n\pi/2$$

$$M = 1, 3, 5, 7. \ . \ .$$

$$P = n\pi a/2L = (n\pi/2L)\ \sqrt{GJg/\gamma I_p}$$

$$\underline{p = n\pi/2\ \sqrt{GJg/\gamma I_p L^2}} \qquad n = 1, 3, 5 \qquad (1)$$

For free-free condition Ref: 9, p. 300, 319

$$p = an\pi/L = n\pi\ \sqrt{GJg/\gamma I_p L^2} \qquad n = 1, 2, 3 \qquad (2)$$

For the fundamental mode the free-free frequency is twice the frequency for fixed free condition and $L_1 = L_2/2$. This would indicate that the node at centerline acts as fixed end.

The beam torsional properties have been calculated as follows:

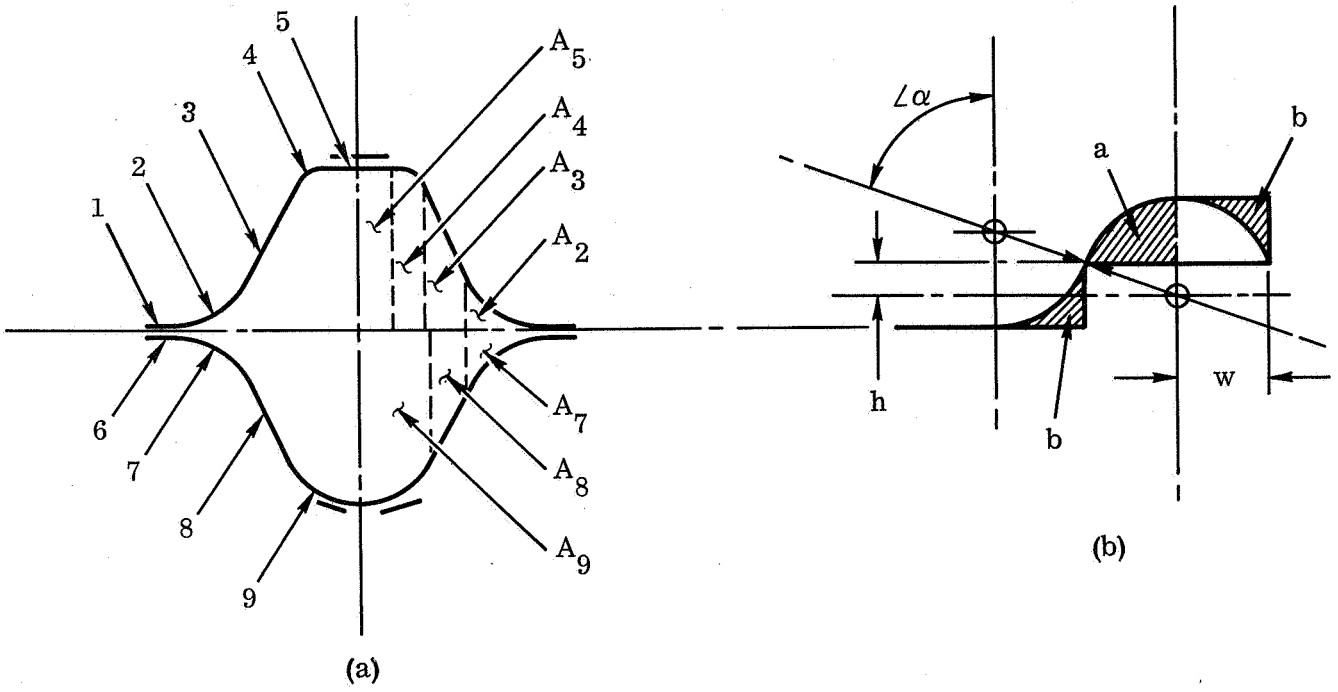

Figure 56. Beam Cross-Section Elements

From Figure 56:

Area of Segment (a)

$$A_a = \alpha_r r^2/2 - \omega h/2$$

$$\omega = r \text{ Sin } \alpha \qquad h = r \text{ Cos } \alpha$$

$$A_a = (r^2/2)(\alpha - \text{Sin } \alpha \text{ Cos } \alpha)$$

Area of Segment (b)

$$A_b = r\omega - r^2\alpha/2$$

$$A_b = r^2(\text{Sin } \alpha - \alpha/2)$$

For the following conditions:

$r_2 = r_7 = r_9 = 0.40$ in. $\qquad \alpha_1 = 65.90^o$

$r_4 = 0.19$ in. $\qquad \alpha_2 = 66.54^o$

2) $A_{2b} = r^2 \text{ Sin } \alpha - r^2\alpha/2 = 0.4^2(0.91283) - 0.4^2(1.150175)/2$

$A_2 = 0.0540388$

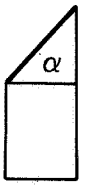

7) $A_{7b} = 0.4^2(0.91729) - 0.4^2(1.16129)/2 = 0.053,8632$

3) $A = \omega_3 \text{ Sin } \alpha \text{ Cos } \alpha/2 + \omega_3 \text{ Cos } \alpha \; R_2(1 - \text{Cos } \alpha)$

$= 0.52140\ (0.91283)(0.40833)/2 + (0.52140)(0.90833)(0.4)(1 - 0.40833)$

$= 0.52140\ (0.40833)[0.91283 + 0.4\ (1 - 0.40833)] = 0.240,508$

8) $A = (0.42095)(0.39822)\ [0.91729 + 0.4(1 - 0.39822)] = 0.194117$

4) $A_{4a} = r^2\alpha/2 - r^2 \text{ Sin } \alpha \text{ Cos } \alpha/2 + r \text{ Sin } \alpha[0.825 - r(1 - \text{Cos } \alpha)]$

$A_{4a} = (0.19^2/2)[1.150175 - 0.91283\ (0.40833)]$
$+ 0.19\ (0.91283)[0.825 - 0.19(1 - 0.40833)]$

$A_{4a} = 0.014033 + 0.123589 = 0.137622$

9) $A_{9a} = (0.4^2/2)[1.16129 - 0.91729\ (0.39822)]$
$+ 0.40\ (0.91729)[0.86756 - 0.4(1 - 0.39822)]$
$= 0.063681 + 0.230000 = 0.293681$

5) $A_5 = \omega h = 0.15\ (0.825) = 0.12375$

$A_t = 2\Sigma A_i = (1.08355)\ 2 = 2.1671 \text{ in.}^2$

$$J = 4A^2\, t/ds = 4(2.1671)^2\, t/6.0 = 3.1309t$$

$\theta = \Sigma\, q\, ds\, \ell/2\, At\, G = T\ell/GJ$ Ref: (11), p. 443

$$q = T/2A$$

$$T/J = \Sigma\,(T/2A)\; ds/2At = \Sigma Tds/4A^2t$$

Converting A to an equivalent circle

$$A = \pi r^2 = 2.1671$$

$$r_{eq} = \sqrt{2.1671/\pi} = 0.8305$$

Mass moment of inertia of beam-panel section related to centerline of deployed panel

$$I_{centerline} = I_o + Md^2$$

For A cylindrical mass about its centerline

$$I_o = mr^2\, \ell/2 = (\rho/g)(\pi r^2)\, r^2\, (1)/2 = (\rho/g)\, \pi r^4/2 \qquad (\ell = 1.0)$$

$$= (\rho\pi/2g)(R_o^4 - R_i^4) = (\rho\pi/2g)(R_o^2 - R_i^2)(R_o^2 + R_i^2)$$

$$= (\rho\pi/2g)(R_o - R_i)(R_o + R_i)(R_o^2 + R_i^2) = (\rho\pi/2g)(t)(R_o + R_i)(R_o^2 + R_i^2)$$

$$= (4\rho\pi/2g)\left[(R_o + R_i)/2\right]\left[(R_o^2 + R_i^2)/2\right] \sim (2\rho\pi/g)[R][R^2]$$

$$I_o = (2\pi\rho/g)(R^3t) = 2\pi rt(\rho/g)(R^2) = mr^2,\ \text{lb. sec}^2\ \text{in.}^2/\text{in.}^*$$

$$m_{act} = (\rho/g)\, V = (\rho/g)(2)(3.0)t = (0.160/386.1)(6)(0.003)$$

$$m_1 = 0.00288/386.1 = (7.459)10^{-6}\ \text{lb. sec.}^2/\text{in.}^*$$

$^*m_1 = (\text{lb./in.}^3)\ 1/(\text{in./sec.}^2)\ (\text{in.}^3) = \text{lb. in.}^3\ \text{sec}^2/\text{in.}^3 = \text{lb. sec.}^2/\text{in.}$

$$I_{o1} = mr^2 = Kmr_{eq}^2 = 0.632(7.459)\ 10^{-6}\ (0.8305)^2$$

$$I_{o1} = 3.2515(10^{-6})\ \text{lb. sec.}^2\ \text{in.}^2/\text{in.}$$

$$Md^2 = 7.459(10^{-6})(41.0)^2\ (10^{-6}) = 12{,}539\ (10^{-6})\ \text{lb. sec.}^2/\text{in.}^2/\text{in.}$$

$$I_{\text{centerline}_1} = (12{,}539 + 3)\ 10^{-6} = 12{,}542\ (10^{-6})\ \text{lb. sec.}^2/\text{in}^2/\text{in.}$$

Mass moment of inertia of Kapton and retainers about centerline.

$$m_2 = [8.46/495 - W_b]/g = [8.46/495 - (2)(3.0)(0.16)(0.003)]/386.1$$

$$m_2 = [0.017091 - 0.00288]/386.1 = 0.014211/386.1$$

$$m_2 = 36.807(10^{-6})\ \text{lb. sec}^2/\text{in.}$$

$$I_{o2} = M\ell^2/12 = m\ell^2/12 = 36.807\ (82)^2\ 10^{-6}/12$$

$$I_{o2} = 0.020624\ \text{lb. sec.}^2/\text{in.}^2/\text{in.}$$

Mass moment of substrate:

$$m = W/gL_b = 44.5/495(386.1) = 232.839\ (10^{-6})$$

$$I_{o3} = m\ell^2/12 = 232.839\ (79)^2\ 10^{-6}/12$$

$$I_{o3} = 0.12110\ \text{lb. sec.}^2\ \text{in.}^2/\ \text{in.}$$

$$I_t = I_{\text{centerline}_1} + I_{o2} + I_{o3} = 0.012542 + 0.020624 + 0.121096$$

$$I_t = 0.154262\ \text{lb sec}^2\ \text{in}^2/\text{in} \qquad \text{(For two beams)}$$

Differential bending due to unit torque applied at centerline deployed panel - Ref: centerline torque, Figure 55.

a. For no torsional rigidity in the intercostal and intercostal considered very stiff, EI $\rightarrow \infty$; the system is redundant but is related geometrically.

$T_{centerline} = 2T_a + 2P_a L_i/2 = 1$ in.-lb.

$T_a = T_b$ and $P_a = P_b$

$2T_a + P_a L_x = 1$

$\theta_a = \Delta/(L_i/2) = 2\Delta_a/L_i$ (a)

$\left.\begin{aligned}\theta_a &= T_a L/GJ \\ \Delta_a &= P_a L^3/3EI\end{aligned}\right\}$ Subst. in (a)

$T_a L/GJ - (P_a L^3/3EI)\ 2/L_i = 0$

$T_a L/JG - 2P_a L^3/3EI\ L_i = 0$

$T_a/JG - 2P_a L^2/3EI\ L_i = 0$ (1)

$2T_a + P_a L_i = 1$ Above (2)

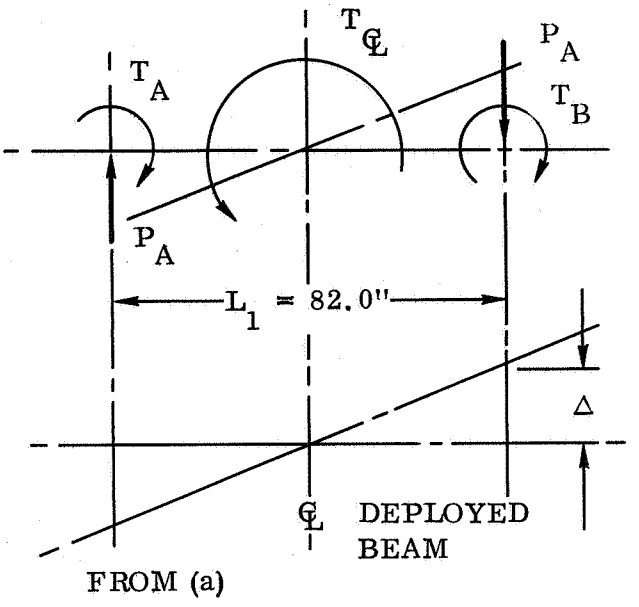

Substituting T_a from equation (2) into Equation (1)

$(1/2 - P_a L_i/2)/JG - 2P_a L^2/3EI\ L_i = 0$

$P_a L_i^2/2GJ + 2\ Pa\ L^2/3EI = L_i/2JG$

$P_a = L_i/2JG\ (L_i^2/2GJ + 2\ L^2/3EI)$

$P_a = \underline{L_i/(L_i^2 + 4JG\ L^2/3EI) = L_i/K_a}$

$T_a = (1/2 - P_a L_i/2) = 1/2 - L_i^2/2(L_i^2 + 4JG\ L^2/3EI)$

$T_a = \underline{(1/2)\left[1 - L_i^2/(L_i^2 + 4JG\ L^2/3EI)\right] = (1/2)(1 - L_i^2/K_a)}$

$2T_a + P_a L_i = 1.0 = 2(1/2)(1 - L_i^2/K_a) + (L_i/K_a)L_i$

$$1 - L_i^2/K_a + L_i^2/K_a = 1.0, \text{ Check}$$

For the following conditions T_i @ 350^oF

$L_i = 84.0$ in. $\quad L = 495$ in. $\quad E = 14.9\ (10^6) \quad I = 1.1377t$

Ref: p. 7.2 - 21

$G = 6.2\ (14.9/16.2)10^6 = 5.59(10^6)$ for $T = 350^oF$ Ref: p. 7.2-21

$J = 3.1309t$ Ref: p. 7.2 - 28

$$K = L_i^2 + 4JG\ L^2/3EI$$

$$K = (84.0)^2 + 4(3.1309)\ t\ (5.59)\ 10^6\ (495)^2/3(14.9)(10^6)(1.1377t)$$

$$K = 7056 + 337{,}301 = 334{,}357 \text{ lb./in.}$$

$$T_a = 1/2\left[1 - 84.0^2/344{,}357\right] = 1/2\ (1 - 0.0205)$$

$$T_b = P_a L_i/2 = L_i^2/2K = (1/2)(0.0205)$$

b. For 100% torsional rigidity in the intercostal considering 1/2 beam

$$\Delta/2 = P_a L_i^3/3EI$$

$$\Delta = 2(\Delta/2) = 2P_a L_i^3/3EI$$

$$\Delta = (2P_a/3EI)(L/2)^3 = P_a L^3/12EI$$

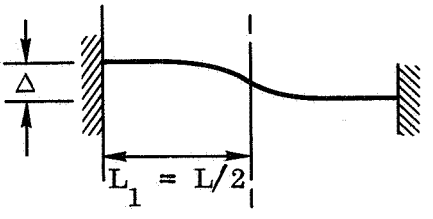

$\theta = T_a L/JG$

$2T_a + P_a L_i = 1.0$ } Same as previous case

$\theta_a - 2\Delta/L_i = 0$ Same as case (a)

$$T_a L/JG - 2\,(P_a L^3/12EI)/L_i = 0$$

$$T_a/JG - 2P_a L^2/12EI\ L_i = 0$$

$$T_a = (1/2)(1 - P_a\ L_i)$$

$$(1/2 - P_a\ L_i/2)/JG - P_a L^2/6EIL_i = 0$$

$$\underline{P_a = L_i/(L_i^2 + JG\ L^2/3EI) = L_i/K_b}$$

$$T_a = (1/2 - P_a\ L_i/2) = 1/2 - (L_i/2)\ L_i/(L_i^2 + JG\ L^2\ /\ 3EI)$$

$$\underline{T_a = (1/2)\left[1 - L_i^2/(1 + JG\ L^2/3EI)\right] = (1/2)(1 - L_i^2/K_a)}$$

Using values given for case (a)

$$K = L_i^2 + JG\ L^2/3EI = 84.0^2 + 3.1309(5.59)(495)^2/3(14.9)(1.1377)$$

$$K = 7056 + 4.288(19^6)/50.855 = 7056 + 84{,}325$$

$G = 5.59$ @ 350^oF Ref: 12 (MIL-HDBK-5A)

$$T_a = (1/2)\left[1 - 84.0^2/91{,}381\right] = (1/2)(1 - .0772)$$

$$T_b = P_a L_i/2 = L_i^2/2K_b = 84.0^2/2(91{,}381)$$

$$T_b = (1/2)(.0772) = T_b(r)$$

For 50% torsional rigidity in intercostal

$$r = (r_1 + r_2)/2 = (0.0205 + 0.0772)/2 - 0.04885 \sim 0.05$$

$$T_a = (1/2)(1 - 0.05) = (0.95)(0.5) = 0.475\ \text{in.-lb.}$$

$$T_b = (1/2)(0.05) = 0.025\ \text{in.-lb.}$$

$K_t = T/\theta = (T)/(T_a L/JG) = (0.50)JG/(0.475)L$

$K_t = (0.50)\ 3.1309\ (0.003)(5.59)\ 10^6/0.475(495)$

$= (0.026253/235.125)10^6 = 111.654$ in.-lb./rad per beam

$T = K\theta,\ K = T/\theta \qquad \theta = TL/JG \qquad K = JG/L$

$f_n = (n/4)\ \sqrt{GJg/\gamma L^2 I_p'}$ Ref: p. 7.2 - 25

$\gamma \cong \rho$ = weight/unit volume

I_p = moment (mass) of inertia per unit length

$f_n = (n/4)\ \sqrt{(GJ/L)/I_p L} = n\ \sqrt{K_t/16 I_p L}$

$I_p = 0.12110$ lb. sec.^{2}/in. Ref: p. 7.2-29

$K_t = 111.654$ Rad/in.-lb.per beam

$f_n = kn\ \sqrt{2(111.65)/16(0.1211)495} = \sqrt{0.11641(2)}\ (n)$

$f_n = kn\ \sqrt{0.23282} = 0.483n$ Hz $\qquad n = 1, 3, 5$

k = Correction factor for length other than 495 inches.

The analysis was based upon a 495-inch original length, which still reflects the actual length of substrate on the panel. The beams were lengthened to accommodate a lightweight thermal wrap. The effect of this increase in length and added inertial moment of inertia will be taken relative to the inverse of the respective lengths, which will be slightly conservative.

$K = L_1/L_2 = 495/544.58 = 0.908$

$f_n = 0.483\ k\ n = 0.483\ (0.908)(1.0)$

n = 1.0 fundamental frequency

$f_n = \underline{0.438}$ Hz

Pendulum effects - When testing the panel with 1.0g acceleration downward the deployed structure behaves as a combination pendulum and cantilever beam. The cantilever effect is idealized as a torsional spring at the pivot point.

$$\Sigma T_o = 0 = T_{acc} - T_k - T_k = 0$$

$$T_{acc} = I_{cr} = I_o\ddot{\theta}$$

$$I_o = M\ell^2/3 = W\ell^2/3g \quad \text{for}$$

rod about one end

For torsional spring @ centerline rotat.

$$T_{sp} = -K_t\theta$$

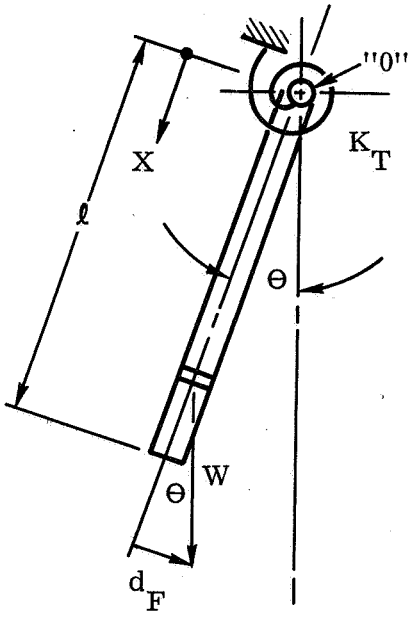

For small amplitudes

$$dF = dW \text{ Sin } \theta = dW(\theta)$$

$$dW = \rho A dx$$

ΣT_f about pivot point "0"

$$dT_f = -(dW)(\theta)(x) = -\rho A\theta(x)dx$$

$$T_f = -\int_0^{\ell} \rho\Delta\theta \; x \; dx = -\theta\rho\Delta\ell^2/2 = -\theta(\rho\Delta L)(\ell/2)$$

$$T_f = -W\theta\ell/2$$

$$\Sigma T_o \quad I\ddot{\theta} - T_f - F_k = 0$$

$$(W\ell^2/3q)\ddot{\theta} = (W\ell/2)\ \theta + K_t\ \theta = 0$$

$$\ddot{\theta} + (3g/2L + 3g\ K_t/WL^2)\ \theta = 0 = \ddot{\theta} + a\ \theta = 0$$

$$f_n = (1/2\pi)\ \sqrt{a}\ = (1/2\pi)\ \sqrt{3g/2L + 3g\ K_t/WL^2}$$

For pure pendulum effect $K_t = 0$

$$f_n = (1/2\pi)\ \sqrt{3g/2L}$$ Pure pendulum

$$f_n = (1/2\pi)\ \sqrt{3(386.1)/2\ (495)}\ = (1/2\pi)\ \sqrt{1.17}$$

$$f_n = \underline{0.172}\ \text{Hz.}$$

It is to be noted that the torsional spring effect which is here considered negligable will have the effect of increasing the frequency. Torsional bending modes would couple and have the effect of decreasing the frequency. The ratio of the pendulum mode to the torsional mode is

$$f_{np}/f_{nt} = 0.172/0.438 = 0.393$$

Summary:

The beam-substrate torsional mode natural frequency (f_n = 0.438 Hz) is well within the requirements of the minimum f_n = 0.040 Hz.

Torsional modal testing of the array in a "1-g" field must consider and allow for the expected coupling of the pendulum mode.

7.2.4.3 Panel Diaphragm Mode

The substrate with the attached solar cells and electrical connections acts as a diaphragm or membrane. There are some fundamental differences that do exist between any solar cell array and classical analysis of membranes. Analyses of membranes assume 100% edge rigidity in both the transverse and lateral panel directions. This is not the case for deployed solar arrays. Further, membrane analysis is based on the assumption of a relatively high pretensioned membrane, which tension does not change

appreciably in amount due to deflection of the membrane. Again, this is not the case for a solar array with very small edge pretension. Both of the above factors combine to make the panel mode coupled nonlinearly with both the cantilever and torsional mode. At the present state-of-the-art in dynamic analysis, a quantitative analysis is the only one presently feasible. Further study of this mode will be undertaken in Phase II. Schematically the panel membrane mode is as shown in Figure 57:

For a membrane with a small edge pretension and considering small deflection conditions and edge rigidity

$$f_{MN} = \frac{1}{2}\sqrt{\frac{gS}{w}\left(\frac{m^2}{a^2} + \frac{n^2}{b^2}\right)}$$

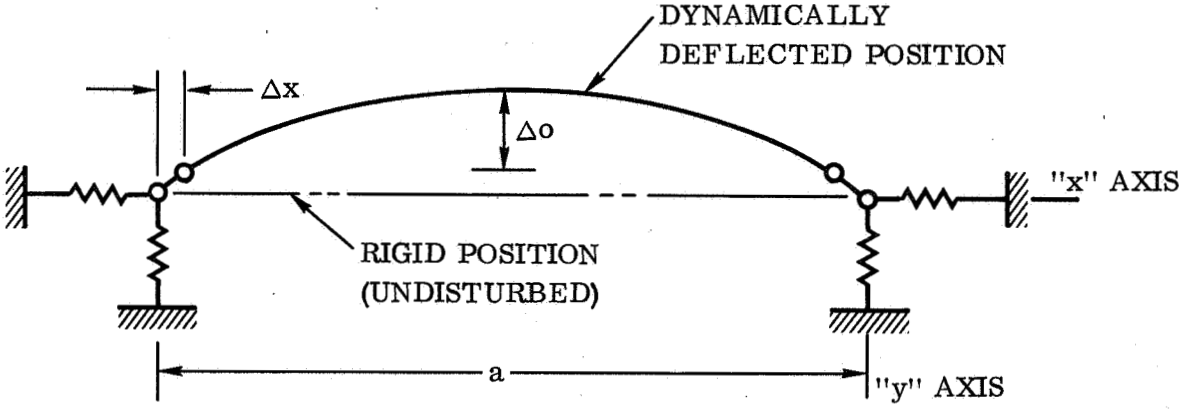

Figure 57. Panel Diaphragm Coupled Mode

For the following conditions:

m = n = 1, fundamental frequency

f_{mn} = 0.04 (Hz)

a = 82.0 inches b = 544.48 inches (length)

g = 386.1 (gravity constant)

w = 42 pounds/250 (144)-pounds/square inch

Substituting the above values in the frequency equation:

S = 0.0001272 pound/inch Edge Tension

It was also shown mathematically that for a membrane that does not stretch:

$$\Delta_x = \Delta_o^2 \pi^2/4\ a \qquad \text{(Reference: Figure 57)}$$

The above two equations indicate that only the smallest edge force is required to give a diaphragm frequency of 0.04 cps (Hz), and that the slightest motion of the panel sets up edge forces due to Δ_x at an even faster rate (nonlinear), in the "S" or short panel direction.

There are edge forces in both the lateral and longitudinal directions due to the side beams and the tip intercostal. The dynamic coupling in the "Y" (cantilever) axis direction is more complex. Due to the "S" axis direction nonlinearity, it can be concluded that coupling can occur only in a small (Δ_o) amplitude range; thereafter, the two motions will be decoupled, since frequency will vary with amplitude.

7.2.5 Guide Sleeve Supports

The magnesium guide sleeve mounts are designed primarily for sufficient rigidity to minimize dynamic deflection, supporting the drive torque tube, when excited at resonance in the drum axis direction during the launch sinusoidal vibration of 4g (Pk). Analysis performed in Phase I (Reference 1) shows that deflections will be 0.10 inch at a resonance of 79.6 Hz. This vibration mode is therefore decoupled from the wrap drum end plate, stowed panel, and spacecraft mount vibration modes. The bending stresses induced in the legs of the guide sleeve mount at resonance showed a small margin of safety (+0.06) on material yield; however, the dynamic transmissibility used in calculation of the stress was conservative by a factor of about 3 to 1, as a transmissibility of 5 is more realistic at 4g excitation than the 16.7 used for analysis, (determined by the vibration test of the 50-square foot rollup panel).

7.2.6 Stowed Panel Axial Mode

Analysis to determine the natural vibration modes of the stowed panel when excited during launch in the drum axis direction was given in Reference 2. The first three frequencies were calculated as:

First Mode = 29.6 Hz

Second Mode = 82.2 Hz

Third Mode = 134.5 Hz

7.3 WEIGHT BREAKDOWN

The calculated structure weight breakdown for the Ryan design reflected in Ryan Drawing No. 400U020 is given in this section. Structure weights shown are calculated based on nominal drawing tolerances and sheet thicknesses. For comparison, target weights generated at the outset of the program are also given.

A separate weight breakdown for the solar cell electrical installation is included. It reflects the weight of solar cells and coverglasses in accordance with JPL TWX, dated 6 May 1968.

Weights are shown for one panel of a four panel array.

7.3.1 Electrical Installation Weight Breakdown

Solar Cell Installation:

(Weights are associated with 2 X 2 cm X 8 mil silicon solar cells and 3 mil covers)

		LBS/FT^2
Solar Cell	(Per JPL TWX 6 May 1968)	0.0840
Coverglass	(Per JPL TWX 6 May 1968)	0.0321
Coverglass Adhesive	14.80 milligrams per cell	0.0073
Solar Cell Adhesive	15.00 milligrams per cell	0.0074
Copper Bus Bar	41.60 milligrams per cell	0.0205
Solder	3.80 milligrams per cell	0.0019
		0.1532

Power Transmission:

(Major Weight Contributing Elements):

ITEM	MATERIAL	WEIGHT, POUNDS
Longitudinal Bus Bars	Aluminum 1 Mil	0.976
Transverse Collector	Aluminum 2 Mil	0.144
Feedthrough and Jumpers	Copper 2 Mil	0.051
Solder		0.029
Adhesives		1.362
Insulation	Kapton 1/2 Mil	0.389
	TOTAL WEIGHT	2.951

Total solar cell area for thirteen modules is 250.72 square feet.

On a square foot basis, power transmission weight is 0.0118 pound/square foot.

Total Subsystem Weight (less substrate):

Electrical	0.1532 pound/square foot
Transmission	0.0118 pound/square foot
TOTAL	0.1650 pound/square foot

The above weights were verified empirically and with reasonable process controls should prove to be realistic. Weights for the cells, covers and bus materials are average weights. The adhesive weights are based on minimum thickness.

For the Ryan design incorporating 250.72 square feet of solar cells, the electrical installation weight becomes,

$$\text{Total Electrical Weight} = 0.1650 \times 250.72$$

$$= 41.366 \text{ pounds}$$

7.3.2 Structure Weight Breakdown

DRUM SUPPORT AND GUIDE SLEEVE MOUNT ASSEMBLY

ITEM	CALCULATED WEIGHT	TARGET WEIGHT
1. Slide Guide Fittings (Fixed End)	0.8651	0.456
2. Slide Guide Fittings (Slide End)	0.628	
3. Slide	0.102	0.171
4. Slide Retaining Angles	0.052	
5. Bulkhead and Adjustment Screws		0.108
6. Springs	0.140	0.140
7. Spring Fittings	0.014	0.027
8. Mount Lugs		0.074
9. Mount Bolts	0.046	
10. Helicoil Inserts	0.024	
11. Retaining Screws	0.026	
12. Stop Mechanism	0.303	
TOTAL WEIGHT	2.200	1.176

BEAM GUIDE SLEEVES

ITEM	CALCULATED WEIGHT	TARGET WEIGHT
1. Side Plates O/B	0.343	0.3131
2. Side Plate I/B	0.234	
3. Top Plates	0.183	0.2660
4. Bottom Plates	0.120	
5. End Plates I/B	0.029	0.0540
6. End Plate O/B	0.022	
7. Internal Bulkheads	0.042	0.1310
8. Attach Angles	0.060	
9. Frame Angle	0.084	
10. Guide Inserts	0.084	
11. Top Plate (Support)	0.043	0.4290
12. Support (Guide Insert)	0.228	
TOTAL	1.472	1.1930

WRAP DRUM ASSEMBLY

ITEM	CALCULATED WEIGHT		TARGET WEIGHT
1. Skin (Mag.) (0.025)	4.171		5.696
2. Intermediate Rings	0.154		0.115
3. Harness Retaining Ring			0.106
4. End Plate Rings			0.113
5. End Plate - Fixed End	1.986		1.786
6. End Plate - Slide End	1.352		
7. Spindle and Bolt Attachment	0.277		
8. Harness Spool			0.101
9. Roller Bearings	0.160		
10. Electrical Harness			1.600
11. Electrical Wiring	0.600		
12. Bushing Supports			0.167
13. Snap Rings	0.009		
14. Sleeve Holder	0.076		
15. End Caps	0.065	Slip Rings	
16. Sleeves	0.246		
17. Sleeve Flanges	0.056		
18. Contact Rings	0.098		
19. Ring Holders	0.164		
20. Insulator	0.005		
21. Contacts	0.100		
22. Screws	0.010		
23. Guide Fence	1.823		
TOTAL	11.352		9.684

SPACECRAFT MOUNT ASSEMBLY

ITEM	CALCULATED WEIGHT	TARGET WEIGHT
1. Top and Bottom Plates	1.292	0.466
2. Side Plates	1.059	0.368
3 Internal Bulkheads	1.220	0.074
4. Closure Angles	0.4160	0.093
5. Spacecraft Mount Fittings (1)	0.136	0.033
6. Drum Mount Fitting (Fixed) (1)	0.490	0.039
7. Drum Mount Fitting (Slide) (1)	0.309	0.098
8. Center Attach Fitting	0.029	
9. Truss Tubes (2)	0.377	1.787
10. Center Truss Tubes (1)	0.188	0.029
11. Truss Pins (12)	0.118	0.132
12. Fasteners Attach Fittings (#6 aluminum huckbolts) (24)	0.096	
TOTAL WEIGHT	5.830	3.119

PANEL ASSEMBLY

ITEM	CALCULATED WEIGHT	TARGET WEIGHT
1. Substrate (0.001)Kapton)	2.513	3.233
3. Substrate-Beam Attach Medium 3 Mil Ind. Tape (ECC-B)	0.161	0.050
4. Attach Doublers	0.044	
5. Substrate Intersheet Attach Medium	0.044	0.045
6. Side Beams (Basic)	3.424	3.272
7. Tip Intercostal	0.263	
8. Stop Damper Pad	0.012	0.502
9. Substrate Doublers (240)	0.151	0.082
10. Drive Strips (1/2-0.010)	1.196	0.599
11. Damper Pads	2.019	2.527
12. Adhesive	1.010	
13. Outer Wrap Coating	0.110	0.158
TOTAL WEIGHT	10.947	10.469

DEPLOYMENT/RETRACTION SYSTEM

ITEM	CALCULATED WEIGHT	TARGET WEIGHT
Extension System		
1. Drive Motor and Pinion	2.750	0.756
2. Motor Brace	0.021	0.017
3. Motor Mount	0.017	0.023
4. Torque Tube Shaft	0.234	0.090
5. Drive Sprockets	0.208	0.230
6. Torque Tube End Caps	0.106	0.111
7. Torque Tube	1.481	1.607
8. Torque Tube Support	0.234	
9. Bushings and Retainers	0.033	0.071
10. Roll Pins	0.013	
11. Attach Bolts (Shaft)	0.060	
12. Attach Bolts (Motor)	0.040	
13. Limit Switch and Drive	0.200	0.100
14. Electrical Wiring	0.200	
Subtotal	5.597	
Retraction System		
15. Retraction Drive Motor	1.500	0.240
16. Fasteners	0.035	
17. Motor Control Unit	0.125	
Subtotal	1.660	
TOTAL WEIGHT	7.257	3.245

7.3.3 Weight Summary

The structure and electrical installation weights given in the breakdown are integrated in this section to give the total weight for one panel.

WEIGHT SUMMARY

ARRAY SUBASSEMBLY ITEM	CALCULATED WEIGHT	TARGET WEIGHT
Drum Support and Guide Sleeve Mount Assembly	2.200	1.176
Beam Guide Sleeves	1.472	1.193
Wrap Drum Assembly	11.352	9.684
Spacecraft Mount Assembly	5.830	3.119
Panel Assembly	10.947	10.469
Deployment/Retraction System	7.257	3.245
TOTAL STRUCTURAL WEIGHT	39.085	28.886
Solar Cell and Electrical Installation weight (2x2x0.008 with 0.003 CG. - 250.72 square feet at 0.165 pound/square foot)	41.366	47.636
TOTAL PANEL WEIGHT	80.451	76.522

The total weight, converted to pounds/square foot based on solar cell area, becomes:

$$\text{pounds/square foot} = \frac{80.451}{250.72} = 0.32$$

7.4 DETERMINATION OF RADIATIVE PROPERTIES OF KAPTON

The solar array utilizes a Kapton "H" film substrate for mounting the solar cells. It was necessary to determine the thermal radiative properties of the Kapton so that the temperature profile of the surfaces could be predicted under the influence of a space environment. The transient temperature history and equilibrium temperature attained under long term worst case environmental conditions can be theoretically derived with the Ryan 1179 Computer Program, using the radiative surface properties of the Kapton as input parameters. These temperatures are used to predict the thermal integrity of the system during space missions.

Monochromatic room temperature reflectance, absorptance, and transmittance data are given for a 0.001 inch thick sheet of Dupont Kapton "H" film. The data are integrated against various source temperature Planckian black body functions to yield curves of total normal emittance and transmittance as functions of source temperature.

7.4.1. Definitions

Definitions of terms used in this report are given below.

ρ_λ Normal Monochromatic Reflectance:
The ratio of the reflected radiant intensity from a body to that incident upon it at a particular wavelength, when the incident radiation is directed normal to the surface.

α_λ Monochromatic Absorptance:
The ratio of the energy absorbed by a body to that incident upon it at a particular wavelength.

ε_λ Monochromatic Emittance:
The ratio of the emitted radiant intensity to that of a black body at the same temperature at a particular wavelength.

ε_n Total Normal Emittance:
The ratio of the emitted radiant intensity (integrated over all wavelengths) in a normal direction to that of a black body at the same temperature.

ε Total Emittance:
The ratio of the radiant intensity, integrated over all wavelengths, emitted by a planar body into a solid angle of 2π steradian to that of a black body at the same temperature.

τ_λ Monochromatic Transmittance:
The ratio of transmitted energy through a body to that incident upon it at a particular wavelength.

τ Total Transmittance:
The ratio of the energy transmitted through a material (integrated over all wavelengths) to the integrated black body energy incident on the surface.

α_s Total Solar Absorptance:
The ratio of the radiant intensity absorbed by a body to that incident upon it from the sun as defined by the F.S. Johnson. curve. (Figure 58.)

H_λ Monochromatic solar intensity (Watts/μ-cm^2) as defined by the Johnson curve. (Figure 58.)

J_λ Monochromatic black body intensity distribution (Watts/μ-cm^2), a function of temperature given by Planck's function.

ρ^* Apparent Experimental Reflectance:
The ratio of energy out to energy in for a system consisting of a semitransparent material backed by a perfect reflector ($\rho = 1$).

The use of emittance, reflectance transmittance and absorptance in these definitions rather than emissivity, reflectivity, transmissivity and absorptivity indicates that the values given are for real surfaces and include the effects of application technique, substrate, and environmental degradation. In this report where the terms having the suffix "ity" are used, a theoretical value or a laboratory measurement of a chemically pure substance on completely flat substrate, is intended.

7.4.2 Apparatus and Procedures

All measurements were made in the Space Science Laboratory of General Dynamics/Convair. The Kapton sample was provided by Dupont. The transmittance of the sample was measured with a Beckman IR4 spectrophotometer which used NaCl and CsBr prisms. The NaCl prism was used for the lower wave lengths (1 to 16μ), and the CsBr prism for the higher wave lengths (11 to 35μ). A smooth curve was fitted over the output strip chart data to average out spurious fluctuations and to facilitate incremental breakdown for computer analysis. The reflectance of the sample was measured with a Perkin-Elmer Model 13 spectrometer in conjunction with a Hohlraum and associated controller.

7.4.3 Results

The total normal emittance of the sample increases from 0.068 at 100°K to 0.330 at 400°K and decreases to 0.310 at 500°K. The hemispherical emittance is slightly higher over the temperature range (See Figure 63).

The total transmittance decreases from 0.796 at 100°K to 0.415 at 400°K and increases to 0.453 at 500°K (See Figure 64).

There is a fairly well defined window from about 5 to 10μ, where the monochromatic transmittance drops by approximately a factor of 7. Also in this bandwidth, the absorptance and reflectance values increase by approximately a factor of 2 to 3 (See Figures 60 through 63).

7.4.4 Computations

A complete description of the radiative properties of the Kapton sample must include the monochromatic values of α, τ and ρ as functions of wave length (λ) and the total values as functions of the incident black body temperature. Actually, only two of the three basic parameters need to be found experimentally since the third can be computed from the law of conservation of energy

$$\rho + \alpha + \tau = 1$$

Monochromatic parameters are discussed in the first part of this section and the total parameters are discussed at the end.

7.4.5 Monochromatic Parameters

In practice, ρ_λ and τ_λ are directly measurable quantities and α_λ is determined from the conservation of energy equation. For semitransparent materials, such as Kapton, τ_λ can be measured directly, but ρ_λ must be measured indirectly as will be shown below.

The transmittance is determined simply by measuring the transmitted energy and taking the ratio of transmitted to incident energy.

The reflectance can be determined in one of two ways: (1) the sample is backed by a theoretically perfect absorber and the ratio of reflected to incident energy is measured, or (2) the sample is backed by a theoretically perfect reflector and the ratio of energy out (including transmitted energy) to energy in is measured. In the first method, the ratio is the true value of reflectance of the Kapton. In the second method, the ratio is the apparent value of reflectance and includes the effects of transmission and absorption in the Kapton.

Since it is easier to obtain a more nearly perfect reflector than absorber of energy over the 1 to 30μ band, the second method was used. A thin sheet of gold was placed behind the Kapton sample and the reflectivity of the gold was assumed to be 1.

See Figure 58. (The subscript λ has been dropped, but it is understood that monochromatic values are implied.) The energy into the system is equal to H. At the top surface of the Kapton, the reflected energy is shown as $H\rho$. Also at this interface, $H\alpha$ is absorbed and $H\tau$ is transmitted.

The transmitted energy, $H\tau$, sees a perfect reflector and is incident again at the bottom surface of the Kapton (labeled n = 0). At this point, $[H\tau]\ \rho$ is reflected, $[H\tau]\ \tau$ is transmitted and $[H\tau]\ \alpha$ is absorbed.

The transmitted energy, $H\tau^2$, passes through the Kapton and is included, along with the reflected energy at the top surface, $H\rho$, as part of the energy out of the system.

At the bottom surface of the Kapton, $[H\tau]\ \rho$ again sees a perfect reflector, and at n = 1, the energy is divided up as before. This time has reflected energy is $[H\tau]\ \rho^2$, the transmitted energy is $H\tau^2\rho$ and the absorbed energy is $H\tau\rho\ \alpha$.

It is apparent that successive reflections between the Kapton and gold generate infinite series of absorbed and transmitted energy. All reflected energy between the Kapton and gold is converted to transmitted and absorbed energy and is therefore not considered in the overall system computations.

By definition, ρ^* is the energy out divided by the energy in. Therefore, from Figure 1:

$$\text{Energy Out} = H\rho^* = H\rho + \sum_{n=0}^{\infty} H\tau^2\rho^n$$

The energy absorbed can be seen from inspection of the figure:

$$\text{Energy Absorbed} = H\alpha + \sum_{n=0}^{\infty} H\tau\ \rho^n\alpha$$

By conservation of energy,

$$\text{Energy In} = \text{Energy Out} + \text{Energy Absorbed}$$

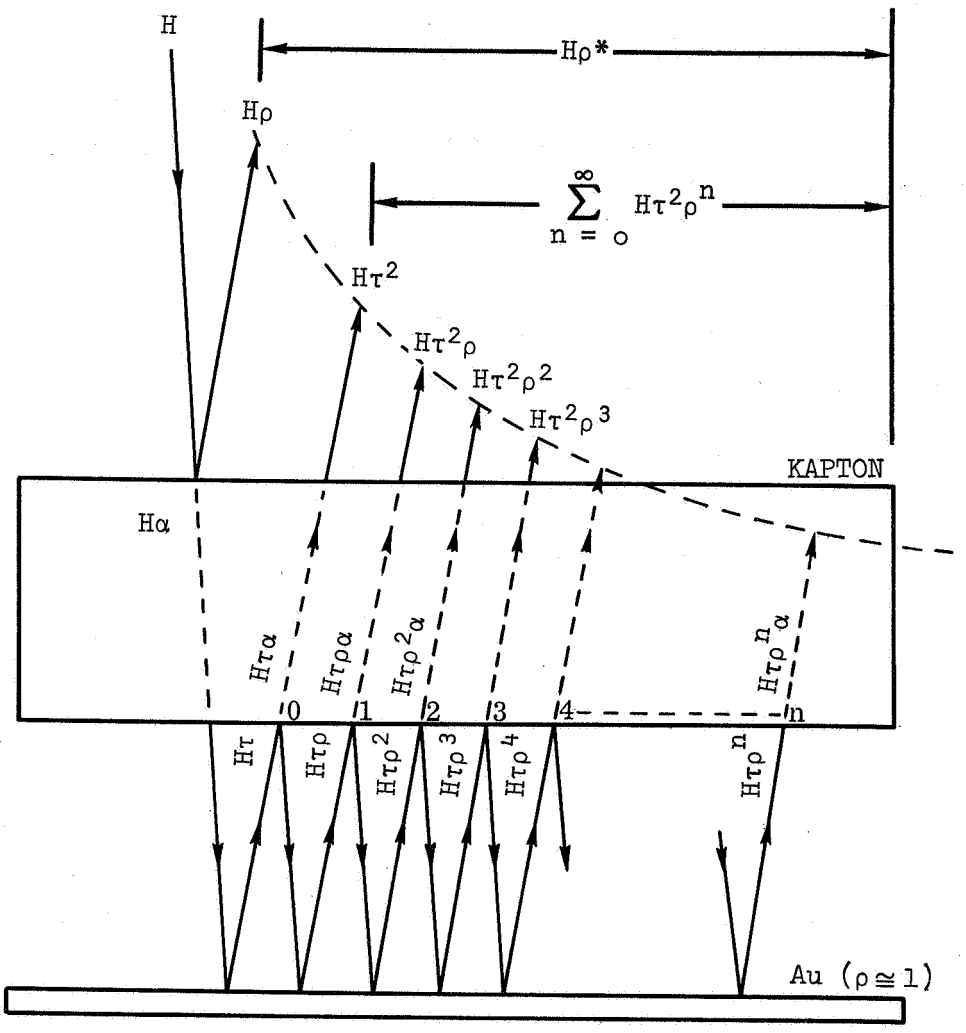

Energy in = H

Energy out = $H\rho^* = H\rho + \sum_{n=o}^{\infty} H\tau^2 \rho^n$

Energy absorbed = $H\alpha + \sum_{n=o}^{\infty} H\tau \rho^n\alpha$

Figure 58 Schematic of Energy Distribution in Sample

$$H = H\rho + \sum_{n=0}^{\infty} H\tau^2 \rho^n + H\alpha + \sum_{n=0}^{\infty} H\tau \rho^n \alpha$$

$$1 = \rho + \alpha + (\tau^2 + \tau \alpha) \sum_{n=0}^{\infty} \rho^n$$

To determine the summation, $\sum_{n=0}^{\infty} \rho^n$,

let $\sum_{n=0}^{\infty} \rho^n = S_n = 1 + \rho + \rho^2 + \rho^3 -- \rho^{n-1} ---$

$$\rho S_n = \rho + \rho^2 + \rho^3 + \rho^4 -- \rho^n ---$$

$$S_n - \rho S_n = 1 - \rho^n$$

$$S_n = \frac{1 - \rho^n}{1 - \rho}$$

$$\lim_{n \to \infty} S_n = \frac{1}{1 - \rho} \qquad \text{since } \rho < 1$$

Therefore,

$$1 = \rho + \alpha + \tau \frac{(\tau + \alpha)}{1 - \rho}$$

which reduces to the conservation of energy equation and verifies that the parameters have been properly identified as fundamental quantities.

It was necessary to relate ρ and α as functions of the measured quantities ρ^* and τ. This was determined as follows:

$$\text{Energy Out} = H\rho^* = H\rho + \frac{H\tau^2}{1 - \rho}$$

$$\rho^* = \rho + \frac{\tau^2}{1 - \rho} \qquad \text{or} \qquad \rho = \rho^* - \frac{\tau^2}{1 - \rho}$$

$$\text{Energy In} = H = H\rho^* + H\alpha + \frac{H\tau\alpha}{1 - \rho}$$

$$1 = \rho^* + \alpha + \frac{\tau\alpha}{1 - \rho}$$

$$\alpha = \frac{1 - \rho^*}{1 + \frac{\tau}{1 - \rho}}$$

The above equations have not been simplified to $\rho = f(\rho^*, \tau)$ and $\alpha = g(\rho^*, \tau)$ which can only be expressed in an unwieldy quadratic form. However, the equations can be solved by an iterative process which lends itself to a computer solution which can be readily adapted for machine computation (see Figure 59, Flowchart).

Since ρ is much less than 1, a good first approximation is:

$$\rho_1 = \rho^* - \tau^2$$

This approximate value is used to get an improved value of ρ:

$$\rho = \rho^* - \frac{\tau^2}{1 - \rho_1}$$

The average of the approximate and improved values is then inserted into the above equation to obtain a new improved value. The process is repeated until the absolute difference between the approximate and improved values is less than .0001. At that time the value of ρ_1 obtained after the final iteration is used to determine α by direct computation. ρ^*, τ, ρ_1 and α are printed out as a function of λ. The computer program is given in Table 15 and the output in Table 16.

Monochromatic transmittance, absorptance and reflectance for the Kapton sample are plotted in Figures 60 through 62.

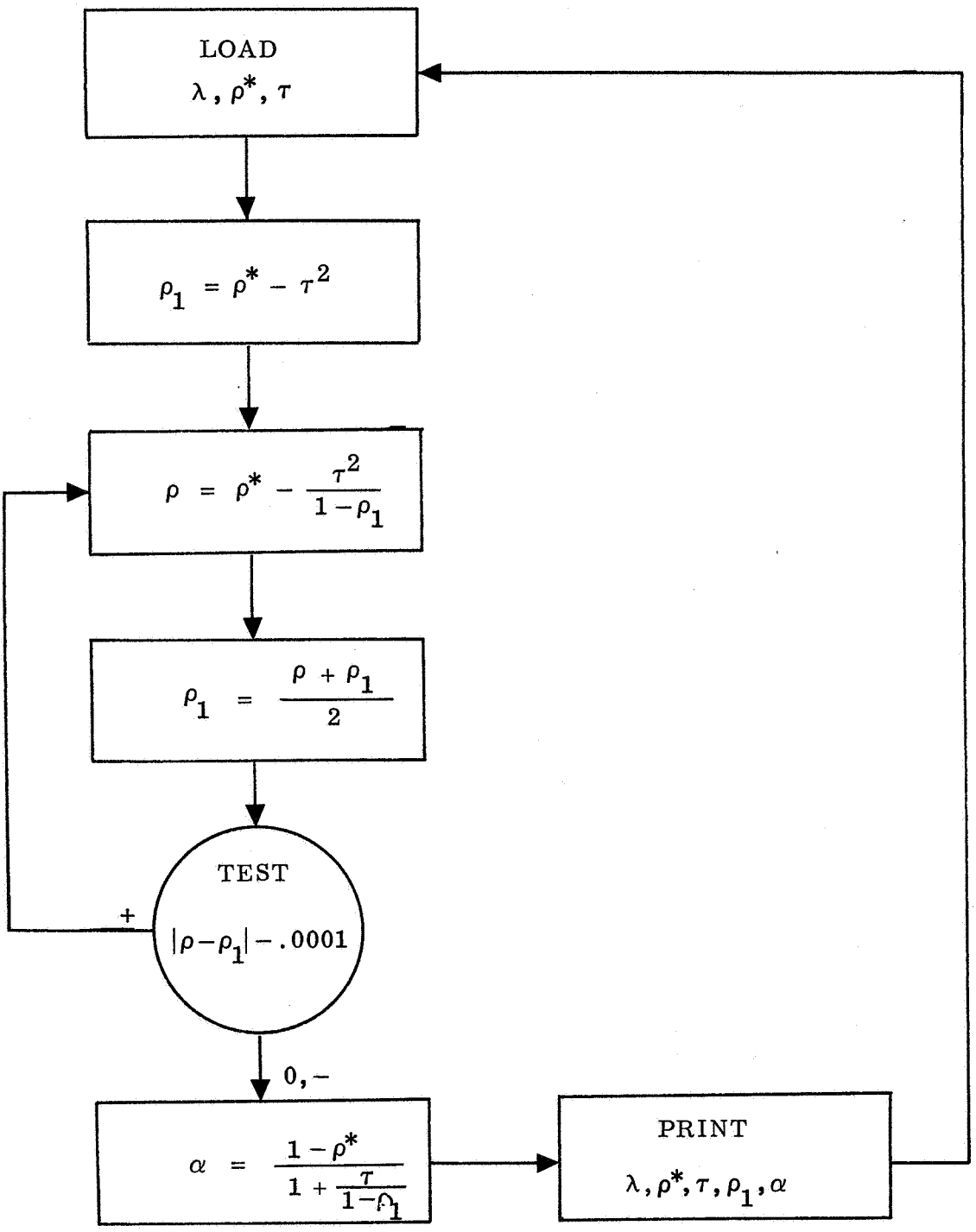

Figure 59 Flowchart

Table 15 Computer Program for the Determination of Monochromatic Values of α and ρ

```
      REAL     LAMDA
      KOUT  =0
      I   = 1
    1 READ(2,100) LAMDA,RHOST,TAU
      KOUNT    = 0
      IF(LAMDA)999, 999, 2
    2 RHO1 = RHOST -TAU*TAU
    3 RHO  = RHOST -TAU**2/(1-RHO1)
      RHO1 = (RHO+RHO1)/2.
      IF(ABS(RHO - RHO1) - .0001)  7,7,5
    5 KOUNT    =KOUNT + 1
      IF(KOUNT-200) 3,6,6
    6 WRITE(3,101)
    7 ALPHA = (1.-RHOST)/(1.+ TAU/(1.-RHO1))
      KOUT = KOUT + 1
      IF(KOUT-33) 75,75,8
   75 GO TO (8,9),I
    8 WRITE (3,102)
      I = 2
      KOUT     = 0
    9 WRITE(3,103) LAMDA,RHOST,TAU,RHO1,ALPHA
      GO TO 1
  100 FORMAT(3F10.0)
  101 FORMAT(' CONVEGENCE HAS NOT BEEN ACHIEVED'/)
  102 FORMAT(1H1/////////12X,'LAMBDA',5X,'RHO*',6X,'TAU',7X,'RHO' ,6X,'A
     1LPHA'/)
  103 FORMAT(10X,F7.2,3X,4(F8.5,2X))
  999 CALL EXIT
      END
```

Table 16 Monochromatic Values of α, ρ and τ

LAMBDA	RHO*	TAU	RHO	ALPHA
1.00	0.95170	0.87500	0.10051	0.02448
1.10	0.95130	0.85500	0.12030	0.02469
1.20	0.95080	0.85500	0.12004	0.02495
1.30	0.95040	0.86200	0.11284	0.02515
1.40	0.95000	0.86200	0.11263	0.02536
1.50	0.95000	0.87000	0.10463	0.02535
1.60	0.94000	0.87000	0.09948	0.03051
1.70	0.94000	0.87000	0.09948	0.03051
1.80	0.93000	0.87000	0.09429	0.03570
2.00	0.94500	0.85500	0.11705	0.02794
2.50	0.93000	0.84600	0.11827	0.03572
3.00	0.89000	0.76000	0.18301	0.05698
3.50	0.69000	0.79500	0.03504	0.16996
4.00	0.82000	0.80500	0.09998	0.09501
4.50	0.95500	0.79000	0.18717	0.02282
5.00	0.76500	0.71000	0.16284	0.12715
5.50	0.69500	0.46500	0.35814	0.17686
6.00	0.50500	0.24500	0.40428	0.35074
6.50	0.31000	0.15500	0.27683	0.56821
7.00	0.32500	0.11000	0.30759	0.58246
7.50	0.32000	0.08300	0.31010	0.60697
8.00	0.33500	0.07300	0.32715	0.59991
8.50	0.36000	0.07900	0.35044	0.57060
9.00	0.35000	0.12900	0.32538	0.54565
9.50	0.36000	0.34500	0.20949	0.44554
10.00	0.57500	0.67500	0.07986	0.24515
10.50	0.70000	0.59500	0.23640	0.16861
11.00	0.50000	0.39500	0.28256	0.32246
11.50	0.44000	0.13800	0.40790	0.45415
12.00	0.40500	0.03750	0.40270	0.55985
12.50	0.40000	0.27000	0.29642	0.43360
13.00	0.56500	0.60500	0.13960	0.25540
13.50	0.48500	0.56500	0.12161	0.31340
14.00	0.40500	0.44000	0.17139	0.38863

Table 16 Monochromatic Values of α, ρ and τ (Continued)

LAMBDA	RHO*	TAU	RHO	ALPHA
14.50	0.59700	0.70000	0.07009	0.22992
15.00	0.79000	0.83000	0.05839	0.11161
15.50	0.72200	0.61000	0.23537	0.15463
16.00	0.65500	0.41500	0.37811	0.20691
16.50	0.62700	0.52000	0.26108	0.21893
17.00	0.60000	0.51500	0.24755	0.23746
17.50	0.58500	0.53500	0.21869	0.24632
18.00	0.57000	0.63500	0.11459	0.25040
18.50	0.59000	0.59500	0.16568	0.23932
19.00	0.61000	0.41500	0.34648	0.23852
19.50	0.58500	0.35600	0.38047	0.26355
20.00	0.56000	0.46500	0.26559	0.26941
20.50	0.67000	0.60500	0.20790	0.18709
21.00	0.78000	0.70000	0.18141	0.11859
21.50	0.71500	0.66000	0.18230	0.15770
22.00	0.65000	0.60000	0.20000	0.19999
22.50	0.59800	0.54500	0.21813	0.23688
23.00	0.54500	0.49300	0.22955	0.27745
23.50	0.57500	0.49000	0.25344	0.25658
24.00	0.60500	0.49500	0.26958	0.23544
24.50	0.67000	0.51000	0.29898	0.19102
25.00	0.73500	0.52000	0.33090	0.14911
25.50	0.72800	0.53500	0.31200	0.15301
26.00	0.72000	0.54500	0.29731	0.15769
26.50	0.74000	0.56000	0.29512	0.14488
27.00	0.76000	0.62000	0.24850	0.13150
27.50	0.84800	0.70000	0.21988	0.08011
28.00	0.93500	0.75000	0.21679	0.03320
28.50	0.93500	0.81000	0.15684	0.03315
29.00	0.93500	0.84000	0.12686	0.03312
29.50	0.93500	0.86500	0.10188	0.03311
30.00	0.93500	0.86500	0.10188	0.03311

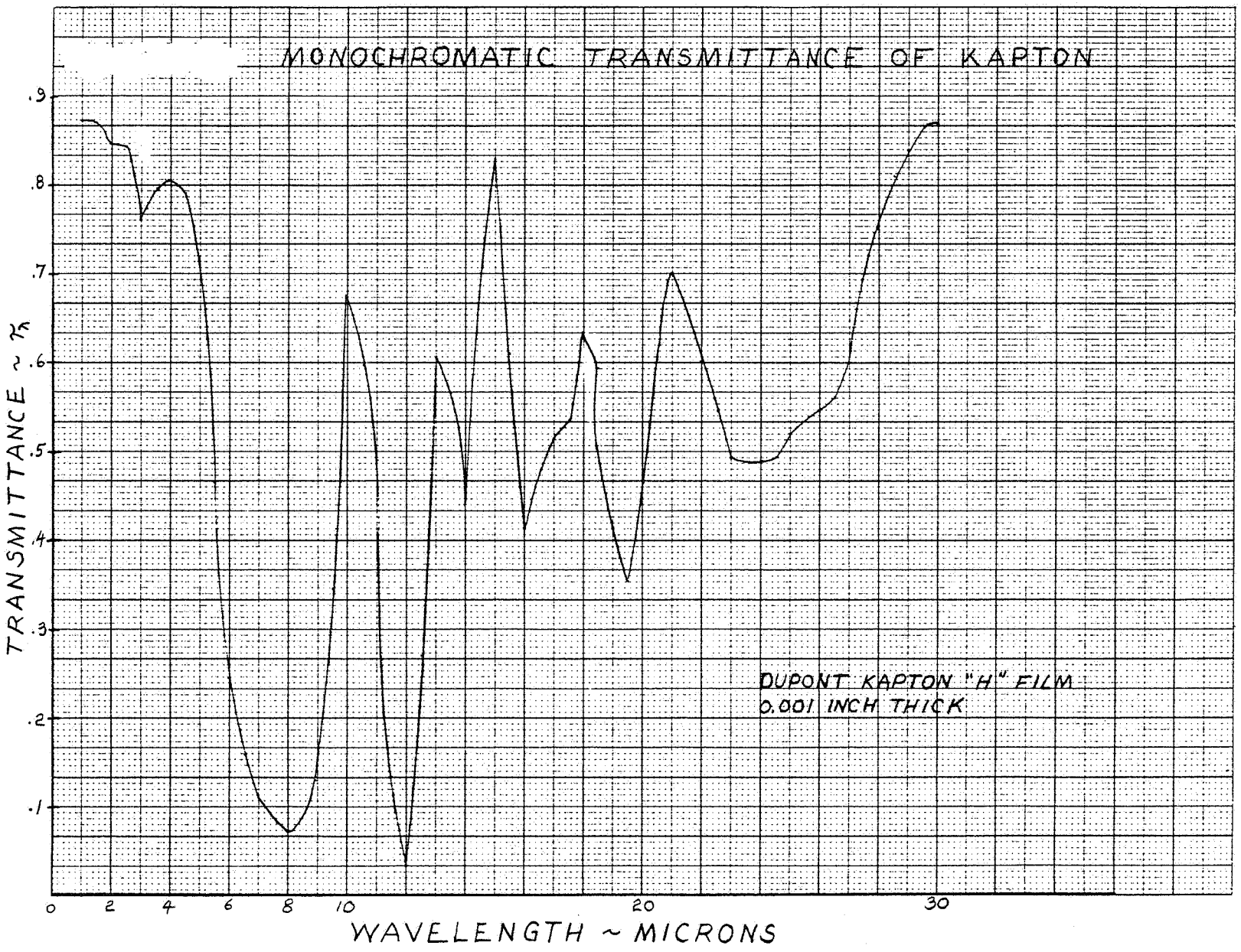

Figure 60 Monochromatic Transmittance of Kapton

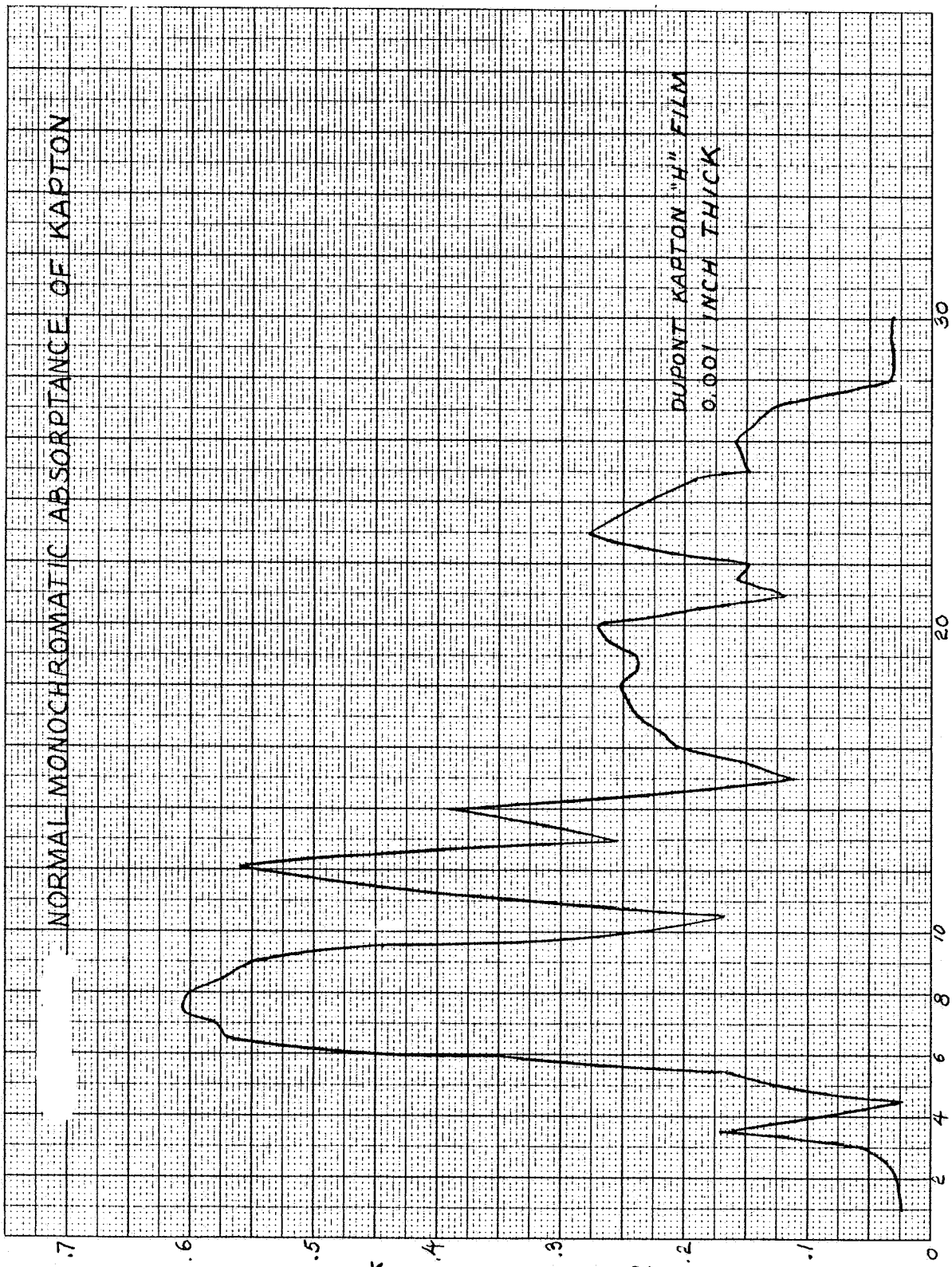

Figure 61 Normal Monochromatic Absorptance of Kapton

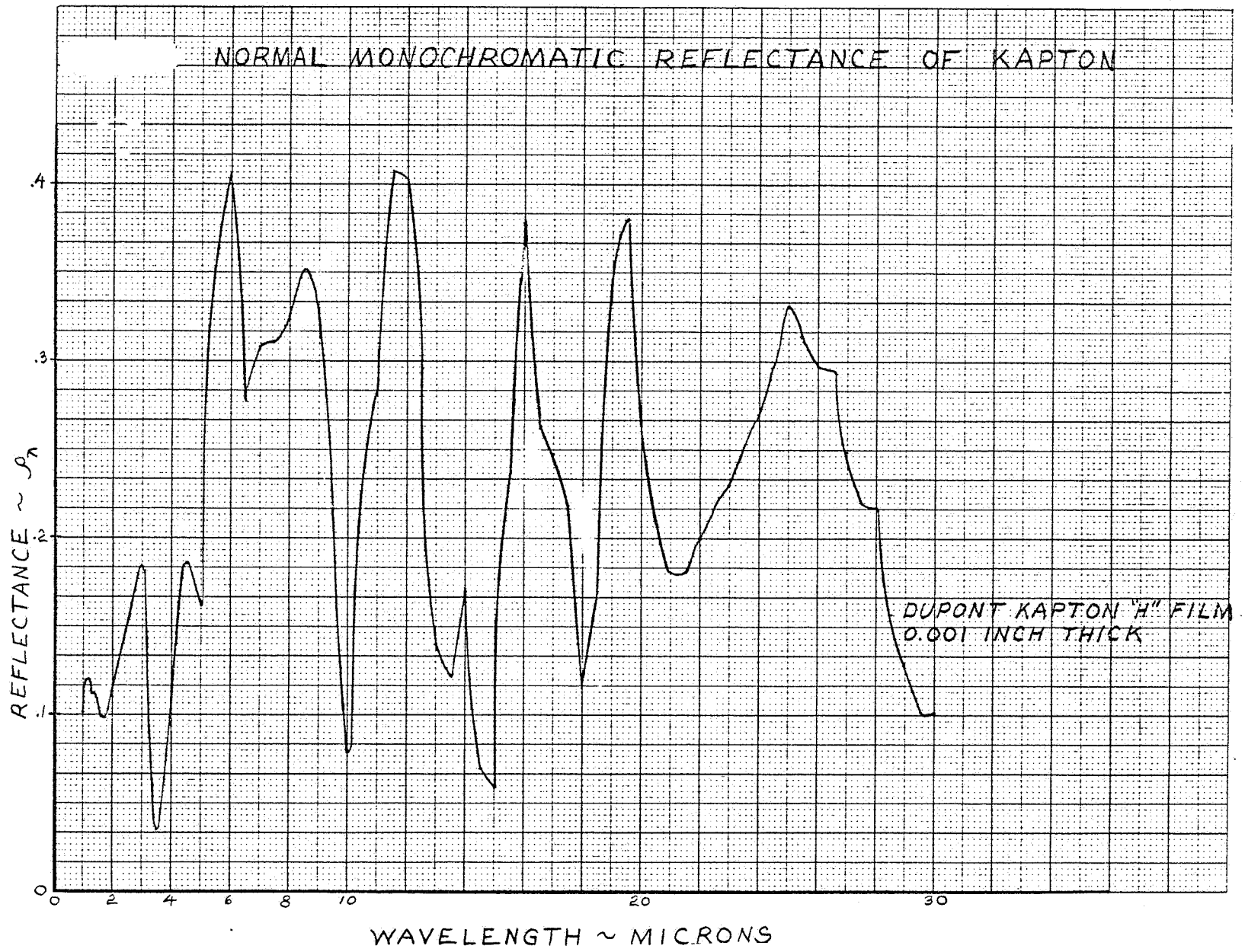

Figure 62 Normal Monochromatic Reflectance of Kapton

7.4.6 Total Parameters

The data of Figures 60 and 61 were processed by means of a GD-Astronautics computer program to produce the values of total normal emittance and total transmittance, given in Tables 17 and 18.

The computer program is set up to solve the following relation directly:

$$\varepsilon_n\ (T^{\circ}K) = \frac{\sum_{\lambda=.3}^{\lambda=32} [(1 - \rho_\lambda)\ J_\lambda \Delta\lambda] + (1 - \rho_\lambda)_{32\mu} \sum_{\lambda}^{\infty} J_\lambda \Delta\lambda}{\int_0^{\infty} J_\lambda\ d\lambda}$$

where ρ_λ, λ and T are inputs, and $(1 - \rho_\lambda) = \alpha_\lambda$ for opaque materials.

Since Kapton is a transparent material, the above relation does not hold directly and the input ρ_λ was modified for this material. The quantity $(1 - \alpha_\lambda)$ was used as the input parameter instead, which effectively converted the equation to:

$$\varepsilon_n\ (T^{\circ}K) = \frac{\sum_{\lambda=.3}^{\lambda=32} \alpha_\lambda\ J_\lambda\ \Delta\lambda + \alpha_{\lambda_{32}} \sum_{\lambda=32}^{\infty} J_\lambda\ \Delta\lambda}{\int_0^{\infty} J_\lambda\ d\lambda}$$

Table 17

REFLECTIVITY DATA RADIANT ENERGY TRANSFER GROUP SPACE SCIENCE LABORATORIES GD-ASTRONAUTICS
RADIANT ENERGY TRANSFER GROUP SPACE SCIENCE LABORATORY GD-ASTRO
SAMPLE IDENT. ONE MINUS ALPHA-CORRECTED
DATE 11-27-67 REQUESTOR RYAN

WAVE LENGTH	1 - α	WAVE LENGTH	1 - α	WAVE LENGTH	1 - α	WAVE LENGTH	1 - α
3.000E-01-0.		3.200E-01-0.		3.300E-01-0.		3.350E-01-0.	
3.500E-01-0.		3.600E-01-0.		3.700E-01-0.		3.750E-01-0.	
3.900E-01-0.		4.000E-01-0.		4.100E-01-0.		4.200E-01-0.	
4.300E-01-0.		4.400E-01-0.		4.450E-01-0.		4.500E-01-0.	
4.650E-01-0.		4.750E-01-0.		4.900E-01-0.		4.950E-01-0.	
5.000E-01-0.		5.100E-01-0.		5.200E-01-0.		5.400E-01-0.	
5.700E-01-0.		7.000E-01-0.		8.000E-01-0.		9.000E-01-0.	
1.000E+00	9.755E-01	1.100E+00	9.753E-01	1.200E+00	9.751E-01	1.300E+00	9.749E-01
1.400E+00	9.746E-01	1.500E+00	9.747E-01	1.600E+00	9.695E-01	1.700E+00	9.695E-01
1.800E+00	9.643E-01	2.000E+00	9.721E-01	2.500E+00	9.643E-01	3.000E+00	9.430E-01
3.500E+00	8.300E-01	4.000E+00	9.050E-01	4.500E+00	9.772E-01	5.000E+00	8.729E-01
5.500E+00	8.230E-01	6.000E+00	6.493E-01	6.500E+00	4.318E-01	7.000E+00	4.175E-01
7.500E+00	3.930E-01	8.000E+00	4.000E-01	8.500E+00	4.294E-01	9.000E+00	4.544E-01
9.500E+00	5.545E-01	1.000E+01	7.549E-01	1.050E+01	8.314E-01	1.100E+01	6.775E-01
1.150E+01	5.459E-01	1.200E+01	4.400E-01	1.250E+01	5.660E-01	1.300E+01	7.446E-01
1.400E+01	6.114E-01	1.500E+01	8.884E-01	1.600E+01	7.931E-01	1.700E+01	7.625E-01
1.800E+01	7.496E-01	1.900E+01	7.615E-01	2.000E+01	7.310E-01	2.100E+01	8.814E-01
2.200E+01	8.000E-01	2.300E+01	7.226E-01	2.400E+01	7.646E-01	2.500E+01	8.509E-01
2.600E+01	8.423E-01	2.700E+01	8.685E-01	2.800E+01	9.668E-01	2.900E+01	9.669E-01
3.000E+01	9.669E-01	3.100E+01	9.669E-01	3.200E+01	9.669E-01	-0.	-0.

MISSIVITY REQUIRED 100 X 300 X 500 X SOLAR ABSORPTIVITY X OTHER
200 X 400 X CARBON ARC ABSORPTIVITY

EMISSIVITY(100 K)=6.782392E-02	SUMMATION RATIO=4.563659E-02
EMISSIVITY(300 K)=2.971583E-01	SUMMATION RATIO=2.938916E-01
EMISSIVITY(500 K)=3.075205E-01	SUMMATION RATIO=3.059031E-01
SOLAR ABSORPTIVITY=6.974892E-01	SUMMATION RATIO=6.974892E-01
EMISSIVITY(200 K)=1.875966E-01	SUMMATION RATIO=1.790716E-01
EMISSIVITY(400 K)=3.303115E-01	SUMMATION RATIO=3.275797E-01

Table 18

REFLECTIVITY DATA RADIANT ENERGY TRANSFER GROUP SPACE SCIENCE LABORATORIES GD-ASTRONAUTICS
RADIANT ENERGY TRANSFER GROUP SPACE SCIENCE LABORATORY GD-ASTRO
AMPLE IDENT KAPTON ONE MINUS TAU
DATE 11-13-67 REQUESTOR RYAN

WAVE LENGTH	1 - τ	WAVE LENGTH	1 - τ	WAVE LENGTH	1 - τ	WAVE LENGTH	1 - τ
3.000E-01	0.	3.200E-01	0.	3.300E-01	0.	3.350E-01	0.
3.500E-01	0.	3.600E-01	0.	3.700E-01	0.	3.750E-01	0.
3.900E-01	0.	4.000E-01	0.	4.100E-01	0.	4.200E-01	0.
4.300E-01	0.	4.400E-01	0.	4.450E-01	0.	4.500E-01	0.
4.650E-01	0.	4.750E-01	0.	4.900E-01	0.	4.950E-01	0.
5.000E-01	0.	5.100E-01	0.	5.200E-01	0.	5.400E-01	0.
5.700E-01	0.	7.000E-01	0.	8.000E-01	0.	9.000E-01	0.
1.000E+00	1.250E-01	1.100E+00	1.450E-01	1.200E+00	1.450E-01	1.300E+00	1.380E-01
1.400E+00	1.380E-01	1.500E+00	1.350E-01	1.600E+00	1.300E-01	1.700E+00	1.300E-01
1.800E+00	1.300E-01	2.000E+00	1.450E-01	2.500E+00	1.540E-01	3.000E+00	2.400E-01
3.500E+00	2.040E-01	4.000E+00	1.950E-01	4.500E+00	2.100E-01	5.000E+00	2.900E-01
5.500E+00	5.350E-01	6.000E+00	7.550E-01	6.500E+00	8.450E-01	7.000E+00	8.900E-01
7.500E+00	9.170E-01	8.000E+00	9.270E-01	8.500E+00	9.210E-01	9.000E+00	8.710E-01
9.500E+00	6.550E-01	1.000E+01	3.250E-01	1.050E+01	4.050E-01	1.100E+01	6.050E-01
1.150E+01	8.620E-01	1.200E+01	9.620E-01	1.250E+01	7.300E-01	1.300E+01	3.950E-01
1.400E+01	5.600E-01	1.500E+01	1.700E-01	1.600E+01	5.850E-01	1.700E+01	4.850E-01
1.800E+01	3.650E-01	1.900E+01	5.850E-01	2.000E+01	5.350E-01	2.100E+01	3.000E-01
2.200E+01	4.000E-01	2.300E+01	5.070E-01	2.400E+01	5.050E-01	2.500E+01	4.800E-01
2.600E+01	4.550E-01	2.700E+01	3.800E-01	2.800E+01	2.500E-01	2.900E+01	1.600E-01
3.000E+01	1.350E-01	3.100E+01	1.350E-01	3.200E+01	1.350E-01	-0.	-0.

MISSIVITY REQUIRED 100 X 300 X 500 X SOLAR ABSORPTIVITY OTHER
200 X 400 X CARBON-ARC ABSORPTIVITY

TRANSMITTANCE	(100 K)=7.959970E-01	SUMMATION RATIO=2.161769E-01
TRANSMISSIVITY	(300 K)=4.648500E-01	SUMMATION RATIO=3.794807E-01
TRANSMISSIVITY	(500 K)=4.534017E-01	SUMMATION RATIO=4.111347E-01
TRANSMISSIVITY	(200 K)=6.148754E-01	SUMMATION RATIO=3.920926E-01
TRANSMISSIVITY	(400 K)=4.151730E-01	SUMMATION RATIO=3.437837E-01

A similar substitution was used for the computation of total transmittance, where $(1 - \tau_\lambda)$ was substituted for ρ_λ, and the effective equation was:

$$\tau\ (T^{o}K) = \frac{\sum_{\lambda=.3}^{\lambda=32} \tau_\lambda J_\lambda \Delta\lambda + \tau_{\lambda_{32}} \sum_{\lambda}^{\infty} J_\lambda \Delta\lambda}{\int_0^\infty J_\lambda \, d\lambda}$$

For this latter case, the output headings in Table 18 have been corrected for proper identification.

J_λ is the Planckian blackbody function corresponding to $T^{o}K$. The summations are performed in two steps since the available data was only to 30μ and the parameter was assumed to be constant above this wavelength.

The results are given in Figures 63 and 64 as functions of blackbody temperature.

Figure 65 shows the theoretical ratios of hemispherical to normal emissivities. Values of total emittance, ε, have been plotted in addition to the normal emittance, ε_n, in Figure 63.

7.5 PRELIMINARY DESIGN DRAWINGS

Copies of the significant engineering drawings, prepared to show the detail arrangement of the selected array concept, are enclosed. These include the following:

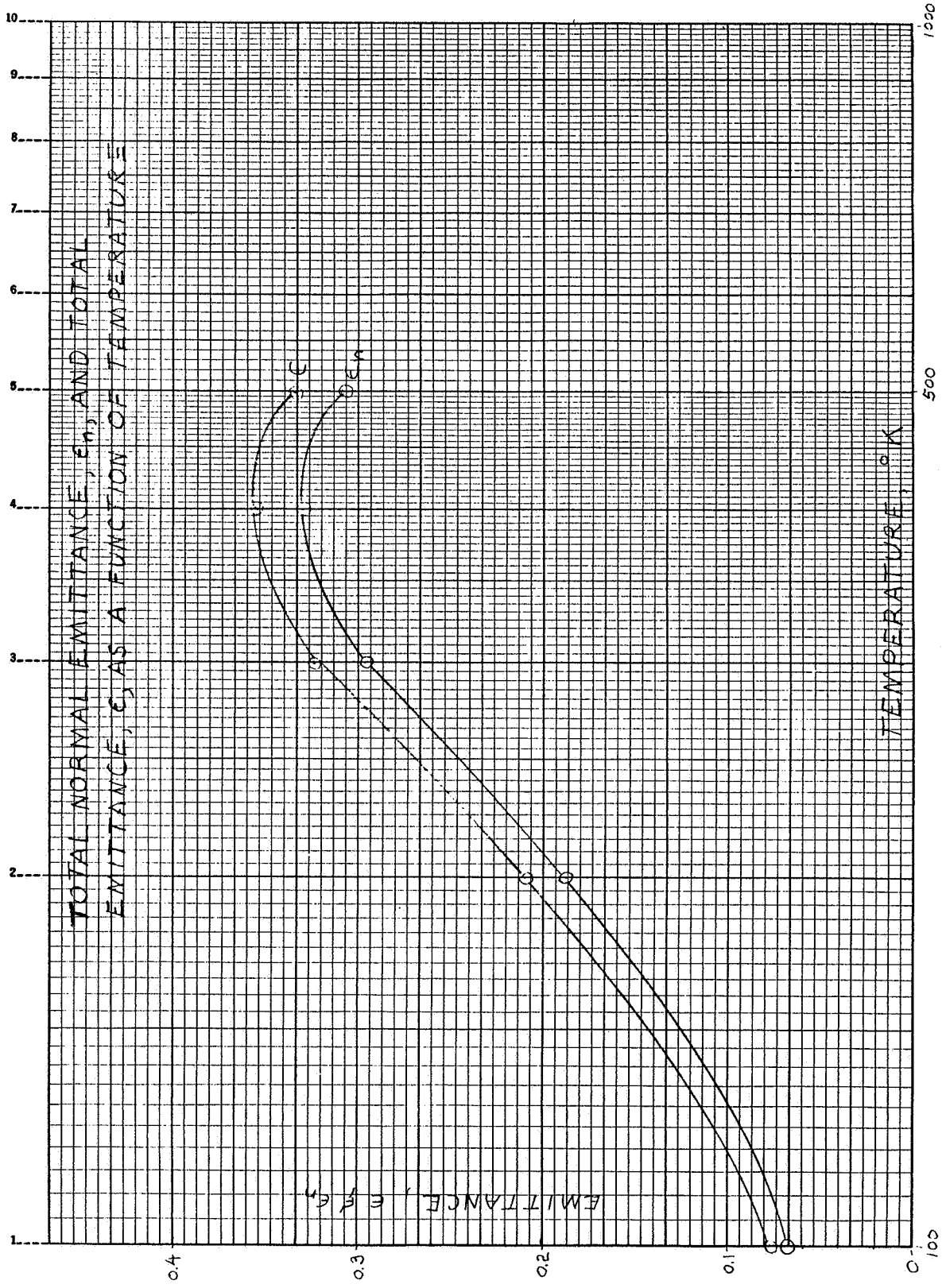

Figure 63 Total Normal Emittance, ε_n, and Total Emittance, ε, As a Function of Temperature

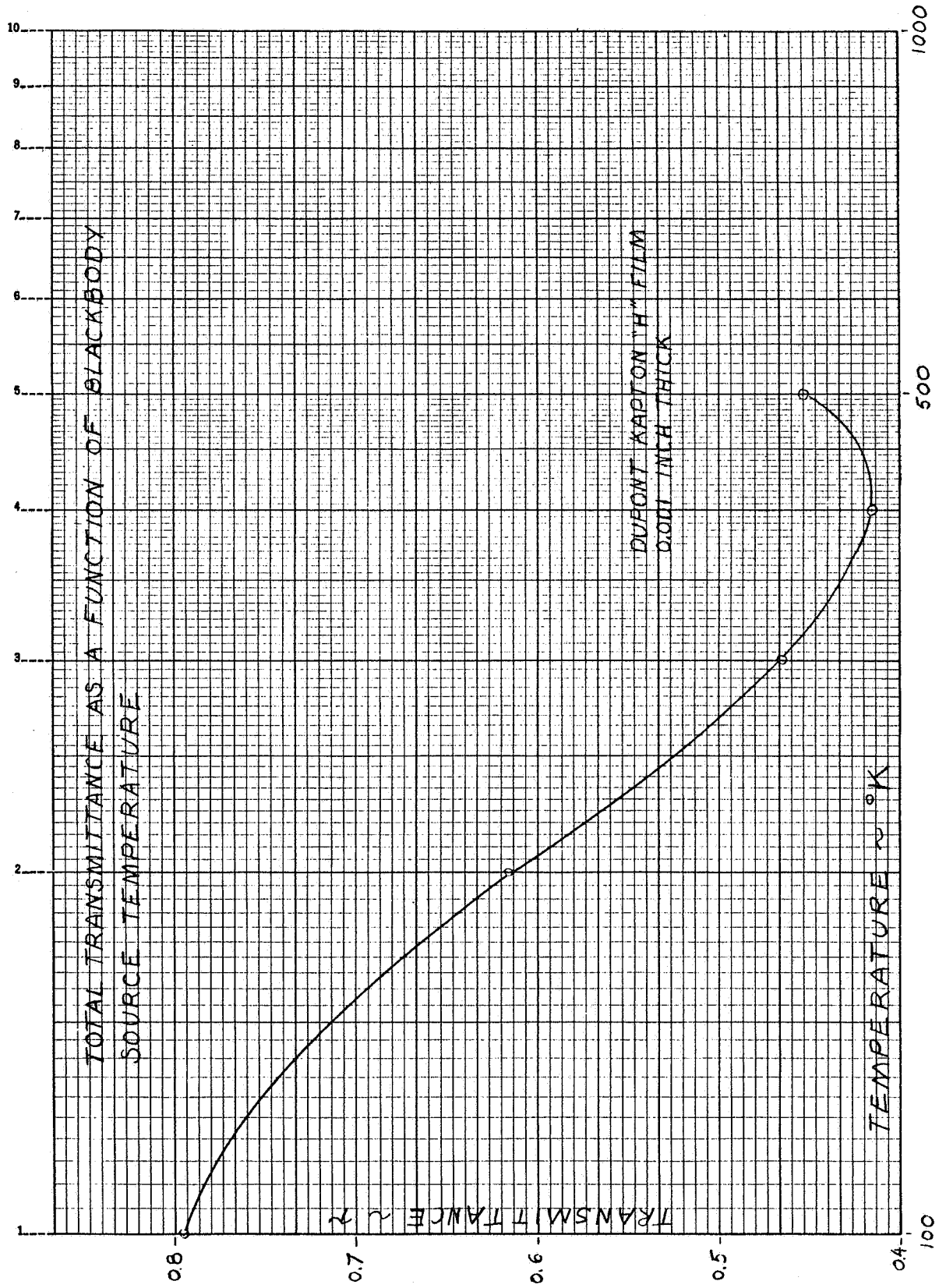

Figure 64 Total Transmittance As a Function of Blackbody Source Temperature

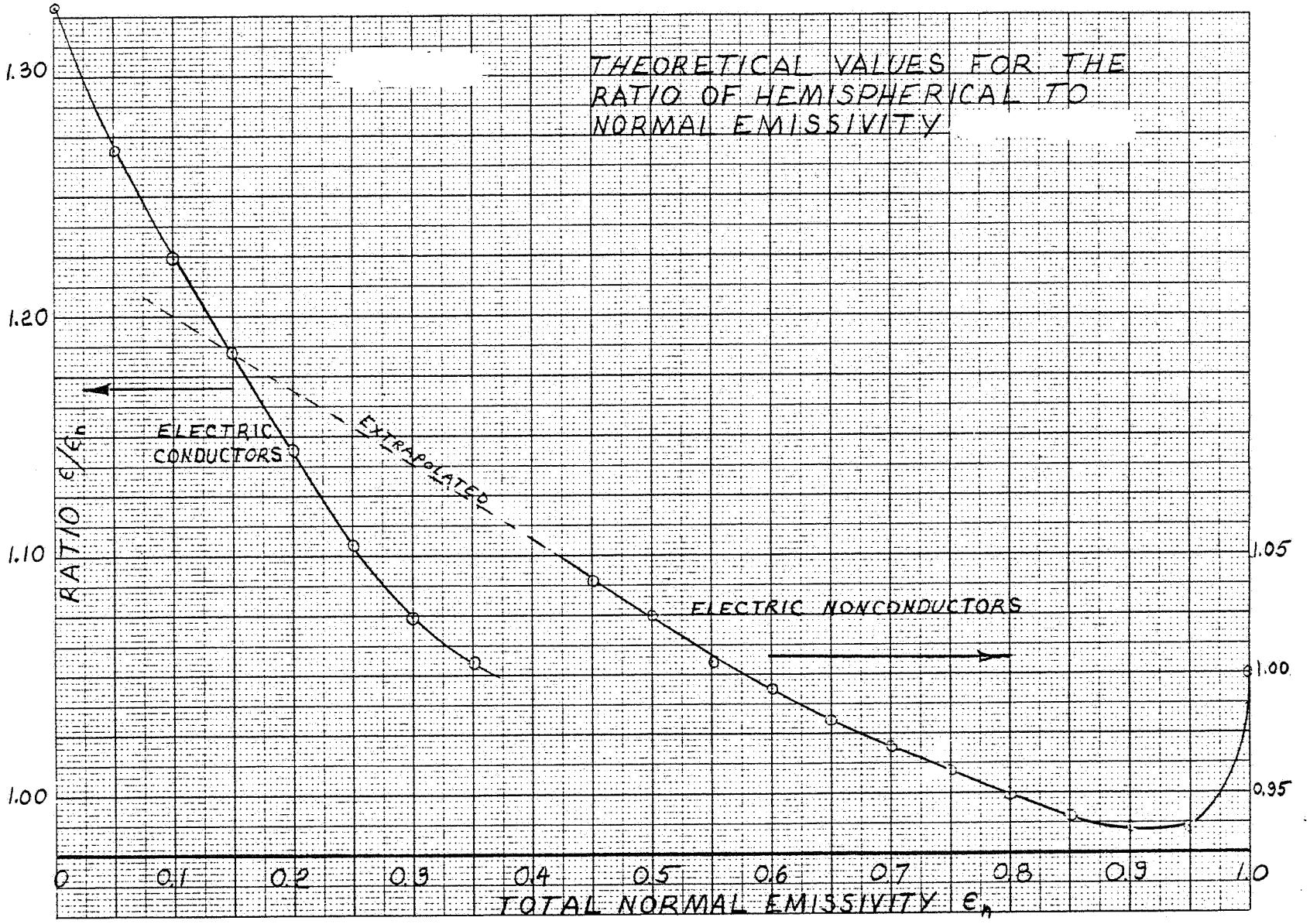

Figure 65 Theoretical Values for the Ratio of Hemispherical to Normal Emissivity

DRAWING NUMBER	TITLE
400U020, Sheets 1 and 2	Assembly - Rollup, Solar Panel, 250-Square Foot.
400U021	Beam Installation - 250-Square Foot, Rollup Solar Panel
400U022	End Support Structure
400U023, Sheets 1 and 2	Drum Assembly - 250-Square Foot, Rollup
400U025	Vehicle Mounting
400U027	Slip Ring and Electrical Harness
400U030, Sheets 1 and 2	Substrate Assembly - Detail, 250-Square Foot Rollup

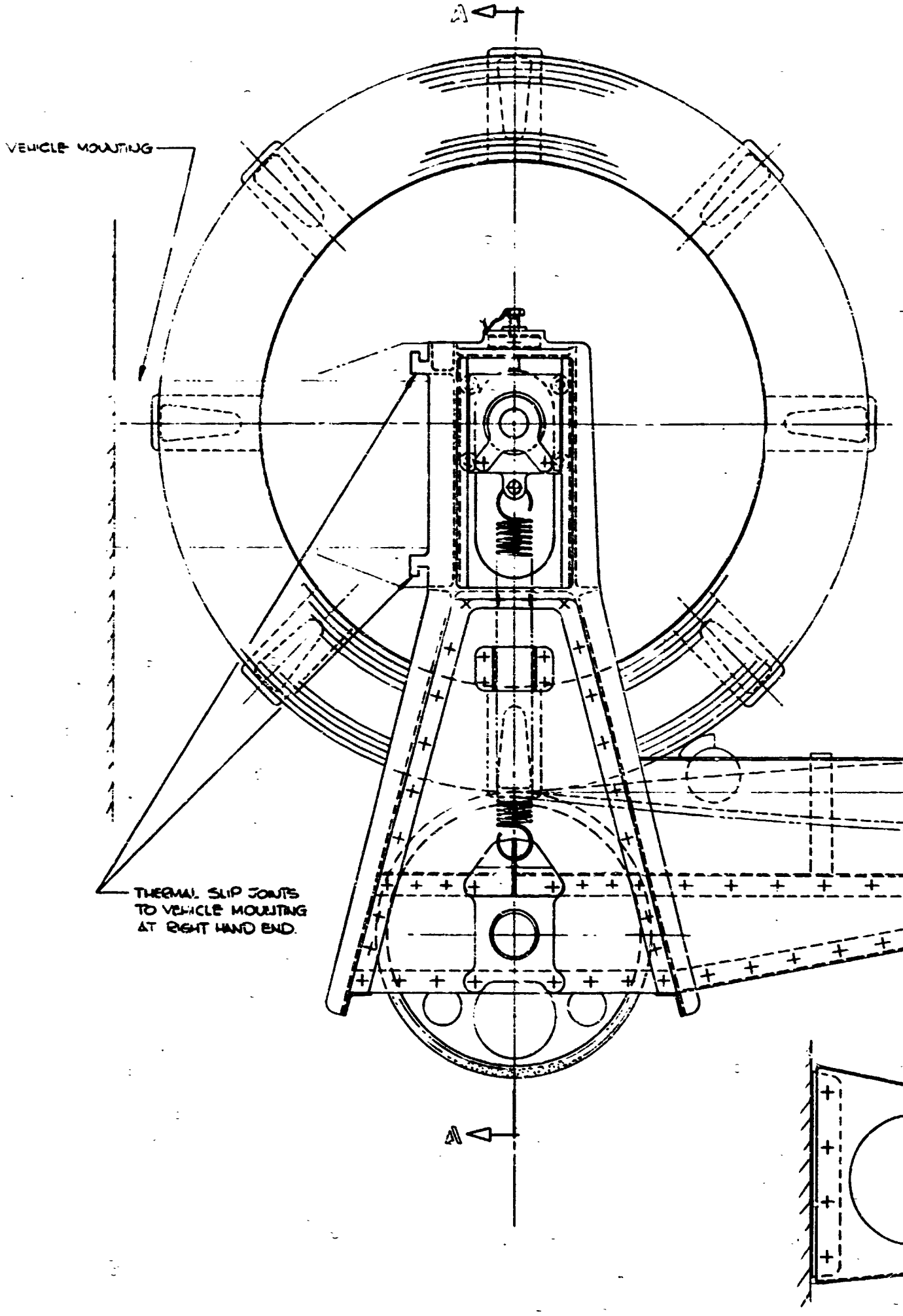

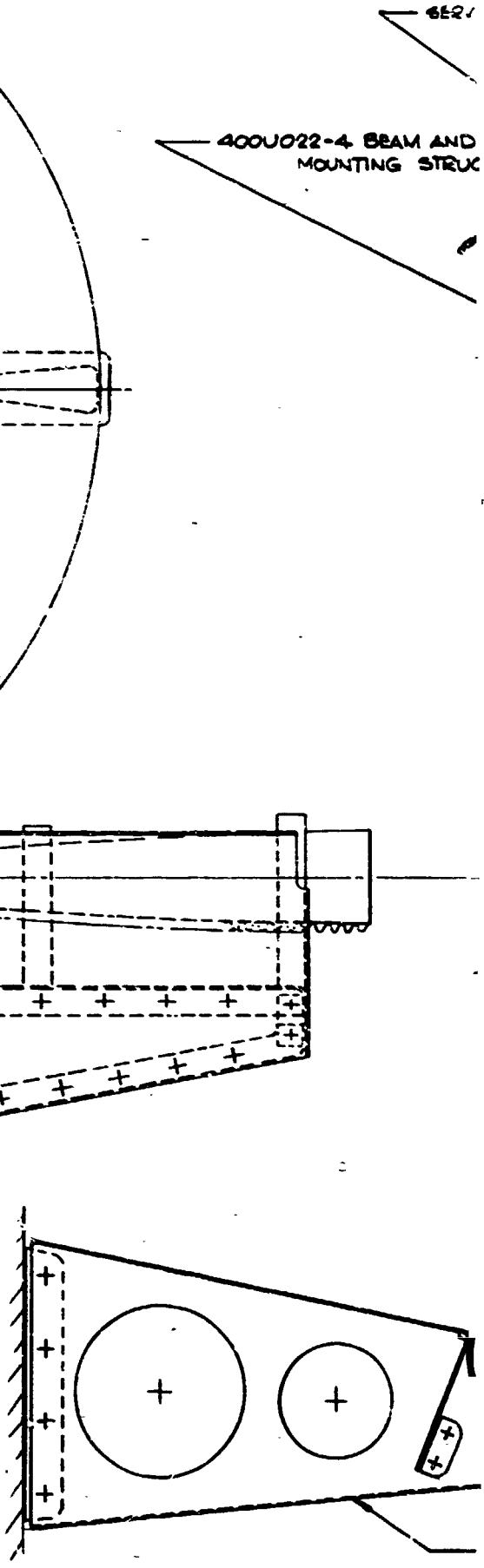

FOLDOUT FRAME

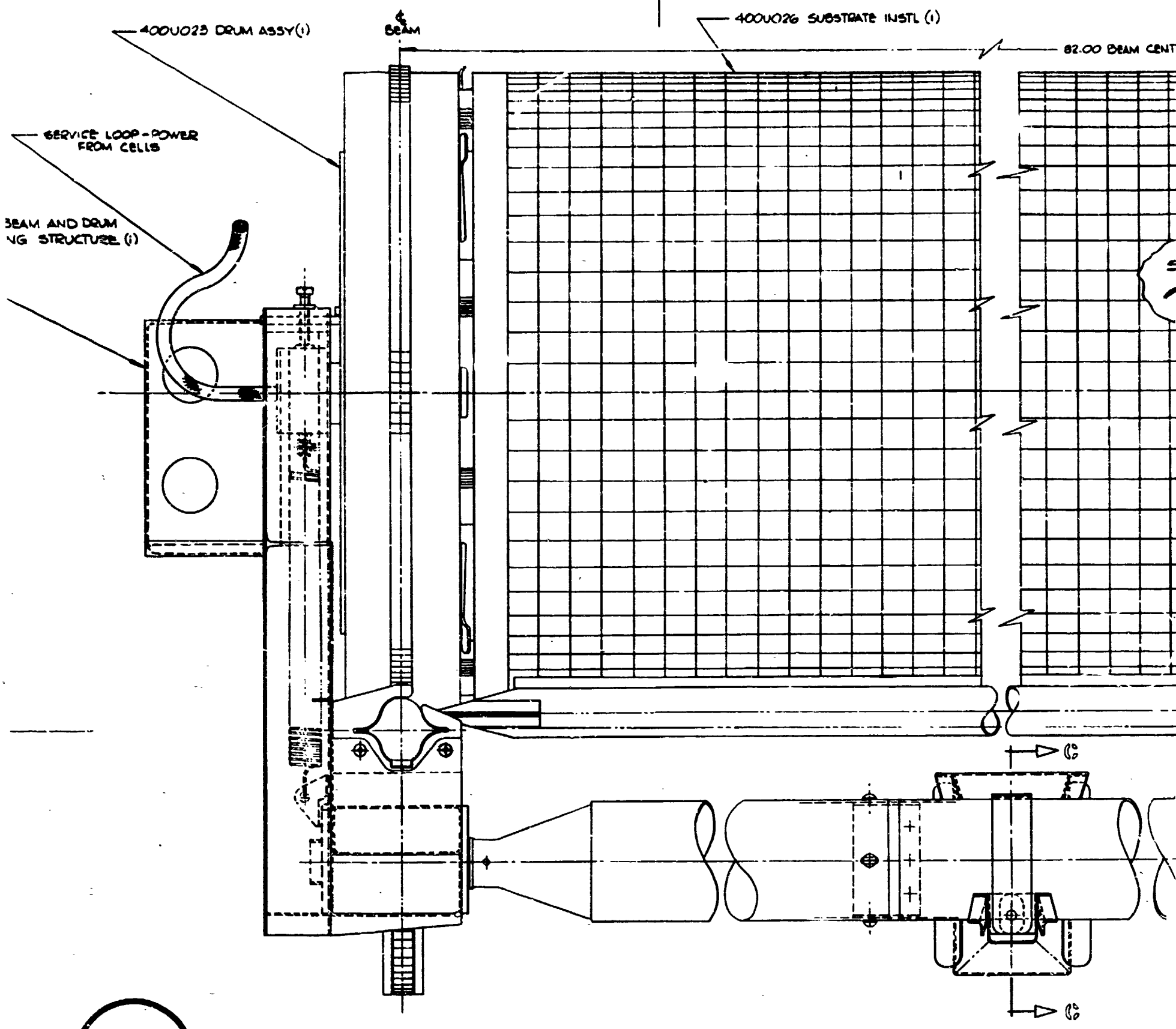
400U023 DRUM ASSY(1)
℄ BEAM
400U026 SUBSTRATE INSTL (1)
82.00 BEAM CENT
SERVICE LOOP - POWER FROM CELLS
BEAM AND DRUM
NG STRUCTURE (1)
TORQUE SHAFT SNUBBER
(.020 MAGNESIUM SHEET AZ31B)
℄ - ℄

400U020 | 1

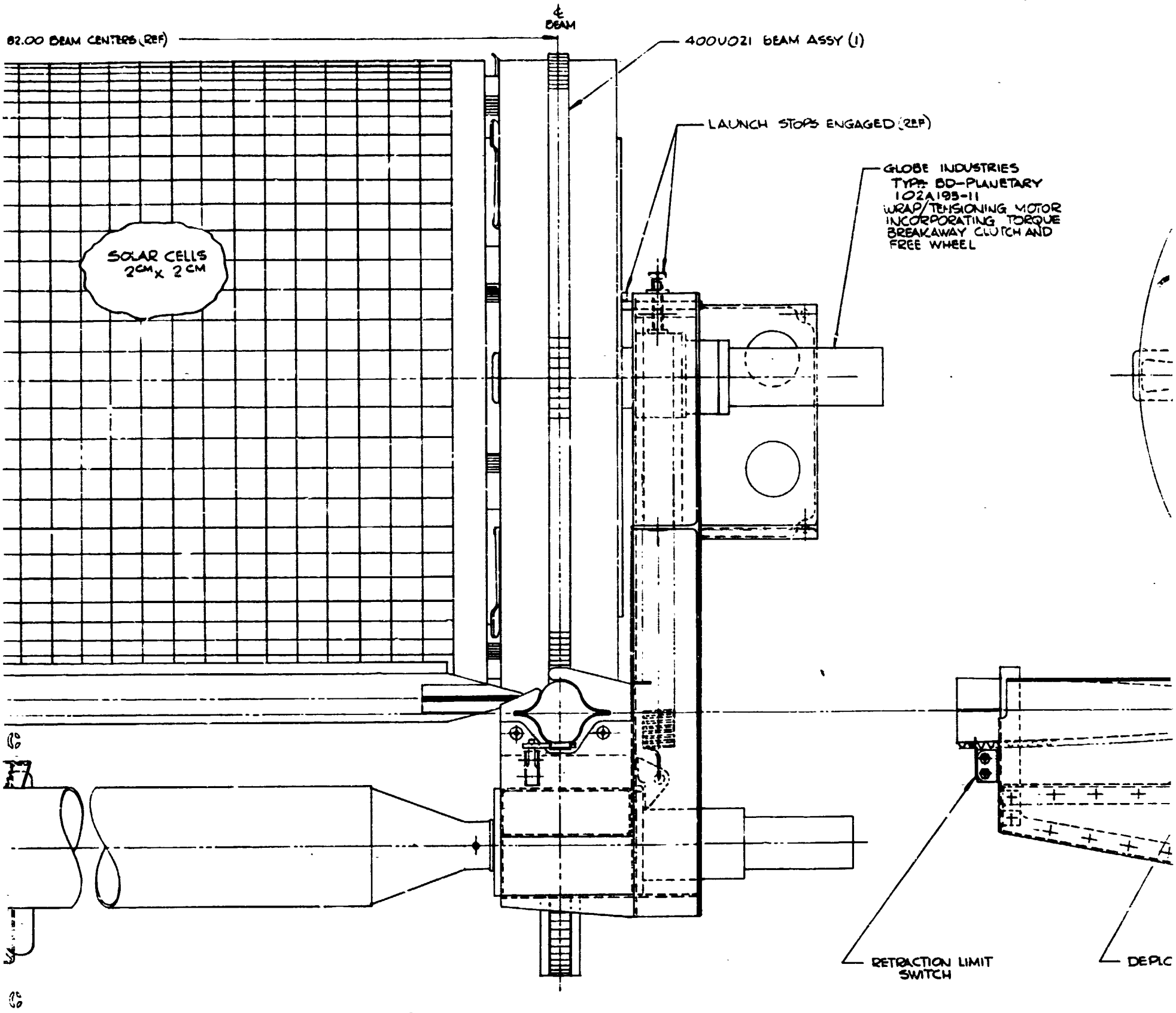
82.00 BEAM CENTERS (REF)
℄ BEAM
400U021 BEAM ASSY (1)
LAUNCH STOPS ENGAGED (REF)
GLOBE INDUSTRIES
TYPE BD-PLANETARY
102A193-11
WRAP/TENSIONING MOTOR
INCORPORATING TORQUE
BREAKAWAY CLUTCH AND
FREE WHEEL
SOLAR CELLS
2CM X 2CM
RETRACTION LIMIT
SWITCH
DEPLO

400U022-3 BE

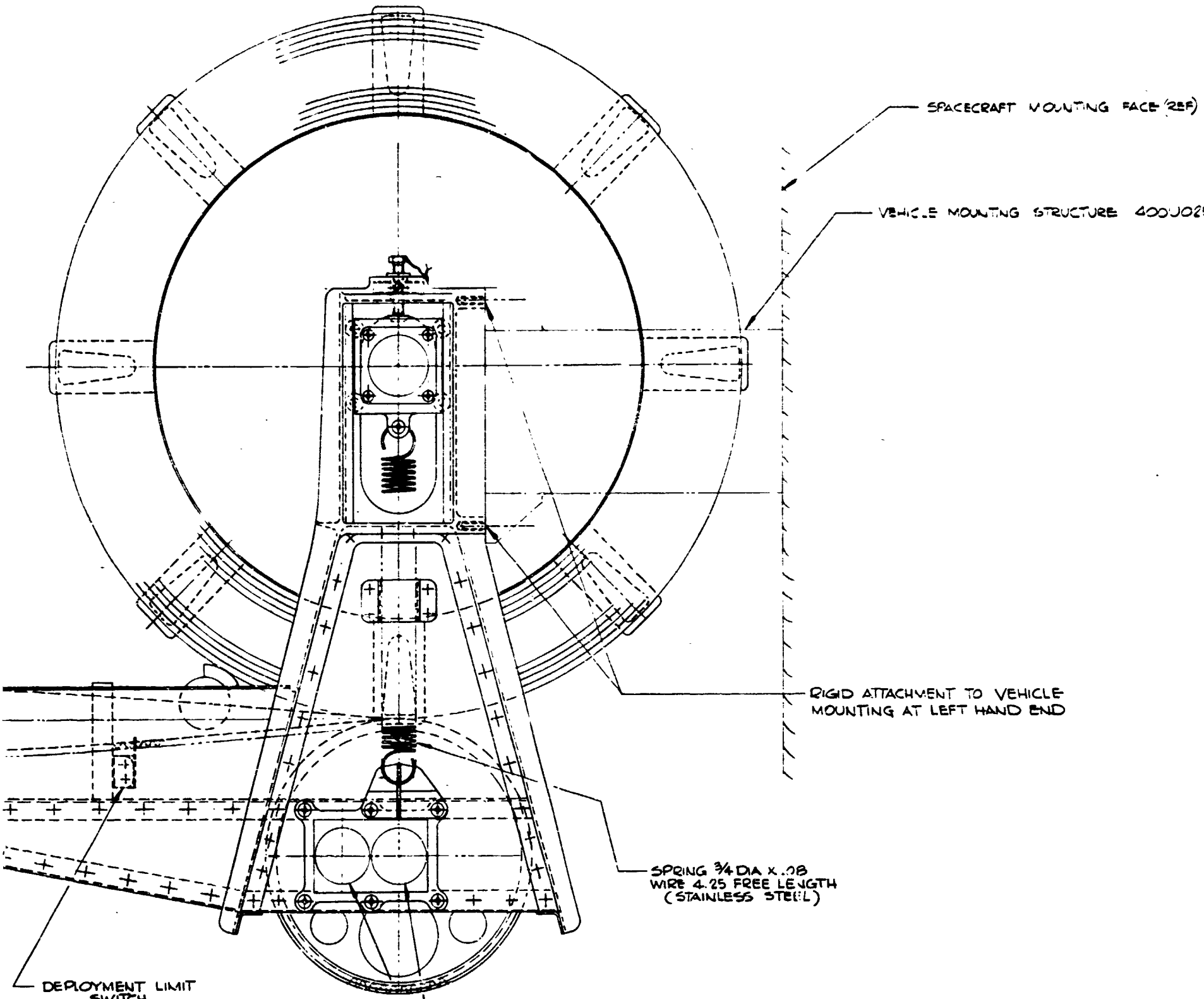

022-3 BEAM AND DRUM MOUNTING STRUCTURE (1)

2 1

REVISIONS

LTR	DESCRIPTION	DATE	APPROVED

D

– SPACECRAFT MOUNTING FACE (REF)

C.E MOUNTING STRUCTURE 400J025

C

-MENT TO VEHICLE
T LEFT HAND END.

B

A

QTY REQD PER ASSY	CODE IDENT	PART NUMBER	DESCRIPTION	STOCK SIZE	MATERIAL	SPECIFICATION	RYAN PART, STOCK NO.	SYMB	ITEM NO.

LIST OF MATERIAL

RELEASE & DATE

UNLESS OTHERWISE SPECIFIED DIMENSIONS ARE IN INCHES AND INCLUDE CHEM APPLIED OR PLATED FINISHES

TOLERANCES

LINEAR		ANGULAR
X	±.1	EXCL OF SHEET
XX	±.02	METAL FLANGES
XXX	±.010	±0° 30'

PARTS TO BE FREE OF BURRS AND SHARP EDGES. MANUFACTURING DEGREE-MENTS PER RYAN ENG. STANDARD NO. 135.

CONTRACT NUMBER

SIGNATURE/DATE

DESIGN ACTIVITY APPROVAL

DESIGN APPROVAL

RYAN AERONAUTICAL COMPANY
SAN DIEGO, CALIFORNIA 92112

ASSY-ROLL-UP, SOLAR PANEL 250 FT²

SIZE J | CAGE IDENT NO. 78022 | DRAWING NO. 400U020 | REV

SCALE 1/1 | WEIGHT | SHEET

FINAL ASSY	NEXT ASSY	NEXT ASSEMBLY	USED ON
QTY REQUIRED		APPLICATION	

2 1

FOLDOUT FRAME

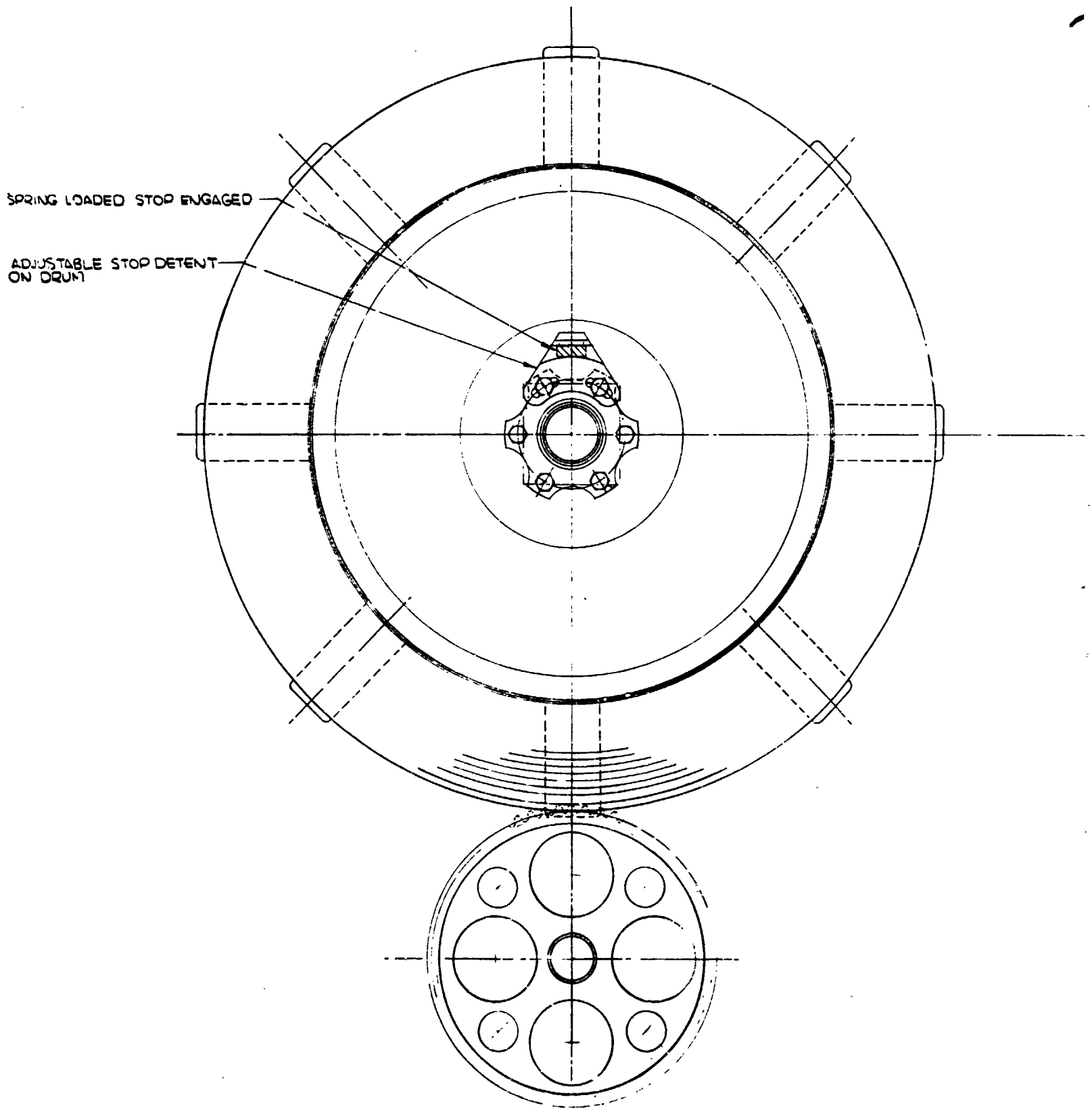

SECTION 13 - 13

400U020 2

FOLDOUT FRAME

4 3 2

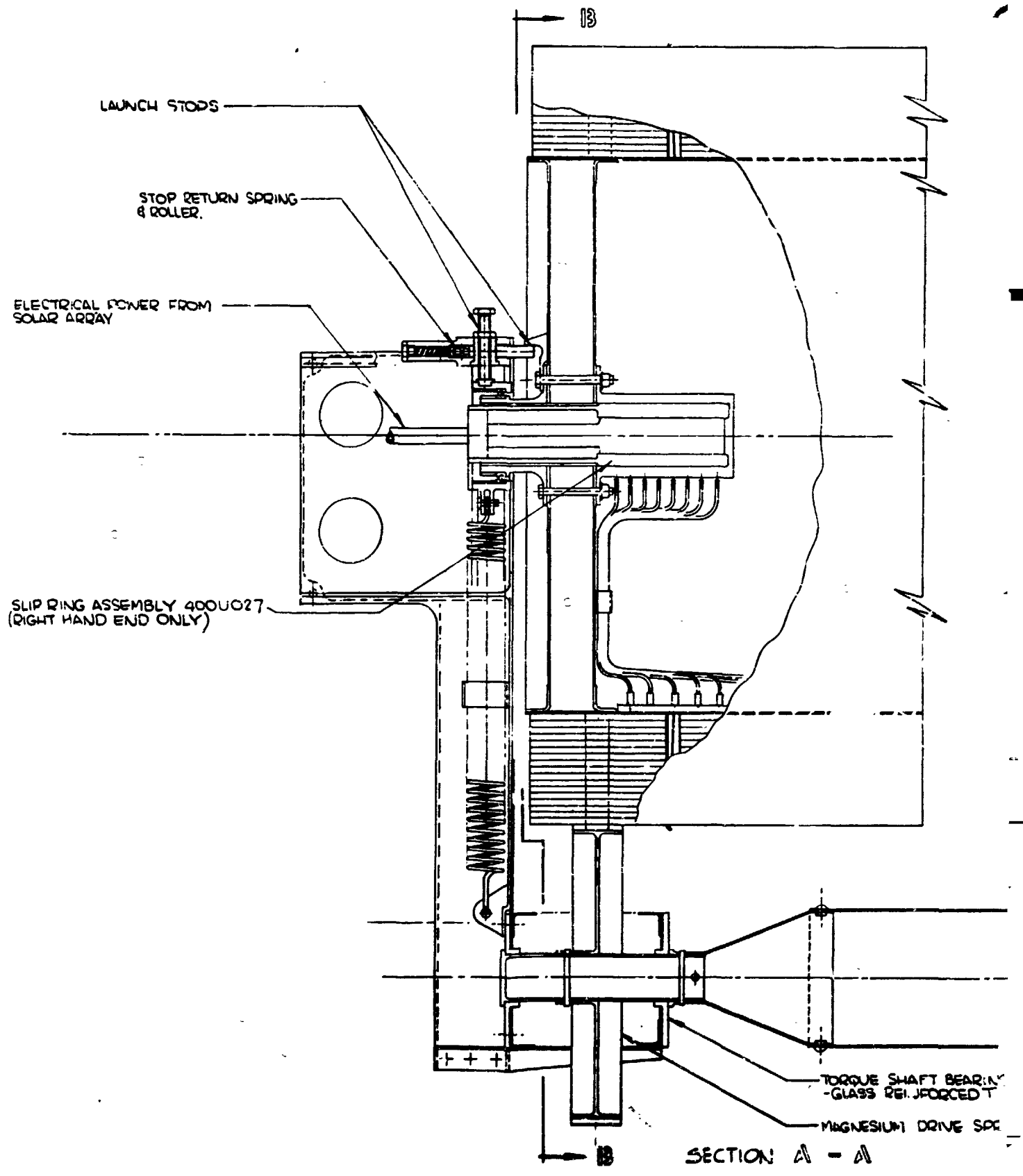

4 3 2

FOLDOUT FRAME

REVISIONS

LTR	DR CK	DESCRIPTION	DATE	APPROVED

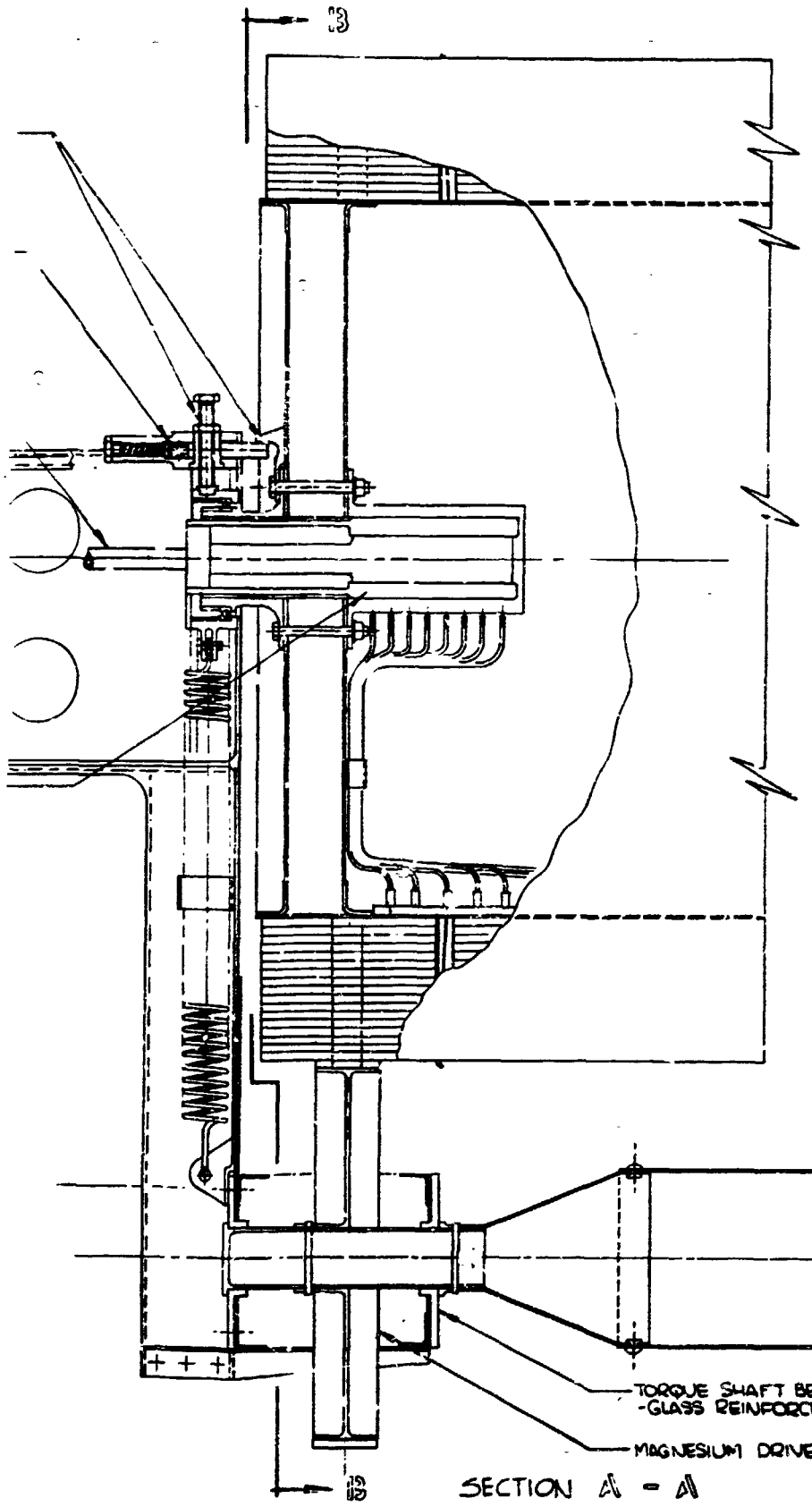

SECTION A - A

J	78/22	4000020	
SCALE		SHEET 2	

FOLDOUT FRAME

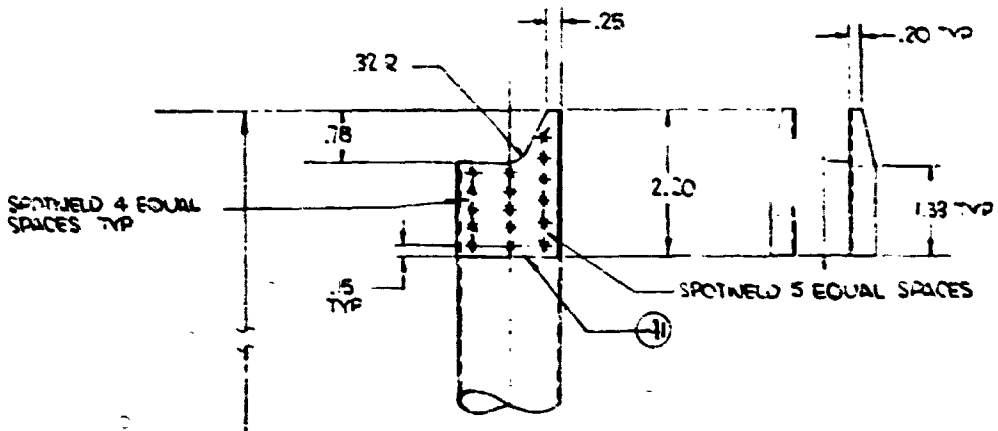

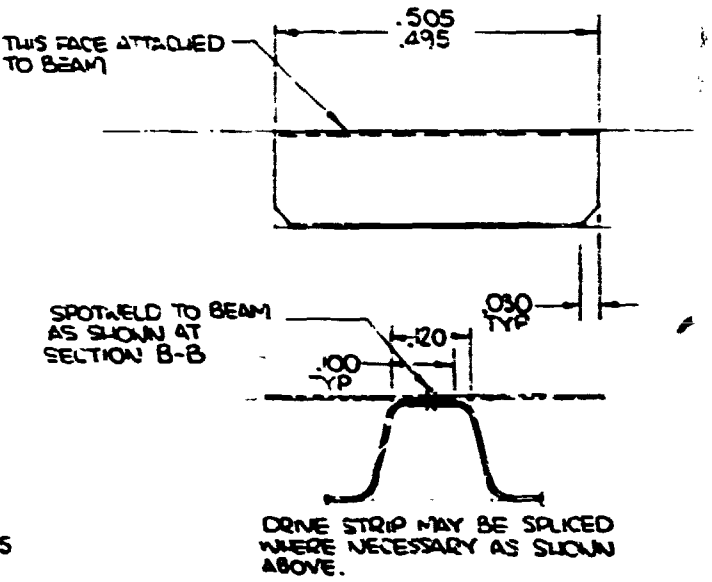

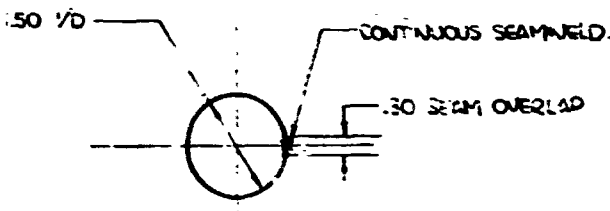

SECTION F-F

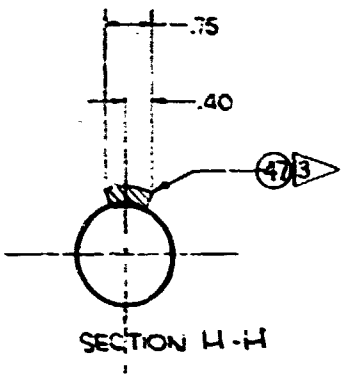

SECTION H-H

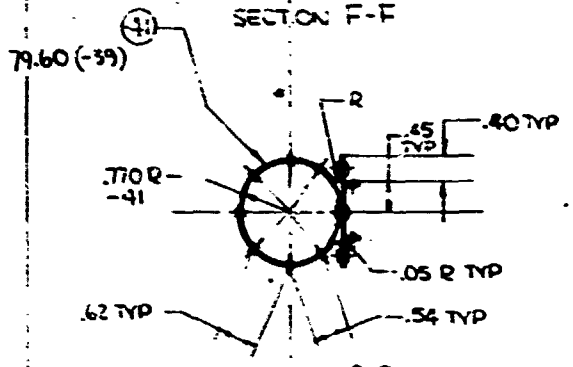

SECTION G-G

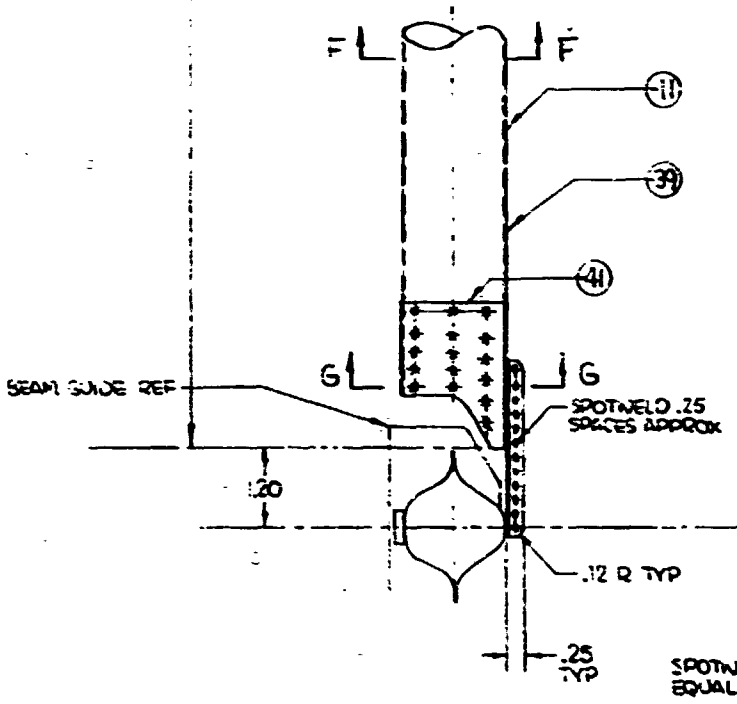

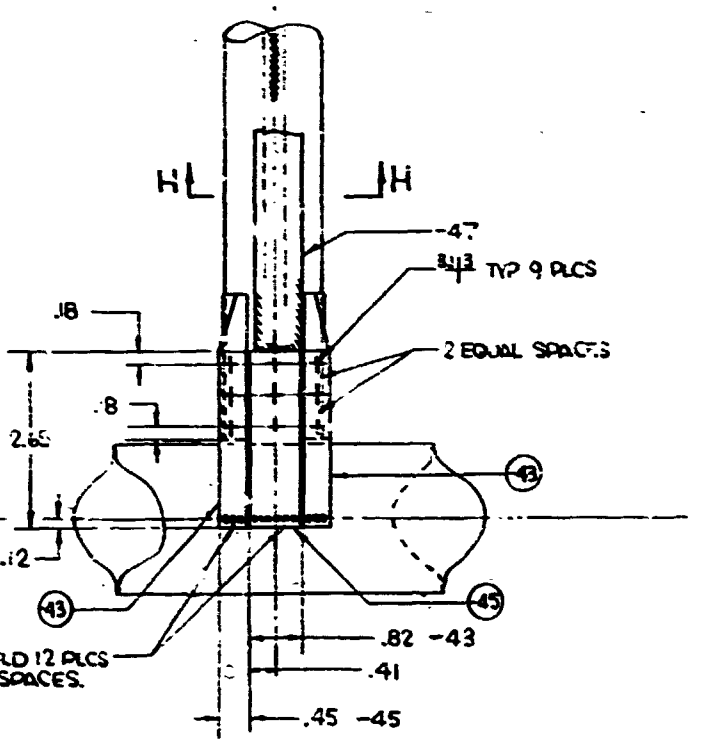

DETAIL J SCALE FULL SIZE

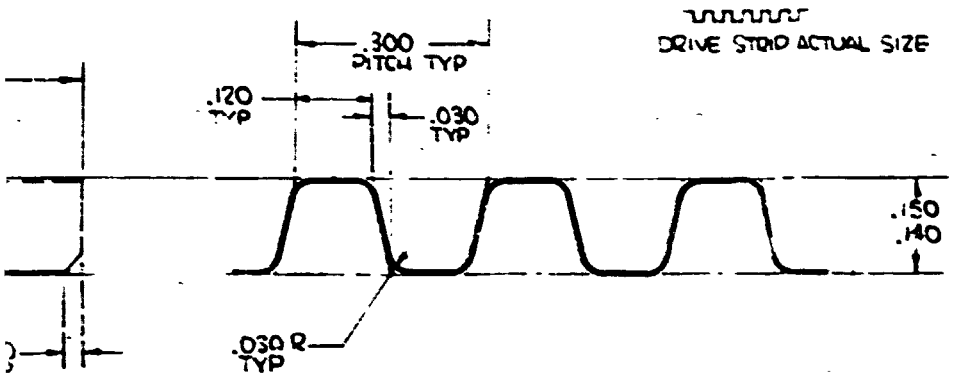

DRIVE STRIP ACTUAL SIZE

DETAIL C DRIVE STRIP -29-31 & -33
SCALE 10 x FULL SIZE
NOTE:- DRIVE STRIP TO BE MADE IN DOUBLE WIDTH & SLIT DOWN CENTER TO OBTAIN MATCHING PAIRS FOR LEFT & RIGHT HAND BEAMS.

SPLICED SHOWN

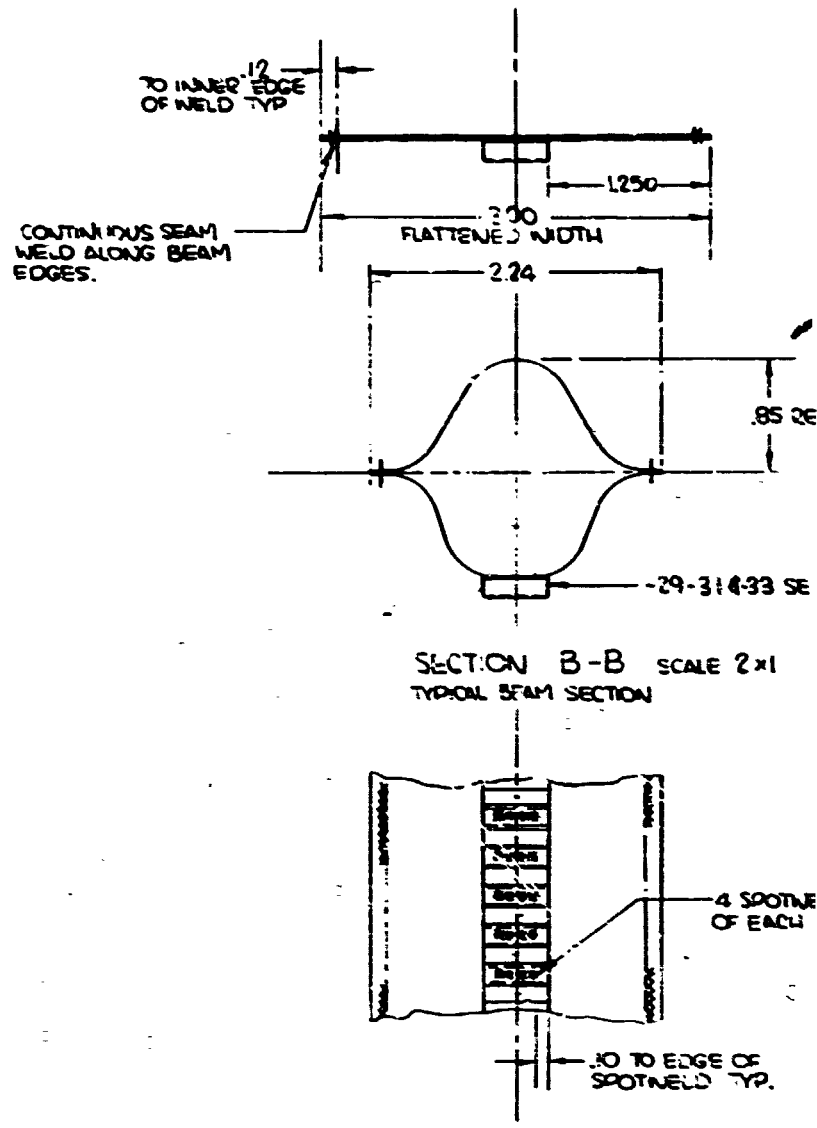

SECTION B-B SCALE 2 x 1
TYPICAL SEAM SECTION

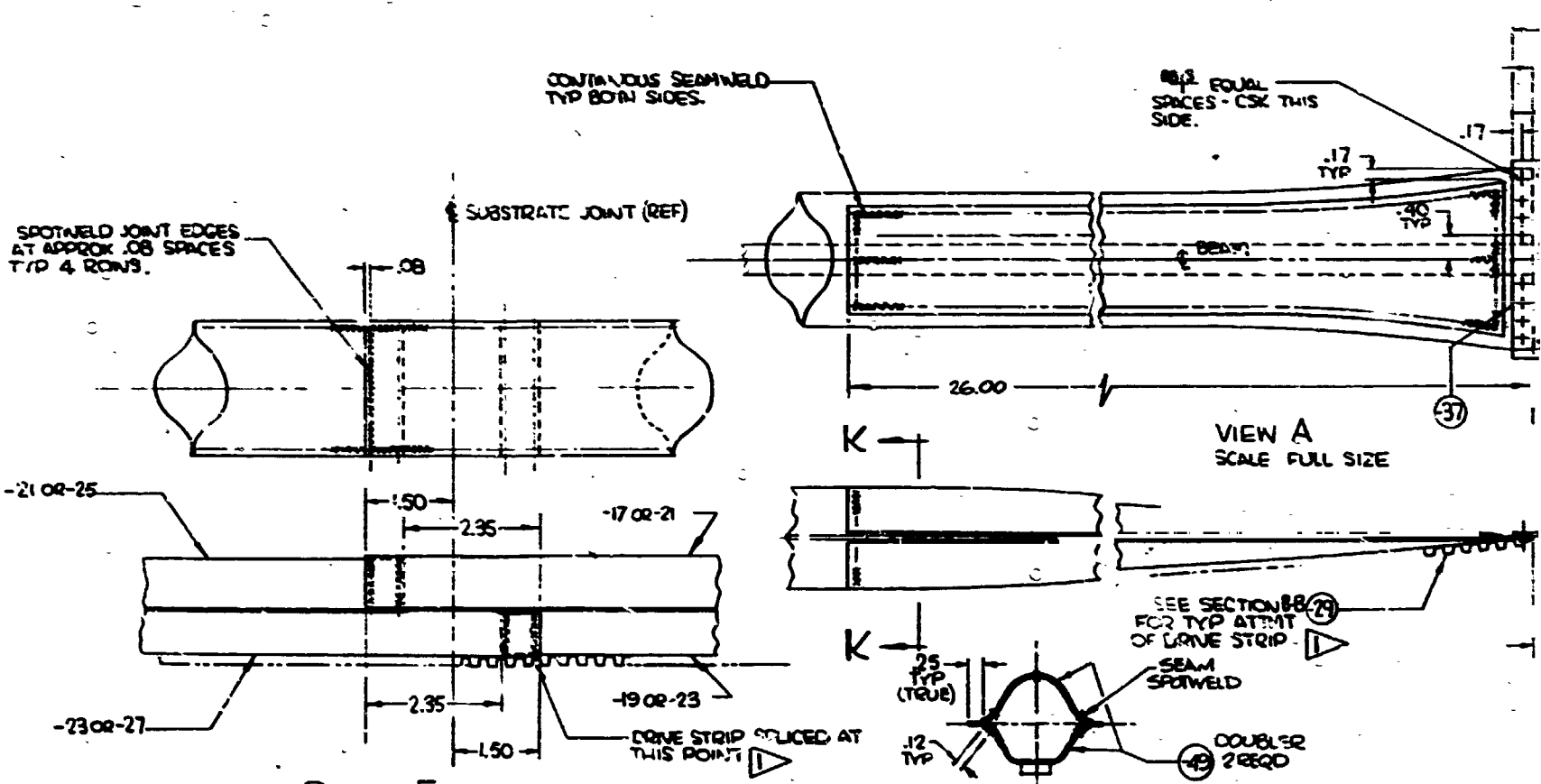

DETAIL E TYPICAL SPLICE
SCALE FULL SIZE.

SECTION K-K

NT FRAME

FOLDOUT FRAME

.250

.85 REF

--29-31-33 SEE DETAIL C

SCALE 2×1

4 SPOTWELDS AT BASE OF EACH CORRUGATION.

TO EDGE OF OTWELD TYP.

TABLE OF MAJOR DIMENSIONS.

ITEM	DISTANCE FROM EXTREME OUTER END (DRUM END)
START OF IW MODULE	19.79
℄ JOINT 1 ℄ 2 MODULES	57.45
℄ JOINT 2 ℄ 3 MODULES	95.11
℄ JOINT 3 ℄ 4 MODULES	132.77
℄ JOINT 4 ℄ 5 MODULES	170.43
℄ SPLICE JOINT 1 ℄ ℄ JOINT 5 ℄ 6 MODULES	208.09
℄ JOINT 6 ℄ 7 MODULES	245.75
℄ JOINT 7 ℄ 8 MODULES	283.41
℄ JOINT 8 ℄ 9 MODULES	321.07
℄ JOINT 9 ℄ 10 MODULES	358.73
℄ SPLICE JOINT 2 ℄ ℄ JOINT 10 ℄ 11 MODULES	396.39
℄ JOINT 11 ℄ 12 MODULES	434.05
℄ JOINT 12 ℄ 13 MODULES	471.71
℄ JOINTS ℄	509.37
THERMAL BLANKET END OF BLANKET	564.57

.85
.50 EOP-5
HOLE(4) 5/16 DIA
.25
.17
.66 TYP
1.08 TYP
.40 TYP
3.25
1.62
.180
HOLE(3) .166 CSK .279 DIA ×100° OTHER SIDE POSITION ON ASSY WITH 400U029
(37)
ZE
.50 (START OF CORRUGATED DRIVE STRIP)

82.00 BEAM CRS.

END THERMAL BLANKET

1.80 REF

(10)

(7)

℄ JOINT THIRTEENTH ℄ THERMAL BLANKET

℄ JOINT TENTH ℄ ELEVENTH SUBSTR MODULES.

188.30

℄ SPLICE 2

(9)

DETAIL J

8.00

177.98

BE SEE

(25)

(21)

(23)

EOP-33

(27)

(33) SEE DETAIL C

(31) SEE DET

FOLDOUT FRAME

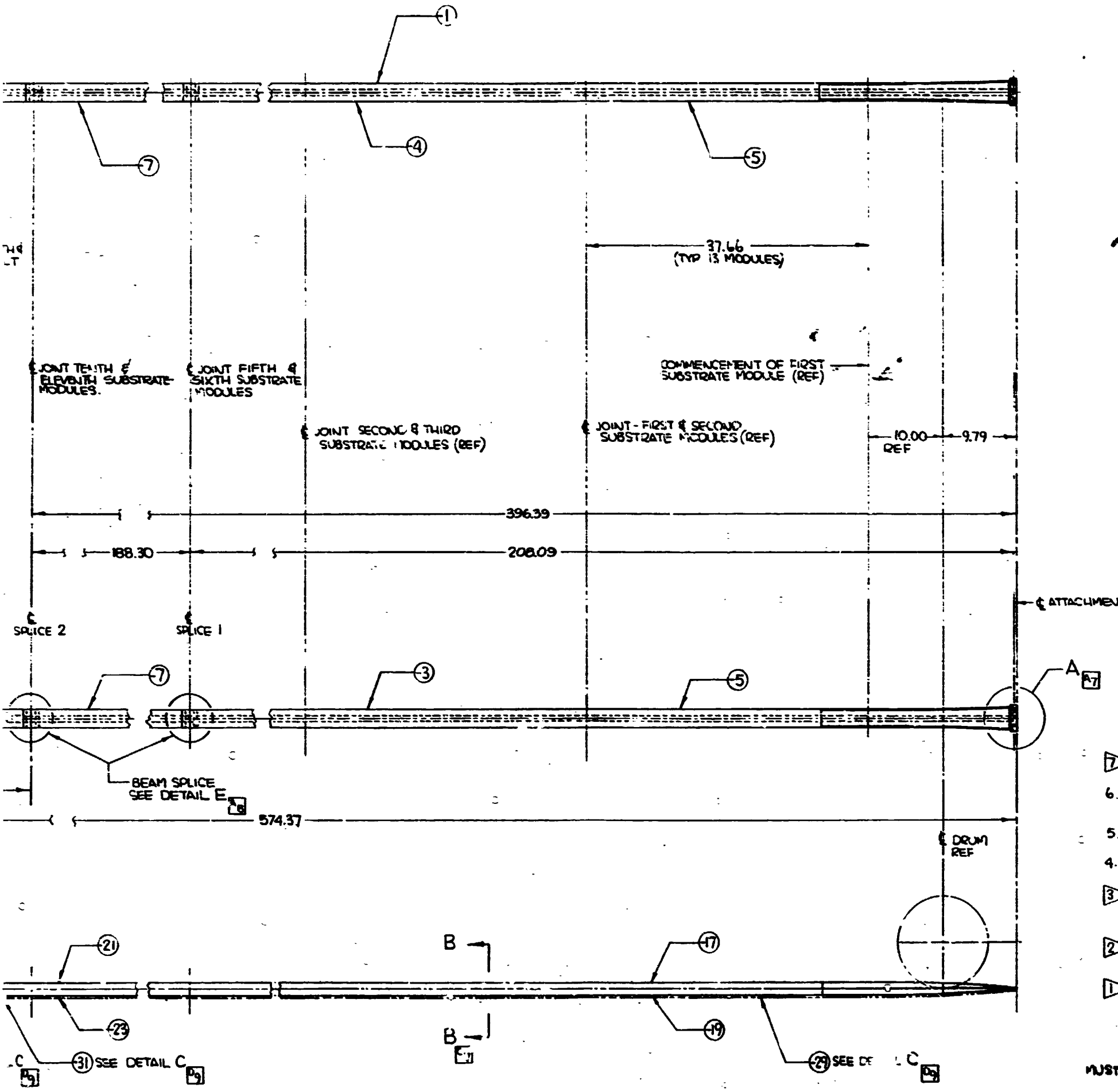

FOLDOUT FR

FOLDOUT FR

THE INFORMATION DISCLOSED HEREIN WAS ORIGINATED BY AND IS THE PROPERTY OF THE RYAN AERONAUTICAL COMPANY AND EXCEPT FOR THE RIGHTS PER ASPR IX GRANTED TO THE UNITED STATES GOVERNMENT AS FOLLOWS: [ ] UNLIMITED, [ ] LIMITED, [ ] NO RIGHTS, RYAN RESERVES ALL PATENT, PROPRIETARY, DESIGN, USE, SALE, MANUFACTURING AND REPRODUCTION RIGHTS THERETO. THIS DOES NOT APPLY TO ANY VENDOR PARTS.

REVISIONS

SYM	ZONE	DESCRIPTION	DATE	APPROVED

℄ ATTACHMENT HOLES (REF)

–A A7

7 DOW CHEMICAL CO. MIDLAND MICH.

6. LIMITS ON STRAIGHTNESS OF -3 & -4 BEAMS TO BE WITHIN ±.12 OF A THEORETICAL STRAIGHT LINE.

5. ALL RESISTANCE WELDING TO BE IN ACCORDANCE WITH RYAN MPO 083

4. ALL PROCESSES TO BE IN ACCORDANCE WITH 400S002

3 BOND -47 TO -39 USING RTV 3145 IN ACCORDANCE WITH 400S002

2 FOAM DENSITY 1.68 lb/CU/FT.

1 ACCUMULATED TOLERANCES ON DRIVE STRIP -29, -31 & -33 ARE NOT IMPORTANT, BUT RELATIONSHIP OF CORRUGATIONS ON LEFT & RIGHT HAND BEAMS ARE TO BE HELD WITHIN ±.010 (NOT CUMULATIVE) PITCH OF CORRUGATIONS MAY BE ADJUSTED SLIGHTLY OVER A GIVEN LENGTH TO MAKE JOINT AT SPLICE - SEE DETAIL E, BUT PITCHES MUST REMAIN WITHIN ±.010 RELATIVE POSITION WITH OPP. HAND BEAM.

NOTES:-

-11	-10	-9	-7	-5	-4	-3	-1	CODE IDENT	PART NUMBER	DESCRIPTION	STOCK SIZE	MATERIAL	SPECIFICATION
AR (7)									RTV 3145	ADHESIVE			
						AR	U12		MS20470AD3	RIVET			
				2					-49	DOUBLER SHEET .0020	2.40 x 26.00	TITANIUM 6AL 4V	MIL-T-9046 CLASS 2
1 (2)									-47	DAMPER PAD SHEET .25 THK	1.0 x 76.0	POLYURETHANE FOAM 3X	MIL-P-26514 TYPE I CLASS 2
	1	1							-45	CHANNEL SHEET .008-.0085	1.1 x 2.7	TITANIUM 6AL 4V	MIL-T-9046 CLASS 2
	2	2							-43	ANGLE SHEET .008-.0085	.75 x 2.7	TITANIUM 6AL 4V	MIL-T-9046 CLASS 2
2									-41	BRKT SHEET .008-.0085	2.1 x 2.3	↕	↕
1									-39	TUBE SHEET .005-.0055	5.20 x 80.0	TITANIUM 6AL 4V	MIL-T-9046 CLASS 2
				1					-37	DOUBLER SHEET .040	1.60 x 3.1	AL ALY 2024-T4	QQ-A-250 -4
	1	1							-33	DRIVE STRIP SHEET .008-.0085	.60 x 300.0	TITANIUM 6AL 4V	MIL-T-9046 CLASS 2
			1						-31	DRIVE STRIP SHEET .008-.0085	.60 x 360.0	↕	↕
				1					-29	DRIVE STRIP SHEET .008-.0085	.60 x 324.0		
	1	1							-27	BEAM HALF LOWER SHEET .008-.0085	3.00 x 163.0		
	1	1							-25	BEAM HALF UPPER ↕	3.00 x 163.0		
			1						-23	BEAM HALF LOWER	3.00 x 192.0		
			1						-21	BEAM HALF UPPER	3.00 x 192.0		
				1					-19	BEAM HALF LOWER ↕	3.00 x 172.5	↕	↕
				1					-17	BEAM HALF UPPER SHEET .008-.0085	3.00 x 172.5	TITANIUM 6AL 4V	MIL-T-9046 CLASS 2
							1		-11	ASSY END INTERCOSTAL			
					1	1			-10 / -9	[illegible]	[illegible]	[illegible]	[illegible]
					1	1			-7	BEAM SECTION MIDDLE			
					1	1			-5	BEAM SECTION INNER			
							1		-4 / -3	BEAM ASSY R.H. / L.H.			
									-1	BEAM INSTL			

LIST OF MATERIAL

[illegible]

BEAM INSTL - 250 SQ.FT. ROLL-UP SOLAR PANEL.

SIZE J 400U021

400U021

2

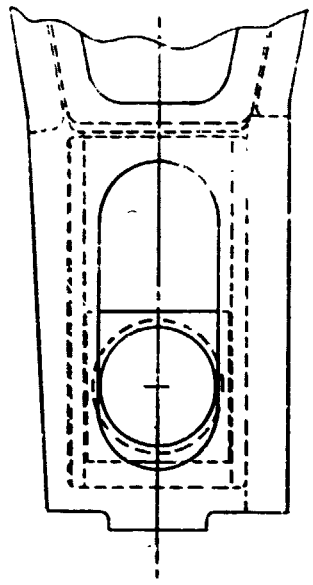

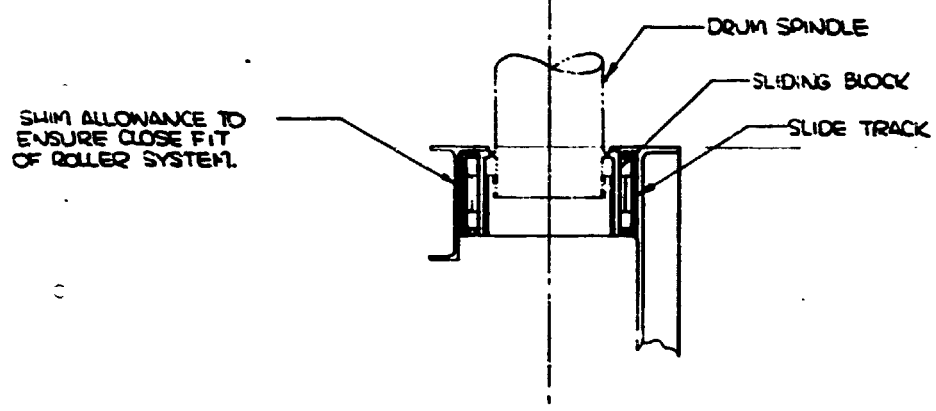

SECTION 12 - 12

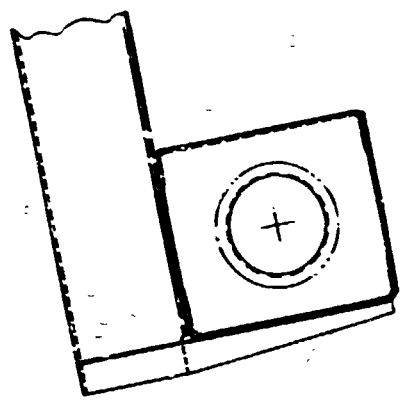

SECTION 13 - 13

FOLDOUT FRAME

FOLDOUT

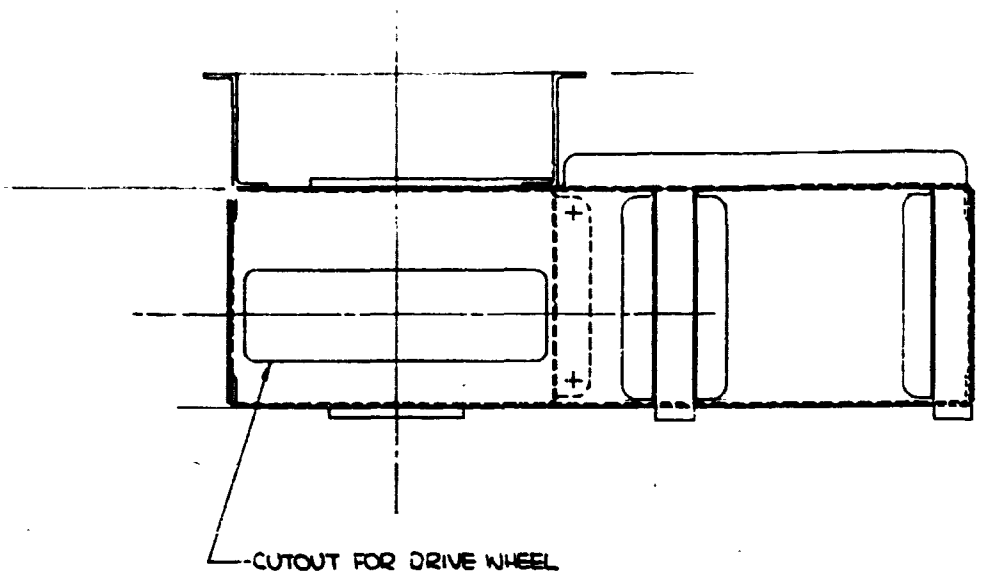
CUTOUT FOR DRIVE WHEEL

SECTION A - A

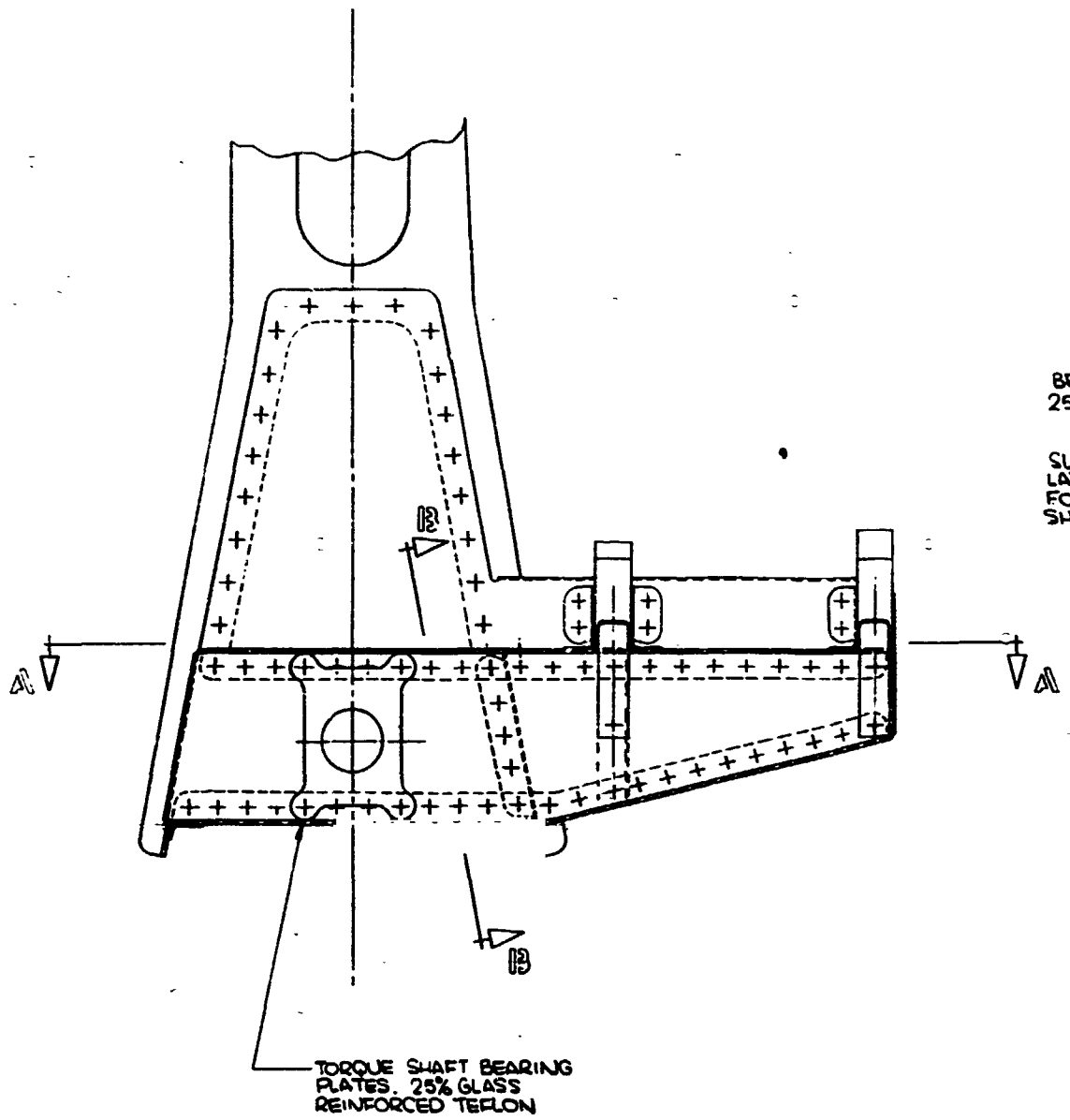
B
B
A
A
TORQUE SHAFT BEARING PLATES. 25% GLASS REINFORCED TEFLON

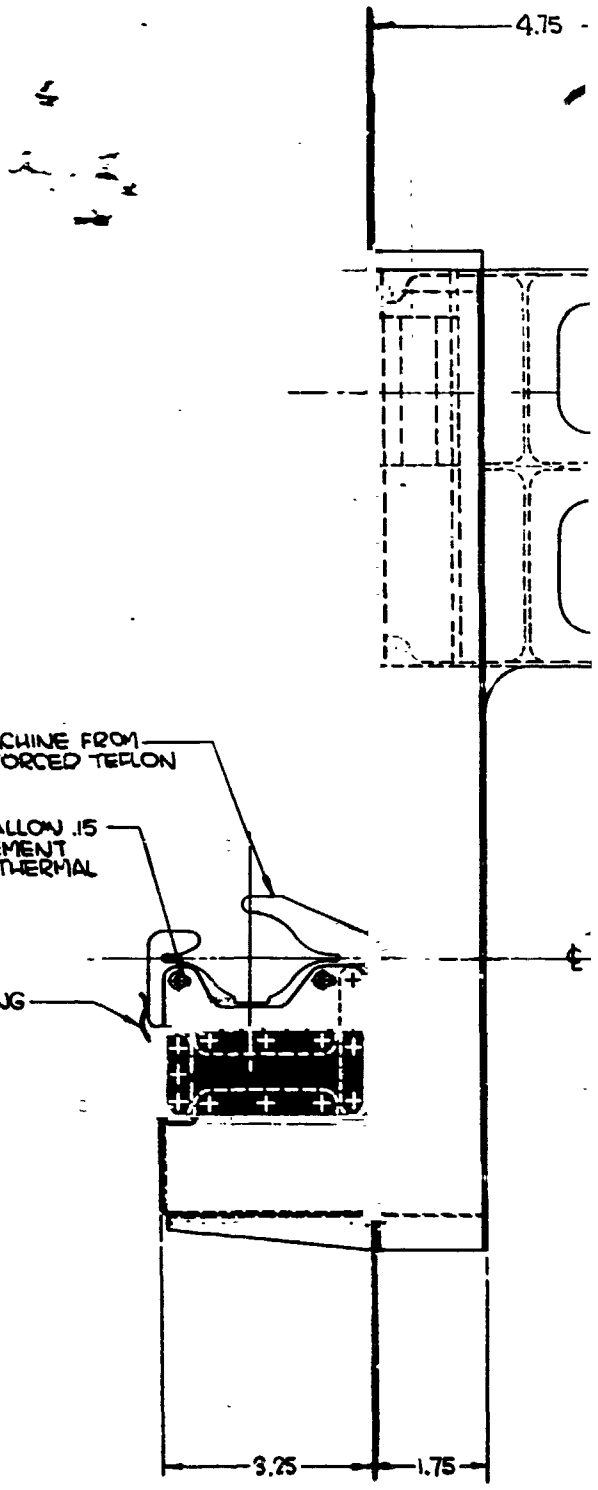
4.15
BEAM GUIDES, MACHINE FROM 25% GLASS REINFORCED TEFLON
SLOTTED HOLES ALLOW .15 LATERAL DISPLACEMENT FOR SUBSTRATE THERMAL SHRINKAGE.
GUIDE RETAINING SPRINGS.
3.25
1.75

7 6 5

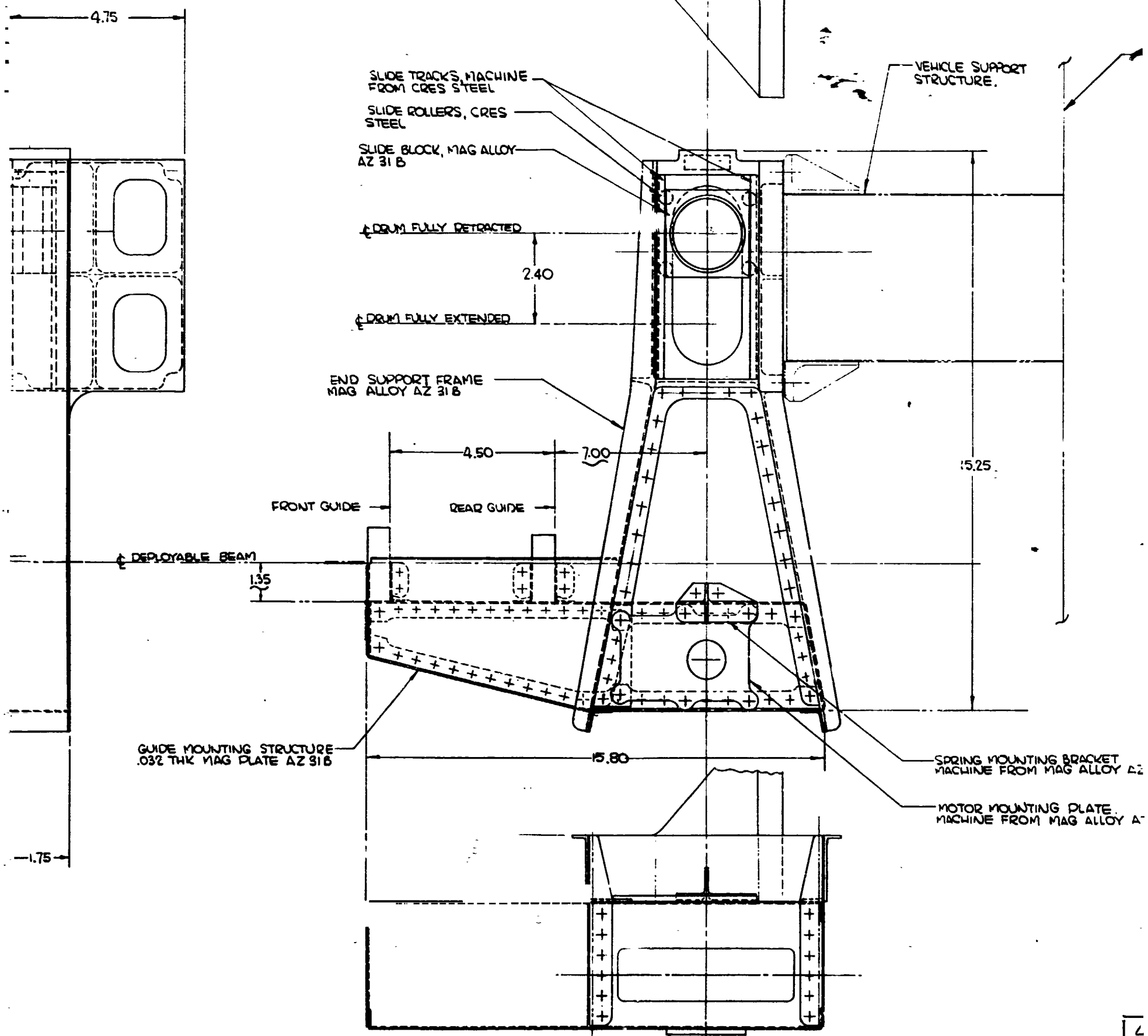

7 6 5

FOLDOUT FRAME

FOLDOUT FRAME

VEHICLE SIDE (REF)

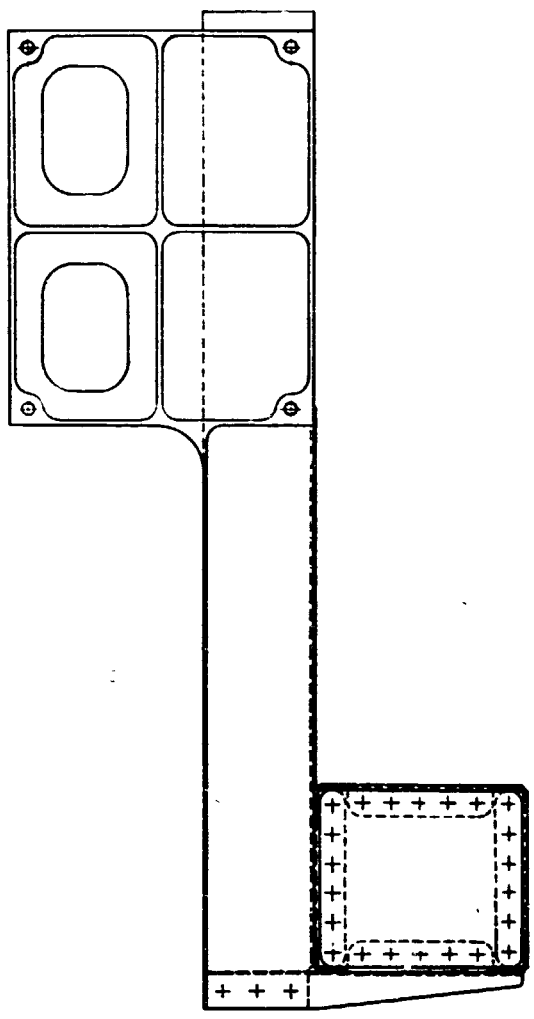

JTING BRACKET
DM MAG ALLOY AZ 31 B

JTING PLATE
DM MAG ALLOY AZ 31 B

ITEM NO.	PART NUMBER	DESCRIPTION
QTY USED PER ASSY		

LIST OF

REVISIONS				
LTR	OFF ON	DESCRIPTION	DATE	APPROVED

CODE IDENT	PART NUMBER	DESCRIPTION	STOCK SIZE	MATERIAL	SPECIFICATION	RYAN MATL CODE	ZONE	ITEM NO.

LIST OF MATERIAL

CODE IDENT	PART NUMBER	DESCRIPTION	STOCK SIZE	MATERIAL	SPECIFICATION	RYAN MATL CODE	ZONE	ITEM NO.

LIST OF MATERIAL

RELEASE & DATE	QTY NEED PER ASSY	FINAL ASSY	NEXT ASSY	QTY REQUIRED	NEXT ASSEMBLY	USED ON APPLICATION

UNLESS OTHERWISE SPECIFIED
DIMENSIONS ARE IN INCHES AND INCLUDE CHEM APPLIED OR PLATED FINISHES
TOLERANCES
LINEAR: .X ±.1; .XX ±.03; .XXX ±.010
ANGULAR: EXCL OF SHEET METAL FLANGES ±0° 30'
PARTS TO BE FREE OF BURRS AND SHARP EDGES. MANUFACTURING REQUIREMENTS PER RYAN SPEC. STANDARD NO. 120.

CONTRACT NUMBER

	SIGNATURES	DATE
DRAWN BY		
CHECK		
ENGINEERING		
STRESS		
PROJECT		

DESIGN ACTIVITY APPROVAL
DESIGN APPROVAL

RYAN AERONAUTICAL COMPANY
SAN DIEGO, CALIFORNIA 92112

END SUPPORT STRUCTURE.

SIZE	CODE IDENT NO.	DRAWING NUMBER	REV LTR
J	78022	400U022	

SCALE | WEIGHT | SHEET 1 OF

FOLDOUT FRAME

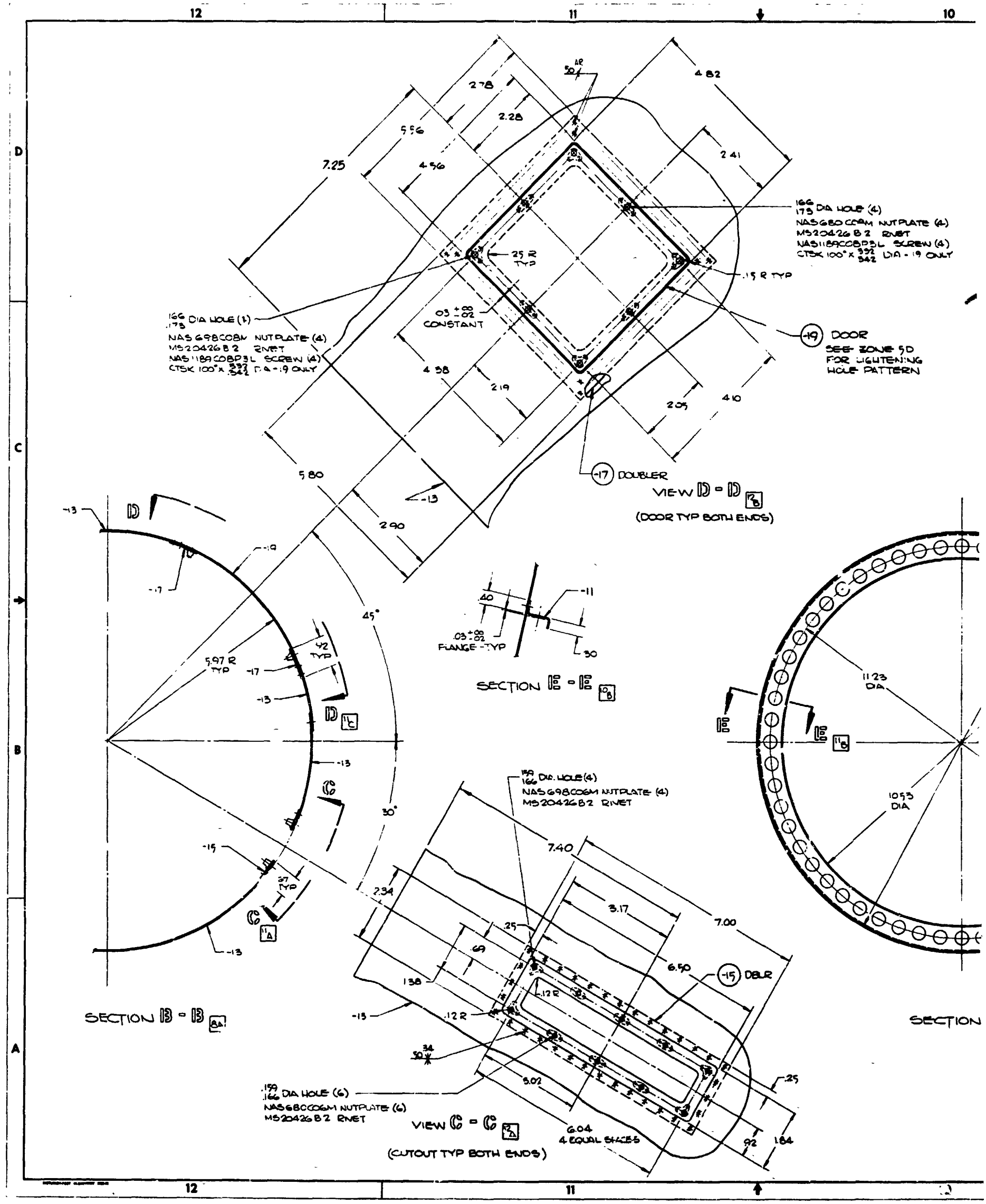

FOLDOUT FRAME

FOLDOUT FRAME

ATE (4)
REW (4)
• ONLY

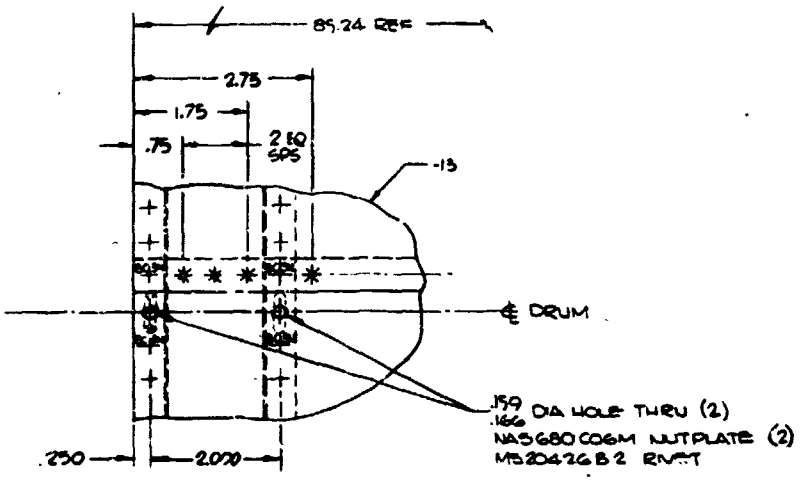

VIEW B [98]

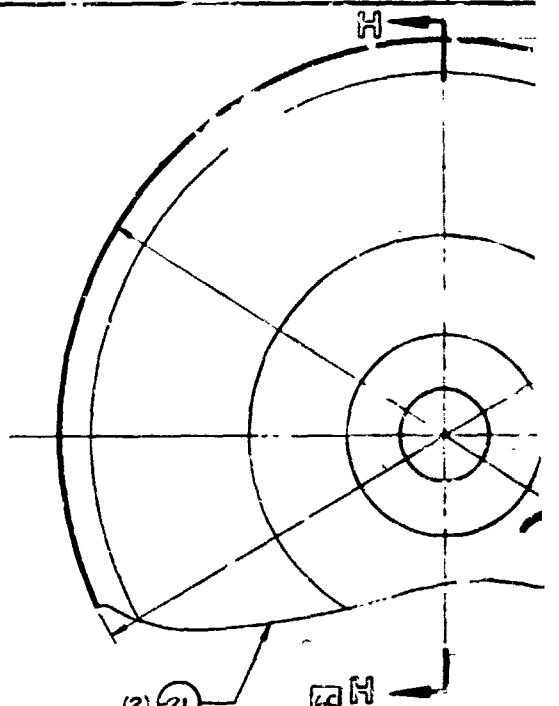

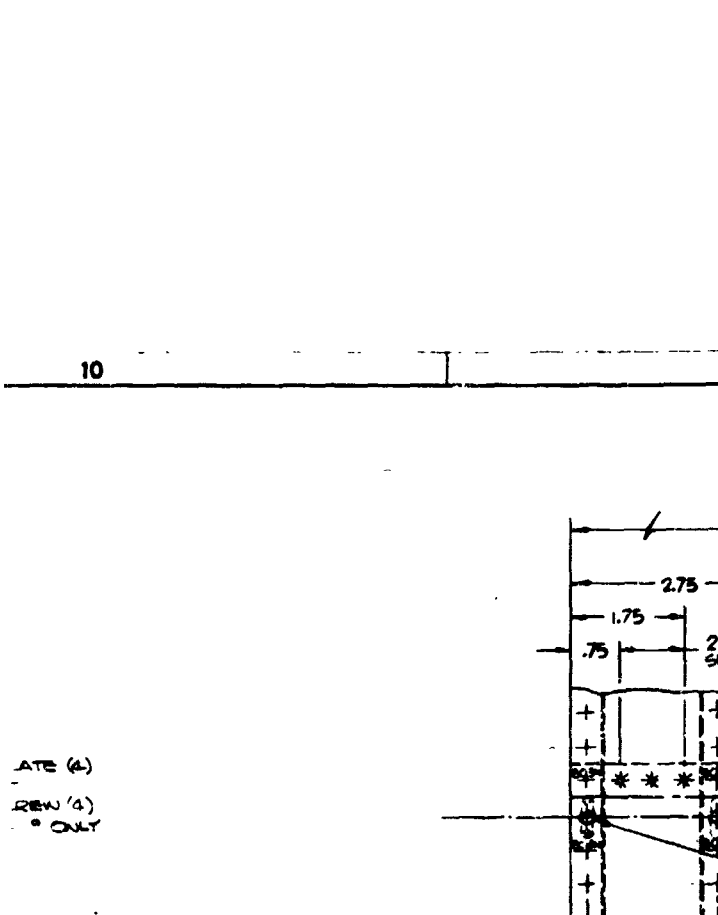

SECTION A - A [6A]

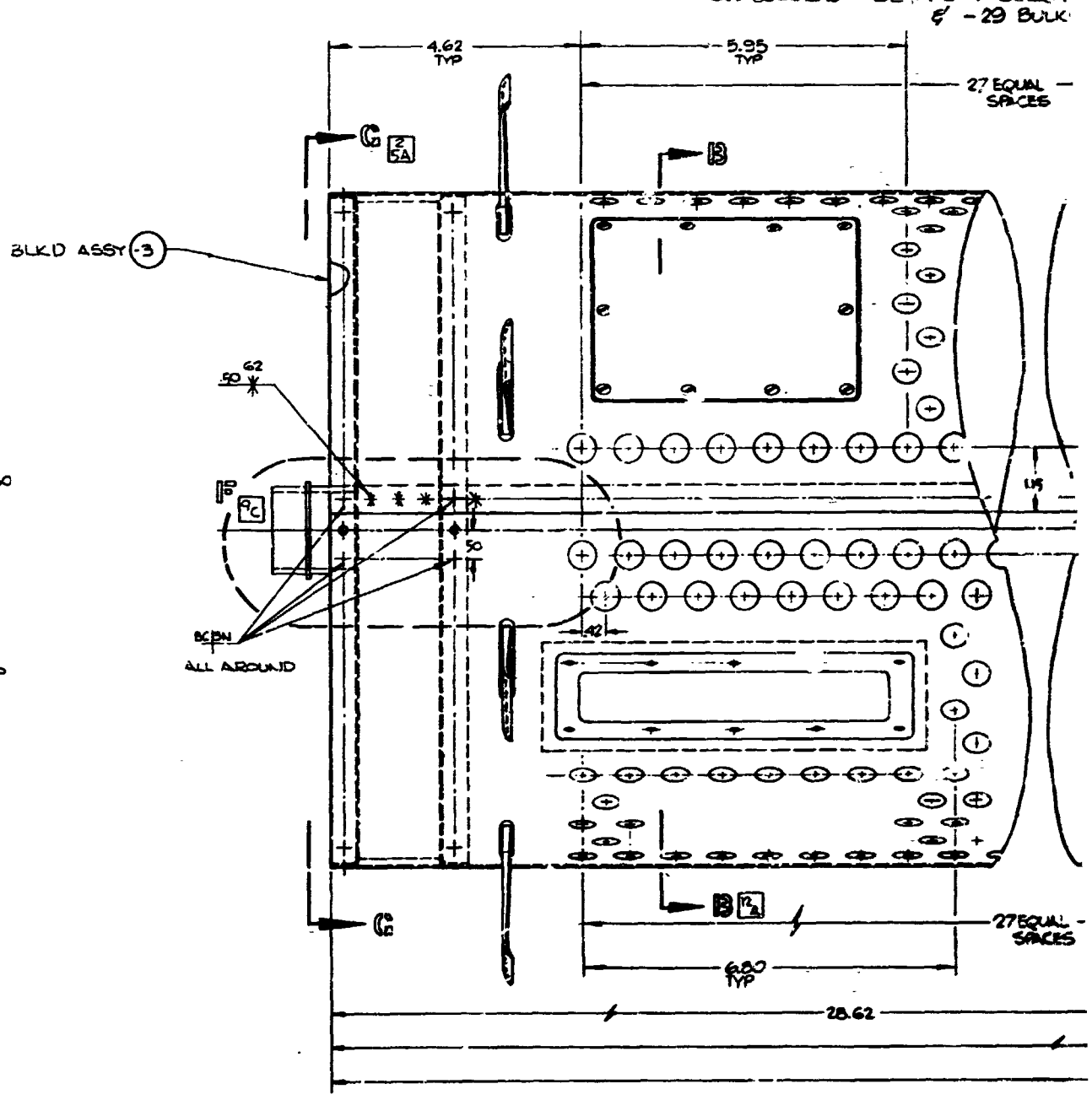

400U023 1

FOLDOUT FRAME

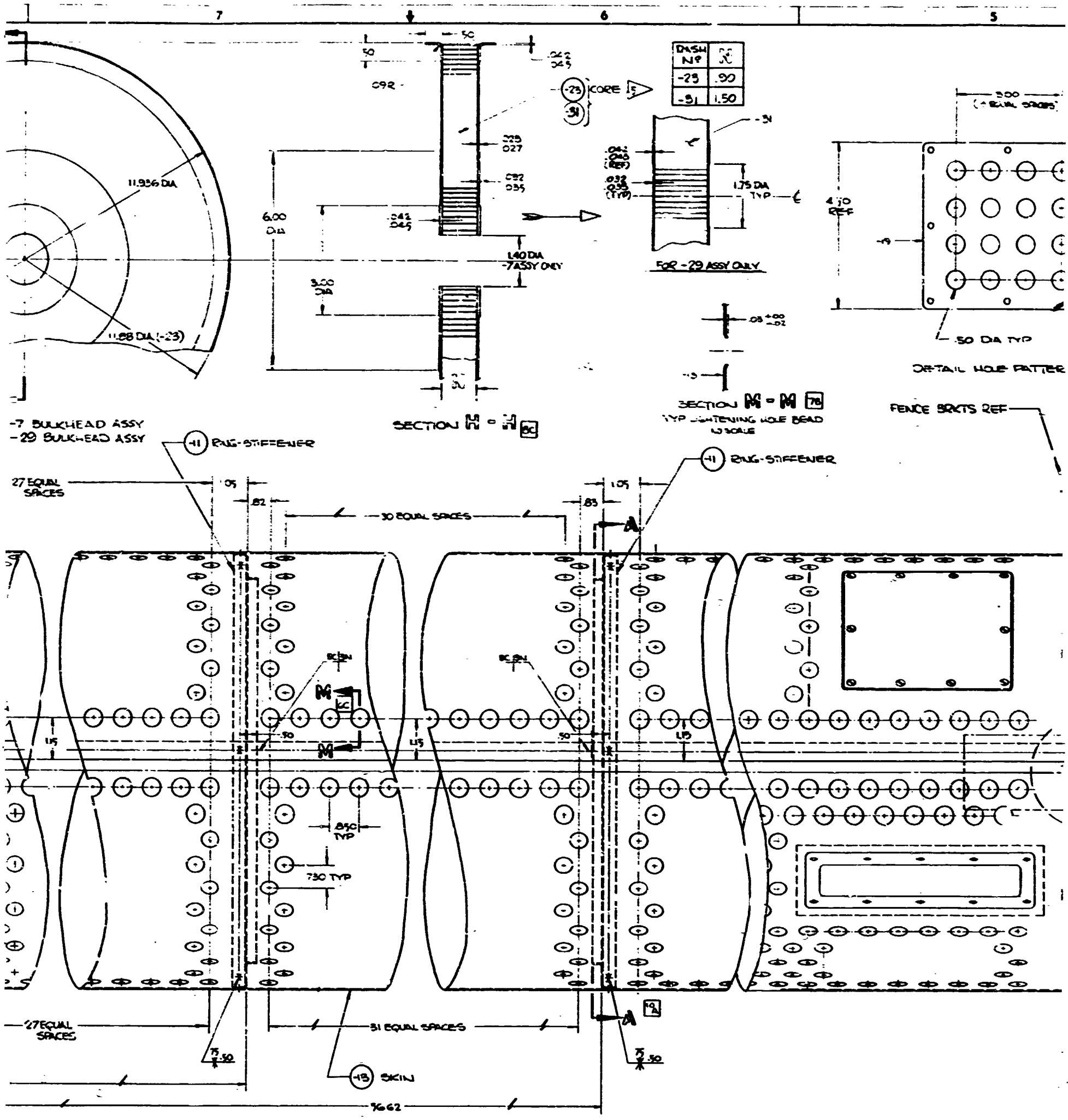

FOLDOUT FRAME

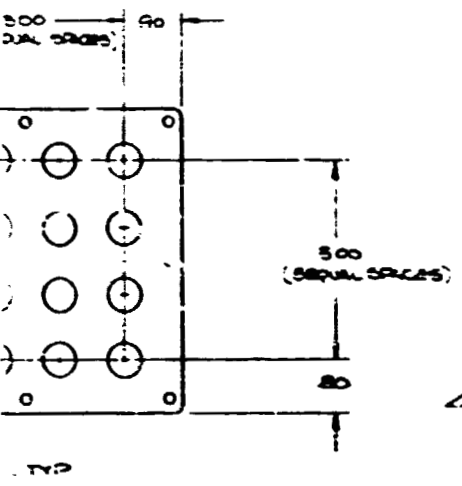

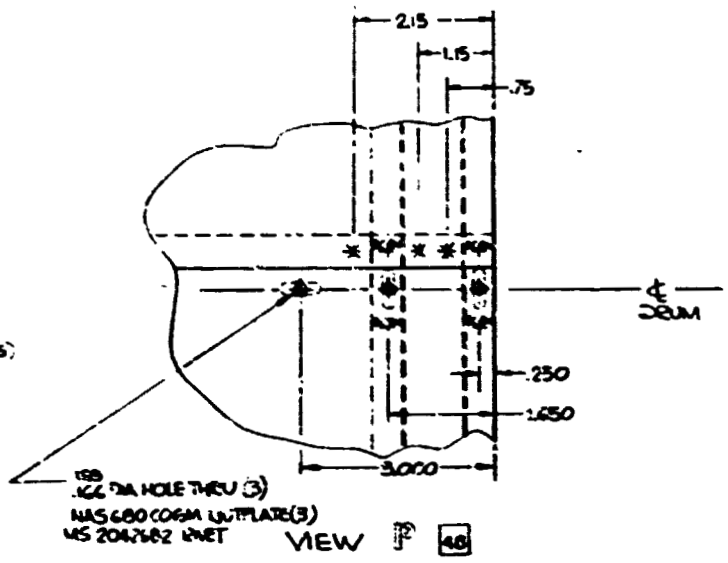

E PATTERN - 9 DOOR

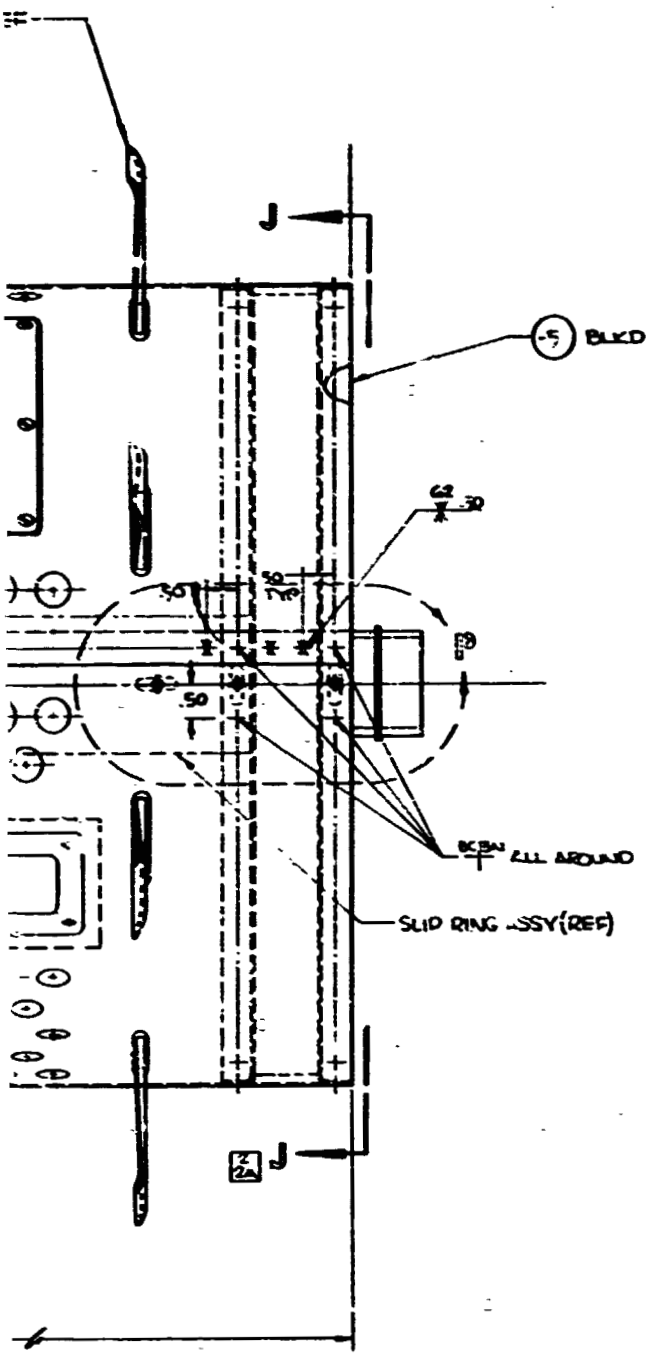

10	AMERICAN CYANAMID, BLOOMDALE DIV, ABERDEEN, MD.
9	SHELL CHEMICAL CO, PITTSBURG, CALIF.
8	SPOTFACE EACH POTTED INSERT FLUSH BOTH SIDES THIS AREA $^{+.005}_{-.000}$.
7	POT BOLT SPACER IN -3 & -5 ASSY'S WITH EPON 828 DION RP-7A WITH 40% MICROBALLOON FILLER MATL
6	BOND WITH EPON 934 AT TIME OF ASSY WITH BOLTS.
5	BOND -23 CORE TO -21 END BLKD WITH FM-96U PER RYAN MPD 1061
4	CHEM ETCH - 21 IN ACCORDANCE WITH RYAN MPD #22.
3	SPOTWELDING TO BE PER RYAN MPD 1068.
2	ALL DETAIL PARTS TO CONFORM TO RYAN SPEC 4005002
1	DIMENSIONING & TOLERANCING PER MIL-STD-8

NOTES

LIST OF MATERIAL

ITEM NO.	PART NUMBER	DESCRIPTION	MATERIAL	QTY REQ PER ASSY

4C0U023 | 1

FOLDOUT FRAME

REVISIONS

LTR	BY	DESCRIPTION	DATE	APPROVED

Flag	-29	-9	-7	-5	-3	-1	Code Ident	Part Number	Description	Stock Size	Material	Specification
						AR		MS20426AD4	RIVET		[illegible]	
						AR		MS20426AD3	RIVET		[illegible]	
		AR				AR		[illegible]	RIVET		[illegible]	
					16			NAS1121C25	BOLT			
				12				[illegible]	RIVET BLIND		[illegible]	
		8		6				[illegible]	NUTPLATE			
		8						[illegible]	NUTPLATE			
		8						[illegible]	NUTPLATE			
		8						[illegible]	NUTPLATE			
		16						[illegible]	SCREW			
				32				[illegible]C16	BOLT			
					22			[illegible]C26	BOLT			
				6				[illegible]08	BOLT			
					38			[illegible]	SPACER			
				38				[illegible]-57	SPACER			
10	AR		AR					FM1000	ADHESIVE		(.05 LB/FT²)	
9				AR	AR			EPON 934	ADHESIVE			
9	AR		AR					EPON 828 [illegible]	FILLER		(40% [illegible] BALLOONS)	
						8		-35	FENCE BRACKET	2.57 x [illegible]	BAR-AL ALY 7075	
						8		-33	FENCE BRACKET	1.85 x [illegible]	BAR-AL ALY 7075	
	1							-31	CORE	1.500	HONEYCOMB [illegible]	
					1			-29	BLKD ASSY			
2	-			1				-27	END HUB RH		MAG BAR AZ31B	H24
2					1			-25	END HUB, LH		MAG BAR AZ31B	H24
			1					-23	CORE	.900	HONEYCOMB [illegible] CORE	
4, 2	2		2					-21	END BLKD	.050	AL ALY SH 7075	T6
		2						-19	DOOR	.032	MAG SH AZ31B	H24
		2						-17	DOUBLER	.032		
		2						-15	DOUBLER	.032		
		1						-13	SKIN	.032		
		2						-11	RING-STIFF	.032		
2		-				1		-9	SKIN ASSY	.025	MAG SH AZ31B	H24
			-	1				-7	BLKD ASSY			
				-		1		-5	BLKD ASSY, RH			
					-	1		-3	BLKD ASSY, LH			
						-		-1	DRUM ASSY			

QTY REQD PER ASSY

LIST OF MATERIAL

APPLICATION: NEXT ASSEMBLY 400U; USED ON MOD 465

RYAN AERONAUTICAL COMPANY, SAN DIEGO, CALIFORNIA

DRUM ASSEMBLY, 250 FT² ROLL UP

SIZE J | CODE IDENT NO. 07765 | DWG NO. 400U023

SCALE 1/1 | SHEET 1

400U023

FOLDOUT FRAME

FOLDOUT FRAME

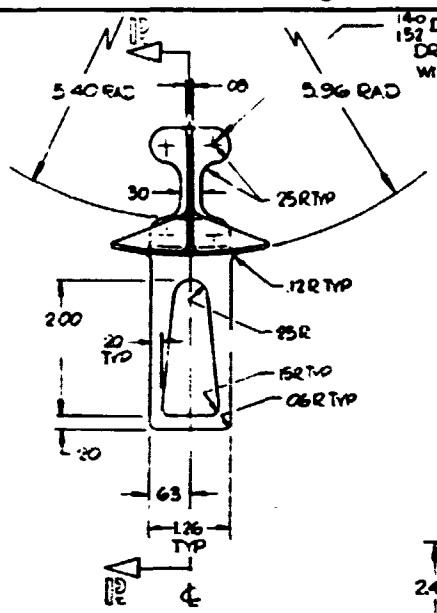

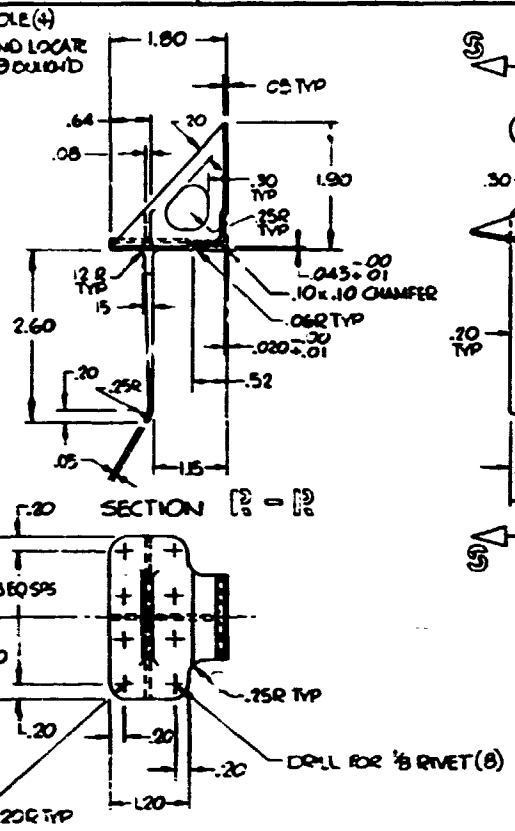

DETAIL - 33

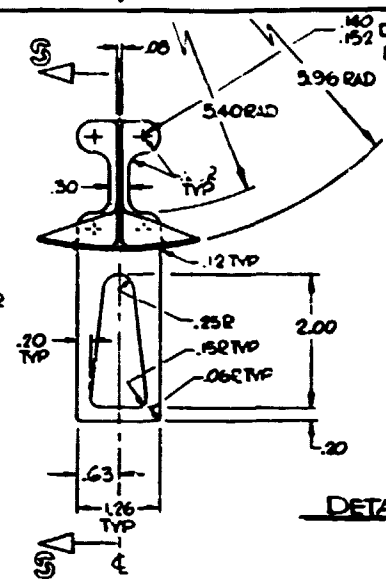

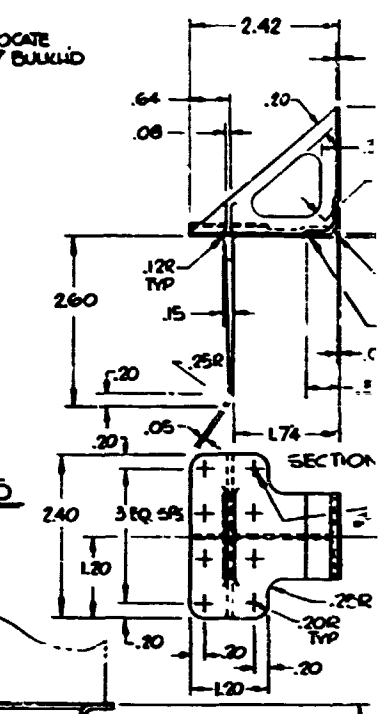

DETAIL - 35

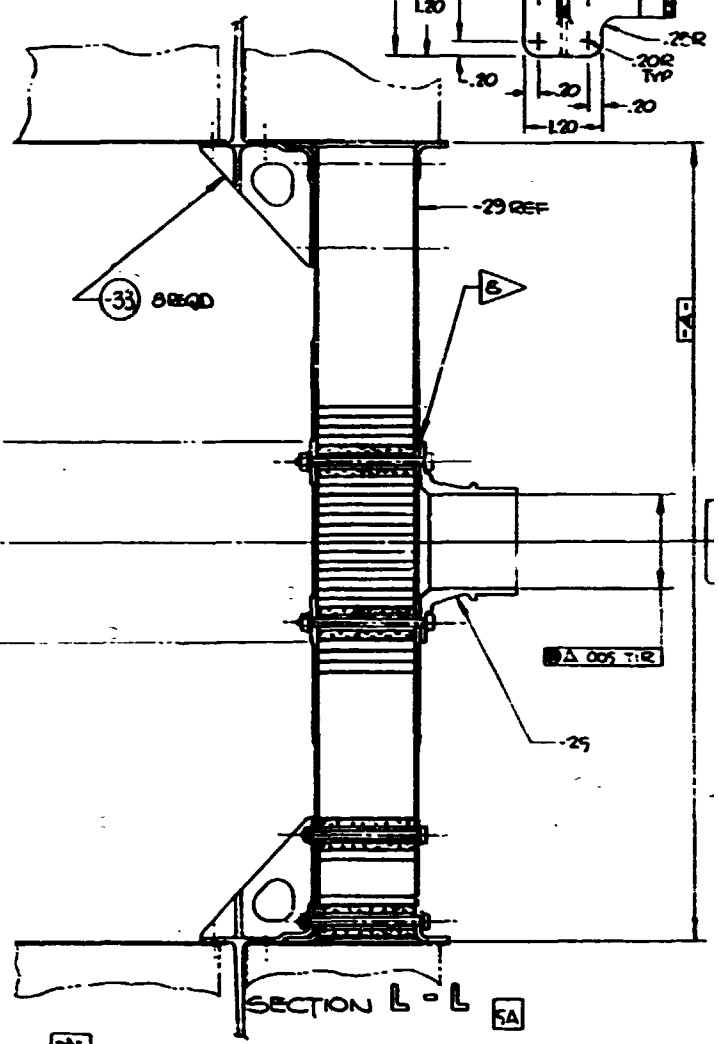

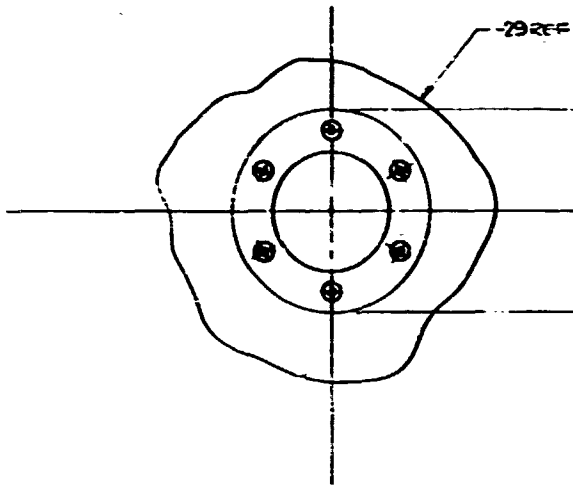

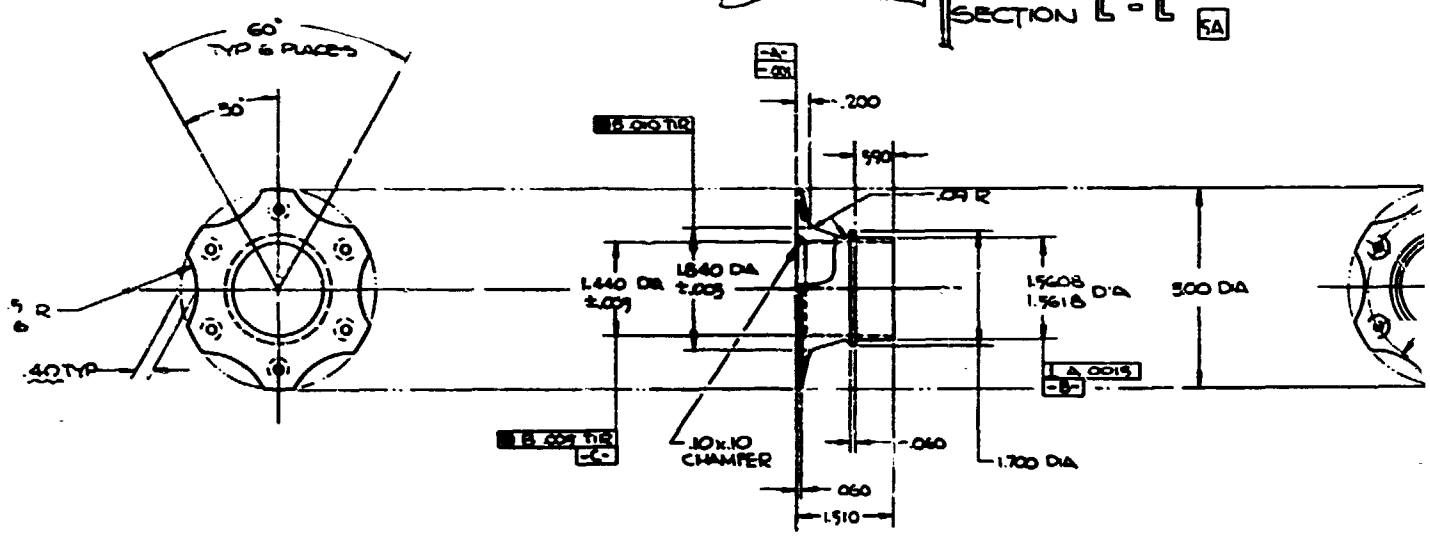

DETAIL -25 END HUB - L.H.

FOLDOUT FRAME

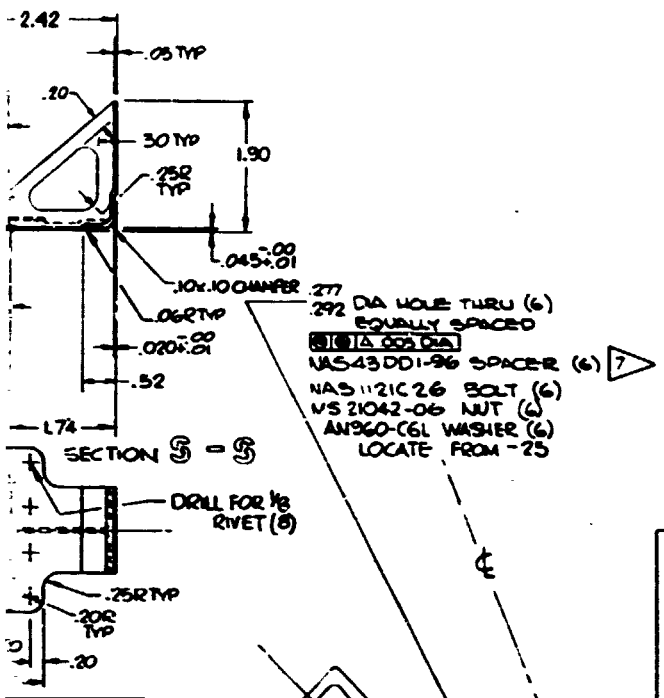

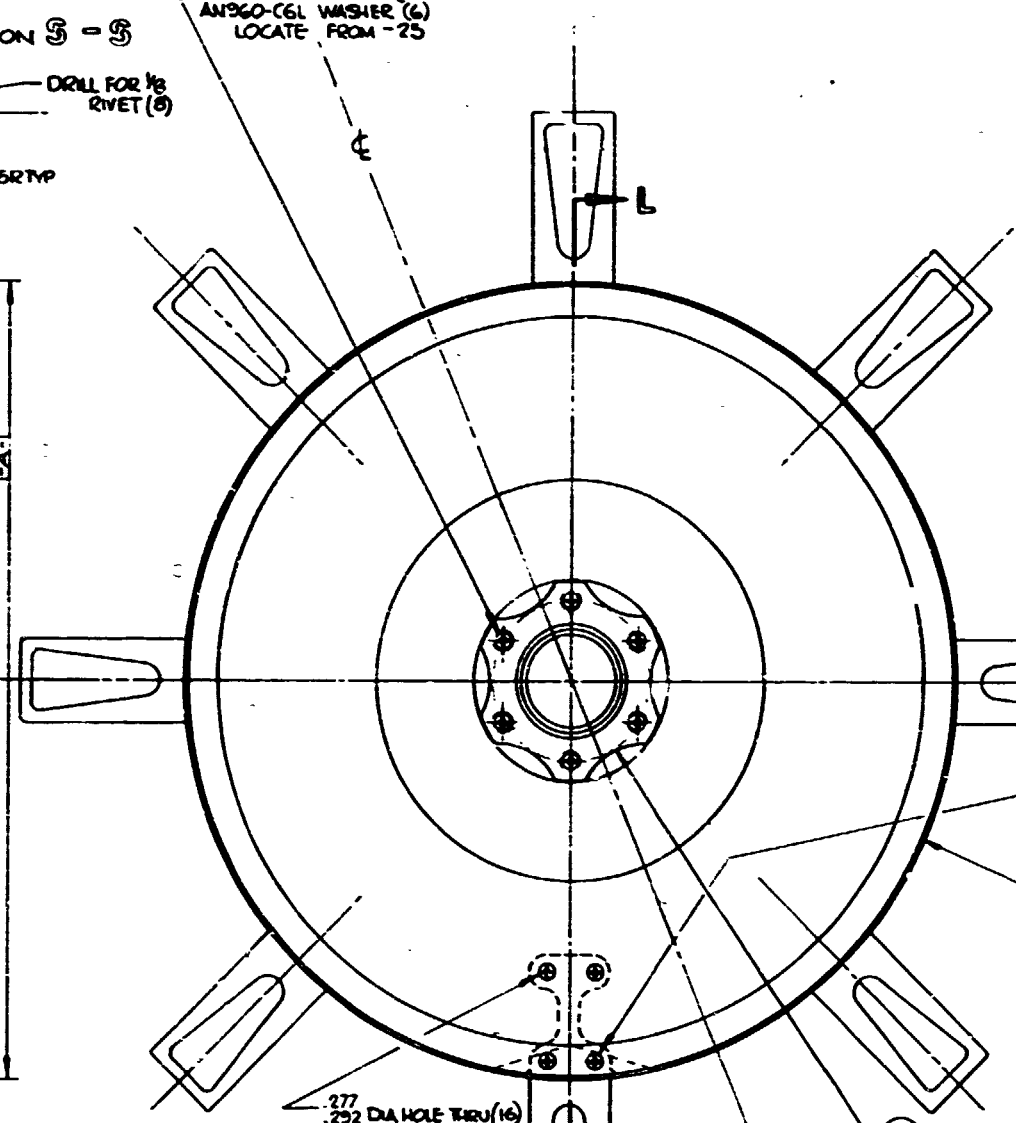

(DETAIL-3 BULKHEAD ASSY)

EDGE OF SUBSTRATE (REF)

BEAM FENCE BRACKET -35

NAS698C06M NUTPLATE (6)
MS20604B3W2 RIVET-BLIND (12)
LOCATE FROM -5 BULKD ASSY

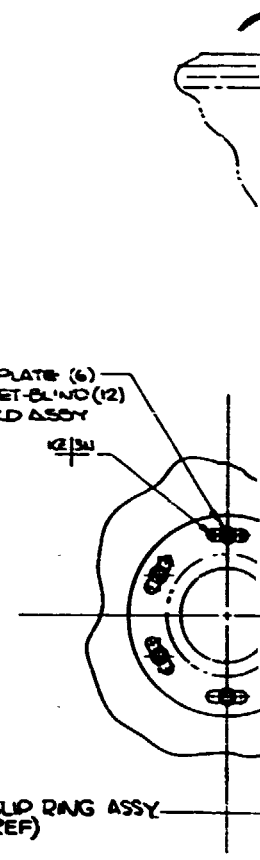

400U027 SLIP RING ASSY (REF)

.277
.292 DIA HOLE THRU (16)
FROM DETAIL-33
Ⓢ Ⓜ Ⓐ .005 DIA
NAS43DD1-96 SPACER (6) 7
NAS1121C26 BOLT (16)
MS21042-06 NUT (16)
AN960-C6L WASHER (16)
LOCATE FROM -33

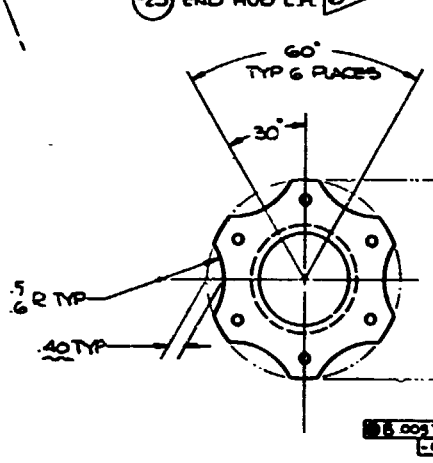

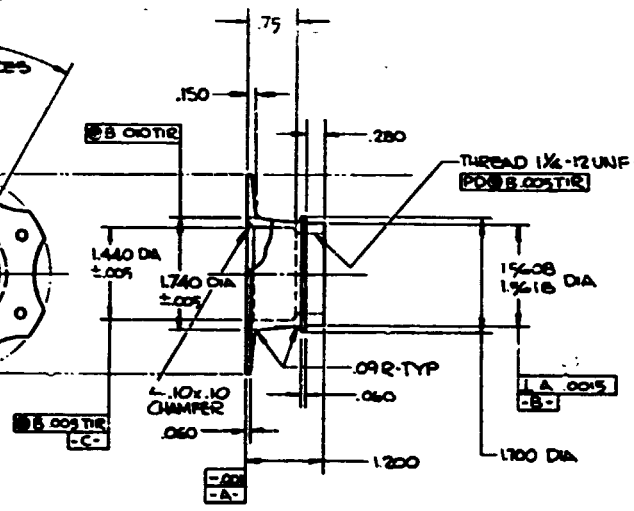

DETAIL-27 END HUB-R.H.

400U023 2

FOLDOUT FRAME

FOLDOUT FRAME

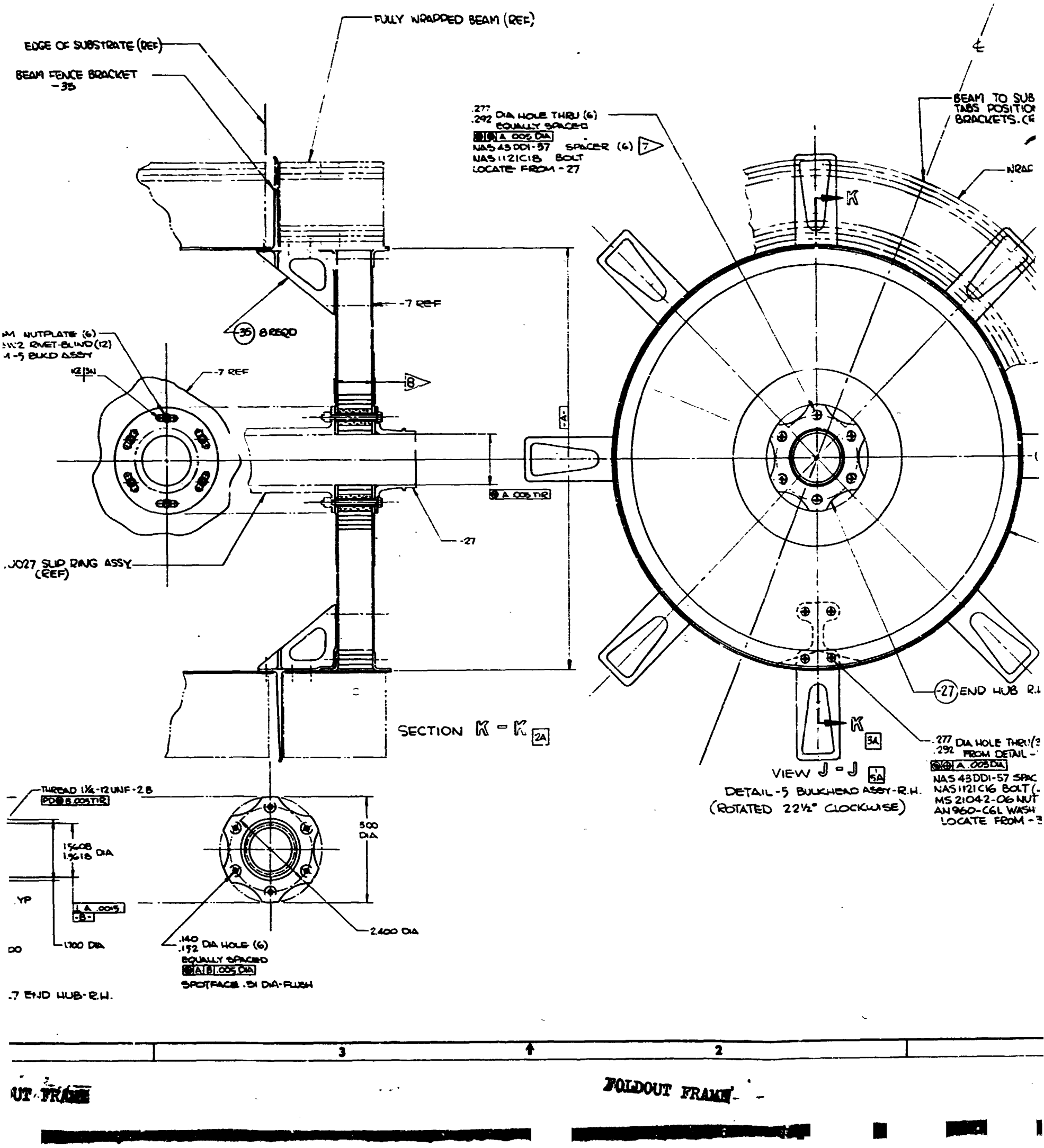

REVISIONS			
LTR	DESCRIPTION	DATE	APPROVED

FULLY WRAPPED BEAM (REF)

.277
.292 DIA HOLE THRU (6)
EQUALLY SPACED
Ⓢ Ⓜ A .005 DIA
NAS43DD1-57 SPACER (6) 7
NAS1121C18 BOLT
LOCATE FROM -27

BEAM TO SUBSTRATE ATTACHMENT TABS POSITIONED TO CLEAR FENCE BRACKETS. (REF)

WRAPPED SUBSTRATE (REF)

-7 REF

8

A .005 TIR

-27

-7 REF

-27 END HUB R.H. 6

SECTION K - K 2A

K

3A

VIEW J - J 6A

DETAIL-5 BULKHEAD ASSY-R.H.
(ROTATED 22½° CLOCKWISE)

.277
.292 DIA HOLE THRU (32)
FROM DETAIL - 35
Ⓢ Ⓜ A .005 DIA
NAS43DD1-57 SPACER (32)
NAS1121C16 BOLT (32)
MS21042-06 NUT (32)
AN960-C6L WASHER (32)
LOCATE FROM - 35

SIZE	CAGE IDENT NO.	DRAWING	REV LTR
J	78022	400U023	
SCALE 1/1		SHEET 2	

FOLDOUT FRAME

FOLDOUT FRAME

D

C

B

A

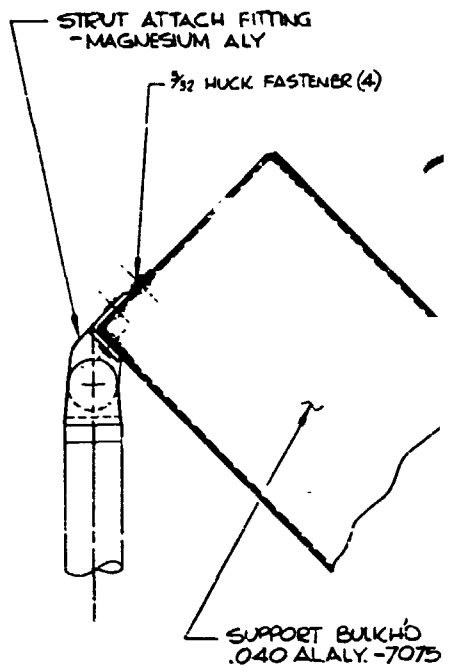

SECTION E - E

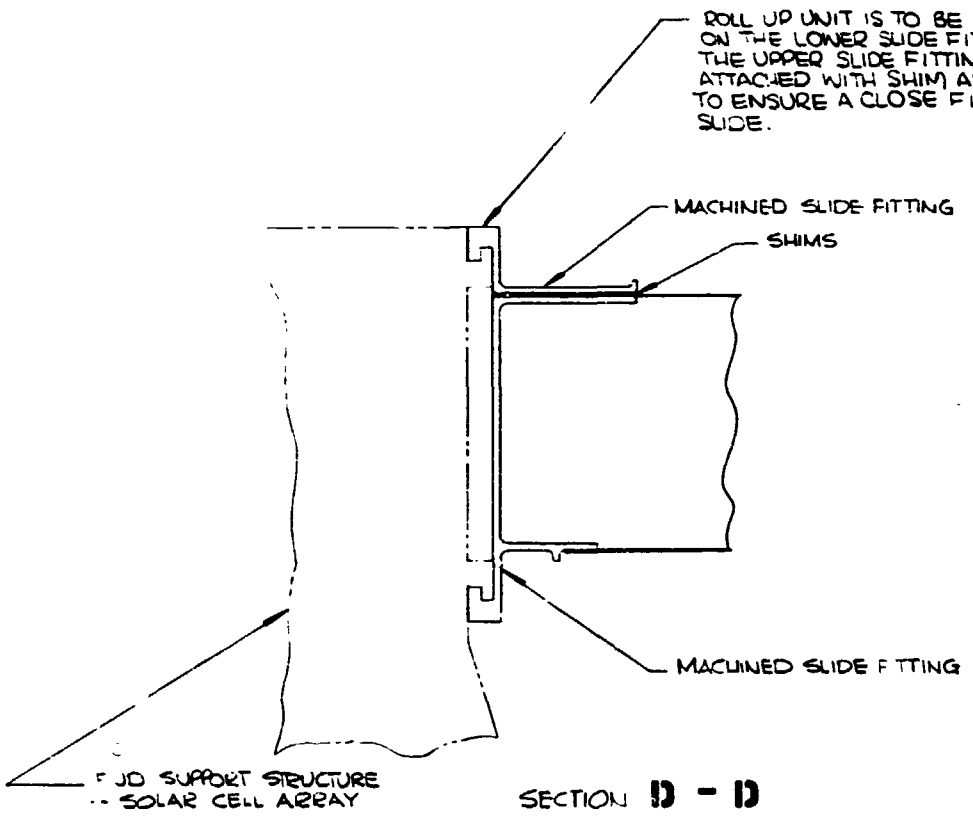

SECTION D - D

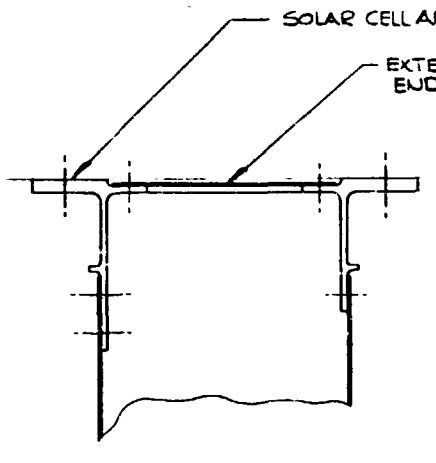

SECTION F - F

10 9 8

TING

ASTENER (4)

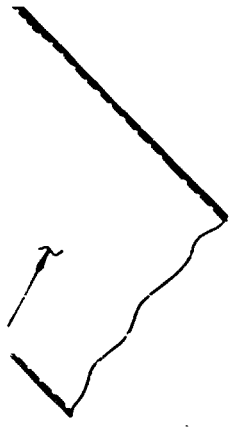

ORT BULKHD
.O AL ALY.-7075

: - E

OLAR CELL ARRAY INTERFACE

EXTENDED SHEET OF
END BULKHD

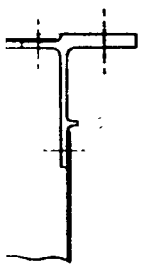

- F

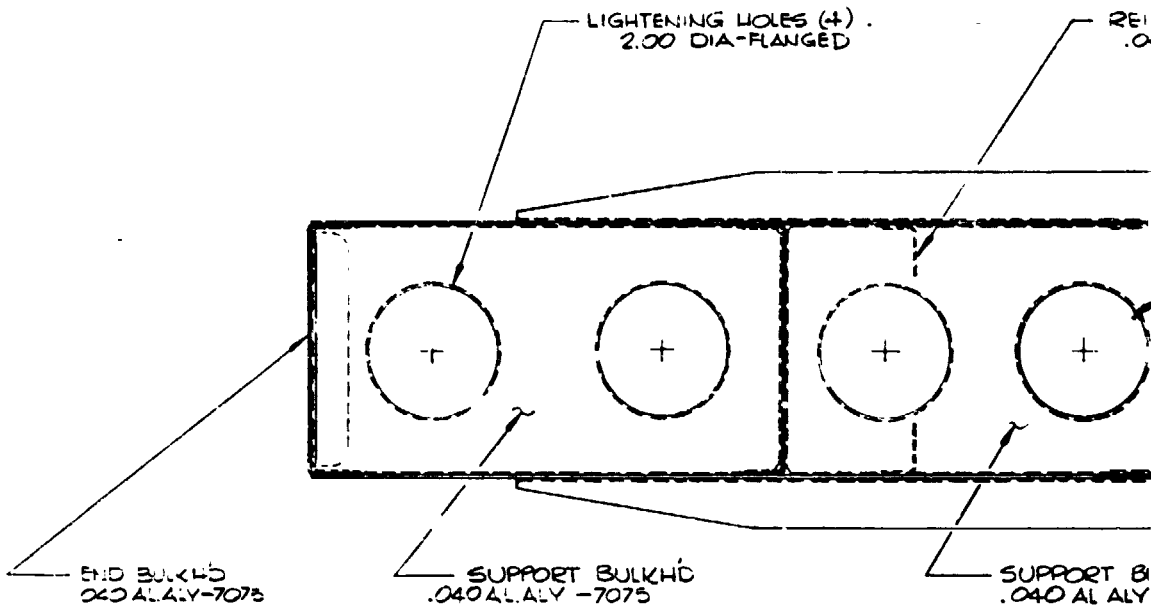

VIEW ON B - B

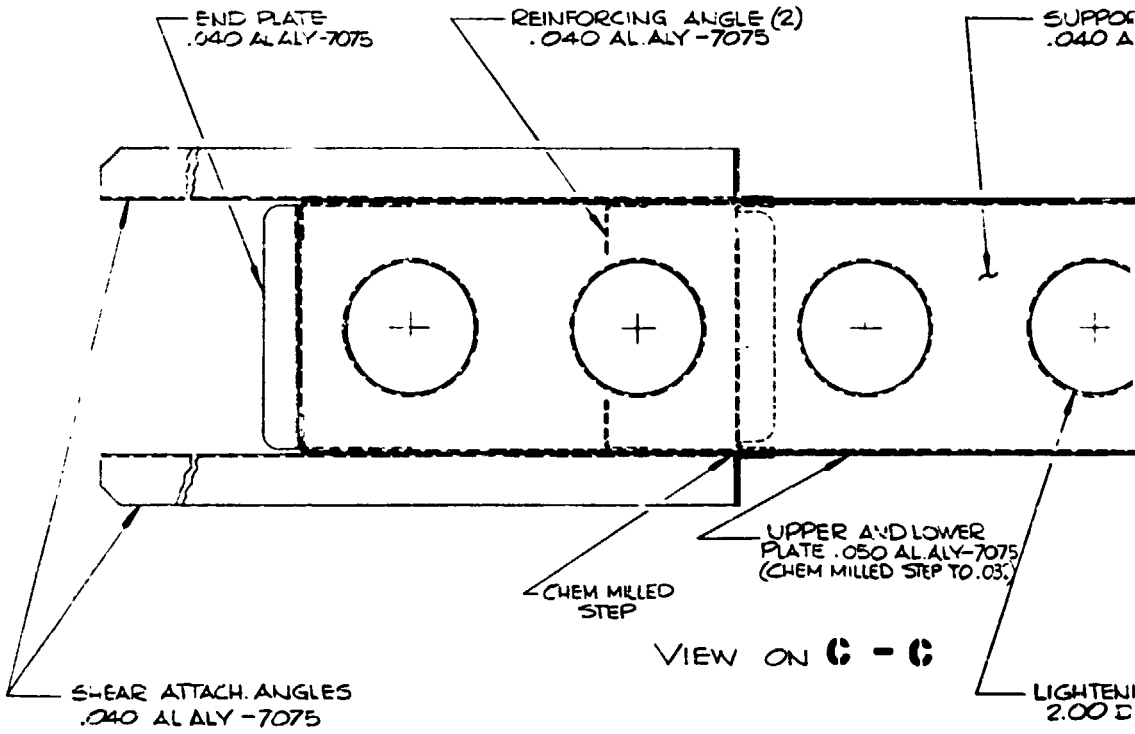

VIEW ON C - C

400U025 1

10 9 8

FOLDOUT FRAME FOLDOUT FRAME

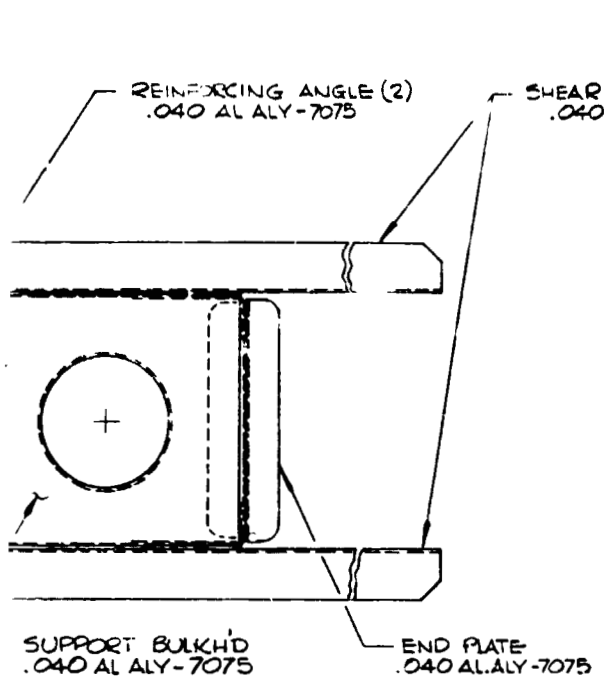

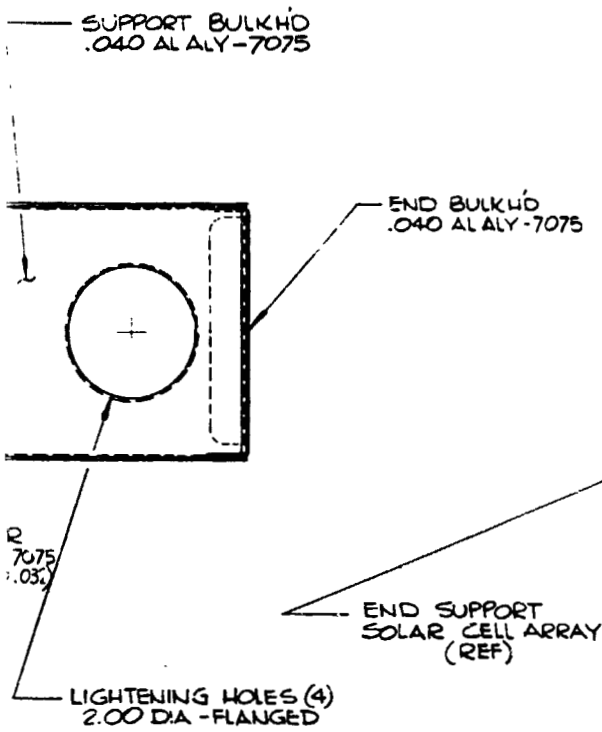

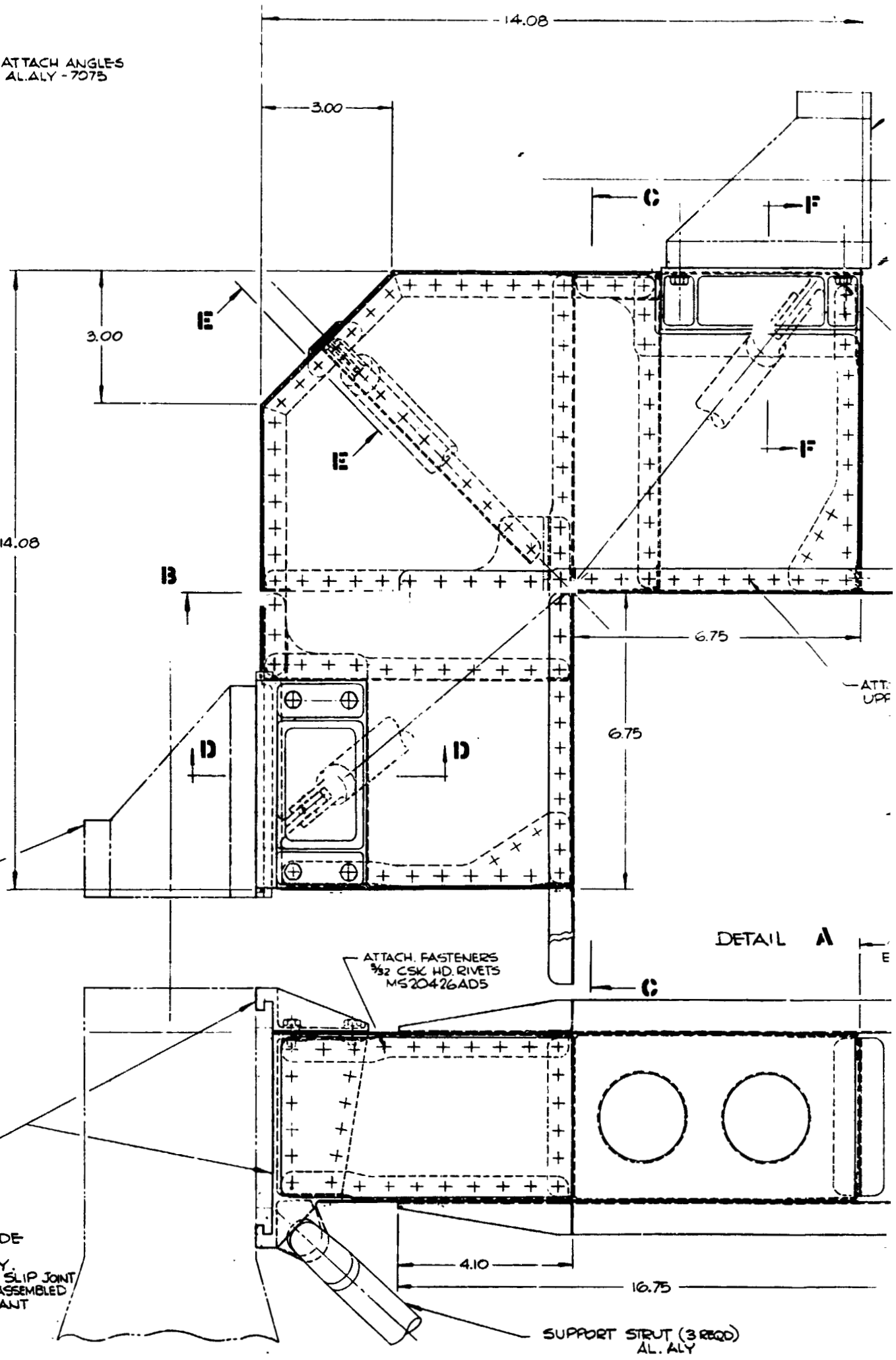

FOLDOUT FRAME

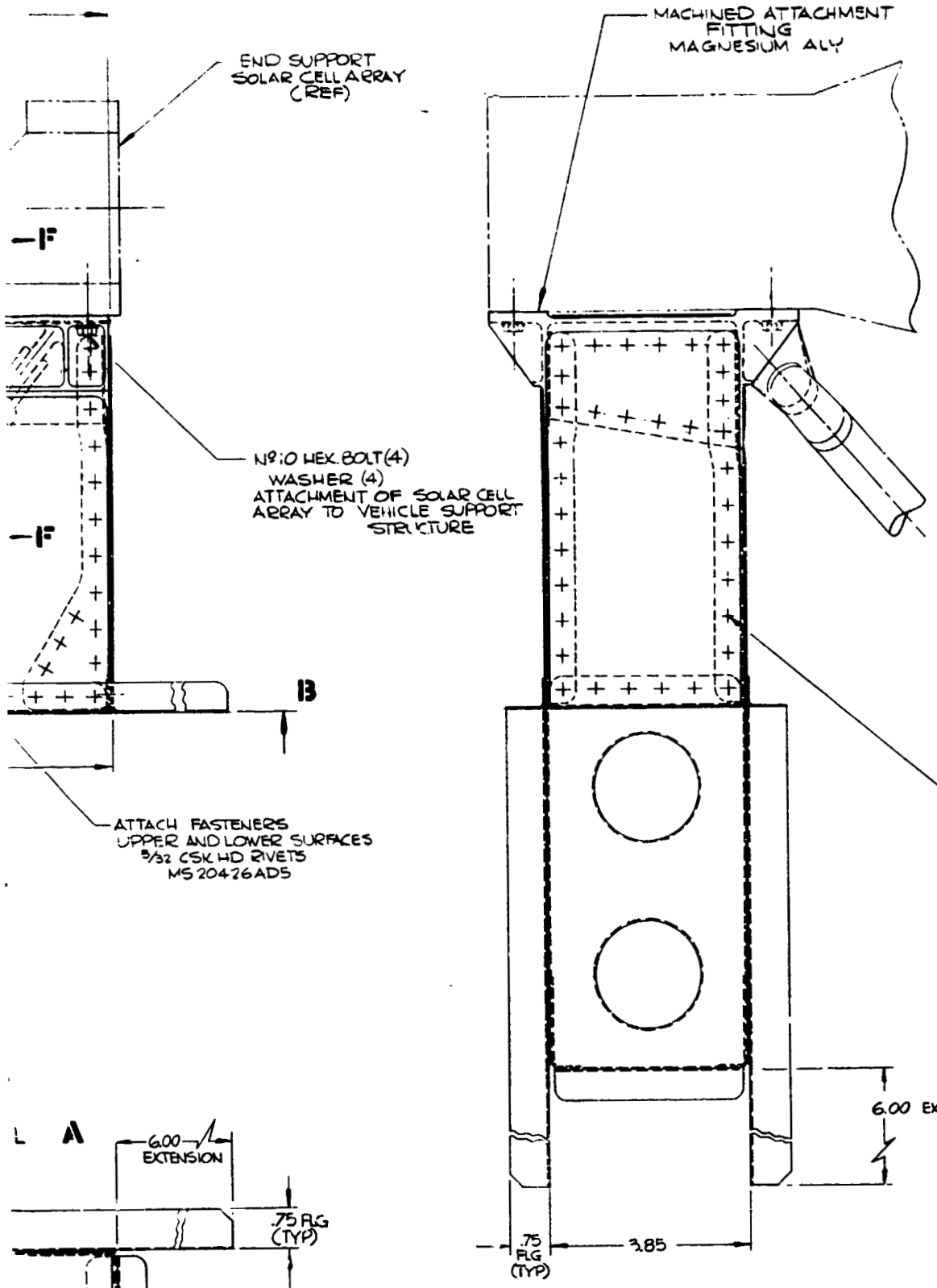

SCALE 1/1

VEHICLE SU
- SOLAR CELL

400U025 | 1

FOLDOUT FRAME FOLDOUT FRAME

REVISIONS				
LTR	EFF ON	DESCRIPTION	DATE	APPROVED

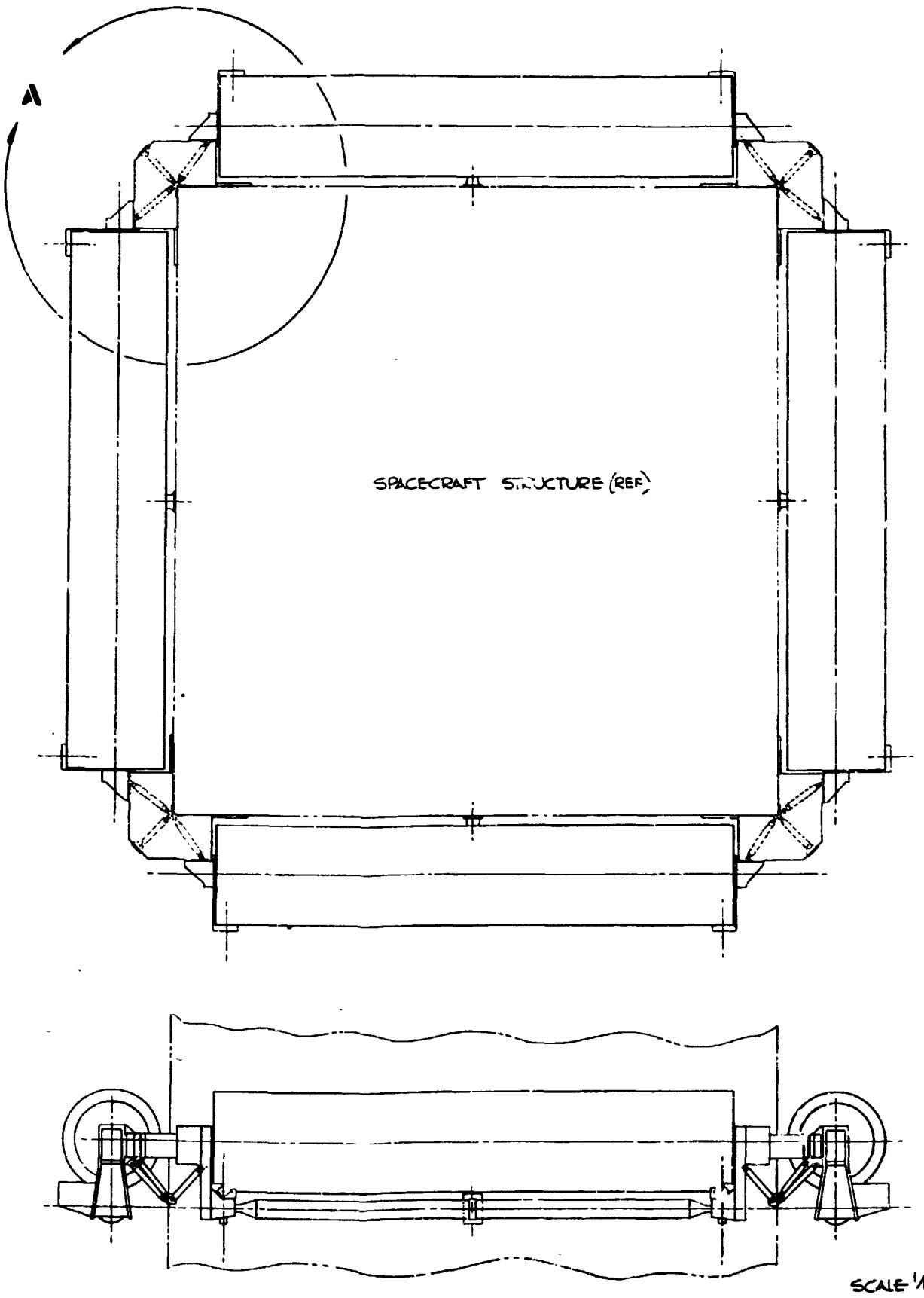

SCALE 1/8

VEHICLE SUPPORT STRUCTURE - SOLAR CELL ARRAY - MODEL 400

J	78022	400U025	
SCALE 1/8		SHEET	

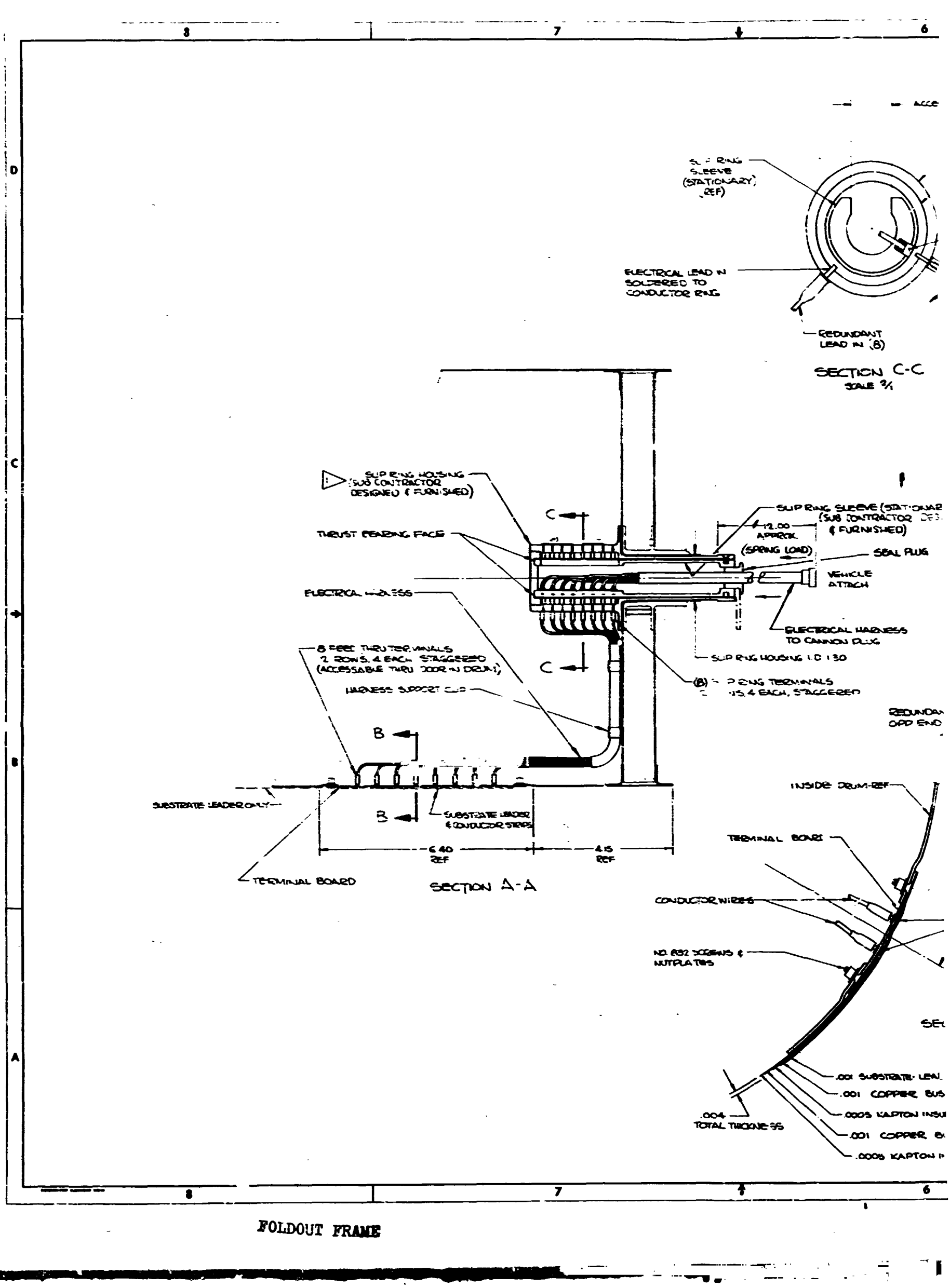

FOLDOUT FRAME

• ACCESS GROOVE

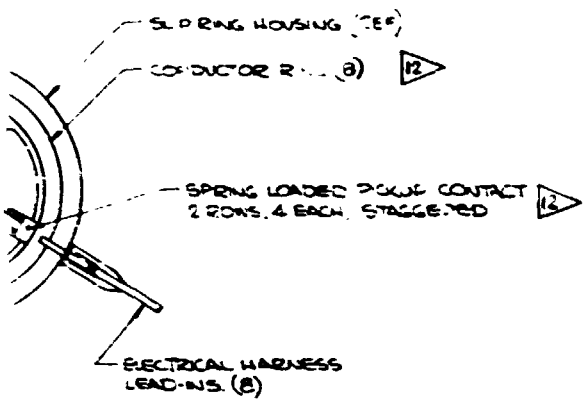

-C

TIONARY)
OR DESIGNED 1
)

PLUG

S

JUNDANT HARNESS
ND END DRUM

VIEW LOOKING INTO END OF DRUM

30° REF

NEGATIVE & POSITIVE BUS'S TO BE SOLDERED TO FEED THRU TERMINALS

ALL INSULATION TO BE BONDED TO TERMINAL BOARD AFTER SOLDERING & INSTALLATION OF BOARD TO DRUM.

SECTION B-B
SCALE 2/1

TE LEADER STRIP
BR BUS (POSITIVE)
ON INSULATION
DER BUS (NEGATIVE)
PTION INSULATION

12 BRUSH MATERIAL - 75% SILVER, 20% GRAPHITE AND 5% M
RING MATERIAL - COIN SILVER
LUBRICATION :-
USE BALL BROS. RESEARCH CORP. VAC-MOTE OR SIMILAR.

11 GENERAL DESIGN PRACTICE - MIL-STD-454 SHALL BE USED TO FABRICATION AND ASSEMBLY TECHNIQ

10 LEADWIRE DE-RATING - ALL LEADWIRE SHALL BE DESIGN FOUR TIMES THE NORMAL OPERATING C

9 CURRENT DENSITY - THE APPARENT CURRENT DENSITY BRUSH INTERFACE SHALL BE 75.

8 BRUSH PRESSURE - BRUSH PRESSURE SHALL BE 8 ± 2

7 TO BE OPERABLE IN AN ENVIRONMENTAL TEMPERATURE
MAX = +300°F
MIN = -150°F
AND AT A VACCUM EQUAL TO DEEP SPACE (10^{-9} TOR).

6 ALL ELECTRICAL CONNECTIONS TO BE SOLDERED

5 ELECTRICAL SYSTEM TO WITHSTAND 10 G'S SINUSOIDAL VIBRATION UP TO 2000 CPS.

4 TOTAL WEIGHT OF SLIP RING ASSY TO BE 7.5 LBS (LES

3 DRUM DEPLOYS (ROTATES) AT A RATE OF (1) TWO REVOLUT PER MINUTE. TOTAL REVOLUTIONS (EXPECTED LIFE) = 500

2 ELECTRICAL SYSTEM DESIGN CRITERIA - TURAL SOLAR CELL C
A VOLTS = 77
P WATTS = 2600
C PERMISSIBLE VOLTAGE DROP ≤ 1%

1. SLIP RING DESIGN AND MANUFACTURE TO BE CAR OUT BY AN APPROVED SUB CONTRACT SOURC

NOTES:

4001027

FOLDOUT FRAME FOLDOUT FRAME

BOARD

MATERIAL - 75% SILVER, 20% GRAPHITE AND 5% MOLYDISULFIDE
MATERIAL - COIN SILVER
CATION :-
ALL BRGS RESEARCH CORP. VAC-MOTE OR SIMILAR
- DESIGN PRACTICE - MIL-STD-454 SHALL BE USED AS A GUIDE TO FABRICATION AND ASSEMBLY TECHNIQUES.
IRE DE-RATING - ALL LEADWIRE SHALL BE DESIGNED TO TRANSMIT FOUR TIMES THE NORMAL OPERATING CURRENT.
ENT DENSITY - THE APPARENT CURRENT DENSITY AT THE RING/BRUSH INTERFACE SHALL BE 75 AMPS/IN²
PRESSURE - BRUSH PRESSURE SHALL BE 8 ± 2 PSI
OPERABLE IN AN ENVIRONMENTAL TEMPERATURE RANGE OF :
+300°F
-150°F
AT A VACCUM EQUAL TO DEEP SPACE (10^{-9} TOR).
LECTRICAL CONNECTIONS TO BE SOLDERED
RCAL SYSTEM TO WITHSTAND 10 G'S SINUSOIDAL RESPONSE TION UP TO 200 CPS
WEIGHT OF SUP RING ASSY TO BE .76 LBS (LESS REDUND. HARDNESS).
DEPLOYS (ROTATES) AT A RATE OF (2) TWO REVOLUTIONS MINUTE. TOTAL REVOLUTIONS (EXPECTED LIFE) = 5000.
OCAL SYSTEM DESIGN CRITERIA - TOTAL SOLAR CELL OUTPUT:
A VOLTS = 77
WATTS = 2800
E PERMISSIBLE VOLTAGE DROP ≤ 1%

RING DESIGN AND MANUFACTURE TO BE CARRIED BY AN APPROVED SUB CONTRACT SOURCE.

LIST OF MATERIAL

FOLDOUT FRAME

FOLDOUT FRAME

2 1

REVISIONS

LTR	DWN BY	DESCRIPTION	DATE	APPROVED

D C B A

(SPECIFICATION CONTROL DWG)

LIST OF MATERIAL

ITEM	PART NUMBER	DESCRIPTION	STOCK SIZE	MATERIAL	SPECIFICATION	MASS UNIT/ASSY	QTY REQD PER ASSY
1		SLIP RING & ELECT HARNESS ASSY					

LIST OF MATERIAL

RELEASE & DATE	QTY REQD PER ASSY	UNLESS OTHERWISE SPECIFIED	CONTRACT NUMBER
FINAL ASSY / NEXT ASSY: QTY REQUIRED	NEXT ASSEMBLY / APPLICATION	DIMENSIONS ARE IN INCHES. TOLERANCES: LINEAR ANGULAR	USED ON

RYAN AERONAUTICAL COMPANY
SAN DIEGO, CALIFORNIA 92112

SLIP RING & ELECTRICAL HARNESS, MODEL 400 (PROPOSED PARAMETERS)

SIZE	CODE IDENT NO.	DRAWING NO.	REV
J	07765	400U027	

SCALE | WEIGHT | SHEET 1 OF 1

FOLDOUT FRAME

FOLDOUT FRAME

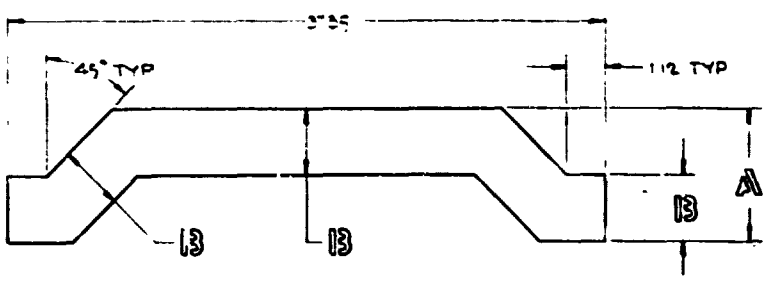

DETAIL BUSS-NEGATIVE LONGITUDINAL -57 THRU -181

DASH NO	A	B
-157	11.00	5.25
-159	10.78	5.14
-161	10.50	5.00
-163	10.12	4.81
-165	9.66	4.58
-167	9.08	4.29
-169	8.42	3.96
-171	7.98	3.54
-173	6.66	3.08
-175	5.62	2.56
-177	4.46	1.98
-179	3.26	1.38

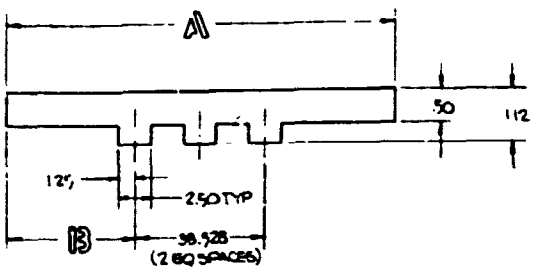

DETAIL BUSS-POSITIVE TRANSVERSE -235 THRU -259

DASH NO	A	B
-235	61.52	14.90
-237	67.74	14.60
-239	68.02	14.75
-241	68.40	14.98
-243	68.86	15.17
-245	69.44	15.45
-247	70.10	15.78
-249	70.94	16.20
-251	71.86	16.66
-253	72.90	17.18
-255	74.06	17.76
-257	75.26	18.56
-259	76.58	19.02

TAB BU

SUBSTRATE ASSY	SUBSTRATE SUB-ASSY	BUSS-POSITIVE LONGITUDINAL	INSULATOR POSITIVE
-1	-27	-105	-131
-3	-29	-107	-133
-5	-31	-109	-135
-7	-33	-111	-137
-9	-35	-113	-39
-11	-37	-115	-141
-13	-39	-117	-143
-15	-41	-119	-145
-17	-43	-121	-147
-19	-45	-123	-149
-21	-47	-125	-151
-23	-49	-127	-153
-25	-51	-	-

57.35

DETAIL BUSS-POS
-105 THRU-129

DASH NO	A
-105	5.25
-107	5.14
-109	5.00
-111	4.81
-113	4.58
-115	4.29
-117	3.96
-119	3.54
-121	3.08
-123	2.56
-125	1.98
-127	1.38

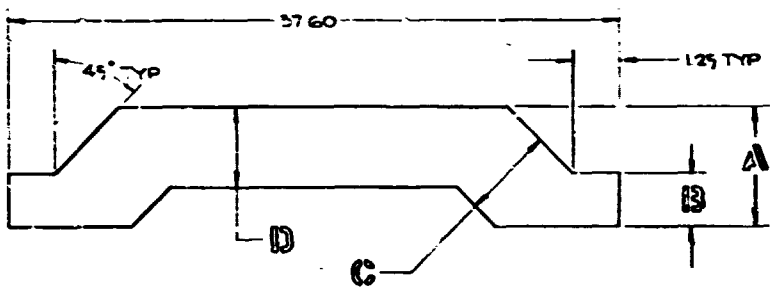

DETAIL INSULATOR-NEGATIVE -183 THRU -207

DASH NO.	A	B	C	D
-183	12.00	5.75	5.75	6.25
-185	11.78	5.64	5.64	6.14
-187	11.50	5.50	5.50	6.00
-189	11.12	5.31	5.31	5.81
-191	10.66	5.08	5.08	5.58
-193	10.08	4.79	4.79	5.29
-195	9.42	4.46	4.46	4.96
-197	8.58	4.04	4.04	4.54
-199	7.66	3.58	3.58	4.08
-201	6.62	3.06	3.06	3.56
-203	5.46	2.48	2.48	2.98
-205	4.26	1.88	1.88	2.38

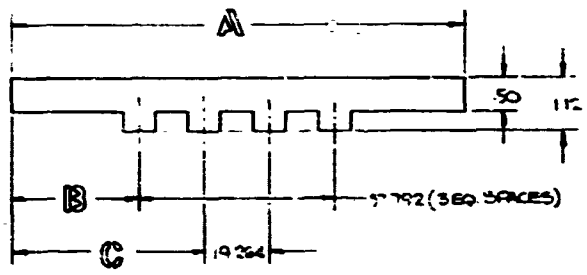

DETAIL BUSS-NEGATIVE TRANSVERSE -287 THRU -311

DASH NO.	A	B	C
-287	56.02	-	13.38
-289	56.16	-	18.60
-291	57.75	.00	9.26
-293	57.79	.00	19.26
-295	58.70	.45	-
-297	59.86	1.03	-
-299	61.18	1.69	-
-301	62.86	2.53	-
-303	64.70	3.45	-
-305	66.78	4.50	-
-307	69.10	5.65	-
-309	71.50	6.85	-
-311	73.14	7.67	-

PARTIAL TABS TYP EACH END

A

DETAIL INSULATOR-NE
TRANSVERSE
-313 THRU-337

DASH NO.	A
-313	56.52
-315	56.96
-317	57.52
-319	58.28
-321	59.20
-323	60.36
-325	61.68
-327	63.36
-329	65.20
-331	67.28
-333	69.60
-335	72.00
-337	73.64

TAB BLOCK "A"

ASSY	SUBSTRATE SUB-ASSY	BUSS-POSITIVE LONGITUDINAL	INSULATOR POSITIVE	BUSS-NEGATIVE LONGITUDINAL	INSULATOR NEGATIVE	BUSS-POSITIVE TRANSVERSE	INSULATOR-POS TRANSVERSE	BUSS-NEGATIVE TRANSVERSE	INSULATOR NEG TRANSVERSE	DOUBLER
	-27	-105	-131	-157	-183	-209	-261	-287	-313	-339
3	-29	-107	-133	-159	-185	-237	-263	-289	-315	-211
5	-31	-109	-135	-161	-187	-239	-265	-291	-317	-213
7	-33	-111	-137	-163	-189	-241	-267	-293	-319	-215
9	-35	-113	-139	-165	-191	-243	-269	-295	-321	-217
11	-37	-115	-141	-167	-193	-245	-271	-297	-323	-219
13	-39	-117	-143	-169	-195	-247	-273	-299	-325	-221
15	-41	-119	-145	-171	-197	-249	-275	-301	-327	-223
17	-43	-121	-147	-173	-199	-251	-277	-303	-329	-225
19	-45	-123	-149	-175	-201	-253	-279	-305	-331	-227
21	-47	-125	-151	-177	-203	-255	-281	-307	-333	-229
23	-49	-127	-153	-179	-205	-257	-283	-309	-335	-231
25	-51	-	-	-	-	-259	-285	-311	-337	-233

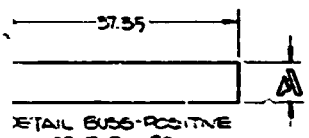

DETAIL BUSS-POSITIVE
-105 THRU-129

DASH NO.	A
-105	5.25
-107	5.14
-109	5.00
-111	4.81
-113	4.58
-115	4.29
-117	3.96
-119	3.54
-121	3.08
-123	2.56
-125	1.98
-127	1.38

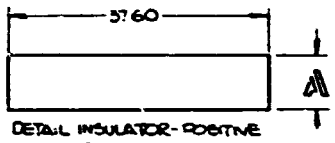

DETAIL INSULATOR-POSITIVE
-131 THRU-155

DASH NO.	A
-131	6.25
-133	6.14
-135	6.00
-137	5.81
-139	5.58
-141	5.29
-143	4.96
-145	4.54
-147	4.08
-149	3.56
-151	2.98
-153	2.38

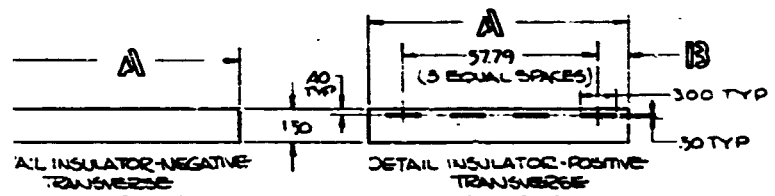

DETAIL INSULATOR-NEGATIVE
TRANSVERSE
-313 THRU-337

DETAIL INSULATOR-POSITIVE
TRANSVERSE
-261 THRU-285

DASH NO.	A	B
-261	68.02	5.11
-263	68.24	5.22
-265	68.52	5.36
-267	68.90	5.55
-269	69.36	5.78
-271	69.94	6.07
-273	70.60	6.40
-275	71.44	6.83
-277	72.56	7.28
-279	73.40	7.80
-281	74.56	8.38
-282	75.76	8.98
-285	77.08	9.64

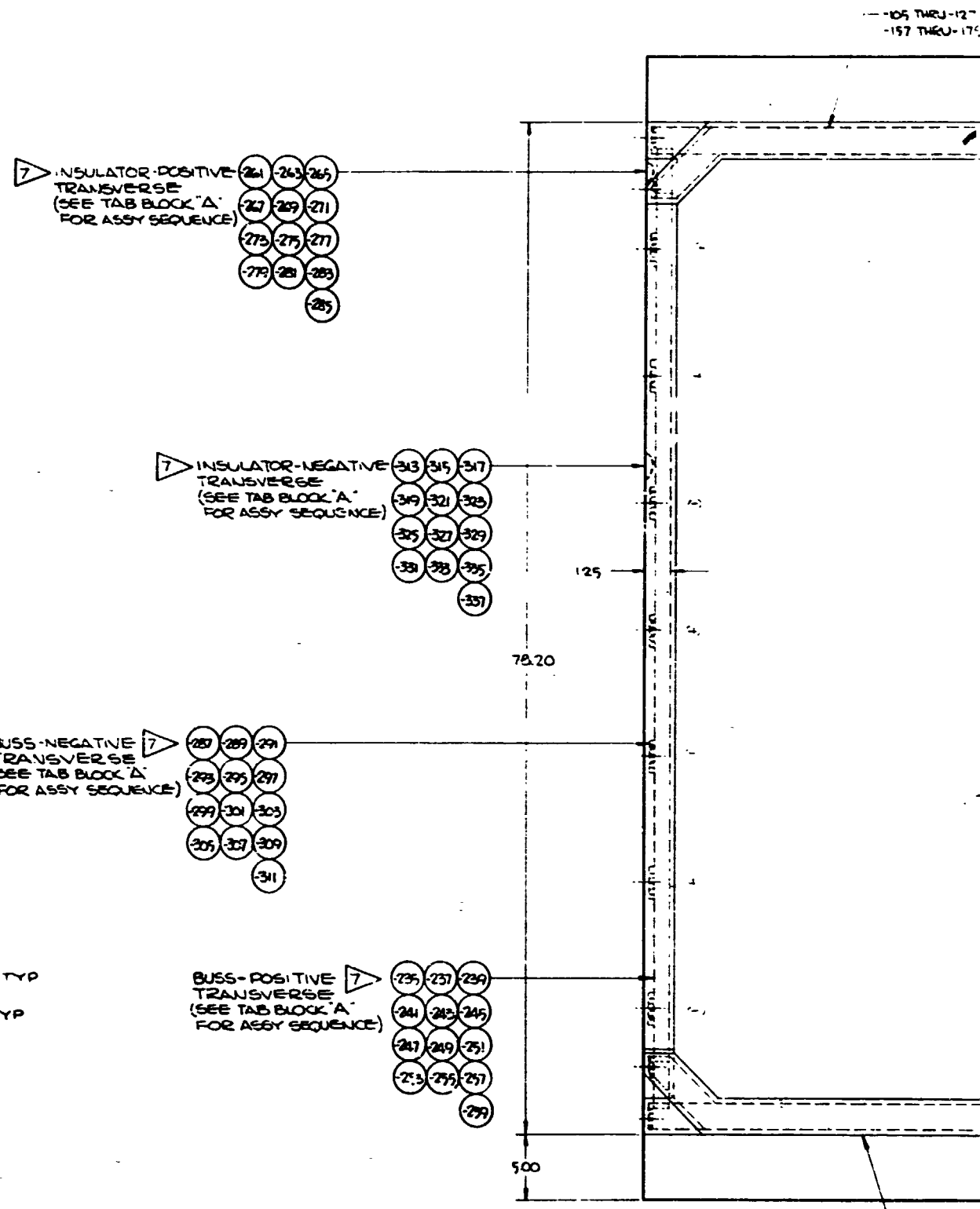

DETAIL SUBSTRATE AS
-1 THRU-25 SHOWN
(SEE TAB BLOCK "A"
FOR ASSY SEQUENC
(SOLAR CELLS INSTALL FA

400U030 | SH 2 | REV

FOLDOUT FRAME

FOLDOUT FRAME

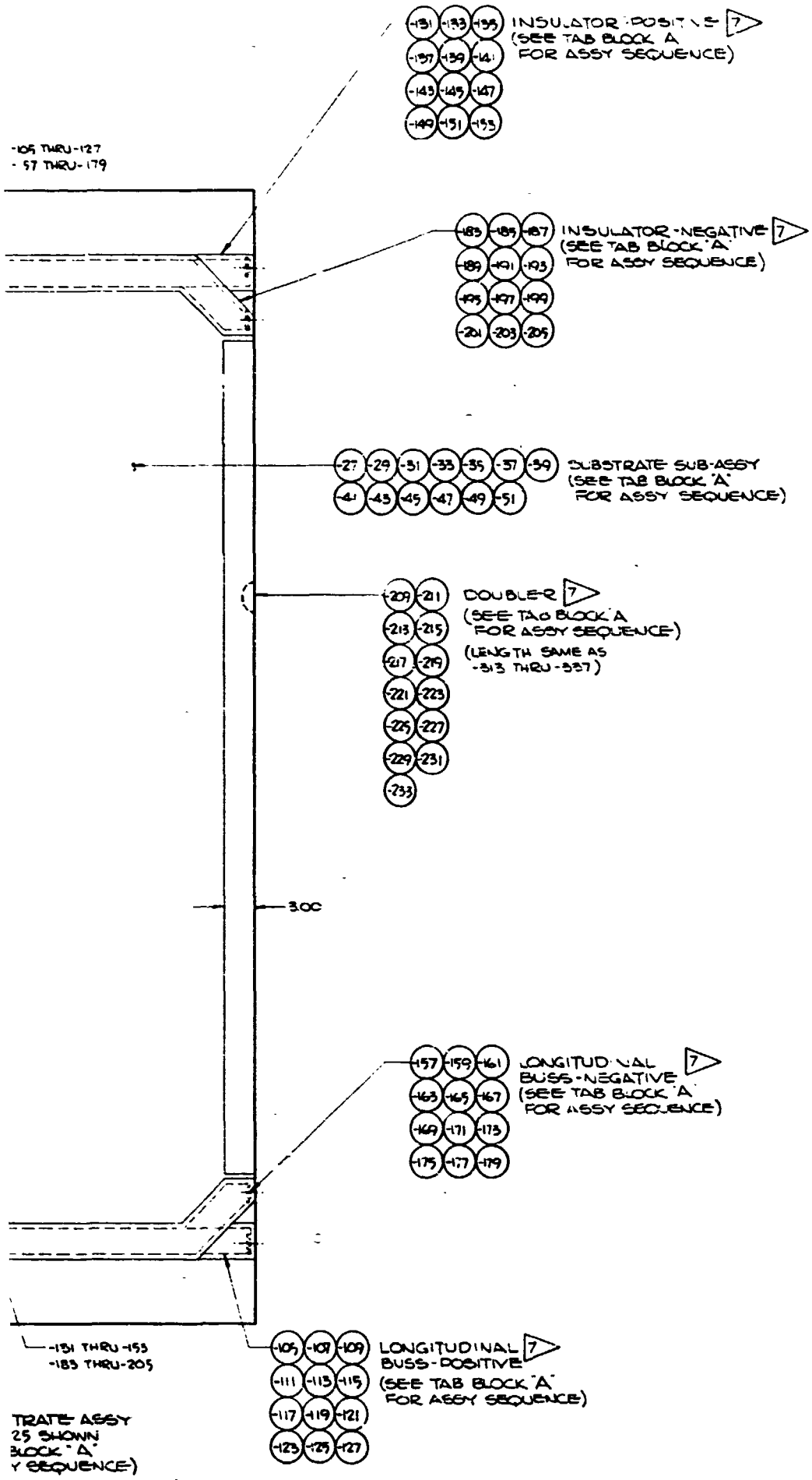

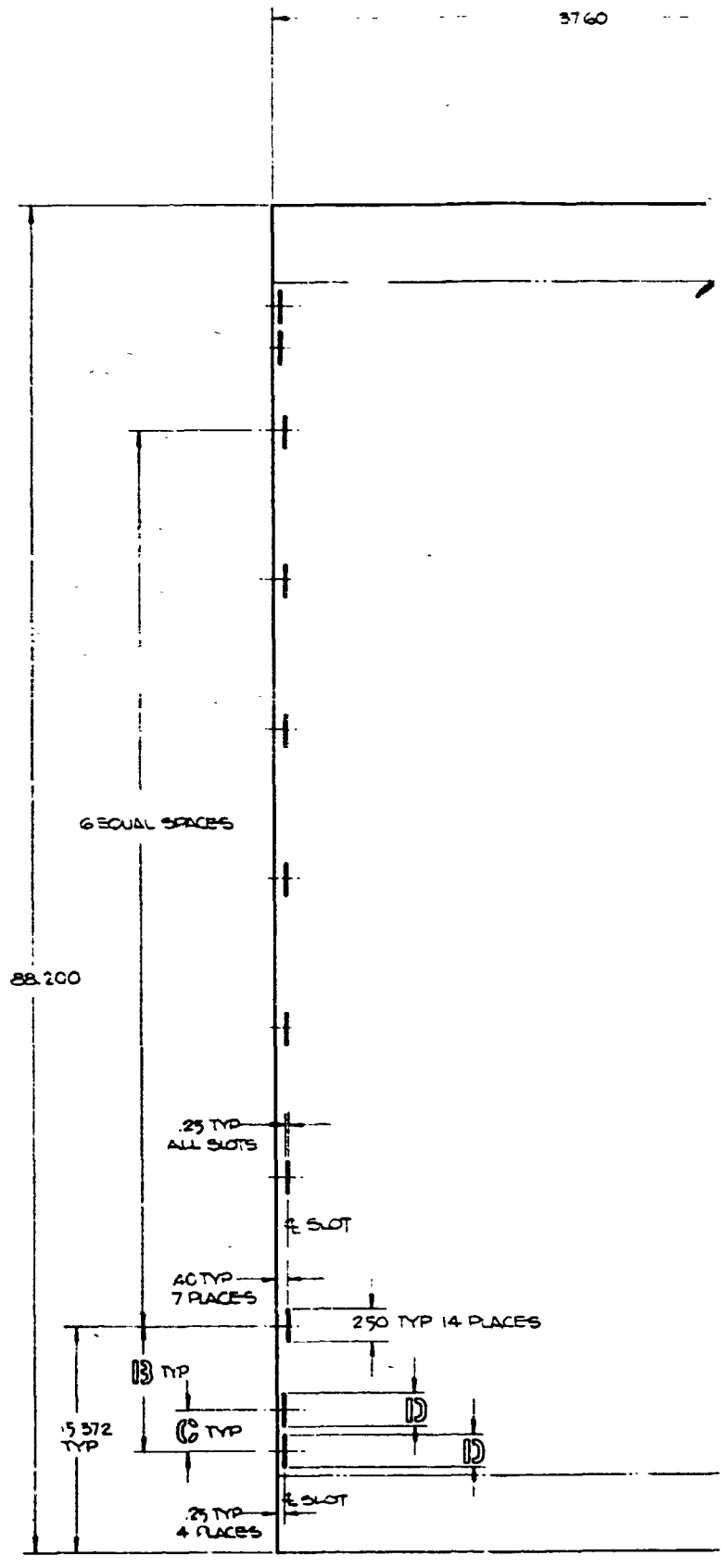

DETAIL SUBSTRATE SUB-ASSY
-27 THRU-51 SHOWN
(SEE TAB BLOCK 'B' FOR ASSY SEQUENCE)
(BUSS'S AND INSULATORS INSTALL NE
SOLAR CELLS INSTALL FAR SIDE)

3760

.25 MIN

7

.79 REF

SOLAR CELLS INSTALL THIS SIDE

.53 REF

BUSSES, INSULATORS, DOUBLER AND BUTTONS INSTALL THIS SIDE

SECTION A = A

A

A

(79) (81) (83) (85) (87) (89) (91) (93) (95) (97) (99) (101) (103) SUBSTRATE (SEE TAB BLOCK 'B' FOR ASSY SEQUENCE)

(53) (55) (57) (59) (61) (63) (65) (67) (69) (71) (73) (75) (77) SUBSTRATE (SEE TAB BLOCK 'B' FOR ASSY SEQUENCE)

THESE SLOTS IN -27 THRU -49 ONLY TYP THIS SIDE

TAB BLOCK 'B'					
ASSY NO	B	C	D	BOND SUBSTRATES	
-27	7.00	5.75	5.25	-53	-79
-29	7.05	5.65	5.15	-55	-81
-31	7.12	5.50	5.00	-57	-83
-33	7.22	5.30	4.80	-59	-85
-35	7.32	5.10	4.60	-61	-87
-37	7.47	4.80	4.30	-63	-89
-39	7.62	4.50	4.00	-65	-91
-41	7.82	4.10	3.60	-67	-93
-43	8.07	3.60	3.10	-69	-95
-45	8.32	3.10	2.60	-71	-97
-47	8.62	2.50	2.00	-73	-99
-49	8.92	1.90	1.40	-75	-101
-51	9.25	1.25	.75	-77	-103
-347				-349	-351

QTY REQD PER ASSY	CODE IDENT	PART NUMBER	DESCRIPTION	STOCK SIZE	MATERI

LIST OF MATERIAL

SUB ASSY
SHOWN
CK 'B'
SEQUENCE)
25 INSTALL NEAR SIDE
LL FAR SIDE)

400U030 | 2

FOLDOUT FRAME

FOLDOUT FRAME

REVISIONS

LTR	EFF ON	DESCRIPTION	DATE	APPROVED

D C B A

ITEM NO.	QTY REQD PER ASSY	CODE IDENT	PART NUMBER	DESCRIPTION	STOCK SIZE	MATERIAL	SPECIFICATION	RYAN MATL CODE	ZONE	ITEM NO.
		ALL	BUSSES (TRANSFER)	OC2 x AR	STRIP AL 00-0		QQ-A 250/1			
		(ALL)	BUSSES (CONST.)	001 x AR	STRIP AL 00-0		QQ-A 250/1			
		(ALL)	DOUBLERS	00 x AR	KAPTON FILM		TYPE 100 H			
		(ALL)	INSULATORS	001 x AR	KAPTON FILM		TYPE 100 H			
		(ALL)	SUBSTRATE	001 x AR	KAPTON FILM		TYPE 100 H			

LIST OF MATERIAL

400U030

ITEM NO.	QTY REQD PER ASSY	STOCK SIZE	MATERIAL	SPECIFICATION	RYAN MATL CODE	FUSE

LIST OF MATERIAL

RELEASE & DATE	QTY REQD PER ASSY

UNLESS OTHERWISE SPECIFIED
DIMENSIONS ARE IN INCHES AND INCLUDE OVER APPLIED OR PLATED FINISHES

TOLERANCES

LINEAR		ANGULAR
X	± 1	EXCL OF SHEET METAL FLANGES
XX	± .03	± 0° 30'
XXX	± .010	

PARTS TO BE FREE OF BURRS AND CHARP EDGES. MANUFACTURING REQUIREMENTS PER RYAN SPEC. STANDARD NO. 130.

CONTRACT NUMBER

SIGNATURES | DATE

DESIGN ACTIVITY APPROVAL

DESIGN APPROVAL

FINAL ASSY	NEXT ASSY	NEXT ASSEMBLY	USED ON
QTY REQUIRED		APPLICATION	

RYAN AERONAUTICAL COMPANY
SAN DIEGO, CALIFORNIA 92112

SUBSTRATE ASSY-DETAIL
250 FT² - ROLL-UP

SIZE	CAGE IDENT NO.	NUMBER	REV SYM
J	78022	400U030	

SCALE 1/2 WEIGHT SHEET 1 OF 2

15 14 13

D C B A

55.00

83.20

J J

M

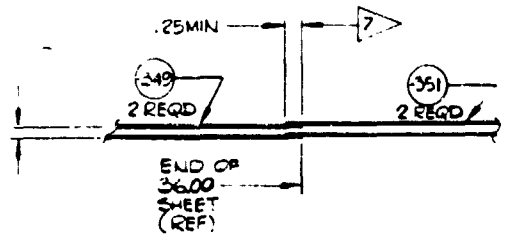

SECTION J - J

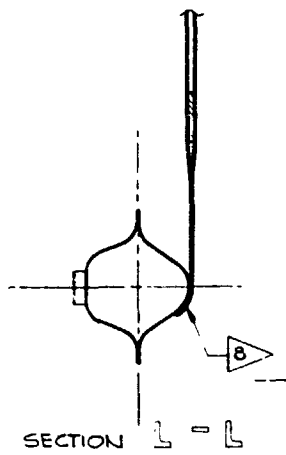

SECTION L - L

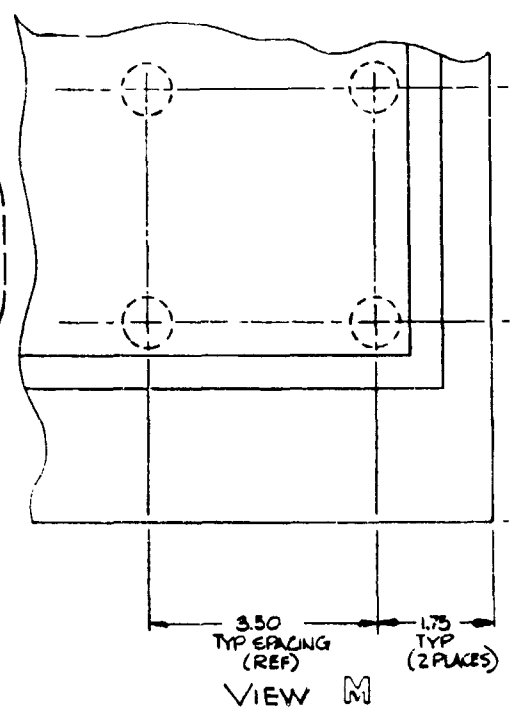

VIEW M

DETAIL SUBSTRATE THERMAL BLANKET SUB-ASSY
-347 SHOWN
(SEE TAB BLOCK '8' FOR ASSY SEQUENCE)

15 14 13

FOLDOUT FRAME

FOLDOUT

13 | 12 | 11

55.00
(FOR BUTTON SPACING THIS AREA SEE TABLE C-APPROX 3.50)

108.59
(FOR BUTTON SPACING THIS AREA SEE TAB C -APPROX 2.50)

94.24
(FOR BUTTON SPACING SEE TAB C - APPROX

11.14 REF

3.26 REF

400U021 REF

-53 SUBSTRATE SUB-ASSY

-25 SUBSTRATE ASSY

-23 SUBSTRATE ASSY

-21 SUBSTRATE ASSY

-19 SUBSTRATE ASSY

-17 SU

END OF WRAP N°12

END OF WRAP N°11

END OF WRAP N°10

END OF WRAP N°8

400U02. REF

3.50 TYP SPACING (REF)

3.00 TYP (2 PLCS)

1.75 TYP 2 PLACES

TAB - REF

THERMAL BLANKET - REF

TAB - REF

400U002 REF

SECTION C - C
TYP CROSSMEMBER/THERMAL BLANKET ATTACH

BUTTONS - REF

SUBSTRATE - REF

CELLS - REF

TAB - REF

TAB - REF

400U002 REF

SECTION B - B
TYP BEAM/SUBSTRATE ATTACH

1.00

1.00

DETAIL -34! TAB

13 | 12 | 11

FOLDOUT FRAME

FOLDOUT FRAME

10 9 8

544.64

94.24 (FOR BUTTON SPACING THIS AREA SEE TAB C - APPROX 2.20)

89.89 (FOR BUTTON SPACING THIS AREA SEE TAB C - APPROX 1.90)

85.55 (FOR BUTTON SPACING THIS AREA SEE TAB C - APPROX 1.80)

22.00 REF

400U021 REF

7.42 REF

-17 SUBSTRATE ASSY

-15 SUBSTRATE ASSY

-13 SUBSTRATE ASSY

-11 SUBSTRATE ASSY

-9 SUBSTRATE ASSY

-7 SUBSTRATE ASSY

END OF WRAP Nº8

END OF WRAP Nº7

END OF WRAP Nº6

END OF WRAP Nº5

END OF WRAP Nº4

VIEW LOOKING NORMAL TO DAMPER BUTTON SIDE
(CELLS INSTALLED FAR SIDE EACH SUBSTRATE MODULE)
ATTACHMENT TABS OMITTED FOR CLARITY)
SCALE 1/8

1.00

1.00

-341 TAB

℄ EQUAL SPACE - REF

.06 REF

-341

VIEW J
TYP CLIP ATTACH

-341

VIEW K
TYP CLIP ATTACH

3.65

1.00

DETAIL -339 BEAM ATTACH TAB

TAB DAMPER SPACI	
ASSY NO.	all
-	1.72
-3	1.5
-5	1.3
-7	1.1
-9	1.0
-11	1.1
-13	1.3
-15	1.5
-17	1.7
-19	1.9
-21	2.1
-23	2.3
-25	2.5
-347	3.5

4C0U030 1

10 9 8

F[illegible]UT FRAME

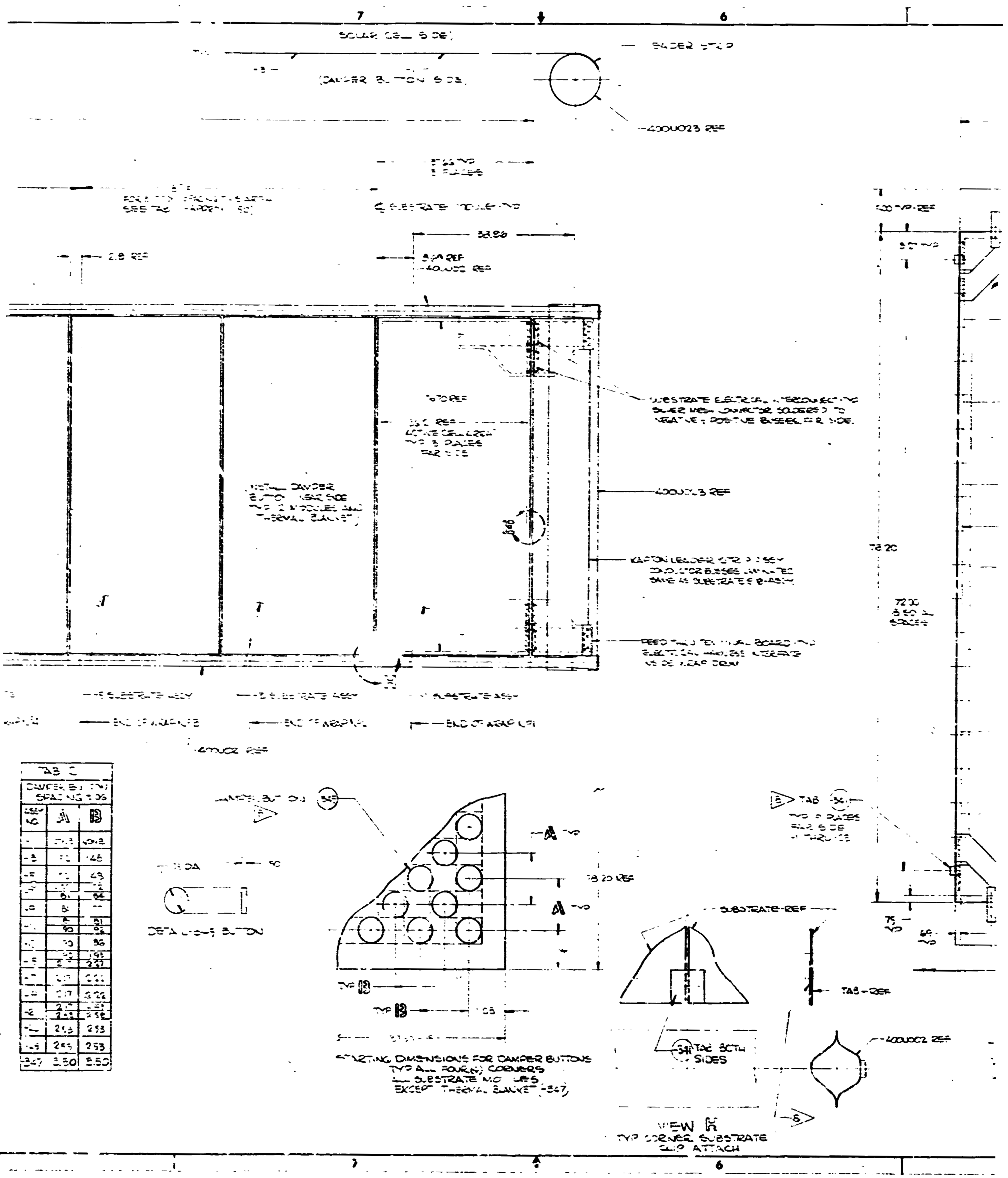

FOLLDUT FRAME

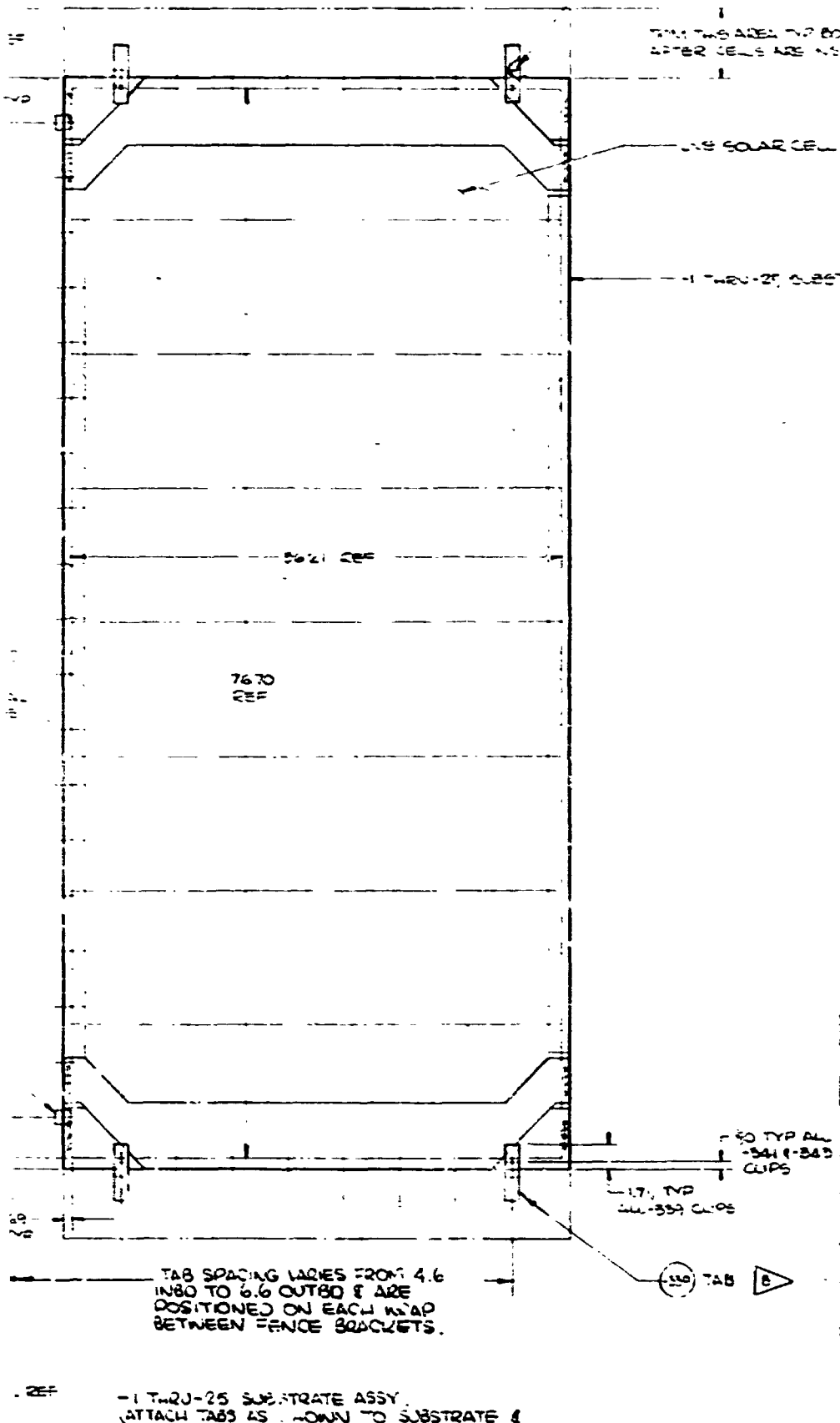

5 BOND ALL BUTTONS, TABS TO BEAM AND TABS TO SUBSTRATE USING RTV 3145 ADHESIVE. PRIME ALL ADHESIVE SURFACES WITH DOW CORNING 92-198 PRIMER PRIOR TO BONDING.

7 BOND ALL SUBSTRATES, SUBSTRATE DOUBLERS, ALL CONDUCTOR BUSSES AND INSULATORS TO SUBSTRATE USING RTV-1044 ADHESIVE. (.0516 LB/FT² MAX)

6 DAMPER BUTTONS TO BE MADE FROM POLYURETHANE FOAM 2.0 LB/CU FT. NOM ECCOFOAM FS.

5 ALL TABS TO BE MADE FROM 3 MIL FIBERGLAS TAPE 1.0 WIDE - SHTNEAVE TYPE ECC-B A-172 FINISH

4 LONGITUDINAL BUSSES TO BE .001 THK & TRANSVERSE BUSSES TO BE .002 THK ALUMINUM FOIL TYPE 1100 EC

3 ALL SUBSTRATE & DOUBLERS TO BE .001 THK & INSULATORS TO BE .0005 - 2 KAPTON H FILM.

2 ALL BONDING THIS DRAWING TO BE IN ACCORDANCE WITH RYAN PROCESS SPECIFICATION 4003002 AS REF ABOVE.

1 DESIGN INFORMATION THIS DRAWING IS AS FOLLOWS

SHEET ONE
1 ASSEMBLED SUBSTRATE ASSYS, CLIPS AND DAMPER BUTTONS.

SHEET TWO
1 SUBSTRATE SUB-ASSY DETAIL (-1 THRU -51)
2 SUBSTRATE ASSY DETAIL (-1 THRU -25).
3 DETAIL ALL BUSSES, INSULATORS AND DOUBLERS.

NOTES:

4000030 | 1

FOLDOUT FRAME

3 2 1

REVISIONS

D

C

B

A

LIST OF MATERIAL

LIST OF MATERIAL

RYAN

SUBSTRATE ASSY-
DETAIL 290 FT ROLL-UP

J | 78022 | 4000030

4000030

FOLDOUT FRAME